BIOPHYSICAL INVESTIGATION OF M-DNA

A Thesis Submitted to the College of Graduate Studies and Research

in Partial Fulfillment of the Requirements for the

Degree of Doctor of Philosophy

in the Department of Biochemistry

University of Saskatchewan, Saskatoon

by

David Owen Wood

Permission To Use

In presenting this thesis in partial fulfillment of the requirements for a postgraduate degree from the University of Saskatchewan, I agree that the libraries of this University may make it freely available for inspection. I further agree that permission for copying of this thesis in any manner, in whole or in part, for scholarly purposes may be granted by the professors who supervised my thesis work, or in their absence, by the Head of the Department of Biochemistry or the Dean of the College of Medicine. It is understood that any copying or publication or use of this thesis or parts thereof for financial gain shall not be allowed without my written permission. It is also understood that due recognition shall be given to me and to the University of Saskatchewan in any scholarly use which may be made of any materials in my thesis.

Requests for permission to copy or make other use of material in this thesis in whole or in part should be addressed to:

Head of the Department of Biochemistry

University of Saskatchewan

Saskatoon, Saskatchewan, S7N 5E5

Abstract

M-DNA is a complex formed between normal double-stranded DNA and the transition metal ions Zn^{2+}, Ni^{2+}, and Co^{2+} that is favoured by an alkaline pH. Previous studies have suggested that M-DNA formation involves replacement of the imino protons of G and T bases by the transition metal ions involved in forming the complex. Owing to the conductive properties of this unique DNA conformation, it has potential applications in nanotechnology and biosensing. This work was aimed at improving existing methods and developing new methods of characterizing M-DNA. The effects of base substitutions, particularly those of G and T, were evaluated in light of the proposed structure. Differences between M-DNA conformations induced by Zn^{2+} and Ni^{2+} were also investigated with a variety of techniques and compared to the effects of Cd^{2+} and Mg^{2+} on double-stranded DNA.

M-DNA formation and stability were studied with an ethidium bromide (EtBr) based assay, M-DNA induced fluorescence quenching of DNA labelled with fluorescein and a compatible quenching molecule, isothermal titration calorimetry (ITC), and surface plasmon resonance (SPR). Production of monoclonal antibodies against the conformation was also attempted but was unsuccessful. The EtBr-based assay showed Ni(II) M-DNA to be much more stable than Zn(II) M-DNA as a function of pH and in the presence of ethylenediaminetetraacetic acid. Sequence-dependency and the effect of base substitutions were measured as a function of pH. With regards to sequence, $d(G)_n \bullet d(C)_n$ tracts were found to form the conformation most easily. Base substitutions with G and T analogues that lowered the pK_a of these bases were found to stabilize M-DNA more

strongly than other base substitutions. A combination of temperature-dependant EtBr and ITC assays showed M-DNA formation to be endothermic, and therefore entropy driven. The SPR studies demonstrated many qualitative differences between Zn(II) and Ni(II) M-DNA formation, allowed characterization of Zn^{2+}, Ni^{2+}, Cd^{2+}, and Mg^{2+} complexes with single-stranded DNA, and provided unambiguous evidence that M-DNA formation results in very little denaturation of double-stranded DNA. Specifically, the SPR study showed Ni(II) M-DNA to be more stable than Zn(II) M-DNA in the absence of transition metal ions, but also showed that Ni(II) M-DNA required higher concentrations of Ni^{2+} than Zn^{2+} to fully form the respective M-DNA conformations. Finally, quenching studies demonstrated Zn(II) M-DNA formation over a pH range from 6.5 to 8.5 provided that a Zn^{2+}:H^{+} ratio of roughly 10^5 was maintained. The K_{eq} for this interaction was 1.3×10^{-8} with 1.4 H^{+} being liberated per base bair of M-DNA formed.

These results support the proposed structural model of M-DNA, as lowering the pK_a of the bases having titratable protons over the pH range studied facilitated M-DNA formation. The fact that Zn(II) M-DNA formation was observed by fluorescence quenching at any pH provided that a constant ratio of Zn^{2+}:H^{+} was maintained was consistent with a simple mass-action interaction for M-DNA formation. The differences between Zn(II) and Ni(II) M-DNA formation show that although it requires a higher pH or transition metal ion concentration, Ni(II) M-DNA is more stable than Zn(II) M-DNA once formed. This difference could play an important role in applications of M-DNA which required modulation in the stability of the M-DNA conformation.

Published Works

The following published articles contain work presented in this thesis:

Wood, D.O. and Lee, J.S. (2005) Investigation of pH-dependent DNA-metal Ion Interactions by Surface Plasmon Resonance. *J. Inorg. Bioch*. 99: 566-574.

Wettig, S.D., Wood, D.O. and Lee, J.S. (2003) Thermodynamic Investigation of M-DNA: A Novel Metal Ion-DNA Complex. *J. Inorg. Bioch*. 94: 94-99.

Wood, D.O., Dinsmore, M.J., Bare, G.A. and Lee, J.S. (2002) M-DNA is Stabilised in G●C Tracts of by Incorporation of 5-fluorouracil. *Nucleic Acids Res*. 30: 2244-2250.

Acknowledgments

First off, I would like to thank my supervisor, Dr. Jeremy Lee. Without his support, guidance, and patience, this project would not have been possible. He granted me a large degree of independence and freedom of action in the direction of my thesis for which I am very grateful. He was also very approachable, funny, and easy to speak with casually. I never thought my supervisor would have an appreciation for history, Monty Python, and even Sid Meier's Civilization!

All of my coworkers over the years in the Lee lab were also very helpful in creating a positive and enjoyable work environment. I'm grateful to all the other graduate students, postdoctoral fellows, summer students, and technicians who I have worked with over the past five years. In particular I would like to thank Shaunavin Labiuk (and later Dr. Shaunavin Labiuk), Dr. Palok Aich, Ryan Skinner, Dr. Shawn Wettig, Grant Bare, Michael Dinsmore, Angela Brown, and Dr. Todd Sutherland for their discussions about the sometimes-confusing behaviour of M-DNA.

All of the surface plasmon resonance and calorimetry work done on machines wned an operated by the Saskacthewan Structural Sciences Centre. The manager of the centre, Dr. Rammaswami Sammynaiken, and the biophysics research officer, Jason Maley, were both of enormous assistance and were willing to go to great lengths to help me with my work. I am not sure how many extra hours Jason worked because of my project, and how many IFC cartridges I clogged up, but I am very grateful for his help and patience.

I would also like to thank the Department of Biochemistry, the College of Medicine, Dr. Jeremy Lee, and NSERC for the financial support they all provided me with during my studies. I also appreciated the opportunity to work as a teaching assistant and lab marker for the Biochemistry 310 class. The funding provided by these sources was very helpful.

I also owe much gratitude to my parents for their support, help, and understanding. Thanks to Christopher and Kimberly, my siblings, and sometimes roommates, for maintaining the condo when my only activity besides sleeping was running SPR experiments. Thanks also to my co-worker and beautiful girlfriend Alina for pushing me to finish on time and giving me a stronger desire to work; that and making me happier than I ever have been before. I love you all.

Finally I would like to thank my friends. You know who you are. Everyone who I've been to Ness Creek with, played paintball with, and otherwise "wasted time" with. Good luck to you all, you're very important to me. There are also some people who will never know who I am but who helped me to work hard and enjoy doing it: Pink Floyd, Radiohead, Ween, Trey Parker, and Matt Stone.

Dedication

This thesis is dedicated to Alina, to my parents, Derek and Barbara Wood, and to my siblings, Janice, Christopher, and Kimberly. Thank you all for your support and love. To Alina, your presence in my life has been immeasurably positive and enriching. I love you. To my parents, I hope to give back some of what you have given me, sooner and not later. To Christopher and Kimberly, may you both be successful in the lives you choose. To Janice, rest in peace.

Table of Contents **Page**

Permission to Use **i**

Abstract **ii**

Published Works **iv**

Acknowledgements **v**

Dedication **vii**

Table of Contents **viii**

List of Tables **xiii**

List of Figures **xiv**

List of Abbreviations **xvii**

1.0 Introduction 1

1.1 DNA structure 1

1.1.1 Subunits of DNA 1

1.1.2 Hybridization and Denaturation of DNA 4

1.2 DNA-Metal Ion Interactions 12

1.2.1 Interaction Sites on DNA and their effects on Duplex Stability 13

1.2.2 Induction of Conformations 16

1.2.2.1 A-DNA 17

1.2.2.2 Z-DNA 18

1.2.2.3 Triplex DNA 22

1.2.2.4 Quadruplex DNA 28

1.2.2.5 M-DNA 34

1.2.2.5.1 pH-Dependent Formation 34

1.2.2.5.2 Electron Transfer properties of M-DNA 38

1.3 Measuring M-DNA Formation 39

1.3.1 Fluorescence Experiments 40

1.3.1.1 Ethidium Bromide based assays 40

1.3.1.2 Quenching of Fluorophore-labelled DNA 44

1.3.2 Isothermal Titration Calorimetry 46

1.3.3 Surface Plasmon Resonance 47

1.3.3.1 Detection of Macromolecular Interactions 52

1.3.3.2 Detection of Conformational Changes 55

1.4 Nucleic Acid Immunogenicity 56

1.4.1 Antibodies Specific for DNA 56

1.4.2 Antibodies Specific for particular DNA conformations or Sequences 58

1.5 Objectives 59

2.0 Materials and Methods 61

2.1 Reagents and Equipment 61

2.1.1 Preparation of Divalent Metal Ion Solutions 63

2.1.2 Purification of Ethylenediamine 64

2.1.3 Determination of Thymidine Analogue pK_as 64

2.2 Nucleic Acids 65

2.2.1 Genomic DNA 65

2.2.2 Production of Nucleic Acids by PCR 65

2.2.2.1 DNA containing Standard Bases 66

2.2.2.2 DNA containing Modified Bases 67

2.2.3 Repeating Sequence Nucleic Acids 67

2.2.4 Oligonucleotides 68

2.3 Ethidium Fluorescence Assay 68

2.3.1 Preparation of Nucleic Acids 69

2.3.2 Detection of M-DNA formation with Zn^{2+}, Ni^{2+}, and Co^{2+} 69

2.3.3 Slow Reversion of Ni(II) M-DNA 70

2.3.4 Effect of DNA Concentration on M-DNA Formation 71

2.3.5 Detection of Zn(II) M-DNA formation in 54% GC double-stranded DNA containing modified bases and repetitive sequence double-stranded DNA 71

2.3.6 Variable Temperature Ethidium Fluorescence Assay 72

2.4 Isothermal Titration Calorimetry 73

2.4.1 Preparation of Nucleic Acids 73

2.4.2 Detection of DNA-Metal Interactions 73

2.5 Surface Plasmon Resonance 74

2.5.1 Preparation of Nucleic Acids 74

2.5.2 Preparation of Surface 74

2.5.3 Detection of DNA-Metal Interactions 76

2.5.3.1 BIAcore Maintenance 77

2.5.4 Estimation of the SPR Response due to Increased Mass 77
2.6 Fluorescence Quenching of Fluorophore-labelled DNA 78
2.6.1 Preparation of Nucleic Acids 79
2.6.2 Quenching Studies 79
2.7 Production of Antibodies Specific for M-DNA 80
2.7.1 Preparation of Nucleic Acids 80
2.7.2 Immunization of Mice 80
2.7.3 Solid Phase Radioimmuno Assay 81
2.7.4 Surface Plasmon Resonance 82
3.0 Results 83
3.1 Preparation of M-DNA-specific Antibodies 83
3.1.1 Solid Phase Radioimmuno Assay 83
3.1.2 Surface Plasmon Resonance 84
3.1.3 Conclusions on Production of M-DNA-Specific Antibodies 90
3.2 Ethidium Bromide Based Assays 91
3.2.1 Formation and Stability of Zn(II), Ni(II), and Co(II) M-DNA 92
3.2.2 Slow Reversion of Ni(II) M-DNA 95
3.2.3 Effect of DNA Concentration on M-DNA Formation 96
3.2.4 Zn(II) M-DNA Formation in Base-Substituted or Repetetive Sequence DNA 99
3.2.5 Effect of Temperature on M-DNA Formation 104
3.3 Isothermal Titration Calorimetry 105
3.4 Surface Plasmon Resonance 108

3.4.1 Surface Preparation 109

3.4.2 Metal Ion-DNA Interactions 112

3.4.2.1 50% GC Double-Stranded DNA 117

3.4.2.2 50% GC Single-Stranded DNA 124

3.4.2.3 Single-Stranded Homopolymers 129

3.4.3 Low pH M-DNA formation 140

3.4.3.1 5-Fluorouracil-substituted Double-Stranded DNA. 140

3.5 Quenching of fluorophore-labeled DNA at Low pH 143

4.0 Discussion 151

4.1 Ethidium Bromide Based Assay 151

4.2 Isothermal Titration Calorimetry 156

4.3 Surface Plasmon Resonance 159

4.4 Quenching of Fluorophore-labeled DNA 169

4.5 Implications for data on M-DNA model 173

4.5.1 Support for the Structural Model 173

4.5.2 Differences between Zn(II) and Ni(II) M-DNA 176

4.5.3 Evidence Against Denaturation 177

4.6 Summary 179

4.7 Future Directions 181

5.0 References 182

List of Tables

Table		Page
2.1	Reagents and Equipment.	61
3.1	The Effect of Sequence and Base Substitutions on the Formation and Stability of M-DNA Measured by the EtBr Assay.	103
3.2	Predicted SPR Responses Due to Mass Change for Each DNA Sequence.	114

List of Figures

Figure		Page
1.1	Structures of Purine, Pyrimidine, and the Bases Found in DNA.	2
1.2	Structure of 2'-deoxyribose and Diagram of Sugar Puckers.	5
1.3	*Anti* and *syn* Conformers of Nucleosides.	6
1.4	A dATCG Four-base Tetramer.	7
1.5	Structures of Modified Bases Relevant to this Study.	8
1.6	Watson-Crick Base Pairing.	10
1.7	Hydrogen-Bonding Patterns in Triplexes.	24
1.8	Schematics of Intramolecular Triplexes.	27
1.9	Hydrogen-Bonding Patterns in Quadruplexes.	31
1.10	Schematics of Different Quadruplex Arrangements.	32
1.11	The Proposed Structure of M-DNA.	37
1.12	The Structure of Ethidium Bromide and its Interaction with DNA.	42
1.13	The Kretschmann Configuration for Detection of SPR.	49
1.14	SPR Spectra.	50
3.1	SPRIA Results for Mice Immunized with F^5U- or I-substituted DNA.	85
3.2	SPRIA Results for Mice Immunized with F^5U-Substituted DNA and a Control SPRIA with Jel 274.	86
3.3	SPRIA Results for Mice Immunized with F^5U-Substituted DNA and Control SPRIAs with various Antibodies.	87
3.4	SPR-based Immunoassay Results with Zn(II) M-DNA.	88

3.5	SPR-based Immunoassay Results with Ni(II) M-DNA.	89
3.6	Formation of Zn(II), Ni(II), and Co(II) M-DNA Measured by the EtBr Assay.	94
3.7	Slow Reversion of Ni(II) M-DNA Measured by the EtBr Assay.	97
3.8	The Effect of DNA Concentration on M-DNA Formation Measured by the EtBr Assay.	98
3.9	The Effect of DNA Sequence and Base Substitutions on M-DNA Formation Measured by the EtBr Assay.	101
3.10	The Effect of Temperature on M-DNA Formation Measured by the EtBr Assay.	106
3.11	M-DNA Formation Measured by ITC.	107
3.12	Preparation of the dsCTL Surface for SPR Studies.	111
3.13	Examples of all Events Studied by SPR.	115
3.14	Exposure of dsCTL to 0.20 mM of all Metal Ions.	118
3.15	Repeated Exposure of dsCTL to Cd^{2+}.	120
3.16	Exposure of dsCTL to Zn^{2+}.	121
3.17	Exposure of dsCTL to Ni^{2+}.	123
3.18	Relationship Between SPR Response and Amount of dsCTL Immobilized	125
3.19	Exposure of btn-CTL-2 to 0.20 mM of all Metal Ions.	126
3.20	Exposure of btn-CTL-2 to Zn^{2+}.	127
3.21	Exposure of btn-CTL-2 to Ni^{2+}.	128
3.22	Exposure of T30 to 0.20 mM of all Metal Ions.	131
3.23	Exposure of T30 to Zn^{2+}.	132
3.24	Exposure of T30 to Ni^{2+}.	133
3.25	Exposure of C30 to 0.20 mM of all Metal Ions.	134

3.26 Exposure of C30 to Zn^{2+}. 135

3.27 Exposure of C30 to Ni^{2+}. 136

3.28 Exposure of A30 to 0.20 mM of all Metal Ions. 137

3.29 Exposure of A30 to Zn^{2+}. 138

3.30 Exposure of A30 to Ni^{2+}. 139

3.31 Exposure of dsCTL to Zn^{2+}, Ni^{2+}, and Mg^{2+} at all pHs. 141

3.32 Exposure of dsCTL with F^5U Subtitutions to Zn^{2+} and Ni^{2+} at all pHs. 142

3.33 Quenching of Fl/QSY7-labeled DNA by Zn^{2+} at pHs 6.5-8.5. 144

3.34 Quenching of Fl/QSY7-labeled DNA by Cd^{2+} or Mg^{2+} at pHs 6.5-8.5. 145

3.35 Quenching of Fl/QSY7-labeled DNA by different Zn^{2+} Solutions at pH 6.5. 147

3.36 The Effect of Each $ZnCl_2$ on the Final pH of 10 mM MES pH 6.5. 148

3.37 The Concentration of Zn^{2+} at 50% Quenching vs pH. 149

4.1 Bar Graph Summary of SPR Responses at 0.20 mM Metal Ion. 163

4.2 Peak SPR Responses of dsCTL to each Metal Ion at pHs 6.5 and 7.5. 167

4.3 Peak SPR Responses of dsCTL to Zn^{2+} or Ni^{2+} with Mg^{2+} Signals Subtracted at pHs 6.5 and 7.5. 168

4.4 The Relationship Between pK_a and the pH at which 50% M-DNA Formation Occurs in the EtBr assay. 175

List of Abbreviations

A_{260}	Absorbance at 260 nm
A	Adenine
m^6A	6-methyladenine
n^2A	Diaminopurine
z^7A	7-deazaadenine
ATR	Attenuated total reflection
bp	Base-pair
btn	Biotin
C	Cytosine
CD	Circular dichroism
CHES	2-[*N*-cyclohexylamino]ethanesulfonic acid
CMD	Carboxymethyldextran
CT	Calf thymus
Br^5C	5-bromocytosine
m^5C	5-methylcytosine
d	2'-deoxy suffix
dd	Double-distilled prefix
d_d	Thickness of a dielectric
DNA	2'-deoxyribonucleic acid
ds	Double-stranded suffix
dNTP	2'-deoxynucleotide-5'-triphosphate
E. coli	*Escherichia coli*
ED	Ethylenediamine
EDTA	Ethylenediaminetetraacetic acid
EtBr	Ethidium bromide
Fl	Fluorescein
FRET	Fluorescence resonance energy transfer
ΔG	Change in Gibb's free energy
G	Guanine
Br^8G	8-bromoguanine
m^8G	8-methylguanine
z^7G	7-deazaguanine
ΔH	Change in enthalpy
I	Hypoxnathine
IFC	Integrated microfluidics cartridge
IR	Infrared
MAb	monoclonal antibody
MES	*N*-(morpholino)ethanesulfonic acid
MOPS	3-(*N*-Morpholino)propanesulfonic acid
n_d	Refractive index of a dielectric layer
n_p	Refractive index of a prism
PCR	Polymerase chain reaction
pu•pu•py	Purine-purine-pyrimidine triplex

py•pu•py	Pyrimidine-purine-pyrimidine triplex
QEFB	Quantitation ethidium fluorescence buffer
RII	Refractive index increment
RNA	Ribonucleic acid
RU	Response unit
SASP	Small acid-soluble protein
SLE	Systemic lupus erythematosus
SPR	Surface plasmon resonance
T	Thymidine
ΔS	Change in entropy
s^2T	2-thiothymidine
s^4T	4-thiothymidine
TBS	Tris-buffered saline
T_m	Melting temperature
TRIS	Tris(hydroxymethyl)aminomethane
UV	Ultraviolet
U	Uracil
Br^5U	5-bromouracil
F^5U	5-fluorouracil
WC	Watson-Crick
Zn-EFB	Zn-ethidium fluorescence buffer

1.0 Introduction

1.1 DNA Structure

There are two types of nucleic acids found in nature: DNA and RNA. Together, they are responsible for the transmission and expression of genetic information. The characterization of these polymers and their subunits is the cornerstone of molecular biology and one of the most important achievements of modern chemistry. This section will outline the important structural features of DNA and its subunits that are relevant to this study.

1.1.1 Subunits of DNA

The basic monomers of DNA and RNA are called nucleotides. These in turn consist of three subunits: a phosphate, a sugar, and a base. There are three bases common to DNA and RNA: adenine (A), guanine (G), and cytosine (C). In addition, uracil (U) is found primarily in RNA while its 5-methyl analogue, thymine (T) is found exclusively in DNA. Adenine and guanine are purine bases whereas cytosine, thymine, and uracil are pyrimidines. All the bases are aromatic and planar, forming rigid structures. The aromatic nature of the bases gives them substantial extinction coefficients in the ultraviolet (UV) range and the absorbance of solutions of DNA and RNA at 260 nm (A_{260}) allows easy quantification of the concentration of monomers in solution. These bases along with the structures of purine and pyrimidine are depicted in figure 1.1.

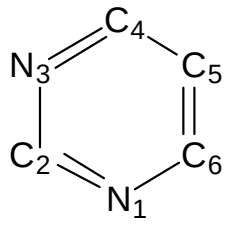

Pyrimidine

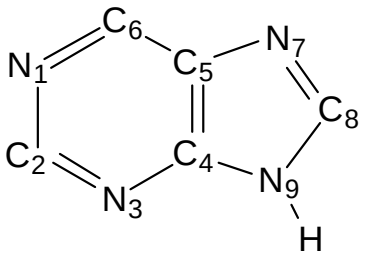

Purine

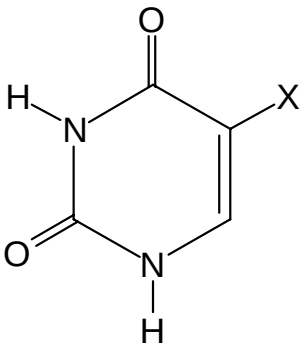

Thymine (X = CH_3)
Uracil (X = H)

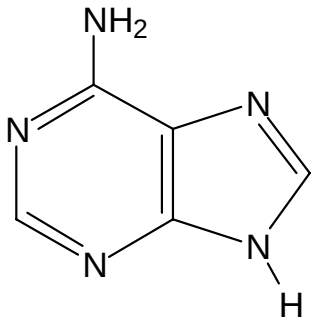

Adenine

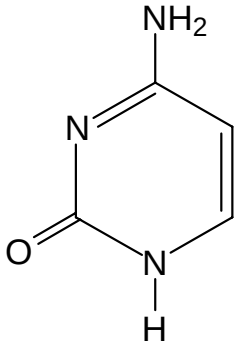

Cytosine

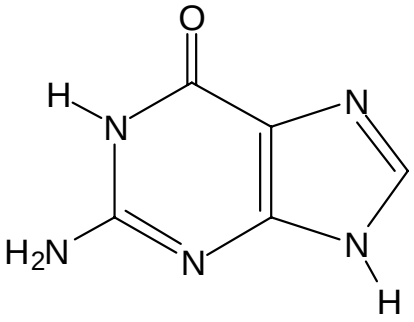

Guanine

Figure 1.1: The ring structures of purine and pyrimidine, the parent molecules of the five bases found in DNA and RNA, as well as the five bases found in DNA and/or RNA: A, C, G, T, and U. The numbering schemes depicted on purine and pyrimidine apply to the five bases as well as their analogues and these positions will be referred to throughout the text.

The combination of a base and 5C furan sugar is referred to as a nucleoside. The base is joined to C1' of the sugar by N1 of pyrimidines and N9 of purines. For clarity, positions on bases are referred to simply as the number of the atom while those on the furan sugar are numbered with a prime symbol. The sugar present in DNA is β-D-2'-deoxyribose and the subunits are referred to as 2'-deoxyribonucleotides. The sugar present in RNA is β-D-ribose and its subunits are in turn called ribonucleotides. Ribonucleosides of the respective bases are called adenosine, guanosine, cytidine, and uridine while those of deoxyribonucleosides simply have deoxy- added as a suffix and include deoxythymidine. Unlike those in the bases, the bonds in the sugar ring display conformational lability. There are two major conformations the furan ring can adopt in DNA and RNA: the C2' *endo* and C3' *endo* conformations. Dubbed "sugar puckers", these are defined by which carbon (C3' or C2') is on the same side of the C4'-O-C1' plane as the base and C5', as depicted for 2'-deoxyribose in figure 1.2. Another conformationally labile portion of nucleosides is the bond between the base and sugar. Thus *syn* or *anti* conformers are illustrated for guanosine and cytidine in figure 1.3. The *anti* conformer is generally preferred due to fewer steric interactions. The rotation about the sugar-base bond and the sugar pucker differ depending on the specific conformation of double-stranded DNA (dsDNA) or double-stranded RNA (dsRNA) present.

A nucleotide consists of a nucleoside and a 5'-phosphate. Ribonucleotides containing each base referred to as adenylic acid, guanylic acid, cytidylic acid, and uridylic acid. From this point forward, the ribonucleotides will be referred to as rA, rG, rC, and rU, while the 2'-deoxyribonucleotides will be referred to as dA, dG, dC, dT, and dU (Although dU is not typically found in DNA in nature, it can be incorporated

artificially). A polymer of 2'-deoxyribonucleotides is called DNA while a polymer of ribonucleotides is called RNA. In either case, the 5' phosphate group of the first monomer is joined to the 3'OH group of the following monomer. Thus, the sequences are listed from the 5' to the 3' end of the polynucleotide chain. A four base DNA oligonucleotide of the sequence dATGC with each base in the *anti* conformation is pictured in figure 1.4.

Although the five bases detailed above are those predominantly found in DNA and RNA in nature, there are many known variations on these structures. Some are present in nature while others are purely synthetic. Those relevant to this thesis are diaminopurine (n^2A), 6-methyladenine (m^6A), 7-deazaadenine (z^7A), 7-deazaguanine (z^7G), 8-bromoguanine (Br^8G), 8-methylguanine (m^8G), 5-bromocytosine (Br^5C), 5-methylcytosine (m^5C), 2-thiothymidine (s^2T), 4-thiothymidine (s^4T), 5-bromouracil (Br^5U), 5-fluorouracil (F^5U), and hypoxanthine (I). The structures of all these modified bases are presented in figure 1.5.

1.1.2 Hybridization and Denaturation of DNA

The vast majority of DNA in the cell is double-stranded, and most single-stranded segments of DNA are present only transiently within larger sequences of dsDNA. The specific interaction of two DNA strands is referred to as hybridization, while the reverse process, the separation of dsDNA into single strands, is referred to as denaturation.

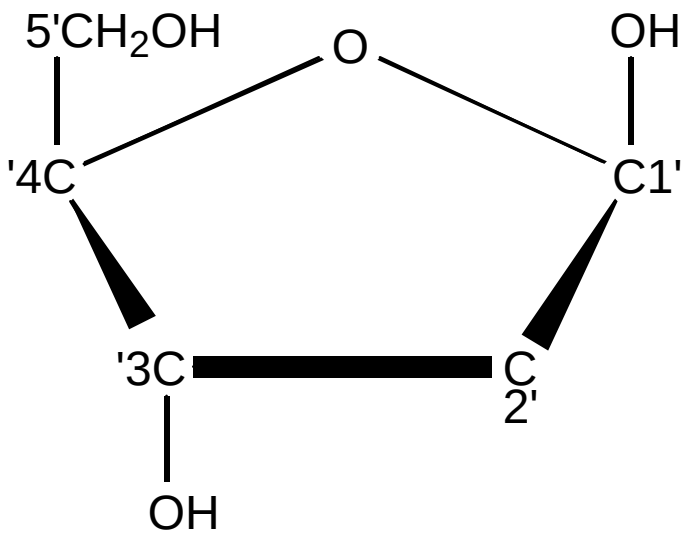

2'-deoxyribose

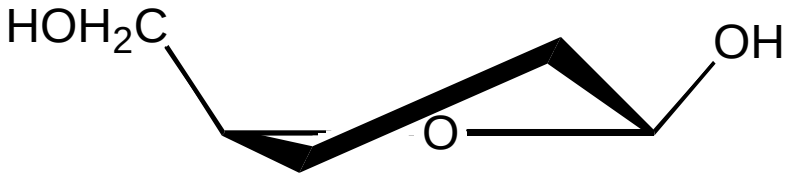

C2' *endo*

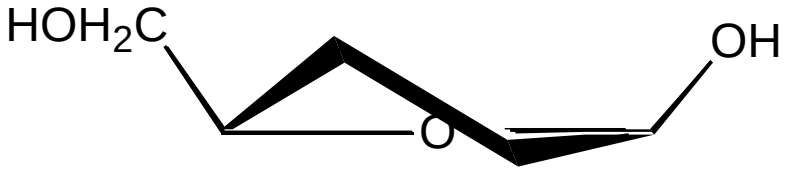

C3' *endo*

Figure 1.2: The numbered structure of 2'-deoxyribose, the sugar found in DNA, and the two possible sugar puckers it can adopt, C2'-*endo*, which is typically found in B-DNA, and C3'-*endo*, which is typically found in A-DNA or dsRNA. In either type of polynucleotide, the bases are attached to C1' by N1 of pyrimidine bases or N9 of purine bases.

2'-deoxyguanosine

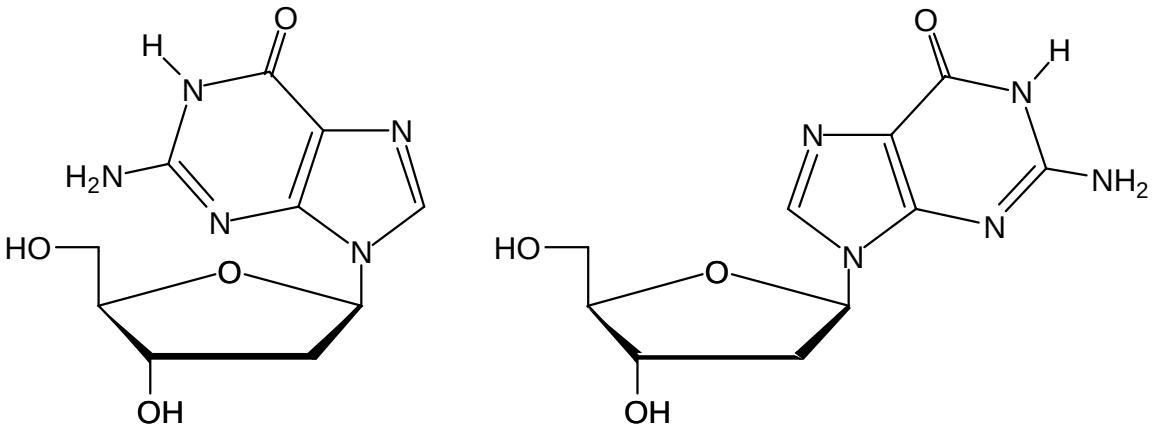

syn *anti*

2'-deoxycytidine

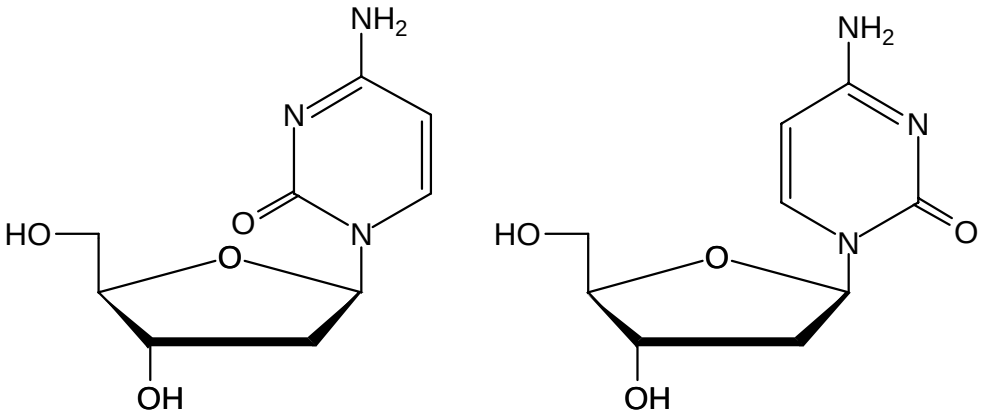

syn *anti*

Figure 1.3: The two possible orientations of the bases of 2'-deoxyguanosine and 2'-deoxycytosine about their bonds between C1' and N9 or N1, respectively. The *syn* and *anti* conformations are named as to whether the bases are arranged with a higher or lower degree of steric interactions with the 2'-deoxyribose sugar, respectively.

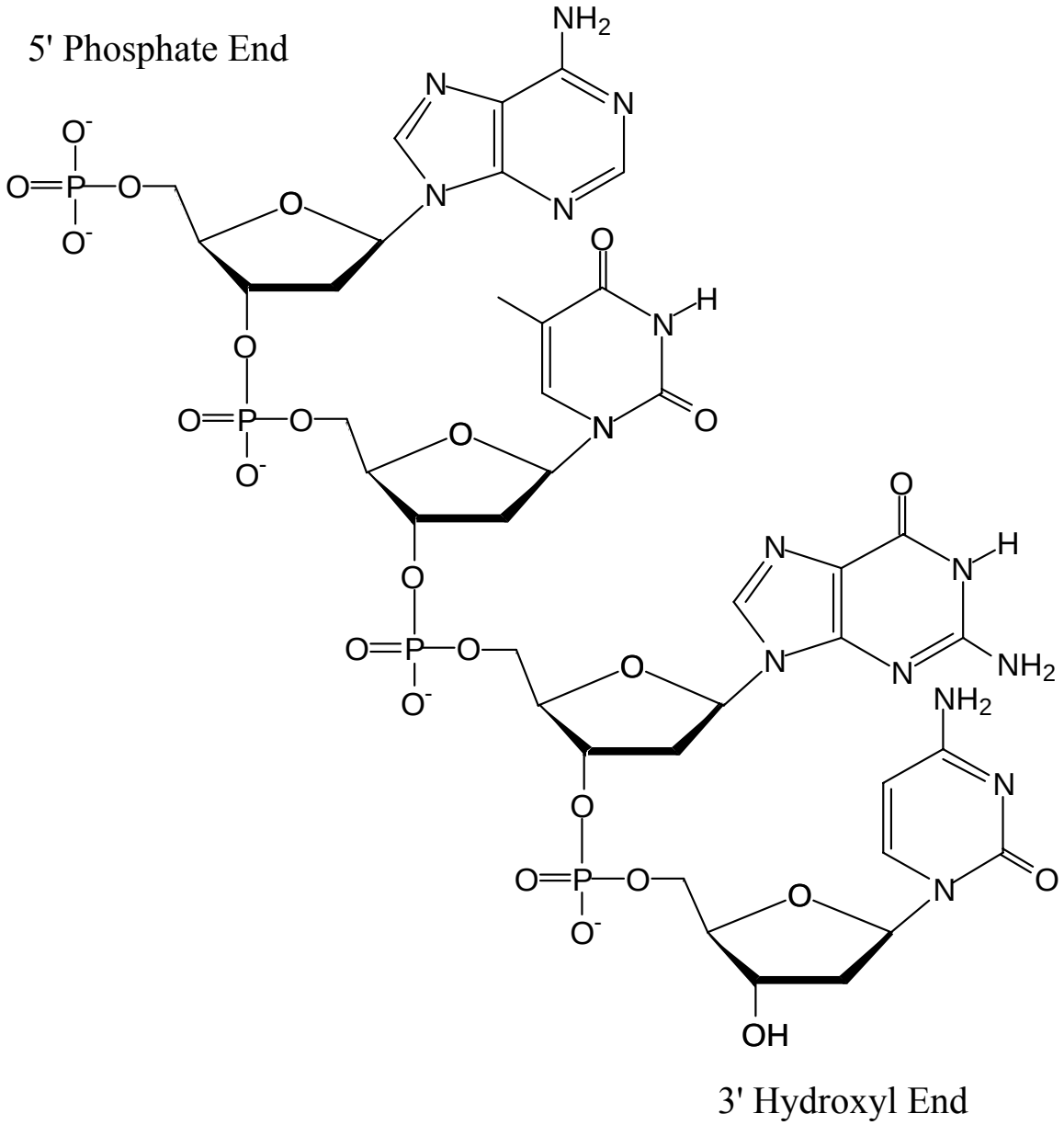

Figure 1.4: A tetranucleotide with the sequence dATGC. The bases are named from the 5' phosphate end of the polymer to the 3' hydroxyl end.

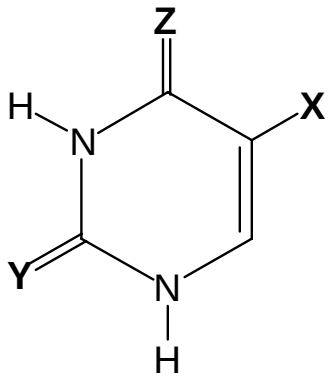

Base	X	Y	Z
T	CH_3	O	O
U	H	O	O
Br^5U	Br	O	O
F^5U	F	O	O
s^2T	CH_3	S	O
s^4T	CH_3	O	S

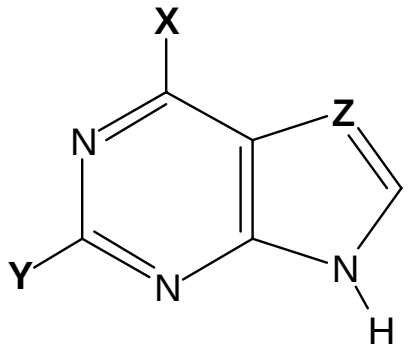

Base	X	Y	Z
A	NH_2	H	N
m^6A	$NHCH_3$	H	N
n^2A	NH_2	NH_2	N
z^7A	NH_2	H	CH

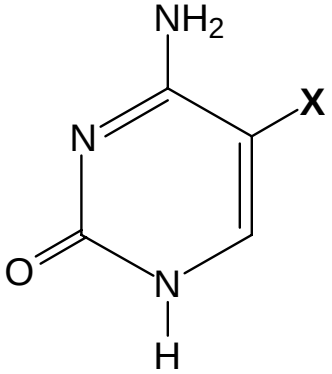

Base	X
C	H
m^5C	CH_3
Br^5C	Br

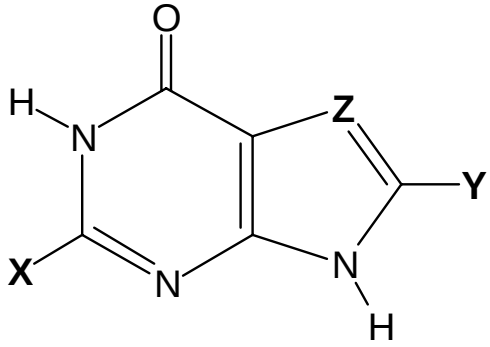

Base	X	Y	Z
G	NH_2	H	N
I	H	H	N
Br^8G	NH_2	Br	N
m^8G	NH_2	CH_3	N
z^7G	NH_2	H	CH

Figure 1.5: The modified bases referred to and in some cases used in this study. For reference, the standard bases are also included in this figure.

Hybridization of two strands is specific and mediated by the formation of Watson-Crick (WC) base pairs. In this base-pairing scheme, first proposed by Watson and Crick (Watson and Crick, 1953), G pairs with C and A pairs with T in anti-parallel strands, meaning that the individual strands run 3'-5' in opposite directions. From this point forward, WC duplexes will be described using a "•" symbol to denote a base pair. Thus, a sequence consisting exclusively of dC on one strand and dG on the complimentary strand would be called $d(C)_n$•$d(G)_n$ while a sequence having repeats of dTG on one strand and dCA on the other would be called $d(TG)_n$•$d(CA)_n$. A sequence having alternating dG and dC on each strand would simply be called $d(GC)_n$ since it is self-complementary.

Another base-pairing scheme, observed by Hoogsteen between 9-methyladenine and 1-methylthymine (Hoogsteen, 1963), is present in folded tRNA molecules as well as in triplexes (which will be discussed in more detail in section 1.2.2.3), but not in normal dsDNA. The WC base pairs are shown in figure 1.6. The WC base-pairing scheme was in agreement with observations that DNA samples contained equivalent amounts of A to T as well as G to C and that the ratio of A:G was equal to that of T:C (Chargaff *et al.*, 1951). WC base pairing allows accurate DNA replication to take place by allowing one strand to act as a template for the other. The specificity of WC base pairing is due to the formation of intermolecular hydrogen bonds between the two DNA strands. There are three such bonds in G•C base-pairs (bps; singular bp) and two in A•T bps. This phenomenon imparts specificity but little stability to the dsDNA structure, as there would be just as many hydrogen bonds present in denatured DNA in contact with solvent. The stability of dsDNA is due largely to the presence of stacking interactions.

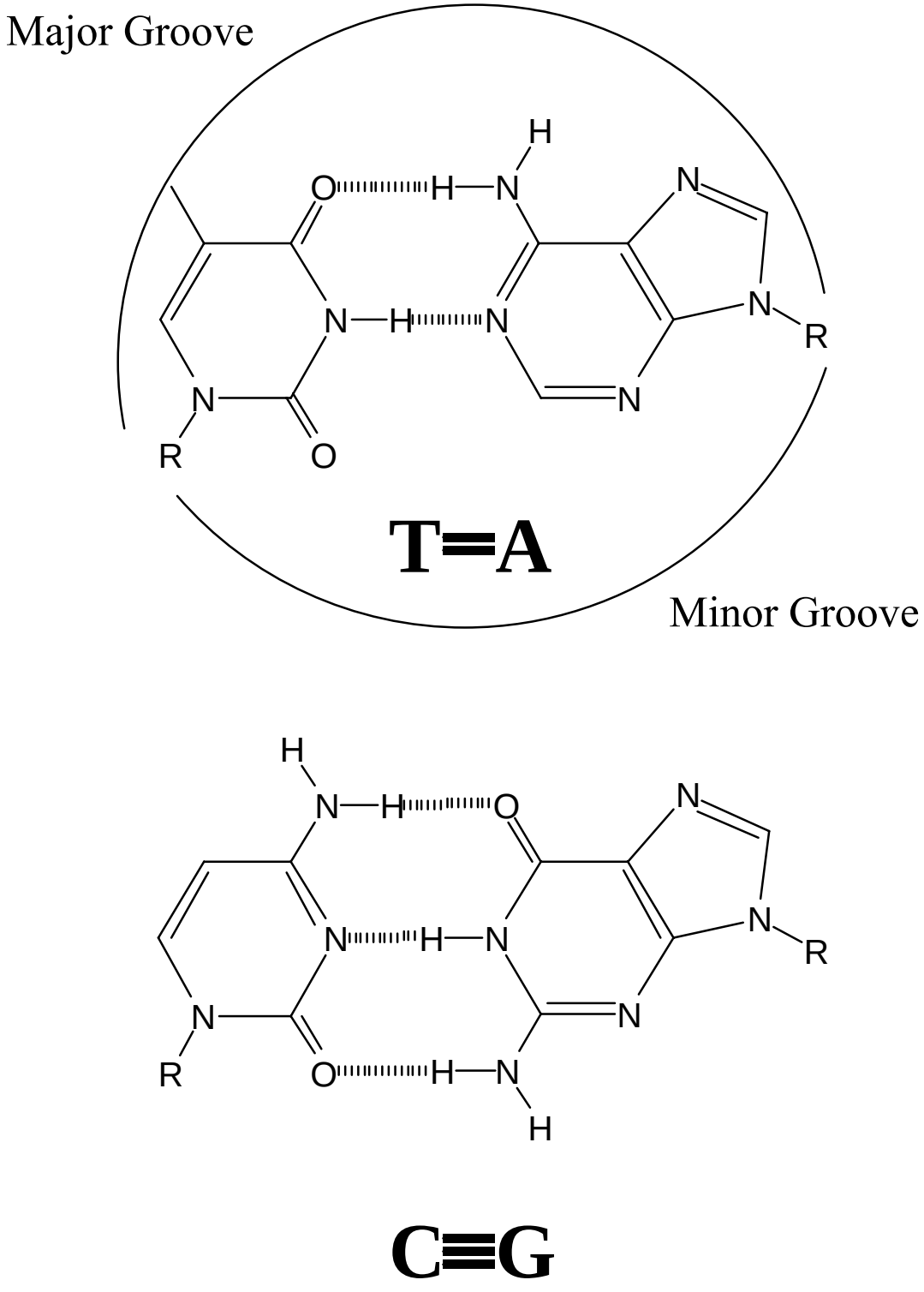

Figure 1.6: The standard WC base pairing schemes for A•T and G•C base pairs. The major and minor grooves of the DNA are indicated for the A•T base pair and apply analogously to the G•C base pairs. This pairing scheme and the indicated grooves apply equally to RNA as to DNA with the exception of U replacing T in RNA.

Once hybridized, the typical structure of dsDNA, referred to as B-DNA, is an anti-parallel right-handed helix. B-DNA has a diameter of ~20 Å and 10.4 bps per turn, with an average rise of 3.4 Å per bp. The helix has a major groove and a narrower minor groove, both deep, which are defined relative to the base pairs as pictured in figure 1.6. The sugar pucker for all residues is C2'-*endo* and all bases are in the *anti* configuration. The bases are almost planar, being tilted on average 6º relative to the helical axis.

Hydrophobic Van der Waals interactions play a large role in determining the stability of a double helix. The planar aromatic bases interact through their π orbitals in what are referred to as stacking interactions. Individual purine nucleoside and mononucleotide molecules show stronger self-associative stacking interactions when a lower degree of phosphorylation and therefore a lower charge is present on the molecule (Yamaguchi *et al.*, 1996). This is due to lowered negative charge density on the molecules, which acts as a repulsive force. This charge-induced repulsion also affects the stability of dsDNA, which cannot remain hybridized without some degree of charge neutralization on the phosphate backbone. In the case of mononucleotides as well as dsDNA, the presence of metal ions shields the negative charge of the phosphates allowing closer association of the bases and hence stronger stacking interactions to occur. This will be covered in more detail in section 1.2.1. Stacking interactions also play a role in intermolecular contacts between proteins and DNA, such as recognition of G residues on RNA by ribonuclease T1 mediated through interaction of a Tyr side chain with the base (Yamaguchi *et al.*, 1996).

Denaturation of DNA occurs at elevated temperatures. Close interaction between base pairs allows a stronger overlap between their π orbitals which in turn results in a

smaller difference in the energy levels for π-π* transitions and hence a weaker absorption relative to isolated bases in single-stranded DNA (ssDNA) (Cowan, 1997). Thus, when DNA undergoes a transition from a double- to single-stranded form, there is an associated hyperchromicity of roughly 1.4 fold. Since denaturation is a cooperative process, there is a well-defined temperature at which the transition occurs, and the midpoint of this transition (T_m) is considered to be the temperature at which denaturation occurs. The T_m is influenced by the ratio of G•C to A•T base pairs. Since G•C base pairs have stronger stacking interactions than A•T base pairs, a higher G•C content will allow a duplex to remain hybridized at higher temperatures. This was quantified in a study of 41 purified genomic DNA samples of varying base composition and led to the conclusion that at 200 mM Na^+ at pH 7.0 ± 0.3, a linear relationship between T_m and G•C content existed such that $T_M = 69.3 + 0.41$ (%G•C) (Marmur and Doty, 1962). The fact that this was done with genomic data, representing an essentially random sequence, ruled out sequence effects, which have a large effect on the T_m, as illustrated in studies on repeating sequence DNA (Saenger, 1984).

1.2 DNA-Metal Ion Interactions

The structures of all nucleotides provide chemically distinct interaction sites for different types of metal cations. Interactions between DNA and metal ions play a crucial role in DNA function *in vivo* and the stability and structure of DNA *in vitro*. This section will summarize some of the more common and important interactions and how they play a role in determining the stability and tertiary structure of DNA helices.

Interactions between DNA and metal ions are also integral to M-DNA formation and, thus, will be discussed in detail.

1.2.1 Interaction Sites on DNA and their Effects on Duplex Stability

There are four chemically-distinct potential interaction sites on nucleic acids: the phosphate backbone, the cyclic base nitrogens, the exocyclic keto groups and the sugar hydroxyls. Each of these sites acts as a ligand of varying strength for different metal ions and these interactions play an integral role in the stability and shape of dsDNA.

Metal ions, which act as Lewis acids towards the ligands present on polynucleotides, are classified as being either hard or soft acids based on their affinities for different types of ligands. Soft ions are more polarizable than hard ions and interactions between soft acids and soft ligands have more covalent character than those between hard acids and hard ligands, which are primarily electrostatic in nature. Examples of hard ions often studied in conjunction with nucleic acids are Li^{+}, Na^{+}, K^{+}, Mg^{+2}, Ca^{2+}, Mn^{2+}, Ba^{2+} and Co^{3+} while soft ions are Cu^{+}, Ag^{+}, Hg^{+}, Hg^{2+} Cd^{+2}, and Pt^{2+}. Many transition metals are intermediate between hard and soft, such as Ru^{+}, Co^{2+}, Ni^{2+}, Cu^{2+}, and Zn^{2+} (Cowan, 1997).

Of the different sites available on dsDNA, sugar hydroxyl groups are bound almost exclusively by hard ions and will not be discussed further. The keto groups of pyrimidines can participate in direct metal ion interactions as can those on position 6 of G. The latter case is unlikely since most metal ions would preferentially interact with N7 and coordination to both of these sites is geometrically unlikely. Despite the fact that they

are hard ligands, phosphate groups are typically bound non-specifically by all metal ions due to their negative charge, which allows ionic interactions to take place (Saenger, 1984). Exocyclic amine groups are present on position 4 of C, 6 of A, and 2 of G, but do not participate in metal ion binding with any type of ion. This is due to partial double bonding character in the C-N bond and consequently electron delocalization into the ring, which imparts partial positive charge to the amine group that is repulsive to cations (Martin and Yitbarek, 1979).

The most intricate interaction patterns between metal ions and DNA are with the heterocyclic ring nitrogens. Since the ring nitrogens are potential protonation sites, their acidity is highly relevant to the binding of metal ions. The pK_a values for the ring nitrogens of nucleotide monophosphates are given in parentheses in the following series:

T3 (9.9) > G1 (9.4) ~ U3 (9.3) >> C3 (4.4) > A1 (3.9) > G7 (2.5) >> A7

For 9-substituted purines, N3 has a pK_a at least four units lower than N7 and therefore is unlikely to bind protons or metal ions under most circumstances. The preference for metal ions to interact with these sites follows the pK_a pattern closely, but not precisely. Despite their low pK_a values, there is a high propensity for metals to interact preferentially with N7 of purines. Thus, the interaction order for metal ions at elevated pH is likely to be as follows:

T3 > G1 ~ U3 > G7 > A7 > C3 > A1

As is apparent from the pK_a series, there are protons present on the first three positions at neutral pH. Thus, the pattern of ligation towards metal ions at netural pH is likely to be:

G7 > A7 > C3 > A1 > G1 ~ U3 > T3

Therefore, pH is important for determining the interaction sites of metal ions with DNA (Martin and Yitbarek, 1979; Martin, 1996).

As described in section 1.1.2, the stacking interactions between purine nucleosides or mononucleotides are stronger when there is less negative charge present on the molecule. The presence of Mg^{2+}, Zn^{2+}, or Cd^{2+} ions has been found to increase the strength of the interaction between the molecules to a higher degree than would be expected simply due to neutralization of charge. Thus, $Mg(ATP)^{2-}$ and $Zn(ATP)^{2-}$ display 2 and 5 fold stronger stacking interactions, respectively, than AMP^{2-}. This difference is due to the fact that the metal ion provides an intermolecular bridge between the two molecules. Further, the higher degree of stabilization imparted by the transition metals is due to the fact that they interact with N7 of the adenine ring as well as with the phosphate group (Yamaguchi *et al.*, 1996).

In dsDNA, the trend is not as simple as in nucleotide monophosphates. The duplex is still stabilized by stacking interactions as described in section 1.1.2, and metal ions, particularly hard ions, still facilitate this interaction by reducing the level of charge repulsion between the phosphate backbones. However, some intermediate and soft divalent ions have a twofold effect on helix stability due to their ability to bind both phosphates and base nitrogens as indicated by T_m measurements with genomic calf thymus (CT) DNA. These ions stabilize the duplex until a threshold is reached (between 0.25 and 1.75 M^{2+}/DNA phosphate depending on the ion) after which they destabilize the DNA and cause denaturation at temperatures lower than in the absence of added divalent ion. It was found that stabilization of the duplex was imparted by $Mg^{2+} > Co^{2+} > Ni^{2+}$ regardless of concentration while denaturation induced by $Cu^{2+} > Cd^{2+} > Zn^{2+} > Mn^{2+}$.

Thus, these metals were classified in order of phosphate vs base binding as such: Mg^{2+} > Co^{2+} > Ni^{2+} > Mn^{2+} > Zn^{2+} > Cd^{2+} > Cu^{2+} (Eichhorn and Shin, 1968). A later study showed that the base binding affinity of Mn^{2+} was more specific for G residues, as increasing G•C content of a sequence allowed for a greater degree of Mn^{2+}-induced lowering of T_m (Anderson *et al.*, 1971). This work was also supported by Raman spectroscopy studies that showed interactions between the above-mentioned transition metals (except Zn^{2+}) and N7 of purine and N3 of pyrimidine rings. These interactions were observed to disrupt stacking interactions and disorder the backbone of B-DNA and paralleled changes associated with thermal denaturation of DNA (Duguid *et al.*, 1993). Various crystal structures have shown N7 coordination to be important in structures of nucleosides, nucleotides, and dinucleotides (Yamaguchi *et al.*, 1996), but a recently solved structure shows that Co^{2+}, Ni^{2+}, and Zn^{2+} only bind terminal N7 positions on the terminal G residues of d(GGCGCC) (Labiuk *et al.*, 2003).

1.2.2 Induction of Specific Conformations

In addition to affecting the stability of dsDNA through interactions on the bases and phosphates, metal ions are capable of inducing major structural rearrangements in these molecules. These changes are often dependent on the identity and concentration of the metal ion, the pH of the medium, and the sequence of and degree of supercoiling in the polynucleotide. Three specific metal ion-induced conformations of dsDNA have been thoroughly characterized and will be reviewed here: Z-DNA, triplex DNA, and

quadruplex DNA. In addition, A-DNA, which is typically present in low humidity conditions, implying a higher ionic strength, is also covered in this section.

1.2.2.1 A-DNA

Early work on DNA structure showed two different conformations of the double helix molecule that shared many characteristics. B-DNA, which has come to be recognized as the typical conformation of dsDNA in biological systems, was the high-humidity form. A-DNA was the low-humidity form (Franklin and Gosling, 1953). Subsequent studies showed that under dehydrating conditions brought on by addition of ethanol, the circular dichroism (CD) spectrum of B-DNA would change which was attributed to formation of A-DNA. The percentage of ethanol necessary to cause this change was reduced in the presence of Na^+ but increased in the presence of Li^+, Cs^+, Mg^{2+}, and Ca^{2+} (Ivanov *et al.*, 1974).

Like B-DNA, A-DNA consists of an anti-parallel duplex of two strands linked by WC base pairs in a right-handed helix. However, the helix is wider and shorter than that observed in B-DNA, with a diameter of ~26 Å and 11 residues per turn with a rise of 2.55 Å per base. Although the bases of A-DNA are in the *anti* conformation relative to their sugar rings like those in B-DNA, the sugar puckers are C3' *endo* rather than C2' *endo* as found in B-DNA. Another dramatic difference between A- and B-DNA is that there is a 20º tilt of the bases relative to the helix axis in A-DNA. In the overall structure of A-DNA, the major groove is narrower and deeper, while the minor groove is wider and shallower (Sinden, 1994).

While dsRNA adopts a conformation similar to A-DNA, the only evidence for actual A-DNA in nature is in complex with small acid soluble protein (SASP) present in the spores of *Bacillus subtilis*. Upon binding CT-DNA *in vitro*, SASP induces a CD-detectable change from B- to A-DNA. The lower humidity of these spores was previously thought to impart UV damage resistance to DNA by sequestering it in the A-conformation and it is thought that binding of the SASP facilitates this conformational change (Mohr *et al.*, 1991). The structure of A-DNA is thought to impart resistance to UV-induced cyclobutane-type thymidine dimers due to the twist of the bases.

1.2.2.2 Z-DNA

While A-DNA is in most respects structurally similar to B-DNA, Z-DNA represents a radical structural departure from standard B-DNA. Z-DNA formation was first observed by CD spectroscopy when the NaCl concentration of a solution of $d(GC)_n$ was raised from 0.2 to 2.5 M or with the addition of 700 mM $MgCl_2$ (Pohl and Jovin, 1972). Following that initial discovery, the crystal structure of Z-DNA, the first crystal structure of a DNA molecule to be solved, revealed a wealth of information about the structure of Z-DNA (Wang *et al.*, 1979).

Like B-DNA, Z-DNA is composed of anti-parallel WC base pairs with a helical tilt relative to the axis of 7º, but the similarity ends there. The most obvious departure from B-DNA structure is that the Z-DNA helix is left-handed rather than right-handed. The alternating $d(GC)_n$ sequence of typical Z-DNA has a dinucleotide repeat unit rather than a mononucleotide repeat as in B-DNA with unusual stacking interactions. The twists

of each base pair relative to the next one in sequence are -9° for dCpG and -51° for dCpG whereas those for B-DNA are +29.8° and +40.0°, respectively. The sugar puckers of G residues are C3' *endo* rather than the C2' *endo* typical of B-DNA and C residues of Z-DNA. These two features, along with the fact that G residues are *syn* relative to the sugar portion of the nucleotide generate the characteristic zig-zag pattern in the phosphate backbone of Z-DNA (Wang *et al.*, 1979).

Other helical parameters of Z-DNA differ from those of B-DNA as well. The minor groove of Z-DNA is deep and narrow compared to that of B-DNA while the major groove is absent altogether. The helix is narrower and longer, having a width of 18 Å and 12 residues per turn with a rise of 3.7 Å per base (Wang *et al.*, 1979). Despite the increased rise per residue the alternating sugar puckers draw the negatively charged phosphate residues of subsequent bases much closer to each other than in B-DNA, explaining the dependence of the conformation on a high ionic strength (Sinden, 1994). Apart from an elevated ionic strength, Z-DNA can be stabilized by covalent modification of bases, supercoiling, and the presence of Z-DNA binding proteins.

The dependence of Z-DNA on ionic strength is not entirely due simply to relaxation of electrostatic interactions between the phosphates. Although all monovalent metal ions stabilize the structure, divalent metal ions have the same effect at lower concentrations, partly owing to their greater ability to shield negative charges (Sinden, 1994). However, early studies showed that whereas $MgCl_2$ allowed Z-DNA formation at 700 mM, less than 5 mM of Co^{2+}, Ni^{2+}, or Mn^{2+} was required to elicit the same response under comparable conditions. Further, when Mg^{2+} was present in 20% ethanol, it had a potency similar to the transition metals (Van De Sande *et al.*, 1988). This effect was

interpreted in the context of increased binding of the transition metals to N sites on the bases and in the case of the ethanol/Mg^{2+} mixture to be due to partial unwinding of the helix by the ethanol, facilitating the change in conformation. A later study using infrared (IR) spectroscopy verified that Co^{2+} and Ni^{2+} were binding more effectively to N7 positions of G residues that stabilized the *syn* conformation required for Z-DNA formation relative to the *anti* conformation of B-DNA. This effect was also observed to increase for Mg^{2+} in the presence of dehydrating agents such as alcohol that allowed better direct coordination of the ion to N7 positions (Taboury *et al.*, 1984).

Co(III)hexamine complexes (Behe and Felsenfeld, 1981; Peck *et al.*, 1982; Stirdivant *et al.*, 1982) and their derivatives (Bauer and Wang, 1997) have been found to be even more potent stabilizers of Z-DNA formation, working in the submillimolar range. X-ray crystallographic studies have shown that the complex binds through its amine groups to O6 and N7 of G residues on the surface of the molecule, as well as to N4 of C residues at sufficiently high concentration (Thiyagarajan *et al.*, 2004). Other studies with complexes of Pt^{4+} and spermidine derivatives, which are potential anti-cancer agents, have shown that they are even more potent Z-DNA stabilizers than Co(III)hexamine. Further, they determined that in the presence of these complexes, Z-DNA was more resistant to ethidium bromide (EtBr)-induced reversion to B-DNA than in the presence of Co(III)hexamine (Qu *et al.*, 2004).

The level of supercoiling present in a DNA molecule also affects the propensity with which it will form Z-DNA. This is due to the fact that Z-DNA formation unwinds the DNA, reducing the number of negative supercoils. Thus, the more negative supercoiling present in a DNA molecule, the larger its propensity to form Z-DNA due to

a more favorable free energy (ΔG) of conversion (Peck *et al.*, 1982; Stirdivant *et al.*, 1982).

Chemical modification of the bases on a Z-DNA forming duplex can also facilitate formation of, as well as stabilize, the Z-DNA conformation. Bromination of 38 % of G residues on C8 and 19% of C residues on C5 locks the molecule in the Z conformation even after removal of high NaCl concentrations by dialysis (Moller *et al.*, 1984). This effect is even stronger if I is substituted for Br (Rich *et al.*, 1984) and methylation of C8 of G residues also favours the Z conformation (Xu *et al.*, 2003). These modifications stabilize Z-DNA by locking G residues in the *syn* conformation, as bulky substituents on C8 prevent its rotation back to *anti* (Rich *et al.*, 1984). Replacement of C residues with m^5C also stabilizes Z-DNA (Behe and Felsenfeld, 1981). This is due to filling of a hydrophobic pocket on the surface of the molecule with the methyl group (Rich *et al.*, 1984).

There is much evidence for Z-DNA formation *in vivo*. The stabilization of Z-DNA under physiological ionic strengths with less supercoiling than nuclear DNA (Peck *et al.*, 1982) as well as its stabilization in m^5C-substituted DNA (Behe and Felsenfeld, 1981) were suggestive of a role for Z-DNA in the cell. Antibodies against Z-DNA have also detected the presence of Z-DNA in the *Drosophila* polytene chromosomes and these antibodies have also been implicated in the pathogenesis of systemic lupus erythematosus (SLE). Sequences favouring Z-DNA formation have also been found in abundance in human chromosome 22 (Rich and Zhang, 2003). It has recently been determined that these sequences are often found in conjunction with promoter binding sites for nuclear factor-I (Champ *et al.*, 2004). The findings resulting from studies using anti-Z-DNA

antibodies must be interpreted with caution however, as it has been found that these proteins can induce the conformation in sequences capable of forming Z-DNA (Lafer *et al.*, 1985). Finally, the helix-turn-helix domain of dsRNA deaminase-1 has been found to bind Z-DNA regions, suggesting that Z-DNA formation may play a role recruiting this enzyme to active sites of transcription (Schade *et al.*, 1999; Schwartz *et al.*, 1999).

1.2.2.3 Triplex DNA

First observed in 1957 (Felsenfeld *et al.*, 1957), triplex polynucleotides, as the name implies, involve coordination of three bases per monomer and are possible in systems with RNA, DNA, or a combination of the two (Frank-Kamenetskii and Mirkin, 1995). Two of the bases are paired in normal WC fashion and run anti-parallel to each other, while the third base is paired to the purine of the WC duplex in a Hoogsteen or reverse-Hoogsteen fashion as depicted in figure 1.7. Each base triad has a central purine residue that must be base paired in a WC fashion to a pyrimidine and in a Hoogsteen or reverse-Hoogsteen fashion to a pyrimidine or purine respectively. Thus, the WC portion of the sequence must have exclusively purines on one strand and pyrimidines on the other, while the third strand has exclusively either type of base. In both cases, the third strand resides in the major groove and runs anti-parallel to the WC strand that has the same type of base. In purine-purine-pyrimidine (*pu*•pu•py; the abbreviation in italics representing the non-WC strand) triplexes, the third strand is symmetrically located in the centre of the major groove, while in pyrimidine-purine-pyrimidine triplexes (*py*•pu•py), the third strand is asymmetrically located closer to the pyrimidine strand of the WC

duplex (Sinden, 1994). The orientations of the bases relative to the sugar rings are similar to those found in B-DNA in both types of triplexes (Malkov *et al.*, 1993). The sugar puckers of the WC portion of *py*•pu•py DNA triplexes are C2' *endo* while those of the third strand show partial C3' *endo* character only at cytosine residues (Asensio *et al.*, 1998); similarly, in DNA/RNA hybrid *py*•pu•py triplexes, the RNA third strand shows only partial C3' *endo* character (Gotfresden *et al.*, 1998).

Formation of triplexes has various requirements depending on the specific sequence involved. Early studies with *py*•pu•py triplexes employing dsDNA and RNA as the third strand demonstrated that $d(A)_n$•$d(T)_n$ formed a triplex with $r(U)_n$ at any pH while a pH of 5.8 or below was necessary to form $d(TC)_n$•$d(GA)_n$•$r(UC^+)_n$ (Morgan and Wells, 1968). It was correctly inferred that the low pH was necessary in order to protonate the N1 position of C, the nucleoside of which has a pKa of 4.5. The presence and identity of divalent metal ions also has a sequence dependent effect on triplex formation. One study showed that at neutral pH, *pu*•pu•py triplexes $d(C)_n$•$d(G)_n$•$d(G)_n$ and $d(TC)_n$•$d(GA)_n$•$d(AG)_n$ were both stabilized by Cd^{2+}, Co^{2+}, Mn^{2+}, Ni^{2+}, and Zn^{2+}, but only the former sequence was also stabilized by Ca^{2+} and Mg^{2+} (Malkov *et al.*, 1993). A later study on GC rich *pu*•pu•py DNA triplexes showed that at sub-millimolar concentrations, stabilization by cations had a pattern of Co^{2+}>Mn^{2+}>Mg^{2+}, while at millimolar concentrations, the pattern was Mn^{2+}>Mg^{2+}>Co^{2+} (Blume *et al.*, 1999). The polyamines spermine and sperimidine (Hampel *et al.*, 1991) and their analogues have also been shown to facilitate *py*•pu•py triplex formation. Modifications of the bases (Lee *et al.*, 1984) or phosphates (Latimer *et al.*, 1989) in a DNA sequence can also modulate triplexe formation. Substitution of m^5C for C increases the propensity for triplex

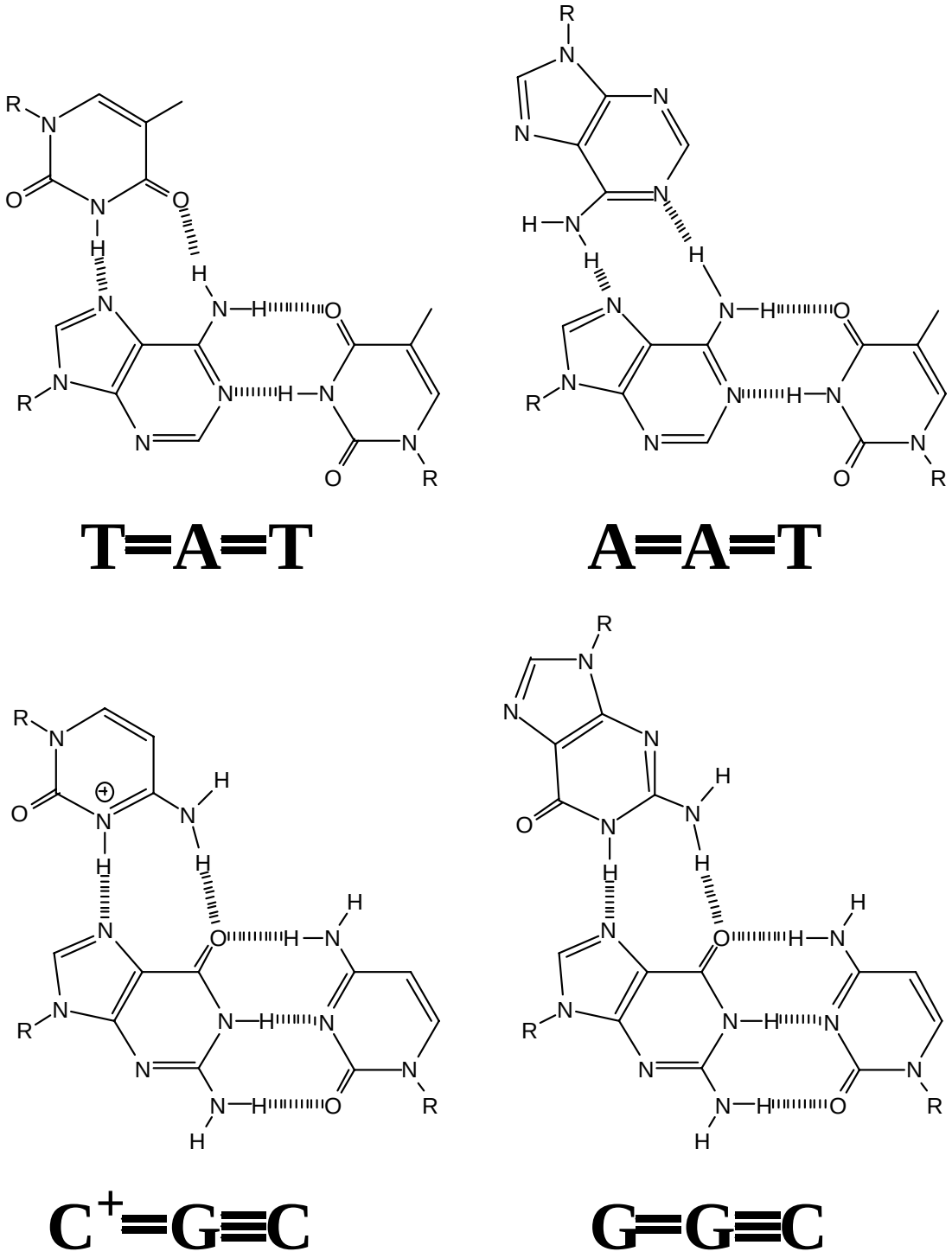

Figure 1.7: The hydrogen-bonding patterns present in each type of triplex. On the left are *py*•pu•py, while *pu*•pu•py triplexes are shown on the right. Those with an A•T duplex base pair are pictured on the top row while those with a G•C duplex base pair are pictured on the bottom row.

formation while substitution of z^7A or m^6A for the central A strand renders triplex formation impossible by eliminating an essential hydrogen bond. Thus, triplex formation is a process dependent on the nucleotide sequence, pH, and the presence of divalent metal ions in a manner that cannot be due simply to electrostatic interactions since the identity of the metal ions present drastically alters their ability to induce the conformation.

Although early work with triplexes showed three separate polynucleotide molecules to be involved in formation of the triplexes (Felsenfeld *et al.*, 1957; Felsenfeld and Rich, 1957; Lee *et al.*, 1979; Morgan and Wells, 1968), later developments suggested (Lee *et al.*, 1984) and demonstrated (Kohwi and Kohwi-Shigematsu, 1988; Mirkin *et al.*, 1987) that it was possible to form intramolecular triplexes from two or one (Sklenar and Feigon, 1990) polynucleotide strand(s). In the case of triplexes formed from one or two strands, there are necessarily regions of single-stranded polynucleotide formed to liberate one strand from part of the duplex to act as the third strand in the resulting triplex. Triplexes formed from one or two DNA strands are illustrated in figure 1.8.

Intramolecular *py*•pu•py triplexes formed from dsDNA, dubbed H-DNA, have been used to explain the sensitivity of py•pu tracts to S_1 nuclease. In order for a dsDNA sequence to form H-DNA, it must contain mirror repeats of py•pu (Mirkin *et al.*, 1987). As is apparent from figure 1.8, due to the presence of the mirror repeat, there are four possible ways for a given intramolecular triplex to form. H-DNA and its *pu*•pu•py counterpart, H*-DNA, can each be formed with the 5' or 3' portion of the third strand, resulting in the possibility of Hy5 and Hy3 isomers for H-DNA and Hr5 and Hr3 isomers for H*-DNA; all of these isomers have been observed (Sinden, 1994). As with

intermolecular triplexes, modification of the bases involved in forming an intramolecular duplex has shown some success in stabilizing the conformation (Phipps *et al.*, 1998).

Although any of the four intramolecular triplex structures are possible within a given mirror repeat, the conditions under which each one forms varies. Formation of Hy3 by $d(G)_n$•$d(C)_n$ at acidic pH can be modulated to Hr3 by addition of Mg^{2+} (Kohwi and Kohwi-Shigematsu, 1988). Another study on $d(G)_n$•$d(C)_n$ at acidic pH showed that Zn^{2+} and Mn^{2+} induced Hr3 in a sequence with a 3 bp interruption between the mirror repeats while Ca^{2+} and Mg^{2+} induced Hr5 in a sequence with a 5 bp interruption and Hy3 in the absence of metal ions (Kang and Wells, 1992). The Hy5 isomer was observed in the presence of Mg^{2+}, Zn^{2+}, Mn^{2+} or Ca^{2+} when a 5 bp interruption was inserted within a mirror repeat of $d(GAA)_4$, while changing the length of the interruption caused it to form Hy3 regardless of metal ions present (Kang *et al.*, 1992). The preference for Hy3 over Hy5 has been attributed to the greater relaxation of negative supercoiling induced by the former isomer compared to the latter (Sinden, 1994). Thus, as with intermolecular triplexes, formation of H-DNA and H*-DNA can be modulated by adjusting the pH, the addition of different metal ions and changing the DNA sequence. In addition, these intramolecular complexes are very sensitive to the degree of supercoiling in the DNA and this as well as previously discussed factors can have a dramatic effect on the specific H-DNA or H*-DNA isomer formed by the dsDNA.

There are numerous findings that suggest triplexes have a role *in vivo*. Early research demonstrated that *py*•pu•py triplex formation with m^5C substituted DNA (Lee *et al.*, 1984) as well as H*-DNA formation in the presence of Mg^{2+} were both possible at neutral pH (Kohwi and Kohwi-Shigematsu, 1988) raising the possibility that formation of

(**A**)

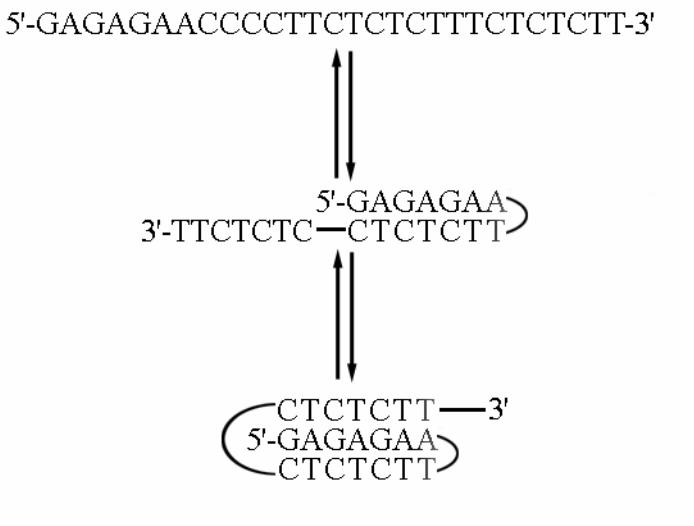

(**B**)

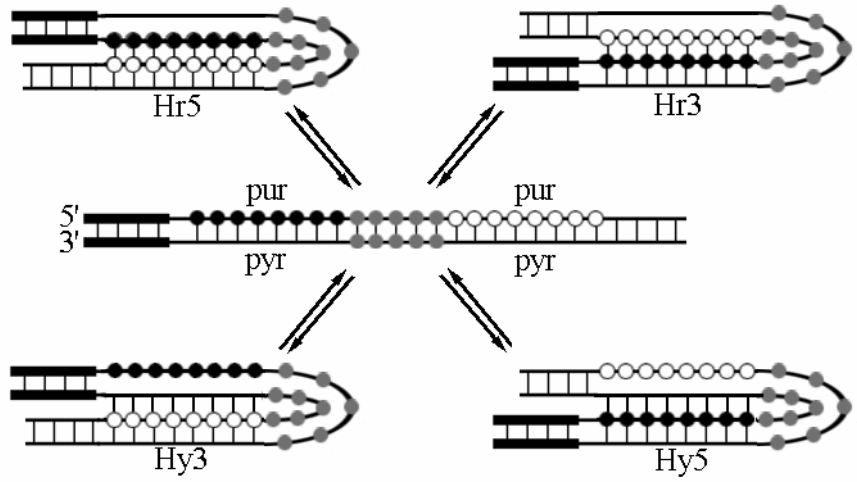

Figure 1.8: (**A**) Schematic illustration of the folding pattern present in a single-stranded triplex molecule. The 3' end is the Hoogsten-paired pyrimidine strand. Adapted from Sklenar and Feigon, 1990. (**B**) Schematic illustrations of the four possible isomers of triplexes generated by unwinding of a duplex DNA sequence with a mirror repeat of pyr•pur sequences in which one strand becomes the third strand in a triplex structure and the other strand remains unpaired. The black and white circles represent 5' and 3' end purine runs, respectively. Adapted from Kang and Wells, 1992.

intramolecular triplexes could be responsible for the sensitivity of py•pu sequences in dsDNA to S_1 nuclease. Several surveys of eukaryotic and prokaryotic genomes showed that potential triplex forming sequences were over-represented in eukaryotes relative to prokaryotes, particularly in promoter regions. An example of this found in intron 21 of the *PKD1* gene, a 2.5 kbp py•pu sequence which is likely to form Hy3 H-DNA at low superhelical densities (Blaszak *et al.*, 1999). Formation of this triplex has been implicated in interfering with replication and causing mutations leading to kidney disease (Patel *et al.*, 2004).

Evidence for triplex formation *in vivo* has also been supplied through binding studies of a monoclonal antibody (MAb), Jel 318. Jel 318 was raised against $d(Tm^5C)_n$•$d(GA)_n$•$d(m^5CT)_n$ and shown to bind to eukaryotic chromosomes but not to sequences from *Escherichia coli* (*E. coli*) (Lee *et al.*, 1987; Lee *et al.*, 1989). Another MAb raised against the same antigen, Jel 466, was later produced and showed greater sequence specificity than Jel 318 and displayed a different binding pattern on chromosomes (Agazie *et al.*, 1994). These two mABs were used in tandem to stain nuclei and it was found that the reactivity of the cell to the mABs was dependent on the stage of the cell cycle, suggesting a role for H-DNA or intermolecular triplexes in chromosome condensation (Agazie *et al.*, 1996).

1.2.2.4 Quadruplex DNA

Quadruplex DNA was first suggested as a possibility during the interpretation of the X-Ray fiber diffraction pattern of $r(I)_n$•$r(G)_n$ (Zimmerman *et al.*, 1975). Later, T_m and

CD studies demonstrated that four-stranded DNA structures were likely in the case of polypurine runs under sufficient monovalent ion concentrations (Lee *et al.*, 1980). Prior to this, four-stranded structures consisting of pairs of WC base pairs joined on the major groove side of the duplex were proposed but no evidence has been found for their existence (Sinden, 1994). The quadruplexes suggested by these early studies and subsequently characterized by a variety of biochemical and structural methods consisted of Hoogsteen paired G residues arranged in a parallel (Sen and Gilbert, 1992) or anti-parallel (Kang *et al.*, 1992; Smith and Feigon, 1992) fashion. The base-pairing scheme of these quadruplexes is illustrated in figure 1.9.

Quadruplexes composed of four strands with G rich runs unable to otherwise hybridize were studied by gel electrophoresis assays and found to assemble into a quadruplex in a concentration dependent manner at physiological ionic strength and pH. Likewise, these sequences were able to form the same complex but at twice the molecular weight when they were mixed as duplexes with their complimentary strands, which were presumed to remain hybridized at their ends but denatured in the region around the G-quartet. The four strands implicated in forming the quartet were presumed to be parallel with their G residues all in the *anti* conformation, as depicted in figure 1.9 (Sen and Gilbert, 1988). This would provide strong stacking interactions, explaining the high T_m values associated with these structures (Lee *et al.*, 1980).

Another type of quadruplex has been characterized in d(G_4T_4) sequences found in the telomeres of *Tetrahymena* and *Oxytricha* (Kang *et al.*, 1992; Smith and Feigon, 1992) species. X-ray crystallography showed separate dsDNA molecules forming two Hoogsteen-bonded hairpin structures with single-stranded T residues in the loops. The

two molecules then associate with anti-parallel strands from each hairpin molecule forming the two remaining G-G interactions to complete the quadruplexes as depicted in figure 1.10. The hydrogen-bonding pattern alternates with each successive tetrad, as illustrated in figure 1.9; one tetrad would have the pattern shown in the all-parallel quadruplex (but with alternating *anti* and *syn* conformations) while the next tetrad would have that shown in the anti-parallel diagram (Smith and Feigon, 1992). NMR studies on the same complex displayed a similar interaction except that the hairpins were bridging the corners of the quadruplex so as to place parallel as well anti-parallel strands beside each other (Kang *et al.*, 1992). This structure is also depicted in figure 1.10. In both cases, successive G residues on the same strand were alternating *syn* and *anti* arrangements to allow the association to take place. As with the all-parallel conformation, stacking interactions stabilize the interaction and high ionic strengths favor the interaction.

As with Z-DNA and triplex DNA, there is some specificity in the metal ions that will induce quadruplexes in different sequences. In quadruplexes formed by strands with multiple G-rich runs it has been found that K^+ ions stabilize the G quartet to such a high degree that the interactions between two hairpin molecules is heavily favored over interactions between four separate strands to yield an all-parallel quadruplex. The all-parallel structure would form in the presence of mM [K^+] with a high overall ionic strength generated by the presence of Na^+. However, in the presence of sufficiently high [K^+], the hairpin parallel quadruplex would form (Hardin *et al.*, 1991; Sen and Gilbert, 1990). Further, studies on parallel quadruplexes formed by $d(GA)_n$, $d(GAA)_n$, and $d(GGA)_n$ showed that formation of a quadruplex had multiple steps that resulted in

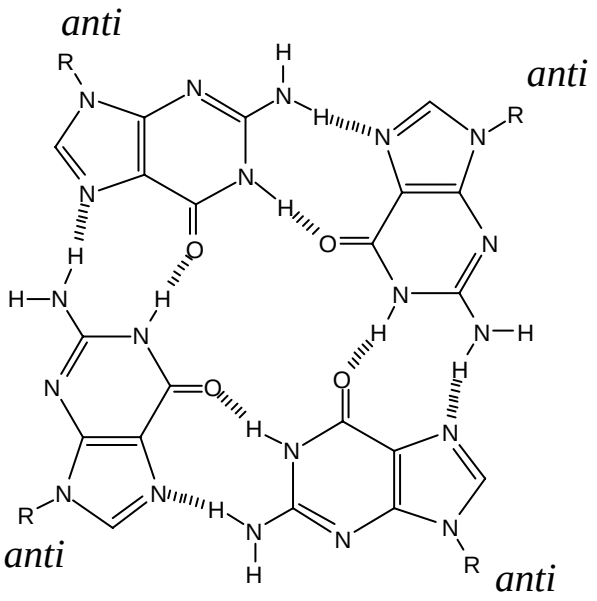

Parallel

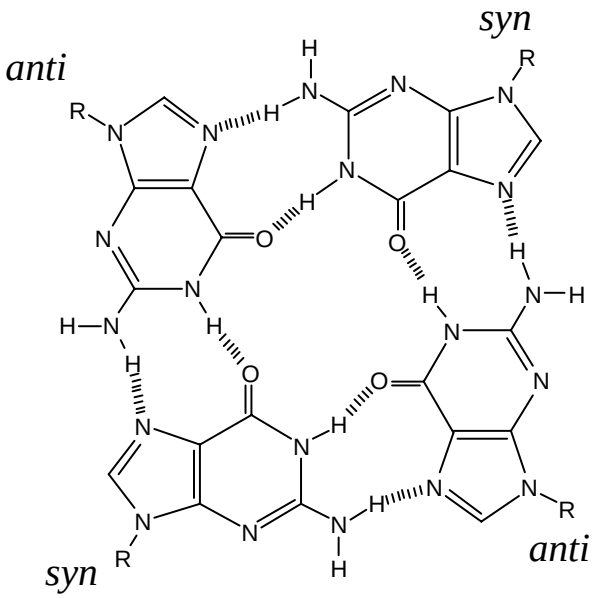

Anti-Parallel

Figure 1.9: The hydrogen-bonding schemes present in G-quadruplex structures. The hydrogen bonding pattern observed in the tetrads of parallel quadruplexes are shown in the upper figure with all *anti* conformations. The hydrogen-bonding pattern present in anti-parallel quadruplexes alternates between that shown in the upper figure (except that the second and fourth bases, clockwise from the top are *syn*) with that shown in the lower with each successive tetrad.

(**A**)

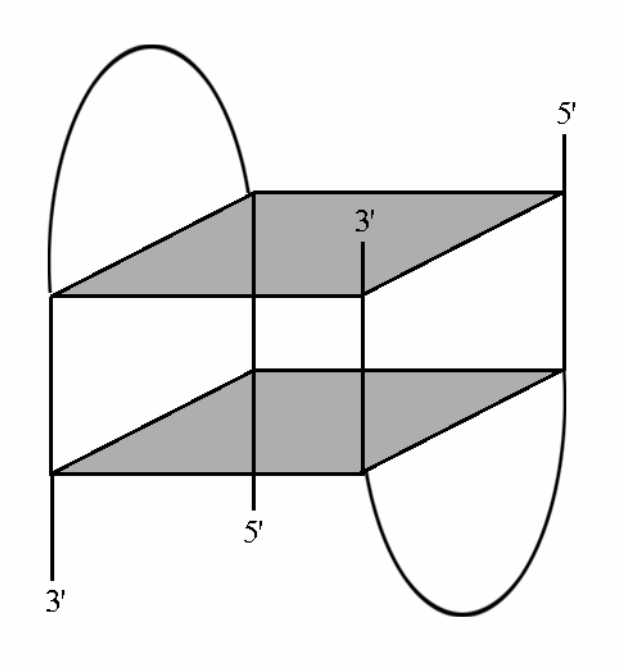

(**B**)

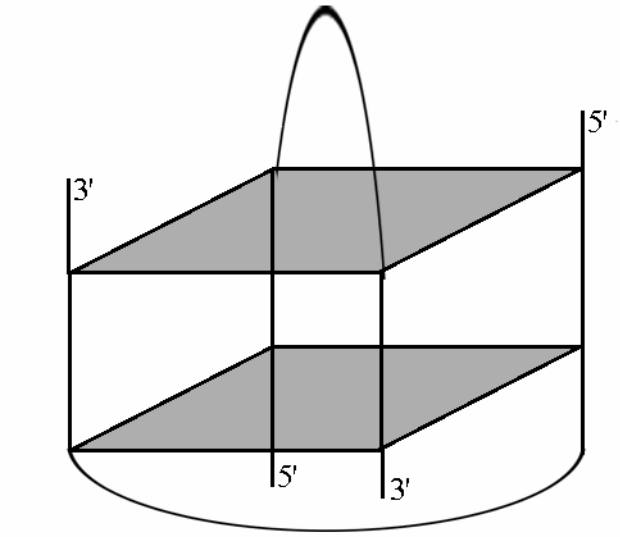

Figure 1.10: Schematic illustrations of the distinct folding of DNA to produce different quadruplexes from two duplex molecules. (**A**) All anti-parallel orientation as observed by X-ray crystallography. Adapted from Smith and Feigon, 1992. (**B**) Anti-parallel as well as parallel orientations as observed by NMR studies. Adapted from Kang *et al.*, 1992. Both of these patterns were observed with sequences from the telomeres of *Oxytricha*.

different denaturation behaviors. Formation of the more stable quadruplex was correlated to the ionic radius of mono- and divalent ions present that stabilized the interaction. It was found that in general, divalent ions stabilized the quadruplex structure at much lower concentrations than the monovalent ions. It was also found that the more stable form of the quadruplex was only formed by ions having an ionic radius near 1.35 Å. Thus, Ba^{2+} and K^{+} stabilized the structure more easily than larger or smaller ions with the same valency (Lee, 1990).

The results from these studies indicated that the size of the cavity formed between successive base tetrads allowed coordination of a mono- or divalent cation and that one with an ionic radius near 1.35 Å was ideal. The 6-keto groups of G residues are believed to coordinate the ion in a similar fashion to crown ethers. The effectiveness of the K^{+} ion at allowing G tetrads to form explains the trapping of sequences that could unwind to form parallel quadruplexes in hairpin intermediates. This is further supported by the fact that sequences too short to form hairpin quadruplexes between two duplexes form parallel quadruplexes equally well with K^{+} or Na^{+}, provided that the concentrations of either ion are sufficient to allow formation of the quadruplex (Sen and Gilbert, 1990).

Since the centromeres and telomeres in most eukaryotic organisms are comprised of G-rich sequences, it has been thought that quadruplex formation may occur in these regions. Further, fragile X chromosome repeats as well as portions of chromosome 19 in humans have been found to contain sequences which could form quadruplexes (Gilbert and Feigon, 1999). Formation of quadruplexes has been shown to inhibit telomerase (Zahler *et al.*, 1991) and has been suspected of playing a role in tethering of chromosomes for meiosis (Sen and Gilbert, 1988). Finally, the recent *in vitro* production

of antibodies against quadruplex structures have provided further evidence that anti-parallel quadruplexes are present in the macronuclei of *Sylonychia lemnae* (Schaffitzel *et al.*, 2001).

1.2.2.5 M-DNA

It can be seen from the above analysis that DNA-metal ion interactions can have a profound effect on DNA conformation. Another alternative conformation in which DNA-metal ion interactions play an intimate role was recently discovered at the University of Saskatchewan. M-DNA is a pH-dependent complex formed between certain transition metals and DNA and has sparked interest due to its unique properties and potential applications.

1.2.2.5.1 Characterization of M-DNA Formation and Inferred Structure

M-DNA formation occurs when dsDNA is exposed to the transition metal ions Zn^{2+}, Ni^{2+}, or Co^{2+} at pH values above 8.0. Zn(II) M-DNA formation at pH 9.0 in CT DNA causes an increase in T_m relative to DNA in the absence of divalent metal ions at any pH up to a Zn^{2+}:phosphate ratio of 10:1 (Lee *et al.*, 1993). This is indicative of a conformational change as at neutral pH, such a high ratio of Zn^{2+}:phosphate would facilitate denaturation of the DNA (Eichhorn and Shin, 1968). Further, raising the pH of a solution would cause the deprotonated forms of T and G to become more abundant, favoring their interactions with metal ions. In the absence of a stabilizing conformational

change, the T_m at elevated pH in the presence of transition metals would be even lower than at neutral pH. M-DNA is also resistant to digestion by DNAse I under conditions in which B-DNA is readily degraded (Aich *et al.*, 2000). All three forms of M-DNA facilitate UV-induced crosslinking of the two strands while Co(II) M-DNA facilitates the same phenomenon induced by γ radiation (Labiuk *et al.*, 2001). M-DNA also shows different electrophoretic mobility than B-DNA, with reduced separation of nicked and supercoiled species and approximately 5% fewer bp per turn (Lee *et al.*, 1993).

Unlike B-DNA, M-DNA does not bind EtBr. This forms the basis of a convenient EtBr-based fluorescence assay that has been a very useful tool in studying M-DNA formation. This assay was used to obtain much of the data detailed in this section (Aich *et al.*, 1999; Aich *et al.*, 2000; Labiuk *et al.*, 2001; Lee *et al.*, 1993). The basis behind this assay will be discussed in more detail in section 1.3.1.1.

Although M-DNA formation has been found to be independent of base composition in genomic DNA, there is a large degree of sequence dependence in repeating sequence synthetic polymers. The propensity of different repeating sequences to form Zn(II) M-DNA was found to follow the following order:

$$d(TG)_n \bullet d(CA)_n > d(TCC)_n \bullet d(AGG)_n \sim d(A)_n \bullet d(T)_n > d(TTC)_n \bullet d(AAG)_n > d(GC)_n >> d(AT)_n$$

Thus, pur•pyr tracts form the conformation better than those with alternating pur/pyr on the same strand and increasing G•C content seems to favour M-DNA formation. (Lee *et al.*, 1993).

There are several findings that suggest M-DNA formation may involve replacement of the imino protons of G and T with the divalent metal ions. First, the imino proton signals of those bases disappear from the H^1 NMR spectrum of $d(TG)_{15} \bullet d(CA)_{15}$ at pH 9.0 upon addition of Zn^{2+} (Lee *et al.*, 1993). Second, one proton is released per

metal ion per base pair upon Ni(II) M-DNA formation as revealed by titration experiments (Aich *et al.*, 1999). Third, GC-rich repeating sequences form Zn (II) M-DNA more quickly and more completely than analogous AT rich sequences, which could be due to the lower pK_a of G (9.4) compared to T (9.9). Further, substitution of dU for dT also facilitates Zn(II) M-DNA formation, which could also be due to the lower pK_a of U (9.3) compared to T (9.9) (Lee *et al.*, 1993).

M-DNA formation has been shown to be reversible, as addition of ethylenediaminetetraacetic acid (EDTA) or lowering the pH of the solution causes it to dismutate back to B-DNA. This feature distinguishes formation of M-DNA from denaturation due to high pH and the presence of transition metal ions, which would also result in a loss of EtBr binding, but would not be fully reversible by chelation. A pH-dependent hysteresis has been observed in the formation and reversion to B-DNA of Ni(II) M-DNA but not with Zn(II) or Co(II) M-DNA. This effect was more pronounced in $d(GC)_n$. Therefore, once formed, the conformation is stable at pH values at which it will not form, suggesting that the transition is cooperative (Aich *et al.*, 2000).

M-DNA formation does not induce large spectroscopic changes. It shows only small changes in its CD spectrum relative to B-DNA and a 10% hypochromicity at 260 nm. Further, M-DNA formation is not inhibited by substitution of z^7A or me^6A for A, indicating that a triplex-like bonding pattern is not occurring, which was an initial concern due to the high propensity of pur•pyr tracts to form the conformation (Aich *et al.*, 2000; Lee *et al.*, 1993). In conclusion M-DNA may have a structure similar to that

(**A**)

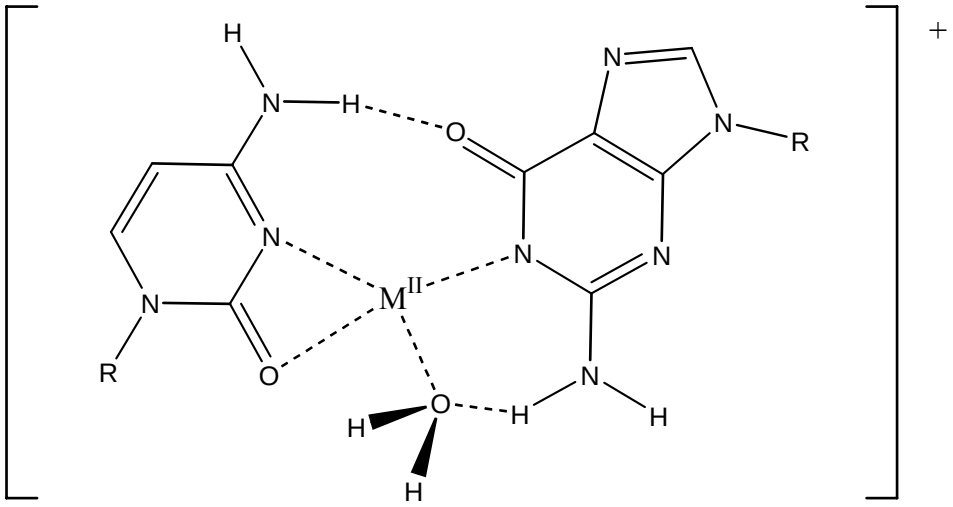

(**B**)

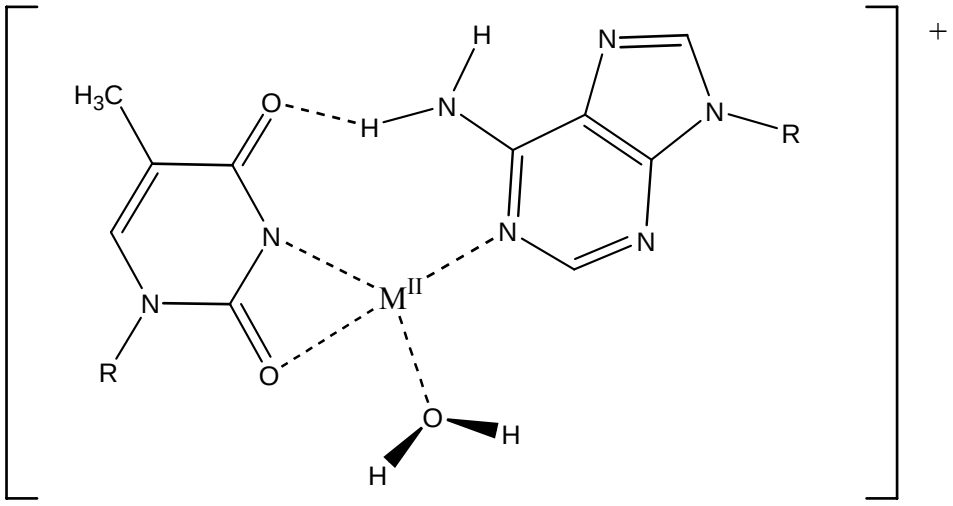

Figure 1.11: The proposed structure of M-DNA. The base pairs indicated are (**A**) G•C and (**B**) A•T. The indicated metal ion, which replaces the 1- and 3-imino protons of G and T, respectively, can be Zn^{2+}, Ni^{2+}, or Co^{2+}.

depicted in figure 1.11 although attempts to crystallize and solve the structure of M-DNA have so far proven unsuccessful.

1.2.2.5.2 Electron Transfer Properties of M-DNA

M-DNA has been shown by direct measurements to allow metallic-like conduction, whereas B-DNA is a semi conductor with a wide band gap (Rakitin *et al.*, 2001). AC impedance studies on immobilized DNA have shown M-DNA to have a much lower resistance than B-DNA (Long *et al.*, 2003), while other electrochemical studies have shown it to have a much faster rate of electron transfer than B-DNA (Li *et al.*, 2003).

Fluorescence quenching studies between fluorophores and quenchers covalently attached to the 5' ends of a duplex have shown that M-DNA allows quenching of fluorescence (implying electronic communication between the attached molecules), while B-DNA does not (Aich *et al.*, 1999; Aich *et al.*, 2002; Wettig *et al.*, 2003). Like the direct electrical studies, this is indicative of electron transfer, and the basis of the assay will be discussed in more detail in section 1.3.1.2.

One of the fluorescence studies employed a three-way DNA junction in which rhodamine as well as anthraquinone were available to act as quenchers for fluorescein (Fl). When the redox state of anthraquinone was modulated, the degree of quenching changed, enabling the three-way DNA junction to act as a molecular switch (Wettig *et al.*, 2003). In another fluorescence study, binding of a sequence-specific protein prevented quenching which was in turn reactivated through addition of proteinase,

suggesting another way in which electron transfer through M-DNA could be modulated (Aich *et al.*, 1999).

These studies have indicated that M-DNA may be useful as a molecular wire with a variety of ways to modulate its activity, so that nano-electronic devices could be constructed. DNA is an attractive template to work with in nanotechnology as a variety of enzymes capable of manipulating DNA on a molecular scale already exist, and DNA replication could be exploited for production of defined sequences that would then be easily converted to M-DNA.

1.3 Measuring M-DNA formation

Since M-DNA formation does not yield large changes relative to B-DNA in UV absorbance or CD studies, these important techniques useful in the characterization of other alternate structures are ruled out. Fluorescence-based methods taking advantage of the lack of appreciable EtBr binding by M-DNA as well as quenching of fluorophores observed in double-labelled M-DNA have been employed to characterize the conformation. As shown in this thesis, the direct biophysical methods of isothermal titration calorimetry (ITC) and surface plasmon resonance (SPR) have also proven useful in characterizing M-DNA.

1.3.1 Fluorescence Experiments

Two fluorescence-based methodologies have been employed in this study. Foremost, an EtBr-based assay has been developed (Lee *et al.*, 1993) that has been of great use in characterizing the conditions under which M-DNA will form as well as its stability once formed. Second, an assay based on quenching of Fl-labeled DNA was developed to measure M-DNA formation (Aich *et al.*, 1999). The principles behind each of these methods will be outlined in this section.

1.3.1.1 Ethidium bromide-based assays

EtBr is a 390 Da cationic DNA-binding drug that is widely used in molecular biology due to its well-characterized interactions with nucleic acids. EtBr was originally used as a trypanocidal agent by inhibiting nucleic acid synthesis (Waring, 1965) and is now commonly used to stain agarose gels for visualization of DNA (Sharp *et al.*, 1973). EtBr binds nucleic acids by intercalation (Jain *et al.*, 1977; Jain and Sobell, 1984; Sobell *et al.*, 1977) and binding of one EtBr molecule to a base pair has been shown to prevent binding of a second molecule to an adjacent base pair of B-DNA, a phenomenon known as neighbour exclusion (Bresloff and Crothers, 1981; Crothers, 1968); in the case of A form DNA or dsRNA sequences, the neighbour exclusion extends to 3 base pairs (Bresloff and Crothers, 1981). The structure of EtBr as well as a crystal structure of it bound with a WC paired dinucleotide of r(CG) is shown in figure 1.12. The binding of

EtBr to nucleic acids has been observed in both DNA and RNA with little sequence specificity (Bresloff and Crothers, 1981; Lepecq and Paoletti, 1967; Waring, 1965).

Visualization of DNA in agarose gels by EtBr takes advantage of the fact that the DNA-EtBr complex fluoresces in the visual range around 600 nm when excited by light around 320 or 520 nm (Lepecq and Paoletti, 1967; Sharp *et al.*, 1973); the absorption spectra in the visual range for various sequences in complex with EtBr all show maximums around 520 ± 3 nm regardless of nucleic acid type or sequence (Bresloff and Crothers, 1981; Waring, 1965), while the visual absorbance maximum for EtBr alone is 480 nm (Hudson and Jacobs, 1975; Latimer and Lee, 1991; Waring, 1965). The fluorescent properties of the EtBr-nucleic acid complex have been exploited to produce a rapid fluorescence assay which can be used to quantify DNA or RNA in solution, to determine the extent of hybridization of the sample (Morgan *et al.*, 1979) and to asses the activity of enzymes which synthesize (Lee *et al.*, 1980) or degrade (Latimer *et al.*, 1989; Morgan *et al.*, 1979) DNA.

The EtBr-nucleic acid complex displays roughly 25 times the fluorescence of free EtBr with CT DNA or RNA when either nucleic acid is in large excess (Lepecq and Paoletti, 1967). This enhancement only occurs when EtBr complexes with double-stranded nucleic acids or with single-stranded ones capable of forming hairpin loops; in the latter case the fluorescence is much lower than in the former (Morgan *et al.*, 1979). The mechanism of enhanced EtBr fluorescence in the presence of nucleic acids is likely due to hydrophobic shielding of the EtBr molecule from solvent, preventing proton exchange to the solvent and extending the lifetime of the excited singlet state thus favoring fluorescence as a means to return to the ground state after the complex has been

(**A**)

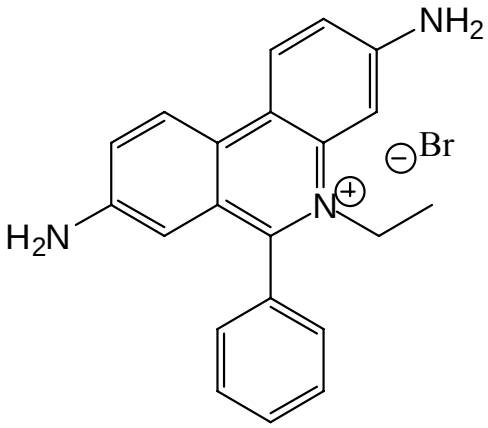

(**B**)

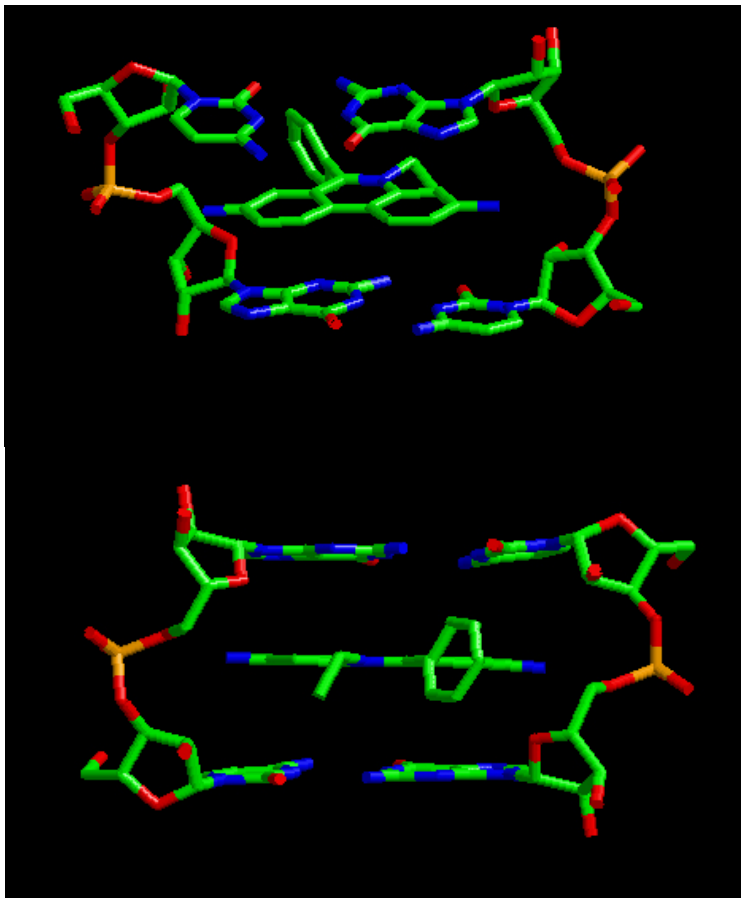

Figure 1.12: (**A**) Structure of EtBr. Note the planar aromatic ring system that intercalates between base pairs with favorable stacking interactions. (**B**) X-ray crystal structure of EtBr bound to the self-complimentary WC paired dinucleotide r(CG). Note the stacking interactions between EtBr and the bases. Adapted from Jain and Sobell, 1984.

excited by the incident light (Hudson and Jacobs, 1975; Olmsted and Kearns, 1977). This mechanism is supported by extentsion of the excited state's lifetime in the presence of D_2O (Olmsted and Kearns, 1977) and larger fluorescence enhancement upon binding of EtBr to triplex than the corresponding duplex sequences. However, if a triplex carries a positive charge no fluorescence is observed in the presence of EtBr (Morgan *et al.*, 1979). The lack of fluorescence in the latter case of triplex formation is likely due to the presence of a positive charge on the DNA, which repulses the positively charged ethidium ions and prevents binding to the DNA (Lee *et al.*, 1979; Lee *et al.*, 1984; Morgan *et al.*, 1979); the presence of metal ions, particularly divalent ones, has been shown to inhibit the binding of EtBR to DNA (Lepecq and Paoletti, 1967).

The enhancement of EtBr fluorescence upon binding nucleic acids is sequence specific to some extent, with sequences having exclusively pyrimidines on one strand and purines on the other showing much less enhancement than mixed sequences and sequences rich in A•T base pairs showing a larger enhancement than those rich in G•C base pairs (Latimer and Lee, 1991; Morgan *et al.*, 1979). Further, sequences with the modified bases 7-deazaadenine and 7-deazaguanine showed 70 % and 0 % of the fluorescence of their parent sequences, respectively, despite the fact that binding of EtBr to DNA containing these modified bases was largely unaffected as demonstrated by absorption studies (Latimer and Lee, 1991).

EtBr fluorescence studies have been used to probe the structure of nucleic acids on *E. coli* tRNA (Bittman, 1969; Tao *et al.*, 1970), CT deoxynucleoproteins (Angerer and Moudrianakis, 1972; Angerer *et al.*, 1974), triplex-forming DNA sequences (Hampel *et al.*, 1991; Lee *et al.*, 1979; Lee *et al.*, 1984; Morgan *et al.*, 1979), Z-DNA (Qu *et al.*,

2004; Van De Sande *et al.*, 1982) and to determine the presence or absence of cross links using fluorescence in conjunction with thermal denaturation studies (Labiuk *et al.*, 2001; Morgan *et al.*, 1979).

M-DNA formation has also been studied by EtBr fluorescence based studies. Like *py*•pu•py triplexes with C^+ residues on the third strand, M-DNA base pairs are believed to carry a positive charge due to the replacement of a proton by a divalent metal ion (Lee *et al.*, 1993) and therefore does not bind EtBr (Lee *et al.*, 1979). Thus, M-DNA will not bind EtBr and no enhancement of fluorescence is observed upon addition of M-DNA to an EtBr solution. Likewise, formation of M-DNA from B-DNA disrupts the DNA-EtBr interaction and the fluorescence drops to baseline. Reversion of M-DNA to B-DNA allows intercalation of EtBr to take place and subsequently restores the EtBr-DNA complex, increasing fluorescence. Millimolar concentrations of EtBr also prevent M-DNA formation, presumably by competing with the metal ions for binding sites on the DNA (Lee *et al.*, 1993). As covered in section 1.2.2.5.1, many properties of M-DNA have been elucidated using this assay.

1.3.1.2 Quenching of Fluorophore-Labeled DNA

Since the proposed structure of M-DNA has metal ions between the base pairs as depicted in figure 1.11, it has been postulated that it could serve as a molecular wire. The stacked aromatic bases of native B-DNA have been evaluated as an electron transfer medium (Arkin *et al.*, 1996; Dandiker *et al.*, 1997; Hall *et al.*, 1996) but other studies have shown that B-DNA is not an efficient conductor (Lewis *et al.*, 1997; Taubes, 1997).

The possibility that M-DNA is capable of charge transfer has been evaluated in several studies employing a fluorescence-based assay in which fluorophores covalently attached to each 5' end of a DNA duplex (Aich *et al.*, 1999; Aich *et al.*, 2002) or three-way junction (Wettig *et al.*, 2003) interact with each other.

In studies employing Fl as an electron donor and rhodamine as an electron acceptor, the quenching observed is likely due to an electron-transfer process as indicated by lifetime measurement studies (Aich *et al.*, 1999). Another type of quenching, fluorescence resonance energy transfer (FRET), is possible when fluorophores display spectral overlap (as Fl and rhodamine do). This mechanism of quenching has a distance dependency of $1/r^6$ and is therefore unlikely at distances greater than 50 Å (Clegg, 1992); the length of a 20mer, the shortest sequences studied, is 60-70 Å, and significant quenching has been observed in duplexes up to 496 bp (Aich *et al.*, 2002). Further, quenching is still observed between fluorophores that do not display spectral overlap, effectively ruling out FRET as a quenching mechanism in this assay (Aich *et al.*, 2002; Wettig *et al.*, 2003). Due to a shallow distance-dependence on the degree of quenching, it was concluded that the most likely mechanism of electron transfer was a "hopping mechanism" in which the electron moves in random directions between metal centers until it is absorbed by the quencher (Giese *et al.*, 2001; Meggers *et al.*, 1998).

A limitation of this assay is that it is restricted to the study of the Zn(II) form of M-DNA. Complexes of Ni(II) and Co(II) often display absorbance around 500 nm. The Ni(II) and Co(II) forms of M-DNA have this characteristic, although the extinction coefficient is too low for this to be a useful method by which to assay M-DNA formation. However, the presence of a weakly absorbing coordination compound at each base pair

allows FRET-based quenching of Fl fluorescence. Thus the Fl emission is quenched in Ni(II) or Co(II) M-DNA even in the absence of an acceptor molecule at the other end of the duplex (Aich *et al.*, 1999). Despite this, it is an effective and simple way to measure the formation of Zn(II) M-DNA in solution.

1.3.2 Isothermal Titration Calorimetry

Isothermal titration calorimetry (ITC) is a biophysical technique commonly used to characterize interactions between two species in solution. It functions by measuring the amount of energy required to heat or cool a solution in order to maintain a constant temperature as a function of the concentration of one of the interacting species. The experiment is typically carried out by adding one interacting species to two separate chambers, one containing the other interacting species in buffer, the second containing only buffer to provide a background heat of dilution. Thus, the change in enthalpy (ΔH) associated with the reaction can be directly measured, whether it is exo or endothermic. Based on binding constants obtained through this value and modelling, ΔG values [and therefore entropy (ΔS) values] can be calculated (Matulis *et al.*, 2000; Zhang *et al.*, 2000).

ITC has been employed in a number of studies to characterize interactions between DNA molecules (Goobes and Minsky, 2001) as well as between DNA and peptides (Keller *et al.*, 2002) and small molecules (Matulis *et al.*, 2000; Ren *et al.*, 2000). It has also been used to characterize interactions between transition metal ions and proteins (Ditusa *et al.*, 2001), peptides (Zhang *et al.*, 2000), DNA (Matulis *et al.*, 2000),

and dinucleotides (Tanner *et al.*, 2002). In each of these cases, an expression for ΔG was obtained by modelling the interactions, which were all relatively simple. Thus, like SPR, ITC is a useful technique for directly studying interactions between biomolecules without the use of labels. However, unlike SPR, large concentrations of interacting species are often necessary to produce a significant signal since the signal depends on the ΔH value associated with the binding event.

1.3.3 Surface Plasmon Resonance

Surface plasmon resonance (SPR) is an optical phenomenon that has been used in recent years to study interactions between biomolecules, interactions between biomolecules and small molecules, and conformational changes in biomolecules (Rich and Myszka, 2002). To measure interactions by SPR, a three-layer system is often used, as depicted in figure 1.13. This configuration is known as the attenuated total reflection (ATR), or Kretschmann configuration (Liedberg *et al.*, 1993) and is employed in the commercially available BIAcore systems (Jonsson *et al.*, 1991; Jonsson and Malmqvist, 1992), the most widely used SPR biosensors in the world (Rich and Myszka, 2002). The three layers that determine the signal are a glass prism, a metal film, and a dielectric with a lower refractive index (n_d) than that of the prism (n_p) (Homola, 1997; Liedberg *et al.*, 1993). When SPR is used to study biomolecules, the dielectric layer consists of immobilized biomolecules that are exposed to a flow system containing an aqueous component consisting of buffer and molecules that interact with the immobilized biomolecules. As shown in figure 1.13, the detector measures the intensity of light

reflected off the metal film after passing through the prism. When the angle θ is larger than the critical angle, θ_c, total internal reflection will occur, meaning that the incident light is reflected back out of the prism on the same side it entered from relative to the metal surface. At these angles, an evanescent electromagnetic field with amplitude perpendicular to the plane of the glass/metal interface will penetrate from the prism into the metal film (Stenberg *et al.*, 1991). Under the correct conditions, this evanescent field can couple to electrons in the metal film to create an electromagnetic charge density wave which propagates along the interface between the metal and the dielectric on the side opposite the prism. The charge density wave is referred to as a surface plasmon, and under the conditions that allow coupling of the evanescent field to the electrons in the metal to form a surface plasmon, SPR occurs (Liedberg *et al.*, 1993).

The conditions that allow SPR to occur are dependent on the wavelength (λ), polarization state, and angle of incidence θ of the incident light, and the optical properties of the prism, metal, and dielectric layers (Jonsson *et al.*, 1991). The incident light must be plane polarized relative to the surface of the metal (Nagata and Handa, 2000) and it must be of a λ suitable to cause resonance in the conduction band electrons of the metal being used. The latter condition is satisfied in the visible and near IR light ranges by Al, Ag, and Au (Jonsson and Malmqvist, 1992). The metal at the interface between the prism and the dielectric must be one in which the electrons display a gas-like behavior, meaning that the electrostatic potential of the ion cores must have little effect on their spatial motion; thus Al, Cu, Ag, and Au are the best choices for the metal to be used (Liedberg *et al.*, 1993). Finally, θ must be such that the wave vector of the surface plasmon (k_{sp}) is equal in magnitude to the component of the incident light's wave vector that is parallel to

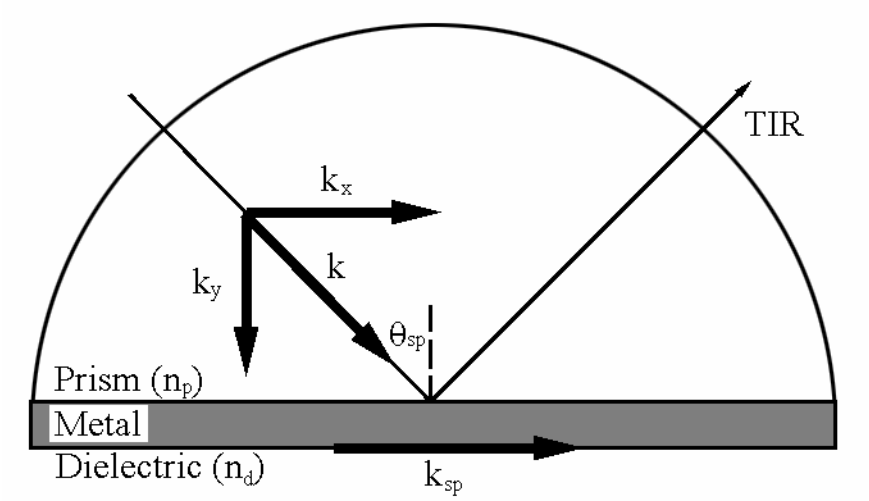

Figure 1.13: The Kretschmann or ATR configuration used in many SPR setups. The indident light is contacting the surface at an angle θ_{sp} and has a wave vector k with k_x and k_y components parallel and perpendicular to the plane of the metal/dielectric interface, respectively. The wave vector of the surface plasmons is represented by k_{sp} while the dielectric constants of the prism and the dielectric are indicated by n_p and n_d, respectively. The conditions of total internal reflection are illustrated by the vector marked TIR, which represents the bulk of the incident light.

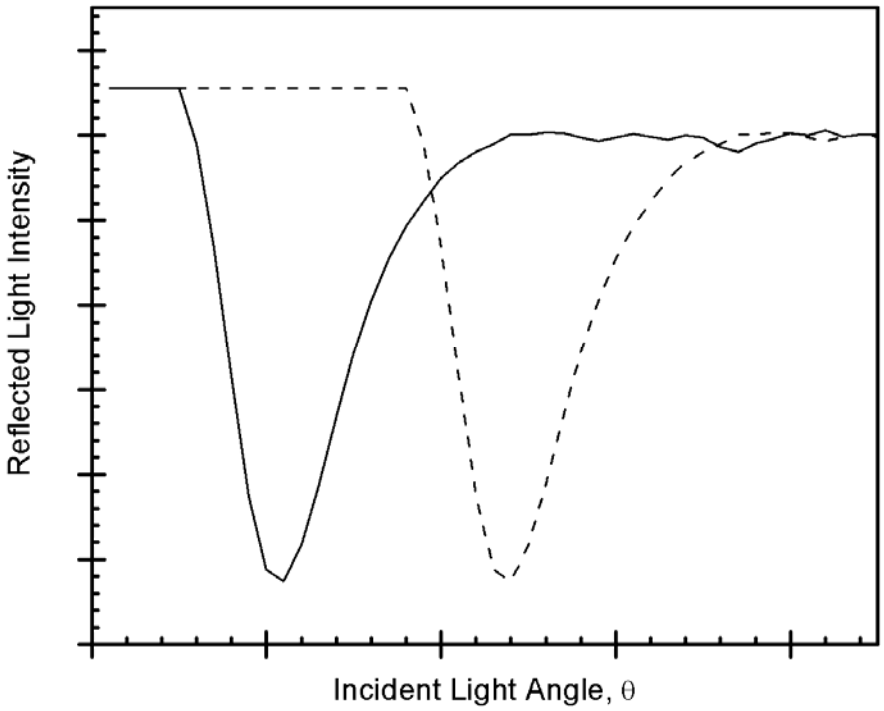

Figure 1.14: The intensity of reflected light as a function of angle. The minimum in reflected light intensity represents the θ_{sp} at which SPR occurs. The dashed line represents a reading obtained from a system with a higher n_d than that represented by the solid line. The higher n_d causes SPR to occur at a larger angle of incidence.

that of k_{sp} (k_x) as shown in figure 1.13; hereafter this angle will be referred to as the resonance angle (θ_{sp}) (Liedberg *et al.*, 1993).

In the case of total internal reflection, the intensity of the reflected light is nearly equal to that of the incident light. However, when employing an ATR device, the reflected intensity drops measurably under conditions that allow SPR (Stenberg *et al.*, 1991). Thus, by keeping all factors described in the previous paragraph equal but varying the angle of incidence, one would generate a spectrum in which the reflected light intensity passes through a minimum at θ_{sp} as depicted in figure 1.14. Angle-resolved SPR biosensors such as the BIAcore series which are employed in the vast majority of commercially available instruments (Rich and Myszka, 2002), measure binding of molecules to the sensor surface as a function of an increase in θ_{sp} which in turn occurs as a result of an increase in n_d due to an increased surface concentration of a given molecule (Jonsson and Malmqvist, 1992; Liedberg *et al.*, 1993). In the BIAcore SPR-based biosensors, the change in θ_{sp} is expressed as in resonance units (RU), where 1 RU corresponds to a 0.0001 º increase in θ_{sp}. This is also illustrated in figure 1.14. An alternative to angle-resolved SPR is to keep θ constant but to modulate λ in order to generate a similar spectrum (Salamon *et al.*, 1994), in which case the value λ_{sp} would increase upon binding of molecules to the surface (Boussaad *et al.*, 2000; Salamon *et al.*, 1997). This approach is not as widely used as angle-resolved SPR (Akimoto *et al.*, 2000). Regardless of the variable used to probe the SPR condition, the increase in n_d is due to displacement of buffer, which has a lower n (~1.33) than protein (~ 1.5 for a protein monolayer) (Boussaad *et al.*, 2000), or other biomolecules or small molecules.

If Al is used as the metal layer between the dielectric and the prism, the dip observed at θ_{sp} is broader than that for Ag or Au, thus lowering the resolution of the signal (Nagata and Handa, 2000). On the other hand, the signal generated by a Ag surface displays a narrower SPR response than that of Au, regardless of θ_{sp} or λ_{sp} (Salamon *et al.*, 1997), making this surface a better choice for determining either n_d or the thickness of an adsorbed monolayer (d_d) (Homola, 1997; Salamon *et al.*, 1997). However, due to its low reactivity with biomolecules and resistance to oxidation, Au is used in the BIAcore series of SPR biosensors (Jonsson and Malmqvist, 1992) as well as some in-house built SPR systems (Gaus and Hall, 1998; May and Russell, 2002; Peterlinz and Georgiadis, 1996; Peterlinz and Georgiadis, 1996; Sarkar and Somasundaran, 2004). Other in-house built systems use Ag to take advantage of the increased sensitivity of this metal (Boussaad *et al.*, 2000; Salamon *et al.*, 1994).

1.3.3.1 Detection of Molecular Interactions

The sensitivity of SPR responses to changes in refractive index has led to its application for studying biomolecular interactions (Jonsson *et al.*, 1991; Jonsson and Malmqvist, 1992; Lofas *et al.*, 1991). Typically, a protein is immobilized covalently to a carboxymethyldextran (CMD) layer bound to the gold surface through formation of amide linkages between free amine groups on the protein and activated carboxylic acid moieties on the CMD matrix (Johnsson *et al.*, 1991; Lofas and Johnsson, 1990). Alternative immobilization chemistries have been performed for ligands in which this standard practice is not acceptable and immobilization of nucleic acids or other molecules

which are not easily covalently bound to this surface can be done by adding biotin (btn) to the molecule and attaching it to covalently bound strepatvidin (Oshannessy *et al.*, 1992). Apart from allowing simple, reproducible immobilization of proteins and other ligands, the CMD matrix provides a more accessible environment for the interaction of immobilized proteins with those in solution than a monolayer. Proteins immobilized to a CMD matrix are also in an environment that more closely resembles a solution than those on a monolayer. Finally, a CMD matrix enhances the binding capacity and sensitivity of the measurements to binding events (Lofas *et al.*, 1991), and blocks non-specific adsorption of molecules to the Au surface (Lofas and Johnsson, 1990). Since proteins between 20 and 200 kDa show similar specific responses, the CMD matrix does not constrain their movement toward the immobilized ligand (Jonsson and Malmqvist, 1992). The signals obtained due to immobilization of protein to the CMD matrix, which extends between 100 and 200 nm from the gold surface, have been verified by parallel studies using radiolabeled proteins (Stenberg *et al.*, 1991).

When SPR is used to study biomolecular interactions, the immobilized biomolecule binds to an interacting species that is delivered through a flow system and the corresponding change in local protein concentration affects the refractive index as detailed in section 1.3.3 (Jonsson *et al.*, 1991). Due to the evanescent nature of the SPR wave, the changes sensed are restricted to the area in the vicinity of the metal/dielectric interface, encompassing the CMD matrix, and not past it (Salamon *et al.*, 1997; Stenberg *et al.*, 1991). Since proteins have a large molecular mass and all have comparable refractive index increment (RII -- an expression of how much a given material changes the refractive index of a solution as a function of mass) values, SPR has achieved great

success as a method for biomolecular interaction analysis (BIA) (Jonsson and Malmqvist, 1992; Perlmann and Longsworth, 1948). Many studies using BIAcore systems and CMD coated chips have been carried out on interactions between purified proteins (Allauzen *et al.*, 1995; Haimovich *et al.*, 1998; Moghaddam *et al.*, 2001; Ozawa *et al.*, 1999; Tufvesson and Westergren-Thorsson, 2002; Vales-Gomez *et al.*, 2001), purified and serum proteins (Cain *et al.*, 2000; Gonzales *et al.*, 2002; Haimovich *et al.*, 1998; Karlsson *et al.*, 1993; Laricchia-Robbio *et al.*, 1998; Takacs *et al.*, 1999; Vikinge *et al.*, 1998), nucleic acids (which have RII values comparable to protein; (Davis and Wilson, 2000)) (Asensio *et al.*, 1998; Bates *et al.*, 1995; Jensen *et al.*, 1997; Nilsson *et al.*, 1995; Sugimoto and Wakizaka, 1998; Sugimoto *et al.*, 2001; Wood, 1993; Zhao *et al.*, 2004), or between nucleic acids and proteins (Jost *et al.*, 1991; Polymenis and Stollar, 1995; Portmann *et al.*, 2004; Schade *et al.*, 1999; Tsoi and Yang, 2004; Yi *et al.*, 1999). Kinetic and equilibrium interaction constants can typically be extracted from these data. More recently, interactions between small molecules and protein (Karlsson and Stahlberg, 1995) or nucleic acids (Bischoff *et al.*, 1998; Ciolkowski *et al.*, 2000; Gambari *et al.*, 2000) have been studied directly, although in the case of small molecule drugs, corrections have to be made for their RII values, which can deviate substantially from those of proteins (Davis and Wilson, 2000). Typically, detection of binding of molecules below 2 kDa is problematic. However, in the case of drug molecules binding to nucleic acids, low molecular weight analytes can generate a significant signal if there is a stochiometric excess of drug molecule in the interaction.

1.3.3.2 Detection of Conformational Changes

Since the SPR signal is a product not only of n_d but also of d_d, it is possible to detect conformational changes in immobilized molecules (Boussaad *et al.*, 2000; Salamon *et al.*, 1997; Salamon *et al.*, 1997). This approach has been used to characterize deposition of small molecules on bare Ag (Salamon *et al.*, 1994) and Au surfaces, in the latter case with one (Sarkar and Somasundaran, 2004) or two (Peterlinz and Georgiadis, 1996; Peterlinz and Georgiadis, 1996) λ values used. Similarly, studies on monolayers of biomolecules using monochromatic techniques on Au (May and Russell, 2002; May and Russell, 2003) or Ag surfaces (Salamon *et al.*, 1994; Salamon *et al.*, 2000) as well as polychromatic techniques on Au (Georgiadis *et al.*, 2000; Peterlinz *et al.*, 1997; Peterson *et al.*, 2000; Peterson *et al.*, 2001; Peterson *et al.*, 2002) or Ag surfaces (Boussaad *et al.*, 2000) have all been undertaken. All studies discussed in this paragraph yielded detailed quantitative information on the thickness as well as the refractive index of the layer, extraction of which was facilitated by the fact that the studies were carried out on a monolayer rather than in a CMD matrix.

There have also been studies that claim to characterize conformational changes in proteins immobilized to CMD matrices (Mannen *et al.*, 2001; Sota *et al.*, 1998) that have since been found to be erroneous on the grounds that the signals observed were likely due to changes in electrostatic interactions between the immobilized protein and the CMD matrix induced by changes in pH (Paynter and Russell, 2002). Other studies of conformational changes in proteins immobilized to CMD matrices have proven (Flatmark *et al.*, 2001; Gestwicki *et al.*, 2001) to be well founded (Winzor, 2003). However, even

when considering these cases, studies on monolayers yielded more quantitative and unambiguous data than those on a CMD matrix, although the environment of the molecules bears less resemblance to those in solution than when using a matrix.

1.4 Nucleic Acid Immunogenicity

Unlike proteins, foreign nucleic acids do not universally provoke a response from mammalian immune systems. However, certain unusual conformations or repeating sequences can elicit an immune response with production of antibodies specific for the structure. In many cases, DNA with modifications to the bases or backbone are even more immunogenic than DNA with standard bases and a normal phosphate backbone. In addition, anti-DNA antibodies have been detected in SLE patients. Thus, anti-DNA antibodies have been of interest both for studying nucleic acid structure and the presence of unusual structures *in vivo* as well as for studies on SLE.

1.4.1 Antibodies specific for DNA

Although most dsDNA is not immunogenic, antibodies specific for DNA are present in the sera of patients or mice with SLE. SLE is an autoimmune disease in which tissues are damaged by pathogenic autoantibodies and immune complexes. There is no cure for SLE and the 20 year survival rate is between 63 and 75% (Hahn, 1998). The antibodies produced are specific for a variety of antigens including histones, immunoglobulin G antibodies (IgG), single- and dsRNA and DNA, phospholipids,

lymphocytes, and platelets. The prevalence of anti-DNA antibodies in SLE is high and increases as the disease progresses. Many of the antibodies are not sequence specific, and bind both single- and dsDNA (Zouali *et al.*, 1988).

A variety of anti-DNA antibodies from lupus-prone mice have been characterized and display a wide variety of specificities. Some bind exclusively to dsDNA with varying degrees of sequence specificity (Braun and Lee, 1986; Lafer *et al.*, 1981; Stollar *et al.*, 1986; Tanha and Lee, 1997) while others bind only to ssDNA (Lee *et al.*, 1982). Others bind either type of DNA (Swanson *et al.*, 1996). In no case was there as large a degree of sequence specificity as that which results from immunization with repeating sequence DNA.

Immunization of mice with repeating-sequence base- or phosphate backbone-modified DNA has shown that such sequences are capable of producing immune responses. Enhanced immunogenicity in modified sequences is believed to be due in part to the nuclease resistance imparted by phosphate backbone modifications. One study showed that some DNA sequences containing phosphorothioates were resistant to pancreatic nucleases, which could cause the DNA to be more immunogenic by having a longer half-life in the body (Latimer *et al.*, 1989). In some cases, the resulting antibodies were specific for the sequence used to elicit the response, and also bound the same sequence in the absence of base modifications (Latimer *et al.*, 1995; Lee *et al.*, 1985). In other cases, the antibodies produced displayed a similar non-specific response to those present in SLE sera or were specific only for the modified phosphate backbone (Latimer *et al.*, 1995).

Anti-DNA antibodies have also been obtained by immunization with M13 phage displaying peptide motifs, which bound to autoantibodies from lupus-prone mice. Some of the reactive epitopes displayed by the phage contained aromatic and negatively charged residues, which were believed to mimic the bases and phosphate backbone, respectively, of DNA (Sibille *et al.*, 1997).

1.4.2 Antibodies specific for unusual DNA conformations

Unlike normal dsDNA, unusual DNA conformations, particularly Z-DNA and triplex DNA, can be immunogenic. Since these conformations can be stabilized by base-modification, DNA containing modified bases is often used as an antigen to generate a response against the conformation in question. Like antibodies generated in SLE, these antibodies have a variety of sequence specificities and some bind only modified DNA while others bind unmodified DNA if it is in the correct conformation.

An early example of this technique employed chemically brominated $d(GC)_n$ to raise antibodies against Z-DNA (Lafer *et al.*, 1981). These antibodies bound both modified and unmodified DNA, provided it was in the Z conformation. Other antibodies recognizing different epitopes on the brominated DNA would not bind Z-DNA if it contained m^5C (Moller *et al.*, 1982). Similarly, antibodies have been raised against $d(Tm^5C)•d(GA)•d(m^5CT)$ which also bind to other triplex forming sequences, albeit with less specificity (Lee *et al.*, 1987). Other antibodies raised with the same triplex react also with unmodified polymers but not with triplexes of other sequences (Agazie *et al.*, 1994). As discussed in section 1.2.2.3, these two antibodies stained different regions of

eukaryotic chromosomes. Thus, it has been shown that in some cases, nucleic acids are immunogenic, particularly if they contain unusual bases, and that their immunogenecity can be due to the conformation they adopt.

1.5 Objective

The objective of this study was to gain a better understanding of the M-DNA conformation by further characterization of the conditions under which it forms using more developed versions of existing techniques as well as developing new techniques. Specifically, the effects of base substitutions, DNA concentration, temperature, and sequence on the equilibrium position of M-DNA formation as a function of pH or metal ion concetration were investigated. Differences between the M-DNA conformations induced by Zn^{2+}, Ni^{2+}, and Co^{2+} were also characterized and compared to the pH-dependent effects of Cd^{2+} on dsDNA. These experiments were designed with a view to testing the hypothesis that M-DNA formation occurs through substitution of the imino protons of G and T bases by the transition metal ions.

The goals of this study were accomplished in part using the EtBr based assay and fluorescence quenching techniques. These techniques have been modified greatly from their original forms for greater versatility. Two other techniques that had not previously been used to characterize the M-DNA conformation, ITC and SPR, were also employed in this study. Development of these assays has allowed new ways to measure M-DNA formation and shown properties of the conformation that would not be obtainable by

other methods. Finally, as another method to characterize the conformation, attempts were made to raise MAbs against M-DNA, but this did not succeed.

Accomplishment of these goals will allow progress toward potential applications of the M-DNA conformation, and will also facilitate structural studies by further defining the conditions under which M-DNA exists. Since M-DNA formation requires an elevated pH as well as the presence of transition metal ions whose solubility decreases with increasing pH, crystallization of the conformation has remained elusive. By characterizing M-DNA formation at lower pH values, more options for crystallization of the structure are available.

2.0 Materials and Methods

2.1 Reagents and Equipment

Item	Supplier
Biological Reagents	
Calf Thymus DNA (type I: sodium salt)	Sigma
Escherichia coli DNA (type VIII: sodium salt)	Sigma
Female Balb-C Mice	University of Saskatchewan Animal Resources
Fetal Bovine Serum	Gibco BRL
Freund's Complete Adjuvant	Sigma
Freund's Incomplete Adjuvant	Gibco BRL
I_{125}-labelled goat anti-mouse IgG	Pharmacia
Jel 42 IgG	Dr. J. Lee
Jel 274 IgG	Dr. J. Lee
Jel 352 IgG	Dr. J. Lee
Jel 542 IgM	Dr. J. Lee
λ phage DNA	Pharmacia
0.54 src-cat plasmid	Dr. K. Bonham
Streptavidin (dessicate)	Sigma
Taq DNA polymerase	Pharmacia
Tth DNA polymerase	Roche
Vent DNA polymerase	New England Biolabs
Chemical Reagents	
2-amino-2'-deoxyadenosine-5'-triphosphate	Trilink Biotechnologies
5-bromo-2'-deoxyuridine-5'-triphosphate	Trilink Biotechnologies
5-bromouridine	Sigma
$CdCl_2$	Fisher
$CoCl_2 \cdot 6H_2O$	Sigma
$Co(ClO_4)_2 \cdot 6H_2O$	Sigma
Concert Rapid PCR purification system	Gibco BRL
2-(*N*-cyclohexylamino)ethanesulfonic acid	Sigma
7-deaza-2'-deoxyadenosine-5'-triphosphate	Trilink Biotechnologies
2'-deoxyadenosine-5'-triphosphate	Pharmacia
2'-deoxycytidine-5'-triphosphate	Pharmacia

2'-deoxyguanosine-5'-triphosphate	Pharmacia
2'-deoxyinosine-5'-triphosphate	P-L Chemicals
2'-deoxythymine-5'-triphosphate	Pharmacia
2'-dexoxyuridine-5'-triphosphate	P-L Chemicals
Ethanolamine	BIAcore
Ethyldimethylcarbodimide	BIAcore
Ethylenediaminetetraacetic acid (disodium salt)	BDH
Ethylenediamine	Dr. M. Majewski
5-fluoro-2'-deoxyuridine-5'-triphosphate	Trilink Biotechnologies
5-fluorouridine	Sigma
HCl	E-M Science
Hepes-buffered saline	BIAcore
N-(2-hydroxyethyl)piperazine-*N*'-(2-ethanesulfonic acid)	Sigma
5-methyl-2'-deoxycytidine-5'-triphosphate	P-L Chemicals
$MgCl_2$	Sigma
$Mg(ClO_4)_2 \cdot 6H_2O$	Sigma
2-(*N*-morpholino)ethanesulfonic acid	Sigma
3-(*N*-Morpholino)propanesulfonic acid	Sigma
NaCl	Sigma
NaOH	BDH
N-hydroxysuccinimide	BIAcore
$NiCl_2 \cdot 6H_2O$	Sigma
$Ni(ClO_4)_2 \cdot 6H_2O$	Sigma
Polyoxyethylenesorbitan monolaureate	Sigma
Polsorbate-20	BIAcore
4-thio-2'-deoxythymine-5'-triphosphate	Trilink Biotechnologies
Tris[hydroxymethyl]aminomethane	Sigma
Uridine	Sigma
$ZnCl_2$	Sigma
$Zn(ClO_4)_2 \cdot 6H_2O$	Sigma

All metal ion solutions and buffers were supplied in solid form with a purity of 97.0 % or greater.

Supplies and Equipment

Accumet Basic pH electrode	Fisher
Absorbance Spectrophotometer 260	Gilford
BIAcore X	BIAcore
Disposable fluorescence cuvettes	VWR
Falcon tubes, 15 mL and 50 mL	VWR
0.20 μM filter discs	Nalgene
F-2000 fluorescence spectrophotometer	Hitachi
F-2500 fluorescence spectrophotometer	Hitachi
18- and 30-guage needles	Becton Dickinson
Micropipettors	Eppendorf

Model 4200 titration calorimeter	Calorimetry Sciences Corp.
Model 1271 Riagamma gamma counter	Wallac
96-well polyvinyl chloride plates	VWR
Mark II Abbe Refractometer	Leica
Quartz cuvettes	Fisher
Sensor chip CM4	BIAcore
Sensor chip SA	BIAcore
Single block easy cycler system	Ericomp
Syringes, 20 mL and 1 mL	Becton Dickinson

Synthetic DNA

Sequences Purchased from the University of Calgary Regional DNA Synthesis Lab

C-src-(–793)	5'-d(TGAGCAGCTTAGCATGGCGC)3'
C-src-(–277)	5'-d(GCAGACGGACGCACGGGAGG)3'
λ-13	5'-d(GCGGGTTTTCGCTATTATG)3'
λ-509	5'-d(CAGCGGAGTCTCTGGCATTC)3'

Sequences Purchased from the Plant Biotechnology Institute

A30	5'-Biotin-d(A_{30})3'
btn-CTL-2	5'-Biotin-d(CATTTGGTCGTGGAATGCGTAGTTAGCCAC)3'
C30	5'-Biotin-d(C_{30})3'
CTL-1	5'-d(GTGGCTAACTACGCATTCCACGACCAAATG)3'
CTL-2	5'-d(CATTTGGTCGTGGAATGCGTAGTTAGCCAC)3'
Fl-CTL-1	5'-Fluorescein-d(GTGGCTAACTACGCATTCCACGACCAAATG)3'
QSY7-CTL-2	5'-QSY7-d(CATTTGGTCGTGGAATGCGTAGTTAGCCAC)3'
T30	5'-Biotin-d(T_{30})3'

-Also ordered were 5FUCTL-1 and 5FUCTL-2, which are CTL-1 and CTL-2 sequences, respectively, with F^5U replacing T. 5FUCTL-2 is biotinylated on its 5' end.

2.1.1 Preparation of Divalent Metal Ion Solutions

All metal ion solutions were prepared by dissolving the solid compounds to 2.0 M concentration in 50 mL of double-distilled H_2O (ddH_2O). The solutions were then filtered through a 0.20 μM filter disc attached to a 20 mL syringe into a 50 mL falcon tube for storage. Due to its acidity, $Zn(ClO_4)_2$ was prepared to 100 mM otherwise it would

damage the filter. Prior to preparation, solid $ZnCl_2$ was heated to 120 °C overnight. Stock solutions of $ZnCl_2$ were acidified to a pH of 4.0 by addition of HCl to prevent precipitation unless otherwise specified. Working solutions for experiments were diluted from these stock solutions.

2.1.2 Purification of Ethylenediamine

Ethylenediamine (ED) was purified by distillation under vacuum with constant stirring using a standard distillation apparatus. The vacuum line ran through a dessicator and sand was used as a medium to conduct heat to the round-bottom flask. The boiling point of ED is normally 116 °C, but under vacuum, boiling was achieved at 91 °C. The ED was harvested and frozen at -20 °C until needed.

2.1.3 Determination of Thymidine Analogue pK_as

The pK_a values for F^5U and Br^5U were unavailable in the literature. Uridine, 5-bromouridine and 5-fluorouridine were dissolved to 10 mM and titrated with 1 N NaOH. The pH values obtained were plotted as a function of added NaOH concentration to determine the pK_a values. It was found that the 5-bromouridine had a pK_a of 8.2 while the corresponding value for 5-fluorouridine was 7.8. The pK_a values for s^4T and s^2 were also unknown and obtaining enough of the nucleosides for a pH titration was cost-prohibitive. Thus, the difference between the pK_a values of these analogues and the corresponding thiolated uracil analogues (Testa *et al.*, 1999) was assumed to be the same as the

difference between the pK_a values of U and T. This estimation gave pK_a values of 9.4 and 8.8 for s^2T and s^4T, respectively.

2.2 Nucleic Acids

All nucleic acid concentrations are expressed in molarity of phosphates. This standard applies to single-stranded and ds- DNA or RNA. In all cases, solutions of nucleic acids were stored at -20 ˚C when not in use and thawed at room temperature. While in use, nucleic acid stock solutions were kept on ice.

2.2.1 Genomic DNA

CT and *E. coli* DNA were purchased as a sodium salt in a dessicated form. In either case, the DNA was dissolved in 10 mM NaCl, 10 mM TRIS-HCl pH 8.0 to at least 1.5 mM and diluted to different concentrations in various buffers depending on the experiment. Final DNA concentrations were determined by A_{260} using quartz cuvettes in an absorbance spectrophotometer with a zero concentration standard being buffer containing no DNA.

2.2.2 Production of Nucleic Acids by PCR

All PCRs contained 0.25 mM of each dNTP, 15 μM of template DNA and 9.6 μM of each primer. The appropriate buffer (as suggested by the supplier) was used for each

polymerase, and Mg^{2+} concentrations were optimised separately for each different PCR. Cycling conditions were 30 sec each at 94, 45 and 72 °C for *Taq* and *Vent* DNA polymerase. PCRs with *Tth* DNA polymerase were cycled at 94 °C for 2 min, then 10 cycles of 94 °C for 30 sec, followed by 50 °C for 30 sec, followed by 72 °C for 45 sec. Twenty more cycles followed, with each successive 72 °C step being elongated by 5 sec and a final 72 °C step of 2 min. All DNA produced by PCR was purified using the Concert Rapid PCR purification system. DNA concentrations were verified by A_{260} or by the standard EtBr fluorescence assay.

The length of PCR products was determined by agarose gel electrophoresis. The samples, along with a molecular weight standard, were loaded into 10 cm long 2% (w/v) agarose gels. The running buffer for the electrophoresis and the liquid component of the gel were composed of 40 mM TRIS-Acetate pH 8.0, 20 mM sodium acetate, and 0.1 mM EDTA. The samples were electrophoresed at 80 V and 100 mA for 2h then stained with 2.0 μg/mL EtBr. The gels were then photographed under illumination by UV light at 365 nm.

2.2.2.1 DNA Containing Standard Bases

Template DNA for amplification by PCR was either λ phage DNA or a plasmid, 0.54 src-cat, containing the human c-*src* proto-oncogene. Primers for the λ genome amplified between bases 13 and 509; 496 bp total with a GC content of 54%. The primers used were λ-13 and λ-509. Primers for the 0.54 src-cat plasmid amplified a 73% GC 516 bp region between bases –793 and –277 of the upstream non-coding sequence of the c-*src*

gene. The primers used were C-src-(–793) and C-src-(–277). Both reactions were catalyzed by *Taq* DNA polymerase.

2.2.2.2 DNA Containing Modified Bases

All PCRs with modified bases employed λ phage DNA as a template and λ-13 and λ-509 as primers. Substitution of 5-methyl-2'-deoxycytidine-5'-triphosphate for 2'-deoxycytidine-5'-triphosphate was performed with *Vent* DNA polymerase. Substitutions of 2-amino-2'-deoxyadenosine-5'-triphosphate for 2'-deoxyadenosine-5'-triphosphate and of 4-thio-2'-deoxythymine-5'-triphosphate for 2'-deoxythymine-5'-triphosphate required *Tth* DNA polymerase. All other substitutions were performed with *Taq* DNA polymerase. Reaction concentrations of all modified dNTPs were 0.25 mM. Reactions with 4-thio-2'-deoxythymine-5'-triphosphate contained 25 % 2'-deoxythymine-5'-triphosphate and had an incorporation efficiency of s^4T of 75 % as judged by absorbance at 340 nm.

2.2.3 Repeating Sequence DNA

The synthetic DNAs $d(GC)_n$, $d(AU)_n$, $d(G)_n \bullet d(C)_n$, $d(A)_n \bullet d(T)_n$, and $d(GGCC)_n$, were gifts from J.S. Lee. Synthetic RNA $r(AU)_n$ and synthetic DNAs $d(AT)_n$, $d(TG \bullet CA)_n$, $d(As^2T)_n$, $d(As^4T)_n$, $d(s^2TG)_n \bullet d(CA)_n$, and $d(s^4TG)_n \bullet d(CA)_n$ were gifts from M.J. Dinsmore.

2.2.4 Oligonucleotides

All PCR primers and labelled oligonucleotides were purchased in a dessicated form. PCR primers were dissolved in ddH_2O to 100X of the concentration needed for the PCR. Other oligonucleotides were also purchased in a dessicated form and dissolved in ddH_2O to between 10X and 200X concentration. In either case, oligonucleotides were synthesized by phosphoramidite chemistry and btn, Fl, or QSY7 were attached via standard six carbon linkers to the 5' end of the sequence.

2.3 Ethidium Fluorescence Assay

A standard fluorescence assay was used to quantify DNA out as follows. The standard quantitation ethidium fluorescence buffer (QEFB) consisted of 1.0 mM EDTA, 0.5 μg/mL EtBr (approximately 1.3 μM), and 10 mM TRIS-HCl pH 8.0. A 10 μL aliquot of DNA was added to 2 mL QEFB and the fluorescence at 600 nm resulting from excitation at 525 nm recorded. All fluorescence experiments were carried out on either a Hitachi F-2000 or F-2500 fluorescence spectrophotometer. The response to DNA concentration is linear when aliquots of 0.015 - 0.30 mM are added; concentrations higher than this can be assayed accurately by adding aliquots smaller than 10 μl. The assay was standardized with an aliquot of 150 μM dsDNA. Detection of M-DNA was possible in a different ethidium fluorescence buffer (Zn-EFB) that contains 0.20 mM $ZnCl_2$, 0.5 μg/mL EtBr, and 10 mM buffer; a 10 μL aliquot of DNA was added to 2 mL Zn-EFB and the fluorescence read in the same manner as with QEFB. The pH and buffer

used to make Zn-EFB depend on the individual experiment. Data from the experiments detailed in section 2.3.4 were plotted as percent B-DNA remaining, with 100% being set at the fluorescence value obtained at pH 6.0. Data for other M-DNA assays were plotted as percent fluorescence, with 100% being set at the fluorescence value obtained in the absence of Zn^{2+}, Ni^{2+}, or Co^{2+}. All EtBr fluorescence readings were obtained at room temperature (21 ˚C) and all incubations were carried out at room temperature unless otherwise specified.

2.3.1 Preparation of Nucleic Acids

All of these assays use either genomic, PCR product, or repeating-sequence DNA. All were prepared as detailed in section 2.2 and purified or dissolved to either 10X concentration in 100 mM NaCl, 40 mM 2-(*N*-cyclohexylamino)ethanesulfonic acid (CHES) pH 9.0 or 1X concentration in 10 or 20 mM buffer, 10 mM NaCl. In the latter case, the buffer and pH used depend on the particular experiment carried out. Concentrations were verified by A_{260} as well as by QEFB.

2.3.2 Detection of M-DNA Formation and Stability with Zn^{2+}, Ni^{2+}, and Co^{2+}

Aliquots of 100 µl of 15 µM λ496mer in 10 mM NaCl, 4 mM CHES pH 9 were converted to M-DNA by addition of 0.2 mM $ZnCl_2$, 0.3 mM $NiCl_2$ or 0.5 mM $CoCl_2$. The aliquots were incubated for 2 h with and without metal ion added. Following M-DNA formation, 100 µl of 25 mM buffer with 10 mM NaCl was added to the incubation, giving

a final DNA concentration of 7.5 μM and the metal ion concentration was adjusted to 0.25 mM in all cases. The pH values of the buffers added were 5.0, 5.5 (sodium acetate), 6.0, 6.5 (2-[*N*-morpholino]ethanesulfonic acid [MES] buffer), 7.0 (*N*-[2-hydroxyethyl]piperazine-*N*'-[2-ethanesulfonic acid] [HEPES]), 7.5, 8.2, 8.5 (TRIS buffer), and 9.0 (CHES buffer). The mixture was allowed to incubate for 10 min, then assayed immediately in Zn-EFB, pH 8.3, before and after addition of 1.0 mM EDTA to the Zn-EFB. Hysteresis experiments with incubations times of 30 or 60 min showed similar results to those with the 10 min incubation time, and so these conditions were considered to be under equilibrium. The readings at the lowest three pH values were averaged and used as a 100% B-DNA standard against which the other readings were normalized.

2.3.3 Slow Reversion of Ni(II) M-DNA

A 75 μM solution of CT DNA in 10 mM NaCl, 20 mM CHES pH 9.0 was incubated in the presence of 0.5 mM $NiCl_2$ or $CoCl_2$ for 2 h to form M-DNA. Following this, EDTA was added at concentrations between 0.1 and 1.0 mM. Aliquots of 20 μl were then taken at intervals over a 22h period and the fluorescence measured immediately in Zn-EFB, pH 8.3, before and after addition of 1.0 mM EDTA to Zn-EFB. The values obtained were normalized against a value obtained from DNA in the absence of divalent metal ion.

2.3.4 Effect of DNA concentration on M-DNA formation

CT-DNA was dissolved in 10 mM NaCl, 20 mM TRIS–HCl pH 8.5 or 20 mM CHES pH 9.0 to concentrations of 4.5, 7.5, 15, 45, 75, 150 and 450 μM. $ZnCl_2$, $NiCl_2$ and $CoCl_2$ were added to aliquots of the DNA over a concentration range of 0.1–1.0 mM and incubated for 2 h. Following incubation, aliquots containing 1.3 nmol of DNA were added to 2 mL of Zn-EFB, pH 8.3, and fluorescence measured immediately before and after addition of EDTA. The concentration of metal ion required for 50% M-DNA formation was estimated by interpolation from a graph obtained by normalizing all readings against one of the same concentration in the absence of divalent metal ion.

2.3.5 Detection of Zn(II) M-DNA Formation in 54% GC DNA with Modified Bases and Repetitive Sequence DNA.

Aliquots of 100 μl of 15 μM DNA in 10 mM NaCl, 4 mM CHES pH 9.0 were converted to M-DNA by addition of 0.2 mM $ZnCl_2$ and incubation for 2 h. Following M-DNA formation, 2 mL of Zn-EFB was added to each sample, as well as to samples of B-DNA, giving a final DNA concentration of 0.71 μM. Zn-EFB preaparations of six pH values were used: pH 6.0 with MES buffer, pH 7.5, 7.75, 8.0, 8.3 and 8.6 with TRIS–HCl buffer. The aliquots were incubated in the Zn-EFB for 30 min then the fluorescence was measured before and after addition of 1.0 mM EDTA. This procedure was applied for $d(AT)_n$, $d(AU)_n$, $r(AU)_n$, $d(GC)_n$, $d(A)_n$•$d(T)_n$, $d(G)_n$•$d(C)_n$, $d(GGCC)_n$, the c-*src* 516 bp fragment, and the λ 496 bp fragments containing standard bases as well as substitutions

of n^2A, z^7A, m^5C, I, U, Br^5U, F^5U for their respective standard bases, and a double-substituted sequence containing I and Br^5U.

A slightly modified procedure was also used in which 10 μL 150 μM DNA in 5 mM NaCl, 10 mM CHES pH 9.0 was added to 2 mL of Zn-EFB, giving a final DNA concentration of 0.71 μM. Eight pH values of Zn-EFB were used: pH 6.0 with MES buffer, pH 7.0 and 7.2 with 3-(*N*-Morpholino)propanesulfonic acid (MOPS), and pH 7.6, 7.8, 8.0, 8.2, and 8.4 with TRIS-HCl buffer. The aliquots were incubated in the Zn-EFB for 30 minutes then the fluorescence measured before and after addition of 1.0 mM EDTA. This procedure was applied for $d(AT)_n$, $d(As^2T)_n$, $d(As^4T)_n$, $d(TG•CA)_n$, $d(s^2TG)_n•d(CA)_n$, and $d(s^4TG)_n•d(CA)_n$. In either procedure, all measurements were normalized against the pH 6.0 values for each sequence.

2.3.6 Effect of Temperature on M-DNA Formation

CT DNA of 15 μM concentration was incubated in 10 mM NaCl, 10 mM TRIS-HCl, pH 8.5 in the presence of various $Zn(ClO_4)_2$ concentrations at temperatures of 4, 10, 21, and 37 °C for 2 h; the long incubation time ensured that the measurements were taken under equilibrium conditions. The pH values of each TRIS buffer were set at the temperatures used in the experiment. Aliquots of 100 μL were then added to 2 mL of pH 8.3 Zn-EFB at room temperature and the fluorescence measured under constant stirring. Fluorescence values were measured before and after the addition of EDTA. All data were plotted as a percentage of the fluorescence intensity observed prior to EDTA addition for the 0 mM $Zn(ClO_4)_2$ reading.

2.4 Isothermal Titration Calorimetry

2.4.1 Preparation of Nucleic Acids

CT and *E. coli* DNA were dissolved in 10 mM NaCl, 10 mM Tris-HCl pH 8.0 to a concentration of 0.75 mg/mL. The DNA solutions were then sheared by being passed through a 30-guage needle five times under maximum thumb pressure. Working solutions were diluted to final concentrations of 50 and 100 μg/mL in 10 mM NaCl, 10 mM Tris-HCl, pH 7.5 or 8.5.

2.4.2 Detection of DNA-Metal Interactions

Enthalpies were measured using a CSC Model 4200 isothermal titration calorimeter with 1.3 mL cells. The sample and reference cells were filled with 1.0 mL of DNA or buffer and 1.1 mL of buffer solution, respectively. A 2.5 mM solution of either $Zn(ClO_4)_2$ or $Mg(ClO_4)_2$ was injected in 10-μL increments every 10 min into the sample cell using a 250-μL Hamilton syringe controlled by the injection apparatus of the instrument. A stir rate of 150 rpm was maintained in the sample cell throughout the experiment. The same titrants were added to buffer solutions without DNA; these data were subtracted from the readings obtained in the presence of DNA to account for the heat of dilution. All of these measurements were carried out at 25 (±0.02) °C.

2.5 Surface Plasmon Resonance

A BIAcore X SPR biosensor was used for all measurements. The sensor chips used were the SA variety, which consist of a CMD matrix with covalently bound streptavidin. This allows easy immobilization of biotinylated oligonucleotides.

2.5.1 Preparation of Nucleic Acids

A total of seven sequences were employed in this study: CTL-1, 5FUCTL-1, CTL-2, 5FUCTL-2, A30, C30, and T30. All oligonucleotides were supplied as a dessicate and dissolved in ddH_2O to at least 150 μM then diluted into TBS buffer (150 mM NaCl, 3.4 mM EDTA, 0.005 % polysorbate-20, and 10 mM TRIS-HCl pH 7.4) prior to use.

2.5.2 Preparation of Surface

Prior to exposure to nucleic acids, the sensor chips were treated with several 8 μL pulses of 50 mM NaOH 1 M NaCl over both flow cells at a flow rate of 20 μL/min to remove loosely bound streptavidin. This was repeated until no further decrease in baseline on either flow cell was observed upon pulsing, corresponding to a decrease of up to 800 RU, or 800 pg/mm^2 of protein. Following this, both flow cells were exposed to 30 μL of CTL-1 at 21 μM in TBS at 5 μL/min to verify that the DNA did not attach non-specifically to the surface. Biotinylated sequences btn-CTL-2, 5FUCTL-2, A30, C30, and

T30 were prepared to 0.21 μM in TBS buffer. Each sequence was immobilized on a separate sensor chip SA by injecting the appropriate DNA solution over flow cell 2 at a flow rate of 5 μL/min with the manual injection command, so that the response due to immobilization could be ascertained 1 minute after a small amount of DNA was added, and then more added incrementally until a response of about +185 RU was achieved. In the case of CTL-2 or 5FUCTL-2, hybridization was then verified by injection of 30 μL CTL-1 or 5FUCTL-1 at 21 μM concentration with a flow rate of 5 μL/min. Thus, duplexes with F^5U on either strand, both strands, or neither strand were generated. This allowed 0, 6, 9, or 15 modified bases to be present in the dsDNA sequence.

A CM4 sensor chip was also used in these experiments as a possible means to reduce background binding. Prior to binding nucleic acids, strepatvidin was immobilized on the surface of the chip. These procedures were carried out at a flow rate of 5 μL/min in HEPES-buffered saline (150 mM NaCl, 3.0 mM EDTA, 0.005 % polysorbate-20, and 10 mM HEPES pH 7.4). The carboxyl groups of the CMD matrix were activated by exposure of the surface to 35 μL of a 0.1 M 1:1 mixture of N-hydroxysuccinimide and ethyldimethylcarbodimide. Immobilization of streptavidin was performed by injection of 95 μL of 400 μg/mL streptavidin in 10 mM Acetate pH 5.0. Following this, deactivation of the surface was carried out by exposure to 35 μL of 1.0 M either ethanolamine or ethylenediamine.

2.5.3 Detection of DNA-Metal Interactions

Most of these experiments used 10 mM NaCl, 10 mM TRIS-HCl pH 7.5 or 8.5 as a flow buffer and were conducted at a flow rate of 50 μL/min. Others, as noted, were performed in 10 mM MES pH 6.5, 10 mM NaCl. Following hybridization (in the case of dsDNA assays), a 100X stock solution of $MgCl_2$, $CaCl_2$, $ZnCl_2$, $NiCl_2$, $CoCl_2$, or $CdCl_2$ was dissolved in flow buffer and 100 μL of this solution was immediately injected over both flow cells. The signals resulting from interactions between the metals and the CMD matrix with streptavidin in flow cell 1 were then subtracted from those obtained on flow cell 2. All sensorgrams shown in figures and all response levels discussed have this baseline subtraction taken into account. One minute after the end of the metal chloride injection, 80 μL of TBS was injected over both flow cells followed by a wash procedure (which the BIAcore X performs automatically upon request) to regenerate the surface, then five minutes were allowed for the baseline to reestablish before another injection of metal chloride was performed. The necessity of this step was judged according to whether the signal on flow cell 1 had returned to baseline as well as that on flow cell two. This procedure was performed on each of the nucleic acids detailed above, and in the case of btn-CTL-2, the assay was performed on the ssDNA as well as on the duplex formed between it and its compliment, CTL-1; hereafter this duplex is referred to as dsCTL. In the case of dsCTL, when 10% or more of the DNA was denatured during the exposure to metal ions, 10 μL of 21 μM CTL-1 was injected over both flow cells to regenerate the dsCTL. All spectra shown are averaged from between 2 and 5 individual readings.

2.5.3.1 BIAcore Maintenance

It is important to note that when doing experiments of this nature, it is possible that metal ion precipitates will deposit in the integrated microfluidics cartridge (IFC) which delivers analytes to the DNA surface. Thus, once per 10 hours of experiments, a customized cleaning procedure was performed. A maintenance chip, which is essentially a glass surface with no gold, was docked and Millipore water was primed twice and unclogged once (prime and unclog are preset procedures which the BIAcore X can perform). The same procedure was then repeated with 100 mM HCl and Millipore water again. Both solutions were heated to ~55 °C prior to cleaning. A sensitivity check was then performed to verify that the IFC was not plugged. These procedures were carried out in addition to standard "desorb" and "sanitize" protocols which are used to clean the BIAcore X.

2.5.4 Estimation of the SPR Response due to Increased Mass

The RII values of Ni^{2+} and Zn^{2+} were not available in the literature. Thus, the RII values of $NiCl_2$ and $ZnCl_2$ were obtinaed. A Leica Mark II Abbe refractometer was used to measure the refractive index values of solutions of the two metal chlorides between 20 mM and 1.0 M concentration. These values were then plotted against concentration and the slope of the resulting linear response is taken as the RII value. This value was then used to estimate the maximum SPR responses due to increased mass on the surface.

The maximum SPR response due to increased mass on the surface was predicted with the following formula, as described in (Davis and Wilson, 2000). The value $(RU_{pred})_{max}$ is defined as:

(1) $$(RU_{pred})_{max} = \frac{RU_L \times MW_A \times RII_A}{MW_L \times RII_L}$$

Where RU_L is the level of immobilization of the ligand in RU; MW_A and MW_L are the molecular weights of the analyte and ligand, respectively; and RII_A and RII_L are the refractive index increments of the analyte and ligand, respectively. This value is then multiplied by the stoichiometry of the interaction (analyte:ligand) to obtain the value $(RU_{pred})_{sat}$. The $(RU_{pred})_{sat}$ value is the estimated maximum response due to the interaction.

This calculation works well for systems in which the analyte is either a macromolecule or a small molecule with sufficient mass for the contribution due to mass to be the main factor in determining the SPR signal. In the case of metal ions binding to DNA, this becomes complicated by the fact that other ions will be displaced to some degree. However, as discussed in section 1.2, ions have different affinities for different sites on DNA and it is not simple to predict to what degree monovalent ions binding to the DNA will be displaced by the divalent metal ion being treated as the analyte. Thus, these calculations assume that no mass in Na^+ is lost, making it likely that the signal due to increased mass is overestimated and therefore provides only an estimate which should at least be correct as to the order of magnitude of the signal.

2.6 Fluorescence Quenching of Fluorophore-labelled DNA

2.6.1 Preparation of Nucleic Acids

Oligonucleotides were dissolved to concentrations of at least 1.5 mM in ddH_2O and diluted to 150 μM in 10 mM NaCl, 10 mM TRIS-HCl pH 8.0. Hybridization was carried out at room temperature for four hours in the dark. Two duplexes were generated: Fl-CTL-1/CTL-2 and Fl-CTL-1/QSY7-CTL-2.

2.6.2 Quenching Studies

A 20 μL aliquot of DNA at 0.15 mM was diluted into 2 mL of 10 mM Buffer with 10 mM NaCl to a final DNA concentration of 1.5 μM. The buffers and pH values employed were as follows: MES pH 6.5, HEPES pH 7.0, TRIS pH 7.5, TRIS pH 8.0, and TRIS pH 8.5. The emission spectrum of Fl was then taken from 500-800 nm following excitation at 490 nm. A peak in the fluorescence was observed around 520 nm with an intensity dependent on the pH. Five μL aliquots of 400X $ZnCl_2$, $MgCl_2$, or $CdCl_2$ were added to the cuvette, stirred for 30 sec, then another spectrum was taken 5 min after addition of metal ion. The increments were 0.02 mM at pH 8.5, 0.04 mM at pH 8.0, 0.20 mM at pH 7.5, 1.00 mM at pH 7.0, and 2 mM at pH 6.5. The fluorescence intensity at a given concentration of metal ion (f) was divided by the initial fluorescence intensity (f_0) to calculate the percent quenching. The values obtained from the Fl-CTL-1/QSY7-CTL-2

duplex were divided by those obtained from the Fl-CTL-1/CTL-2 duplex to account for background quenching of the Fl by metal ions. All spectra shown are the average of at least three independent trials.

2.7 Production of Antibodies Specific for M-DNA

2.7.1 Preparation of Nucleic Acids

I- and F^5U-substituted λ 496mers were produced by PCR and purified to 0.40 mM in 10 mM NaCl, 10 mM CHES pH 9.0. They were then converted to M-DNA by addition of either 10 mM $NiCl_2$ or 2 mM $ZnCl_2$. The DNA for the solid-phase radioimmuno assay (SPRIA) was diluted to 6 μM in the same buffer and converted to M-DNA by incubation with 0.20 mM $NiCl_2$ or $ZnCl_2$. The target DNA for the SPR-based immunoassay was the CTL-1/CTL-2 duplex and was prepared as described in section 2.5.2.

2.7.2 Immunization of Mice

Female Balb/c mice were immunized with 100 μL of a 1:1 mixture of M-DNA and Freund's complete adjuvant on day 1 using an 18 guage needle. They were reimmunized with a 1:1 mixture of M-DNA and Freund's incomplete adjuvant on days 10, 20, and 30. On days 13, 23, and 33, a blood sample of at least 20 μL was collected by tail bleeding. This was used for immunological assays. As a control, mice immunized with only buffer and $NiCl_2$ or $ZnCl_2$ as well as mice that were not immunized at all were

also bled at the same intervals and assayed. Two mice were immunized with each combination of metal ion and base substitution, as well as two of each class of control mice. After collection, the blood was centrifuged in a microcentrigue to separate the serum from the cells and the serum was harvested while the cells were discarded.

2.7.3 Solid-Phase Radioimmuno Assay

The SPRIA was performed on each blood sample. The wells of a 96-well polyvinyl chloride plate were coated with M-DNA by incubation with 50 μL of 6 μM M-DNA in each plate for 2 h. The serum was then diluted 1:1 in 20 mM TRIS-HCl pH 8.5, 20 mM NaCl, 1.0 % (v/v) fetal bovine serum, and 0.20 mM $ZnCl_2$ and then added to the second well. The contents of the second well were then diluted 1:1 with those of the third and a similar procedure was in turn applied to each successive well up to the twenty-third well. The first well was incubated only in the presence of the secondary antibody to determine background binding to the DNA. As a control, the test was repeated with Jel 274, an anti-DNA IgG, as well as Jel 42, an anti-protein IgG, Jel 352, a catalytic IgG, and Jel 542, an anti-protein IgM, for the serum to determine the specificity of the response. All purified antibodies were diluted 1:1 with the same buffer as the serum from a 0.67 mg/mL stock solution. Antibody concentrations were determined by UV absorbance at 280 nm. Following incubation with the serum or primary antibody for 4 hours, the wells were washed three times with 20 mM TRIS HCl pH 8.5, 20 mM NaCl, 0.05 % (v/v) polyoxyethylenesorbitan monolaureate, and 0.20 mM $ZnCl_2$ and exposed to approximately 50,000 counts per minute of I^{125}-labelled goat anti-mouse IgG for 2 hours.

The plates were then washed again and the radioactivity was measured in a gamma counter. The relative responses to antigen provoked in the mice could thus be assessed. As a control, the same procedure was also performed in the absence of $ZnCl_2$ with B-DNA coated plates.

2.7.4 Surface Plasmon Resonance Immunoassay

As an alternative to the SPRIA, an SPR-based immunoassay was also performed. The SPR immunasssay was carried out by exposing serum diluted 1/40 or 1/80 into 10 mM TRIS-HCl pH 7.5 or 8.5, 10 mM NaCl, which was also used as a running buffer, to the dsCTL surface. The sera used were from either pre-immunized mice or mice immunized with F^5U substituted Zn(II) or Ni(II) M-DNA. These assays were performed after exposing the surface to 0.20 mM $ZnCl_2$ or $NiCl_2$ using the three applications wash command followed by replacement of the running buffer with one containing the metal ion being used to convert the dsCTL to M-DNA. The metal ion used to form M-DNA was in all cases the same one used to form the M-DNA with which the mice were immunized. They were also performed in the absence of added metal ion. When antibodies bound the DNA, dissociation was achieved by injecting 30 μL of 10 mM acetate pH 5.0 with 1.0 M NaCl. All experiments were performed at 25 °C and a flow rate of 5 μL/min.

3.0 Results

3.1 Preparation of M-DNA-Specific Antibodies

Antibodies to M-DNA were to be prepared in order to provide another method of detecting M-DNA. This would be applicable to *in vitro* studies aimed at characterization of the conformation as well as detection of M-DNA *in vivo*. Further, if antibodies specific for M-DNA (with lower or no specificity for B-DNA) were produced, this would provide additional confirmation that the conformation is unique. Due to its great stability as a function of pH (see section 3.2.4) I- and F^5U-substituted DNA was used to form the M-DNA with which the mice were immunized. No adverse effects were observed in the mice immunized with M-DNA or control preparations. All assays with serum from immunized animals were performed with serum from the final serum collection.

3.1.1 Solid Phase Radioimmuno Assay

The SPRIA is a well-established immunological procedure to detect and characterize serum antibodies. Mice immunized with either I- or F^5U-substituted Ni(II) M-DNA both showed slightly higher binding against B-DNA following immunization, but when assays were conducted in the presence of Zn^{2+}, all sera showed very high responses regardless of whether they were harvested before or after immunization, suggesting that a non-specific interaction was producing the signals. These results are illustrated in figure 3.1. Further, Jel 274, an IgG specific for B-DNA, also showed higher

responses against M-DNA than B-DNA as shown in figure 3.2. Finally, as shown in figure 3.3, incubation with Jel 541 (an IgM specific for protein) as a primary antibody produced even higher counts than Jel 274, serum immunized against F^5U-containing DNA, or pre-immunization serum. IgG antibodies specific for proteins, Jel 42 and 352, gave small signals in the presence or absence of added metal ions. Thus, it appeared that IgM molecules were giving rise to non-specific interactions with the DNA mediated by the metal ions. All SPRIA data shown are single experiments that are representative of at least three independent trials.

3.1.2 Surface Plasmon Resonance

One of the chief applications of SPR-based biosensors is to detect the presence of and characterize antibodies. A procedure for serum detection of anti-M-DNA antibodies was performed on immobilized dsCTL. These experiments were carried out multiple times and representative results will be described. Responses of serum samples from the Zn(II) M-DNA immunized mice are shown at a serum dilution of 1:40 in figure 3.4. The responses are higher for immunized serum than pre-immunized serum and in either case are higher in the presence of Zn^{2+}. However, the increased response in the presence of Zn^{2+} is not pH dependent and the overall responses are much higher at pH 7.5 than at pH 8.5. The responses of serum samples from Ni(II) M-DNA immunized mice are shown at the same dilution in figure 3.5. As with the samples in the presence of Zn^{2+}, responses were higher at pH 7.5 than 8.5 and higher in the presence of Ni^{2+} regardless of pH or whether the sample was from an immunized animal. Unlike the Zn^{2+} samples, in some

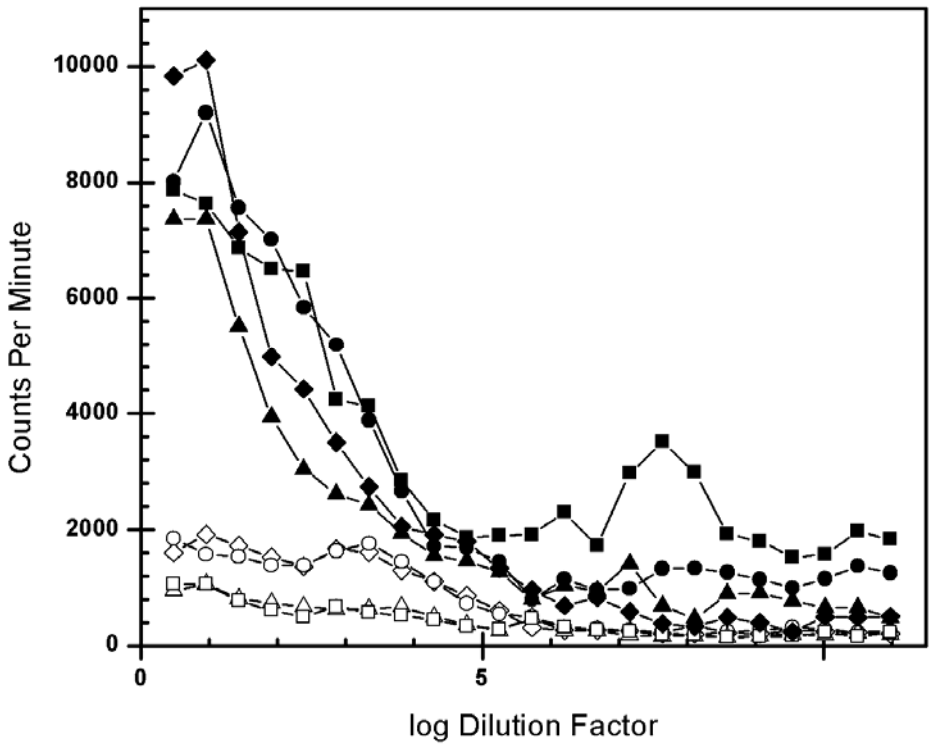

Figure 3.1: SPRIA results obtained with serum from mice immunized with I- (circles) or F^5U-substituted DNA (diamonds) as well as with serum harvested from each mouse prior to immunization (squares and triangles, respectively). The white symbols are against B-DNA while the black symbols are against M-DNA.

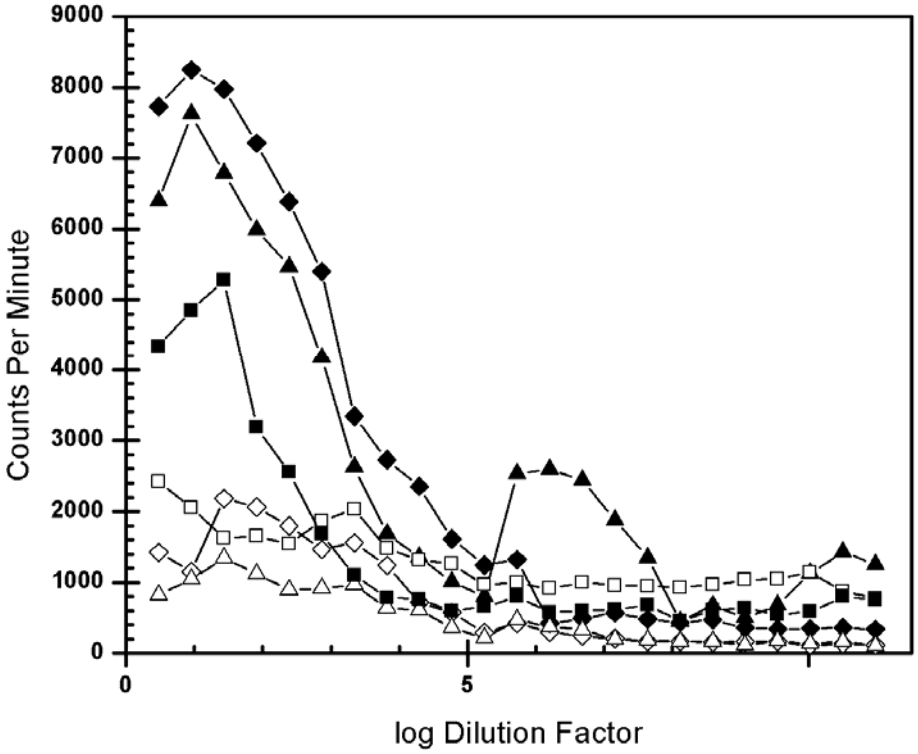

Figure 3.2: SPRIA results obtained with serum from mice immunized with F^5U-substituted DNA (diamonds), serum harvested prior to immunization (triangles), and with an anti-DNA IgG, Jel 274 (squares). The white symbols are against B-DNA while the black symbols are against M-DNA.

(**A**)

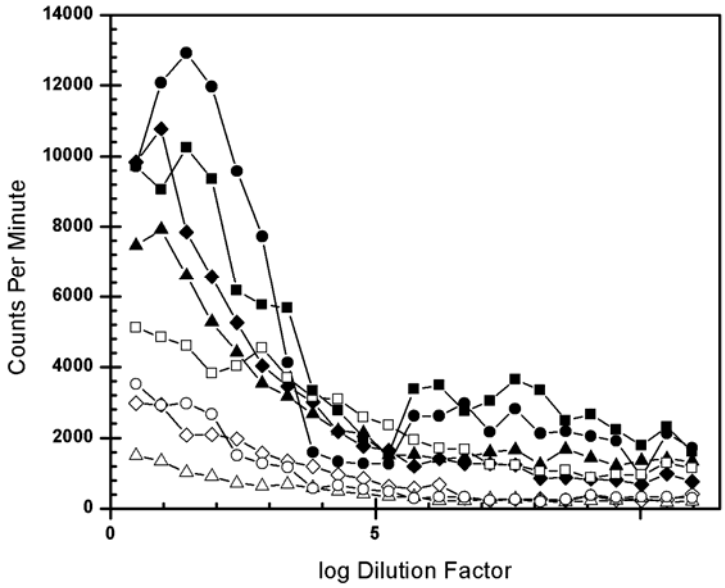

(**B**)

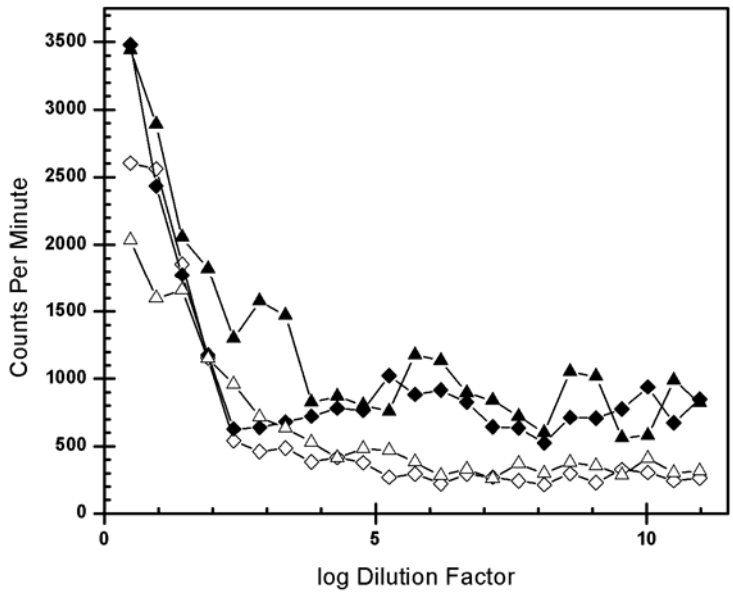

Figure 3.3: (**A**) SPRIA results obtained with serum from mice immunized with F^5U-substituted DNA (diamonds), serum harvested prior to immunization (triangles), an anti-DNA IgG, Jel 274 (squares), and an anti-protein IgM, Jel 542 (circles). (**B**) SPRIA results obtained from an anti-protein IgG, Jel 42 (triangles) and a catalytic phophatase abzyme, Jel 352 (diamonds). The white symbols are against B-DNA while the black symbols are against M-DNA.

(**A**)

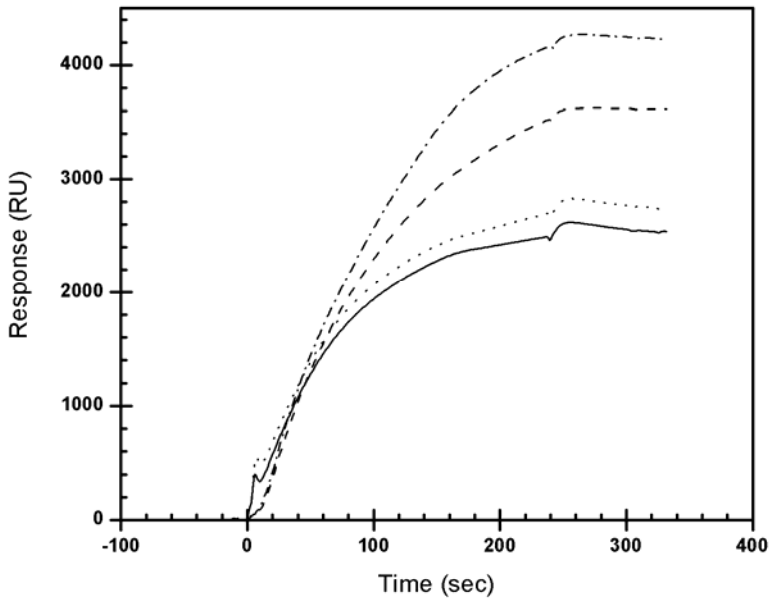

(**B**)

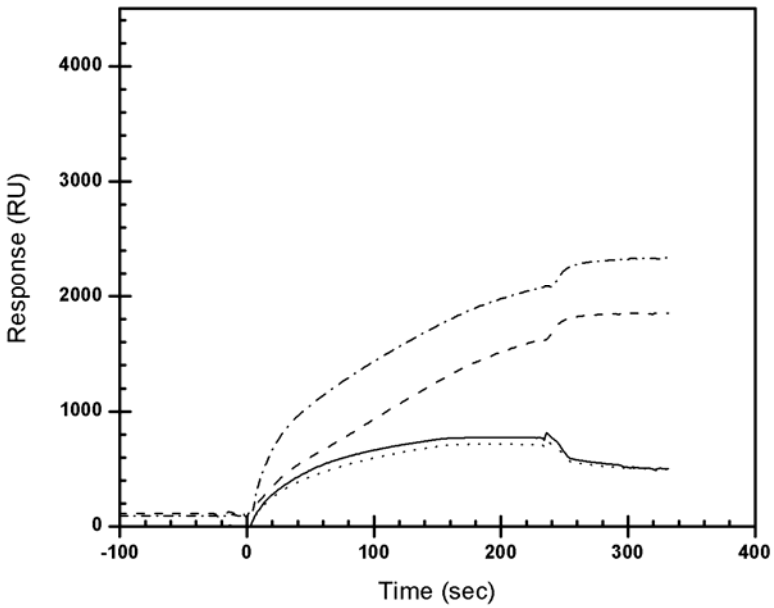

Figure 3.4: SPR responses from exposure to serum harvested before (solid lines) and after (dotted lines) immunization with Zn(II) F^5U-substituted M-DNA. Pre- (dashed lines) and post-immunization (dot-dashed lines) in the presence of 0.20 mM Zn^{2+} in the running buffer are also shown. The responses are shown at pH 7.5 (**A**) and pH 8.5 (**B**).

(**A**)

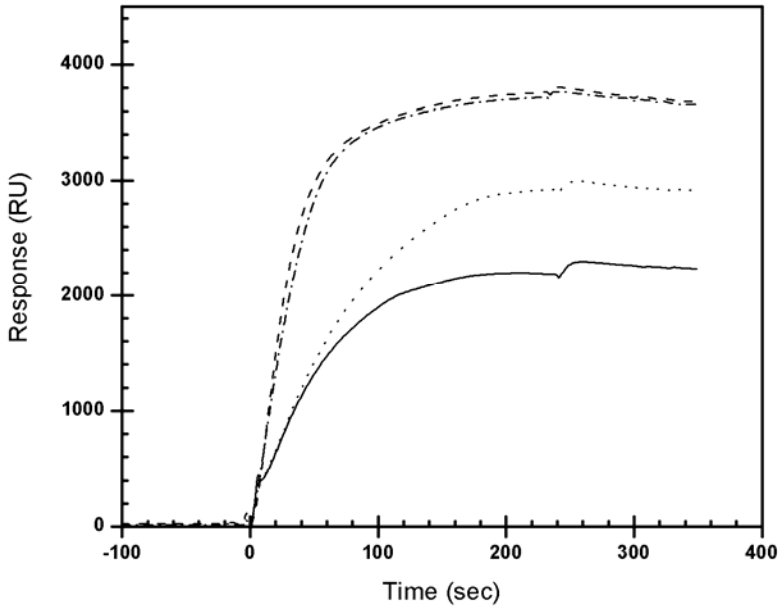

(**B**)

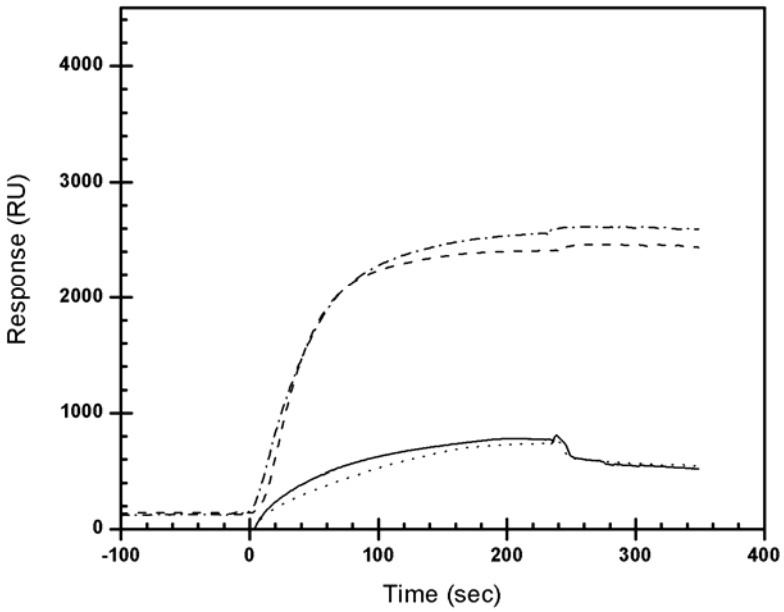

Figure 3.5: SPR responses from exposure to serum harvested before (solid lines) and after (dotted lines) immunization with Ni(II) F^5U-substituted M-DNA. Pre- (dashed lines) and post-immunization (dot-dashed lines) in the presence of 0.20 mM Ni^{2+} in the running buffer are also shown. The responses are shown at pH 7.5 (**A**) and pH 8.5 (**B**).

cases the pre immunization animals' sera gave higher responses. All SPR immunoassay data show representative single experiments from at least three independent assays.

3.1.3 Conclusions on Production of M-DNA-Specific Antibodies

It is possible that anti-M-DNA antibodies are produced during immunization of mice. However, attempts to detect the antibodies were confounded by artefacts in the assays used. Non-specific interactions between IgM molecules and DNA caused false positives in the SPRIA. The SPR studies showed very large differences in signal in the presence or absence of metal ions, necessitating a control based on pH to be used. However, large differences in the signals obtained at pH values of 7.5 and 8.5 and the fact that the difference in response caused by the presence of Zn^{2+} or Ni^{2+} was not specific to pH 8.5 made interpretation of the results very difficult. Most SPR-based immunoassays are with proteins, which are not likely to be bound by components of the plasma. DNA, on the other hand, is bound by a variety of proteins which could be present in the plasma due to damaged cells and thus the response in a study with DNA as an immunogen is likely to have more interactions that are not due to an immune response. Further, it was concluded in a study aimed at reducing background-binding signals in SPR-based immunoassays that a key component of a running buffer in this regard was EDTA (Vikinge *et al.*, 1998), which obviously could not be included in these experiments. In conclusion, with the techniques at hand, it was impossible to discern a positive immunogenic response against M-DNA and thus this aspect of the project was abandoned in favour of further characterization of the structure.

Should the difficulties surrounding detection of antibodies specific to M-DNA discussed in the previous paragraph be unsolvable by improved methodology, there are several alternatives to immunization of mice with M-DNA. Phage display is a well-proven technique for *in vitro* production of monoclonal antibodies and has been successfully used in the Lee lab to create anti-DNA antibodies that bound a variety of DNA sequences with varying specificities (Tanha *et al.*, 1997). Further, as indicated in section 1.4.2, antibodies specific for quadruplex DNA have also been created using this technique (Schaffitzel *et al.*, 2001). Random mutagenesis induced in cells producing antibodies specific for other DNA conformations could also produce antibodies specific for the M-DNA conformation. However, whatever the method used to create the antibodies, the method used to detect and characterize the antibodies must be subjected to stringent controls, as MAbs specific for B-DNA could be inducing B-DNA under M-DNA conditions; the inverse would also likely occur. The potential for false positives or negatives (relative to B-DNA bindng) would be great in an assay to characterize antibodies specific for M-DNA but not for B-DNA.

3.2 Ethidium Bromide Based Assays

In the past, the EtBr assay has been used to characterize many aspects of M-DNA formation (Aich *et al.*, 2000; Lee *et al.*, 1993). These include the effects of changing the sequence, base composition, base substitution, temperature, metal ions, and pH. This study expands on these findings, using the EtBr assay to further characterize the effects of these factors on the equilibrium position of M-DNA formation. The parameters studied

are the different effects of each metal ion on M-DNA formation, characterization of the high degree of stability observed in Ni(II) M-DNA, the effect of changing the DNA concentration on M-DNA formation, the effects of drastically different sequences or base substitutions on Zn(II) M-DNA formation, and the effect of changing the temperature on Zn(II) M-DNA formation. The experiments are discussed in that order and in each case, the EtBr assay employed is slightly different. The differences as well as the rationale behind them are described for each set of experiments. All EtBr assay data presented (figures 3.6 – 3.10 and table 3.1) are averages of between 3 and 12 individual experiments.

3.2.1 Formation and Stability of Zn(II), Ni(II), and Co(II) M-DNA

Although all of the divalent metal ions Zn^{2+}, Ni^{2+}, and Co^{2+} are capable of forming M-DNA, the properties of each form of M-DNA are different. An EtBr assay similar to the original assay was employed to detect M-DNA formation, to asses M-DNA stability, and to characterize differences between these three forms of M-DNA. In this assay, a 200 μL aliquot of 7.5 μM DNA is added to 2 mL of pH 8.3 Zn-EFB for a final DNA concentration of 680 nM. The pH of this buffer was chosen during early studies on M-DNA (Lee *et al.*, 1993) as it allowed both M- and B-DNA to be transiently stable, although if left for periods in excess of 10 minutes, most of the DNA converted to the M form. The 200 μL sample consisted of a 100 μL aliquot of 15 μM DNA in 4 mM CHES pH 9.0 and 100 μL of 25 mM buffer with a pH between 5.0 and 9.0, both with 10 mM NaCl. The low concentration of CHES was sufficient to keep the DNA at pH 9.0 in the

absence of additional buffer but weak enough to allow the final mixture to adopt the pH of the 25 mM buffer added. This method allowed formation and stability of M-DNA to be measured as a function of pH since M-DNA can be formed in the 4 mM CHES buffer and the pH of the solution then adjusted to a desired value by addition of the second buffer. Formation of M-DNA for stability studies required different concentrations of metal ion for each species of M-DNA. Zn(II) M-DNA required 0.20 mM Zn^{2+}, while 0.30 and 0.50 mM of Ni^{2+} and Co^{2+}, respectively, were required to cause complete dismutation to their respective forms of M-DNA with 15 μM DNA at pH 9.0. In all cases, stability studies as well as formation studies were carried out at a final concentration of 0.25 mM of divalent metal ion for 7.5 μM DNA. All readings were normalized against the average value obtained from the B-DNA incubated at pH values of 5.0-6.5. Thus, some formation of M-DNA occurred immediately upon addition of DNA to the Zn-EFB and therefore the values obtained are given as "Percent Fluorescence", as opposed to "Percent B-DNA".

As can be seen in figure 3.6, Zn(II) and Co(II) M-DNA display a similar degree of pH-stability, although Zn(II) M-DNA is formed much more readily than the Co(II) form. Ni(II) M-DNA, on the other hand, displayed radically different properties. Formation of Ni(II) M-DNA occurred sharply at pH 9.0, while Zn(II) M-DNA formation occurred over a pH range of 8.2 - 9.0. Further, while little hysteresis was observed with Zn(II) or Co(II) M-DNA, the Ni(II) form displayed strong hysteresis, being stable down to pH 5.5. This is in agreement with previous results with $d(GC)_n$ and CT-DNA (Aich *et al.*, 2000). All of the fluorescence readings were raised to values comparable to those obtained in QEFB upon addition of 1.0 mM EDTA to the DNA/Zn-EFB mixture with the

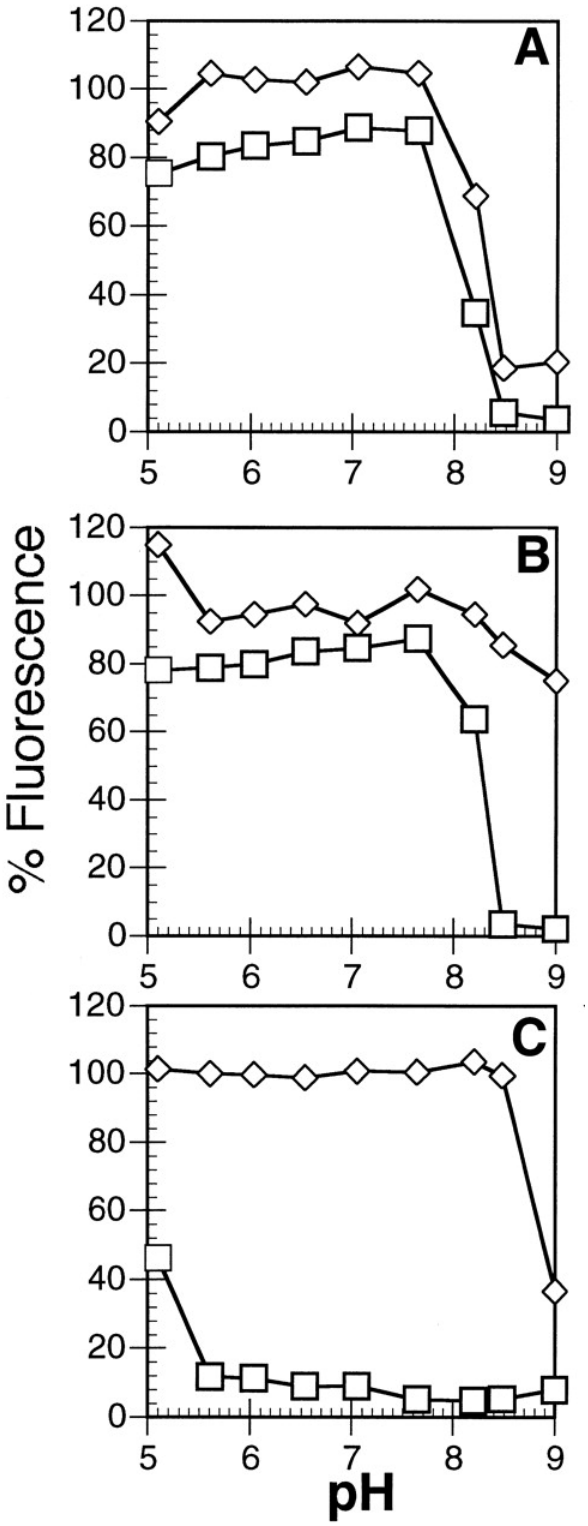

Figure 3.6: Conversion of the λ 496 bp fragment from B- to M-DNA (diamonds) or M- to B-DNA (squares) as a function of pH. The metal ions used are Zn^{2+} (**A**), Co^{2+} (**B**), and Ni^{2+} (**C**).

exception of Ni(II) M-DNA, in which no fluorescence was restored upon addition of EDTA. A similar effect was observed with Co(II) M-DNA, although some fluorescence was restored with addition of EDTA; this was observed when M-DNA was formed for 2 h, but not when it was formed for only 30 min. Inability of EDTA to restore fluorescence would appear to be indicative of denaturation. However, heat-denatured CT-DNA placed in QEFB or Zn-EFB with added EDTA shows roughly 50% of the fluorescence of native DNA, presumably due to the formation of hairpin structures (Morgan *et al.*, 1979) while this sample did not display any enhancement of fluorescence. This led to further experiments aimed at determining whether or not Ni^{2+} and Co^{2+} were causing denaturation of the DNA.

3.2.2 Slow Reversion of Ni(II) M-DNA

To evaluate whether Co^{2+} and Ni^{2+} were denaturing the DNA, an assay similar to that just described was carried out. CT-DNA was dissolved to 75 μM concentration in 20 mM CHES pH 9.0, 10 mM NaCl and 500 μL samples were fully converted to M-DNA by addition of 0.50 mM $CoCl_2$ or $NiCl_2$. Conversion to M-DNA was verified by addition of a 20 μL aliquot to 2.0 mL Zn-EFB. Addition of EDTA had little or no effect for Co(II) and Ni(II) M-DNA, respectively. Following this, EDTA concentrations between 0.25 and 1.00 mM were added to the remaining 480 μL of 75 μM M-DNA. The fluorescence was then measured in Zn-EFB before and after addition of 1.0 mM EDTA to the 2 mL at varying intervals over the next 22 h. After several hours had passed, the samples with more than 0.50 mM EDTA had reverted completely to B-DNA, as illustrated in figure

3.7. Samples incubated with 0.50 mM Ni^{2+} or Co^{2+} did not revert completely to B-DNA in the presence of 0.25 or 0.50 mM EDTA but did so in the presence of 0.75 or 1.0 mM EDTA. Thus, these experiments also indicate that the DNA is not denatured.

The Ni(II) form of M-DNA required a long period of time and excess concentrations of EDTA to revert to B-DNA, while the Zn(II) form reverts instantly. In addition to the increased pH-stability of Ni(II) M-DNA relative to Zn(II) M-DNA, it is more stable it the presence of EDTA. Another distinction between Ni(II) and Zn(II) M-DNA is the higher pH necessary to form Ni(II) M-DNA.

3.2.3 Effect of DNA Concentration on M-DNA Formation

Although earlier studies have shown that M-DNA formation was dependent on the concentration of metal ion present (Lee *et al.*, 1993), it was also found that modulating the DNA concentration has a substantial effect on M-DNA formation, with higher concentrations of DNA requiring higher metal ion concentrations in a logarithmic relationship, as depicted in figure 3.8. This assay was performed in a similar way to the work of the previous two sections, with CT-DNA of concentrations between 4.5 and 450 μM being dissolved in 10 mM NaCl with either 20 mM TRIS-HCl pH 8.5 or CHES pH 9.0. These were then incubated in the presence of Zn^{2+}, Ni^{2+}, or Co^{2+} at concentrations between 0.1 and 1.0 mM for 2 h. Aliquots containing 1.3 nmols of DNA were then added to 2.0 mL Zn-EFB and the fluorescence read before and after addition of 1.0 mM EDTA to the Zn-EFB. The fluorescence values were then compared to those obtained from samples which did not contain added divalent metal ion. The concentrations of Zn^{2+} and

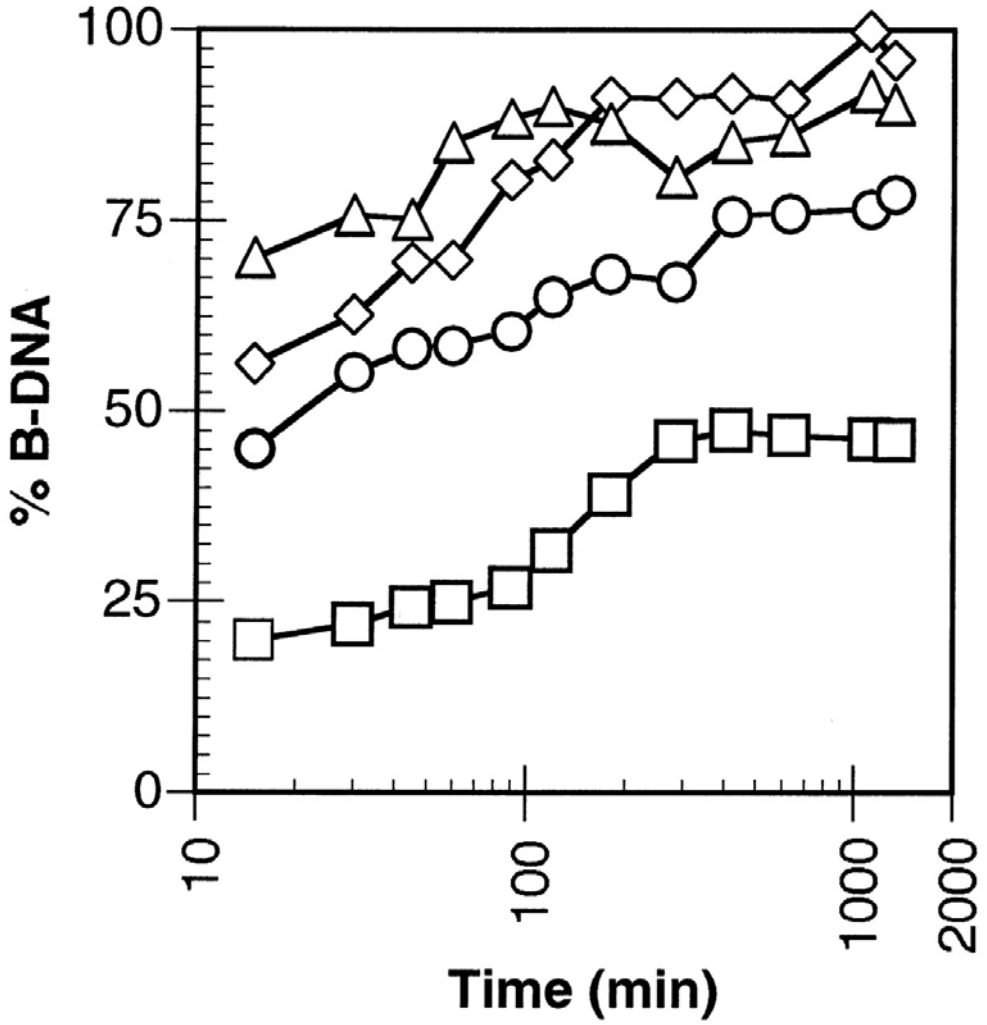

Figure 3.7: Slow conversion of CT DNA from the M- to the B-form. Samples are shown for exposure of Co(II) M-DNA to 0.50 mM (circles) and 1.00 mM (triangles) EDTA. Analogous experiments with Ni(II) M-DNA are shown with 0.50 mM (squares) and 1.00 mM (diamonds) EDTA.

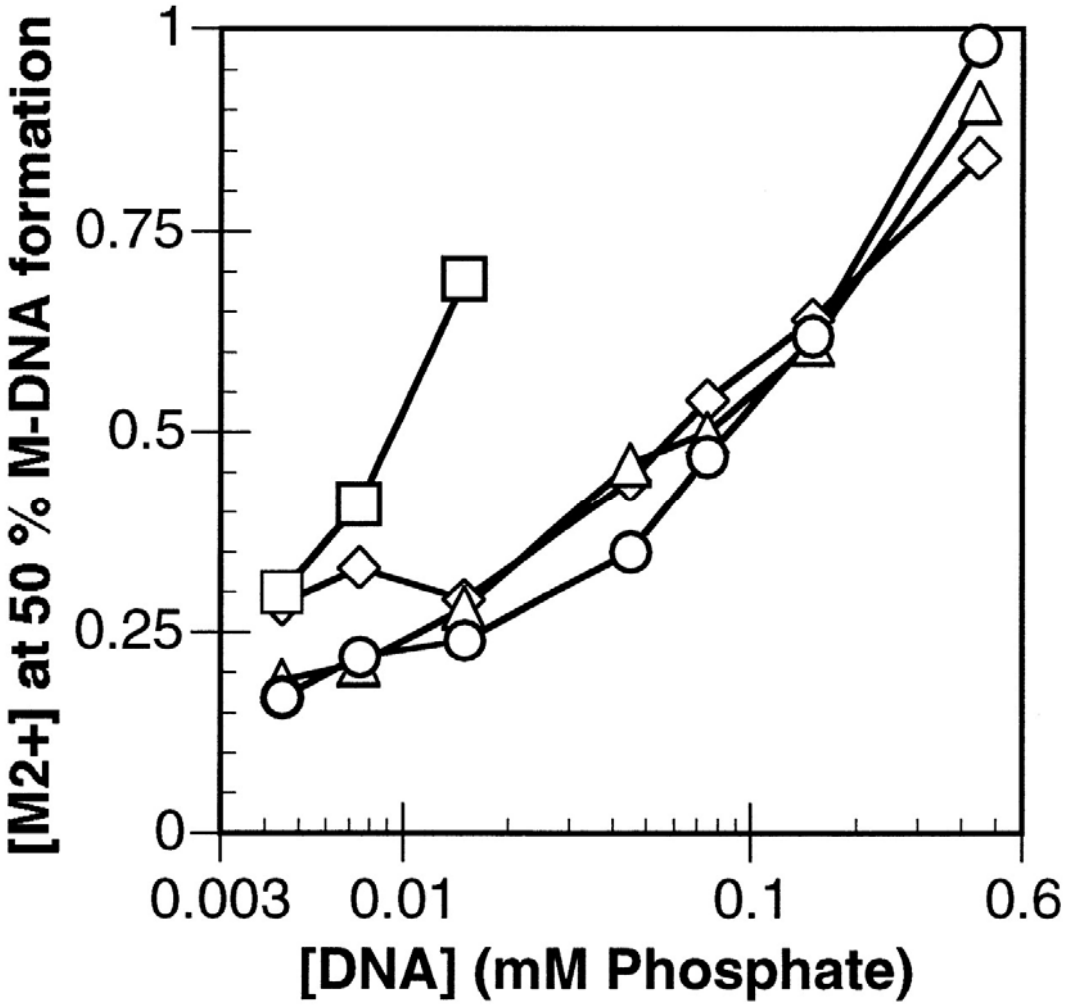

Figure 3.8: The metal ion concentrations necessary to convert 50% of the CT DNA to M-DNA as a function of DNA concentration with Zn^{2+} (diamonds), Co^{2+} (triangles), and Ni^{2+} (squares) at pH 8.5 and with Ni^{2+} (circles) at pH 9.0.

Co^{2+} necessary to convert 50% of the DNA to M-DNA were found to be similar at pH 8.5, while much higher concentrations of Ni^{2+} were required at DNA concentrations below 15 μM, and dismutation did not occur even with 1.0 mM Ni^{2+} at DNA concentrations higher than this. However, when assayed at pH 9.0, the relationship between $NiCl_2$ concentration required to convert 50% of the DNA to M-DNA and the DNA concentration were similar to that observed for the other two metals at pH 8.5. Thus, not only is Ni(II) M-DNA more stable than the other forms, it also requires either a higher pH or a higher metal ion concentration to form.

3.2.4 Zn(II) M-DNA Formation in Base-Substituted or Repetative Sequence DNA

When assaying the effect of various base substitutions on M-DNA formation, it was observed that some base-substituted sequences did not cause an enhancement of fluorescence when added to Zn-EFB, although they did when added to QEFB or when EDTA was added to Zn-EFB. Thus, it was hypothesized that the substitutions were facilitating M-DNA formation to such a high degree that the Zn-EFB was causing them to convert immediately and fully to this conformation. This led to a modified EtBr based assay in which several pH values of Zn-EFB were used. In this form of the assay, a final DNA concentration of 0.71 μM was incubated in Zn-EFB with pH values varying from 6.0 to 8.6 and 0.20 mM $ZnCl_2$. The assay could not be performed at pH 9.0, since the $ZnCl_2$ would not remain soluble at this pH. Precipitation of 0.20 mM $ZnCl_2$ did not occur at pH 9.0 in the presence of 15 μM DNA, but 0.71 μM DNA was not sufficient to solubilize that concentration of $ZnCl_2$ at that pH. The added DNA, which consisted of a

100 μL aliquot of 15 μM DNA in 10 mM NaCl, 4 mM CHES pH 9.0, was converted to M-DNA prior to addition to the Zn-EFB by incubation with 0.20 mM Zn^{2+} for 2 h. Thus, this method allowed stability as well as formation of the base-modified M-DNA to be measured. Further, since an equilibrium is reached in the presence of EtBr and added metal ion, the readings can be normalized against the pH 6.0 Zn-EFB, where it is assumed that no M-DNA formation can take place. Although the DNA-EtBr fluorescence obtained was lower prior to addition of EDTA in pH 6.0 Zn-EFB, this is likely due to inhibition of EtBr binding by electrostatic competition between the 1.3 μM EtBr and the 0.20 mM $ZnCl_2$. This type of fluorescence inhibition occurs with addition of any divalent metal ion to the Zn-EFB. Thus, these normalized values can be referred to as "% B-DNA" rather than "% Fluorescence". The results of this assay with several base substitutions and some repetitive sequences are shown in figure 3.9. As shown in figure 3.8, DNA concentration has a substantial effect on M-DNA formation, but Zn(II) M-DNA formation was similar over a range of 4.5 - 15 μM, suggesting that results obtained at 0.71 μM would be comparable to these results. Comparison of figures 3.6a and 3.9a shows this to be true: roughly 60% B-DNA/fluorescence remains around pH 8.2 while there is less than 20% remaining around pH 8.5 in both cases.

While this technique proved useful to measure the formation and stability of Zn(II) M-DNA with any sequence or any base substitution, it could not be employed to measure the analogous interactions between DNA and Ni^{2+} of Co^{2+}. When 0.20 mM of any of these metals was substituted for Zn^{2+} in the Zn-EFB, the fluorescence values obtained were very low and had little pH-dependence. The low fluorescence values greatly lowered the signal to noise ratio of the readings, leaving little difference between

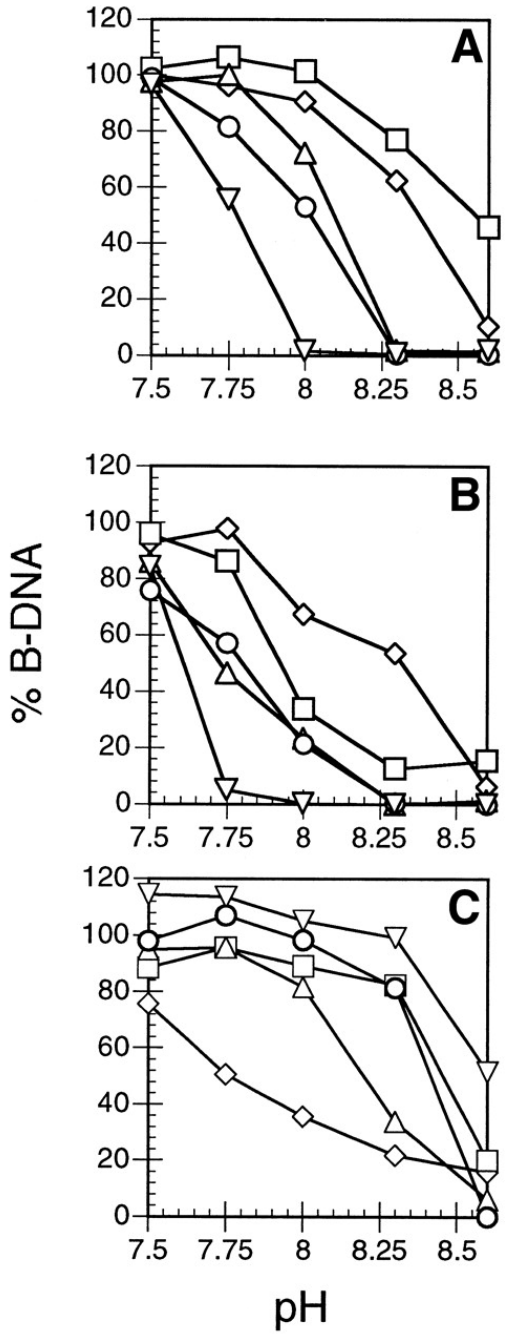

Figure 3.9: Effect of base substitutions in the λ 496 bp fragment on (**A**) the conversion of B-DNA to M-DNA and (**B**) the conversion of M-DNA to B-DNA with 0.2 mM $ZnCl_2$. The following base substitutions are shown in those figures: n^2A (squares), control (diamonds), I (triangles); Br^5U (circles), Br^5U and I (inverted triangles). (**C**) The conversion of B-DNA to M-DNA for repeating sequence nucleic acids: poly(dG)•poly(dC) (diamonds), poly[d(GGCC)] (triangles), poly[d(GC)] (squares), poly[d(AU)] (circles), poly[r(AU)] (inverted triangles).

M- and B-DNA readings. This is likely due to quenching of EtBr fluorescence by available empty 3d orbitals. This was not a problem in the assays described in sections 3.2.1-3.2.3 likely due to the lower concentrations 10 fold lower of Ni^{2+} or Co^{2+} ions present and the presence of 0.20 mM Zn^{2+}.

Representative results of this assay are depicted in figure 3.9 while the midpoint of the transition from M- to B-DNA or vice versa (pH_m) for all sequences and substitutions are listed in table 3.1. As is apparent from the table, some base substitutions strongly facilitate the formation of and stabilize M-DNA. Substitutions of F^5U, Br^5U, or s^4T for T or of I for G most strongly favoured the M-DNA conformation. Further, a double substitution of Br^5U for T and of I for G in the same sequence had a cumulative effect, lowering the pH_m of formation to 7.8 while either substitution alone gave values of 8.0 and 8.1, respectively. Substitution of U for T had little effect on the pH_m values. However, s^4T and s^2T substitutions showed effects that depended strongly on the sequence into which they were inserted. This will be addressed in detail in section 4.1. A dsRNA sequence, $r(AU)_n$, showed similar results to $d(AU)_n$. Thus, the substitutions which replaced bases with titratable imino protons with bases having lower pK_a values at that site more strongly favoured M-DNA formation than those which replace bases lacking titratable imino protons.

The sequence of the DNA also had a large impact on the propensity of the sequences to adopt the M-DNA conformation. This assay showed that sequences with pur•pyr motifs formed the conformation at lower pH values than those with alternating pur and pyr on each strand. Random sequence DNA fell between these two extremes. The base composition of different sequences showed that in general, a higher GC content

DNA	pH_m B- to M-DNA	pH_m M- to B-DNA
Control 54 % GC	8.4	8.3
c-*src* 73 % GC	8.2	7.9
n^2A	8.6	8.0
z^7A	8.2	8.0
m^5C	8.5	8.2
I	8.1	7.8
U	8.3	8.1
Br^5U	8.0	7.8
F^5U	7.9	7.7
s^4T	8.1	-
Br^5U/I	7.8	7.6
$d(G)_n•d(C)_n$	7.8	7.6
$d(GGCC)_n$	8.2	7.8
$d(GC)_n$	8.5	8.3
$d(A)_n•d(T)_n$	8.1	7.8
$d(AT)_n$	8.6	8.4
$d(AU)_n$	8.4	8.1
$r(AU)_n$	8.5	8.1
$d(TG)_n•(CA)_n$	8.1	-
$d(As^2T)_n$	8.3	-
$d(As^4T)_n$	8.3	-
$d(s^2TG)_n•d(CA)_n$	8.3	-
$d(s^4TG)_n•d(CA)_n$	7.7	-

Table 3.1: The effect of base substitutions or sequence changes on the formation and stability of 0.71 μM M-DNA with 0.20 mM Zn^{2+} in the presence of 1.3 μM EtBr. All base substitutions are for the λ 496mer.

favoured the M-DNA conformation. A notable exception to these generalizations is that the sequence $d(TG)_n \bullet d(CA)_n$ formed the conformation much better than any repeating polymer except $d(G)_n \bullet d(C)_n$. All of these results are in agreement with previously obtained data (Lee *et al.*, 1993). The 73% GC DNA showed M-DNA formation at a lower pH than the 54% GC DNA for sequences of 516 and 496 base pairs, respectively. This may appear to conflict with previously obtained data, in which there was little difference observed between genomic DNAs of differing base content (Lee *et al.*, 1993). However, that data was measured as a function of time following addition of $ZnCl_2$, while the current data was ascertained as a function of pH under equilibrium conditions. Thus, while the GC content of the DNA did not appear to have a large impact on the kinetics of M-DNA formation, it had a substantial impact on the position of the equilibrium between B- and M-DNA at different pH values.

3.2.5 Effect of Temperature on M-DNA Formation

The effect of temperature on Zn(II) M-DNA formation at pH 8.5 was evaluated by measuring the formation of M-DNA as a function of $Zn(ClO_4)_2$ concentration at temperatures between 4 and 37 °C. The level of M-DNA formation at each temperature was normalized against the readings obtained in the absence of Zn^{2+} ions. Zinc perchlorate was used instead of $ZnCl_2$ to more closely parallel complimentary studies done by ITC. Control experiments have shown that perchlorate salts give similar results to the analogous chloride salts in EtBr studies. As previous studies had suggested (Lee *et al.*, 1993), increased temperature favours M-DNA formation. This was supported by this

study, as is apparent from figure 3.10. The higher the temperature of incubation, the less Zn^{2+} was required to induce M-DNA formation. This is suggestive of an endothermic process.

3.3 Isothermal Titration Calorimetry

ITC was chosen as a method to measure M-DNA formation since it is a direct biophysical method that does not rely on measuring the binding of a third molecule. That is, only the DNA and the metal interacting with each other generate the signal and no other molecules are present in the equilibrium. A drawback to this assay was that in order to generate a signal, DNA concentrations in excess of 0.15 mM had to be used. It was not possible to cause a conversion to M-DNA at soluble Zn^{2+} concentrations at DNA concentrations higher than 0.30 mM. Thus, the lower sensitivity limit of the instrument was close to the maximum concentration of sample that could be successfully converted to M-DNA. This resulted in large deviations in the measurements, and the error of the ΔH values was 10% or greater. At sufficient DNA concentrations, a signal was obtained in the presence of soluble $Zn(ClO_4)_2$ concentrations at pH 8.5, but not at pH 7.5. Aliquots of 25 μM $Zn(ClO_4)_2$ were added every 10 min to allow equilibration to occur between injections. The readings were normalized against the same injections into buffer without DNA at each pH, and the net ΔH values obtained at each pH are depicted in figure 3.11.

As can be seen in figure 3.11, there is no substantial enthalpic change at pH 7.5 over the concentration of $Zn(ClO_4)_2$ added. Further, exposure to titrations of $Mg(ClO_4)_2$

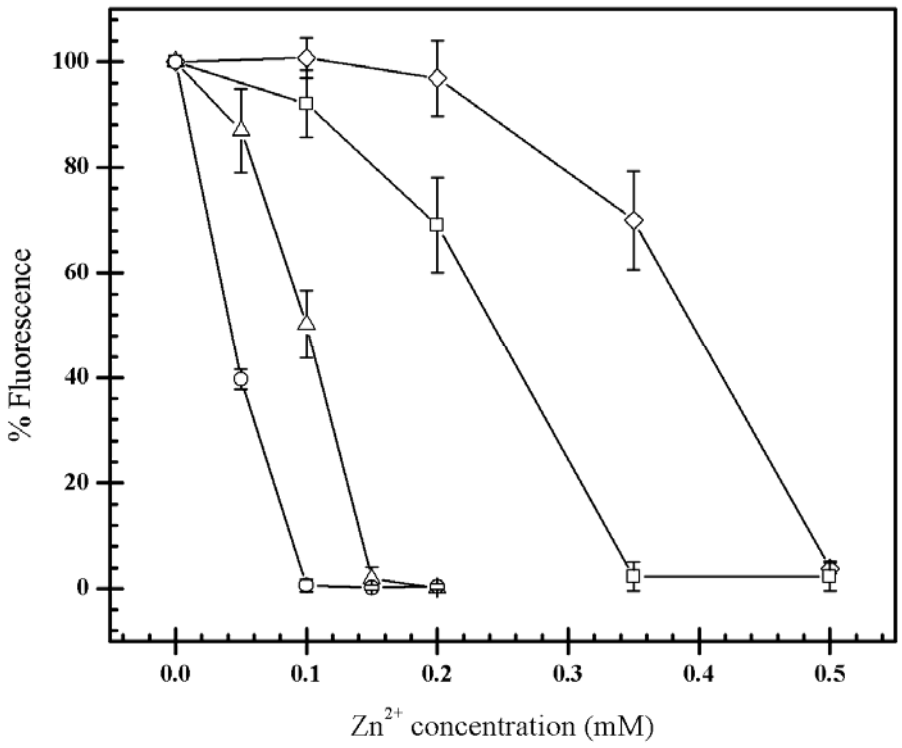

Figure 3.10: Conversion of 15 μM CT-DNA into M-DNA at pH 8.5 as a function of Zn^{2+} concentration at temperatures of 4 (diamonds), 10 (squares), 21 (triangles), and 37 (circles) ˚C.

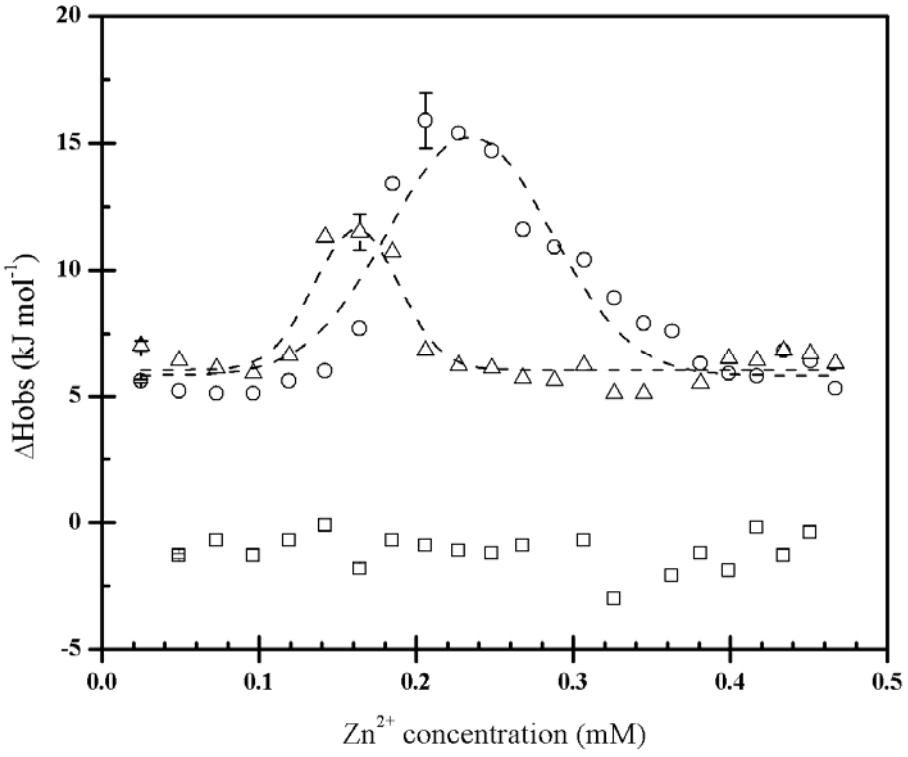

Figure 3.11: Effect of pH and DNA concentration on the formation of M-DNA with CT-DNA at 25 ˚C. Plots are shown for 0.15 mM (triangles) and 0.30 mM (circles) DNA at pH 8.5 and 0.30 mM (squares) DNA at pH 7.5. The curves at pH 8.5 have been shifted by 5 kJ/mol to assist in visualization. This work was done in close cooperation with Dr. S. Wettig, whose work in preparation of this figure is gratefully acknowledged. The data shown in this figure are averages of 3 independent trials.

at pH 7.5 or 8.5 shows weak signals similar to those obtained with $Zn(ClO_4)_2$ at pH 7.5. However, at pH 8.5, $Zn(ClO_4)_2$ causes significant changes at DNA concentrations of 0.15 and 0.30 mM. Further, the transition begins at a higher concentration of $Zn(ClO_4)_2$ at 0.30 mM than at 0.15 mM DNA. It also occurs over a broader range of $Zn(ClO_4)_2$ at the 0.30 mM DNA. This is in agreement with the results of the experiments in section 3.2.3, which show that higher DNA concentrations require higher concentrations of Zn^{2+} to allow conversion to M-DNA. The ΔH values calculated for each concentration of CT-DNA were 18 ± 4 and 21 ± 1.4 kJ per mole of phosphate (kJ/Mol PO_4^-) for 0.15 and 0.30 mM DNA, respectively. This illustrates the higher degree of accuracy at higher DNA concentrations and also demonstrates that the same process was occurring at either concentration, since the ΔH values were within error on a per mole basis. *E. coli* DNA, which has a similar base composition to CT-DNA, showed a ΔH of 26 ± 6 kJ/Mol PO_4^- at 0.150 mM. The enthalpies were also positive, indicative of an entropy-driven process. This is in agreement with data obtained by the variable temperature EtBr assay detailed in section 3.2.5.

3.4 Surface Plasmon Resonance

Like ITC, SPR was chosen as a method to assess M-DNA formation due to the direct nature of the technique. Since signals arising during an SPR experiment are due solely to changes in the properties of the probed layer, it was considered likely that changes in DNA conformation would be detectable by this method. Indeed, although no precedent had been established with nucleic acids, changes in the conformation of

surface-immobilized proteins are detectable by SPR as discussed in section 1.3.3.2. The data presented in figures 3.12, 3.13 and 3.15 are all single experiments representative of multiple assays, while the data shown in figure 3.18 was only obtained once. The data presented in figures 3.14, 3.16, 3.17, and 3.19 – 3.32 are averages of between 3 and 6 individual experiments, all of which had a standard deviation of less than 5 %.

3.4.1 Surface Preparation

The SA type of sensor chip was used in this study. This is the most common choice for studies on immobilized nucleic acids using a BIAcore as oligonucleotides can be easily modified with biotin on their 5' ends and anchored by strong non-covalent interactions to streptavidin which is covalently attached to the CMD matrix on the chip. In this study, between 180 and 200 RU of ssDNA was immobilized in this manner on the surface of a chip. The sequences immobilized consisted of either a 50% GC random sequence or one of three homopolymers, all thirty bases in length. The immobilization was performed on flow cell 2 because the interaction anchoring the DNA to the surface, while strong, was not covalent. Thus, if a biotinylated sequence were to detach, it would simply flow out of the system and not onto a bare surface that was to be referenced as a background signal. Immobilization was performed in small increments to ensure that no more than the desired amount of DNA was immobilized. If too much ssDNA is attached to the surface, complete hybridization cannot be achieved due to crowding (Peterson *et al.*, 2001). This was observed experimentally when more than 325 RU of btn-CTL-2 was immobilized.

In the case of the random sequence, hybridization was verified by addition of the complimentary strand at a low flow rate. Immobilization of btn-CTL-2 and hybridization with CTL-1 in TBS are shown in figure 3.12. The increase in RU corresponding to hybridization was typically 95% or more of that achieved due to immobilization, corresponding to complete hybridization. Exposure of dsCTL surface to 50 mM NaOH for 24 sec completely denatured the surface, leaving only the CTL-2. A second exposure to CTL-1 would result in rehybridization of the DNA to produce dsCTL. This cycle is also depicted in figure 3.12. When hybridizing, the flow rate was low, 5 μL/min, to allow the molecules to interact, but when denaturing, the flow rate was set much higher, at 50 μL/min, to limit exposure of the IFC to harsh chemical conditions. Regardless of the running buffer in use, the actual exposure of the surface to complementary strand during hybridization was always carried out in the high ionic strength TBS.

It was observed that after several days of experiments, the hybridization capacity of the surface would drop by up to 10%. When this occurred, more btn-CTL-2 was added to flow cell 2 to bring the hybridization activity back up to the original values observed. In the case of surface with homopolymers immobilized, there was no simple way to verify how much DNA remained on the surface, so all necessary M-DNA formation experiments were carried out quickly over a period of 2-3 days. Within this time frame, the results observed were reproducible. However, when a three-week-old chip with immobilized A30 was assayed once again, the results were not similar to the first trials. Thus, in all cases, the experiments were performed in as small a time frame as possible, particularily in the case of homopolymers, to ensure reproducibility.

(**A**)

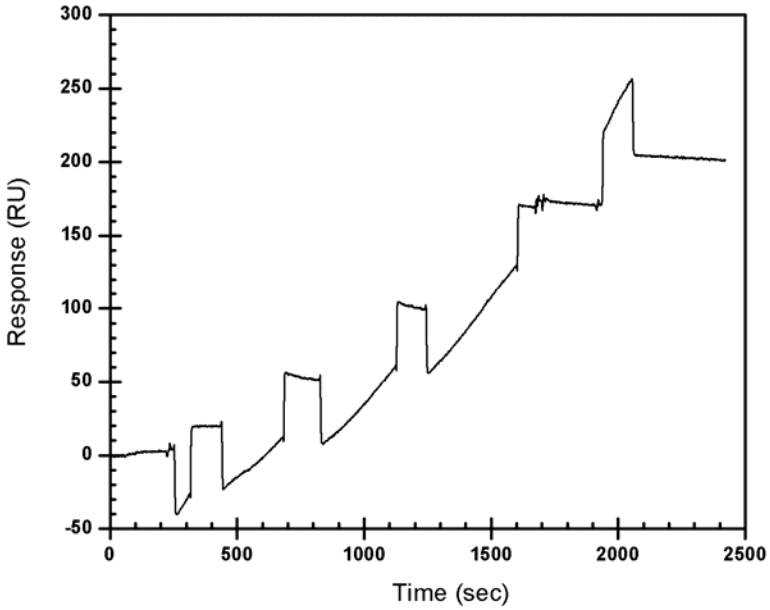

(**B**)

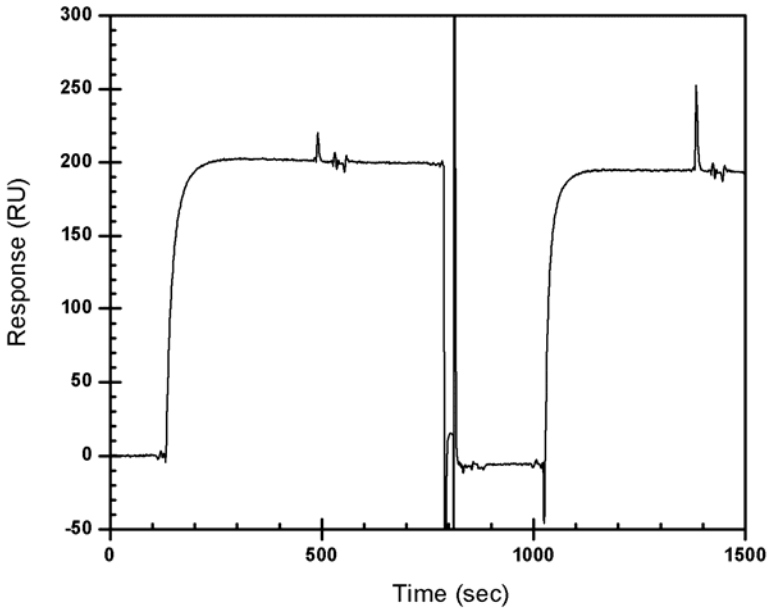

Figure 3.12: (**A**) immobilization of btn-CTL-2. Injections of between 5 and 50 µL volume were repeatedly administered until the desired level of immobilization was obtained. (**B**) Hybridization of CTL-1 with immobilized CTL-2 to form dsCTL, denaturation of the resulting duplex, and renaturation.

3.4.2 DNA-Metal Ion Interactions

The interactions between DNA and a variety of divalent metal ions were characterized at pH values of 6.5, 7.5, and 8.5. The metal ions studied were Mg^{2+}, Ca^{2+}, Zn^{2+}, Ni^{2+}, and Cd^{2+}. Interactions between DNA and Co^{2+} were not evaluated as the reproducibility of these studies was very low. All data shown is for the chloride salts of the metal ions. Parallel trials were performed with perchlorate salts but the data was identical to that obtained with the chlorides. Under no conditions did the use of $ZnCl_2$ that originated from 2.0 M stocks in which the pH was or was not lowered to solubilize the $ZnCl_2$ have any substantial impact on the signals obtained. The flow rate was set at 50 μL/min to eliminate mass transport effects, which were apparent at flow rates of 30 μL/min or lower. Experiments were not carried out at pH 9.0 because the $ZnCl_2$ had a tendency to precipitate at this pH and this not only resulted in poor-quality sensorgrams but also had the potential to damage the IFC. The principal experiments examined a 50% GC duplex, dsCTL, while studies were also carried out on CTL-2, T30, C30, and A30. The results of these experiments will be presented in that order.

As detailed in section 2.5.4, the RII values of $NiCl_2$ and $ZnCl_2$ were determined and the maximum responses due to increased mass upon metal ion binding to the various DNA sequences were calculated. The RII values of $NiCl_2$ and $ZnCl_2$ were found to be 0.216 and 0.195 mL/g, respectively. The RII values of the various DNA sequences were estimated from literature values (Davis and Wilson, 2000) and these values, along with their molecular weights and immobilization levels are presented in table 3.2. The calculated $(RU_{pred})_{sat}$ values for each polymer are also given in table 3.2. In some cases,

the responses obtained were significantly larger than these values. The large responses elicited by some metal ions upon exposure to some of the DNA sequences studied were likely due to formation of M-DNA or to an analogous single-stranded conformation. Data obtained at pH values of 7.5 and 8.5 over metal ion concentration ranges in which M-DNA normally forms at pH 8.5 are detailed in the following subsections and the implications of these findings are addressed in section 4.3. Signals resulting from exposure of dsCTL to higher concentrations of Cd^{2+}, Zn^{2+}, and Ni^{2+} at pH values of 7.5 and 6.5 are detailed in section 3.4.3 and discussed in section 4.3.

For clarity, complete representative sensorgrams of the results presented in the following subsections are given for the interaction of Zn^{2+} with dsCTL at pH 7.5 and 8.5 in figure 3.13. The figure shows hybridization as well as NaOH-induced denaturation events with 10 mM TRIS-HCl pH 7.5 or 8.5 10 mM NaCl as a running buffer. Exposure of the dsCTL surface to 0.20 mM Zn^{2+} at each pH is also shown. The differing responses dependent on pH are covered in section 3.4.2.1. Section A of figure 3.13 shows the baseline of CTL-2 in flow buffer. Section B shows injection of 30 μL of 21 μM CTL-1 in TBS at a flow rate of 5 μL/min; all other sections are at a flow rate of 50 μL/min. Section C follows injection of CTL-1 and is about 185 RU higher than the response level of A, representing complete hybridization; this is the baseline value for the sensorgram. Section D shows exposure of dsCTL to 0.20 mM $ZnCl_2$ in flow buffer. At pH 7.5 (top panel), little change occurs during the injection, on the order of +10 RU, while at pH 8.5 (bottom panel), the $ZnCl_2$ induces a response of about +130 RU, indicating that a conformational change has taken place. Section E shows resumption of running buffer without $ZnCl_2$ over both flow cells and the subsequent rapid dissociation of the $ZnCl_2$, returning the

DNA	MW (g/mol)	RII (mL/g)	Imm. (RU)	Zn^{2+} (15)	Ni^{2+} (15)	Zn^{2+} (30)	Ni^{2+} (30)
CTL-2	9678.3	0.212	185	17.2	17.1	34.4	34.2
DsCTL	19356.6	0.212	370	17.2	17.1	34.4	34.2
T30	9427.2	0.207	220	21.5	21.4	43.0	42.8
C30	8706.6	0.212	214	22.1	22.0	44.2	44.0
A30	9156.9	0.217	206	19.8	19.7	39.6	39.3

Table 3.2: Molecular weights, RII values, and immobilization levels of each polymer used. The estimated $(RU_{pred})_{sat}$ values for 15 or 30 binding sites are also given for each polymer with Zn^{2+} and Ni^{2+}.

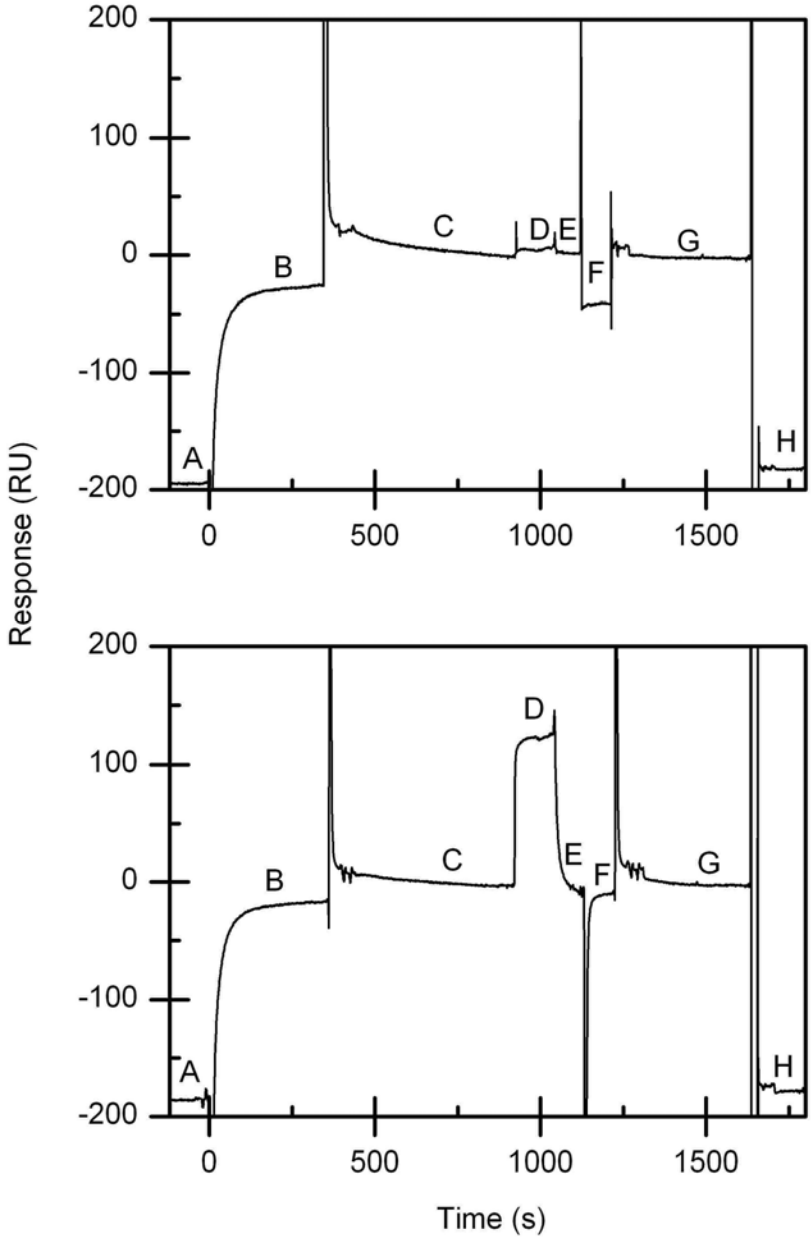

Figure 3.13: Sensorgrams showing the events involved in M-DNA detection on a chip with immobilized dsCTL, carried out in pH 7.5 (top panel) and pH 8.5 (bottom panel) running buffer at a flow rate of 50 μL/min unless otherwise stated. The labelled portions of the graph indicate the following: A, CTL-2 only; B, during injection of 21 μM CTL-1 in TBS at 5 μL/min; C, dsCTL in running buffer; D, during injection of 0.20 mM $ZnCl_2$ in running buffer; E, resumption of running buffer without $ZnCl_2$; F, during injection of 80 μL TBS; G, resumption of running buffer; H, in running buffer after injection of 50 mM NaOH 1 M NaCl, leaving CTL-2 on the surface. The response baseline is set to equal the level of dsCTL while time zero is set at the time of injection of CTL-1. Both experiments are performed on the same sensor chip.

signal to the baseline value. Section F corresponds to injection of 80 μL of TBS, which contains EDTA and can chelate any metal ions bound to either the DNA or the CMD matrix, allowing the net baseline to return to the value in section C. Section G corresponds to resumption of running buffer, and is at least 5 minutes to allow each flow cell to return to baseline. This is required as the ionic strength difference between flow buffer and TBS is sufficient to cause residual effects in the CMD matrix which, although not apparent in the net signal, are substantial on either flow cell. Section H shows the baseline after injection of 20 μL of 50 mM NaOH, 1 M NaCl. This treatment denatures the DNA and leaves btn-CTL-2 on the surface. If the magnitude of the change from G-H corresponds to the magnitude of the change from A-C, then dsCTL has not been denatured during treatment of C-G as is the case in figure 3.13. The large spikes that occur after section B, before and after section F, and between sections G and H are due to large changes in the ionic strength of the solution being measured which in turn cause large changes in the bulk refractive index between the injected buffer and flow buffer. Sensorgrams shown in subsequent sections only show the exposure to metal ions over the periods 50 sec before and 60 sec following this exposure. This corresponds to the end of section C and all of sections D and E. When the level of the baseline following exposure is discussed, it is implied that the baseline being referred to is that observed 5 min after administration of TBS unless otherwise specified, corresponding to the end of section G.

Since the analyte being studied is a metal ion and the CMD matrix is negatively charged over the pH range being analyzed, there is a substantial degree of background interaction. Attempts were made to alleviate this by using CM4 chips with streptavidin immobilized following purchase rather than SA chips, which are purchased with

streptavidin already immobilized with standard immobilization chemistry. The CM4 have a lower degree of carboxylation on the CMD, leaving fewer sites for the cations to interact with. Immobilization chemistries in which unreacted carbodiimide groups were deactivated with ethanolamine (standard reagent used in SA chips and most studies with immobilized proteins) and with ED were both assayed. However, despite the lower degree of carboxylation, neither immobilization chemistry produced background signals that were significantly lower than those observed with SA chips.

3.4.2.1 Double-Stranded DNA with 50% GC Content

The effect of the metal ions on dsCTL varied greatly depending on which metal ion was being exposed to the surface and at what pH the interaction was occurring. The response of the surface to 0.20 mM of several metal ions at pH values 7.5 and 8.5 is shown in figure 3.14. As is apparent from figure 3.14, Mg^{2+} does not cause a substantial change in the SPR signal regardless of the pH. The response of the surface to Ca^{2+} is not shown but was very similar to that of Mg^{2+}. On the other hand, Cd^{2+}, Zn^{2+}, and Ni^{2+} ions had differing effects that were all heavily pH-dependant. The results of exposure of these metal ions to dsCTL will be discussed in that order.

Although Cd^{2+} lowers the melting temperature of DNA at neutral pH (Eichhorn and Shin, 1968) it had not been previously observed that it causes room temperature denaturation of DNA at alkaline pH. This was observed to occur by SPR since exposure of the surface to 0.20 mM Cd^{2+} lowered the baseline signal by over 70 RU, corresponding to denaturation of over 40 % of the duplex on the first exposure. A similar

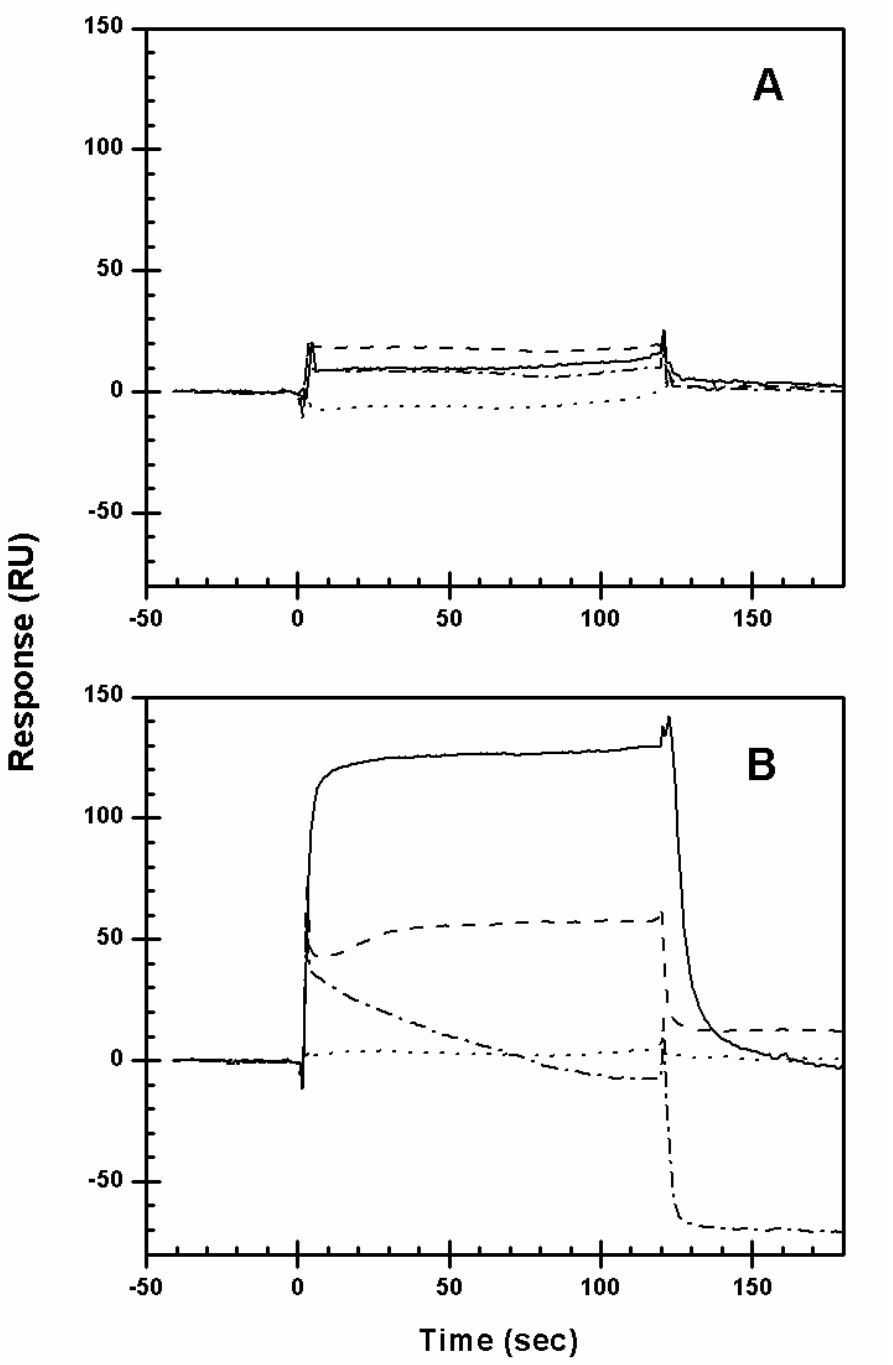

Figure 3.14: Sensorgrams showing the response of ~370 RU dsCTL to 0.20 mM metal ions with a pH 7.5 (**A**) and pH 8.5 (**B**) running buffer. The region between time points 0-120 sec corresponds to the D portion of figure 3.13, while that between time points 121-180 sec corresponds to portion E of figure 3.13. This holds true for all remaining figures in section 3.4 unless otherwise indicated. The metal ions used are: solid lines, Zn^{2+} (solid lines), Ni^{2+} (dashed lines), Mg^{2+} (dotted lines), and Cd^{2+} (dot-dashed lines). The response baseline is set to equal the level of hybridized DNA while time zero is set at the time of injection of the metal ion.

effect was observed at 1.00 mM Cd^{2+}. Subsequent exposures to Cd^{2+} further lowered the baseline until only 20 % of DNA remained hybridized. At pH 7.5, repeated exposure to Cd^{2+} concentrations in excess of 5.0 mM also causes denaturation, although not as completely as that caused by 0.20 mM Cd^{2+} at pH 8.5. The results of repeated exposure to Cd^{2+} at pH values of 7.5 and 8.5 are shown in figure 3.15. In agreement with previous work (Eichhorn and Shin, 1968), exposure to Cd^{2+} at pH 6.5 does not denature dsDNA.

The responses obtained at pH values 7.5 and 8.5 over a Zn^{2+} concentration range of 0.05 - 0.20 mM are shown in figure 3.16. As is apparent from the figure, there is little change in signal under these conditions at pH 7.5. At pH 8.5, however, signals well in excess of the estimates of $(RU_{pred})_{sat}$ are observed at Zn^{2+} concentrations as low as 0.10 mM. The signals show a maximum of ~130 RU at Zn^{2+} concentrations of 0.15 and 0.20 mM. This value does not increase at Zn^{2+} concentrations up to 0.40 mM and above that, precipitation occur which disrupt the signal. At concentrations below 0.15 mM, the response reaches an equilibrium value below that obtained at 0.15 mM or above. Unlike experiments with EtBr, the $ZnCl_2$ is not added to a system containing DNA, which solubilizes the Zn^{2+} somewhat and prevents precipitation. In the SPR experiments, a solution containing only $ZnCl_2$, NaCl, and buffer is added and thus the maximum concentration of Zn^{2+} that can remain soluble is lower. The sensorgrams return to baseline quickly in the absence of Zn^{2+} even before TBS is added, indicating a weak binding event. This is observed on the individual signals obtained on each flow cell as well as on the net signal. Following exposure to Zn^{2+}, some denaturation occurs, but never more than ~8 RU, corresponding to less than 5 % of the total dsCTL.

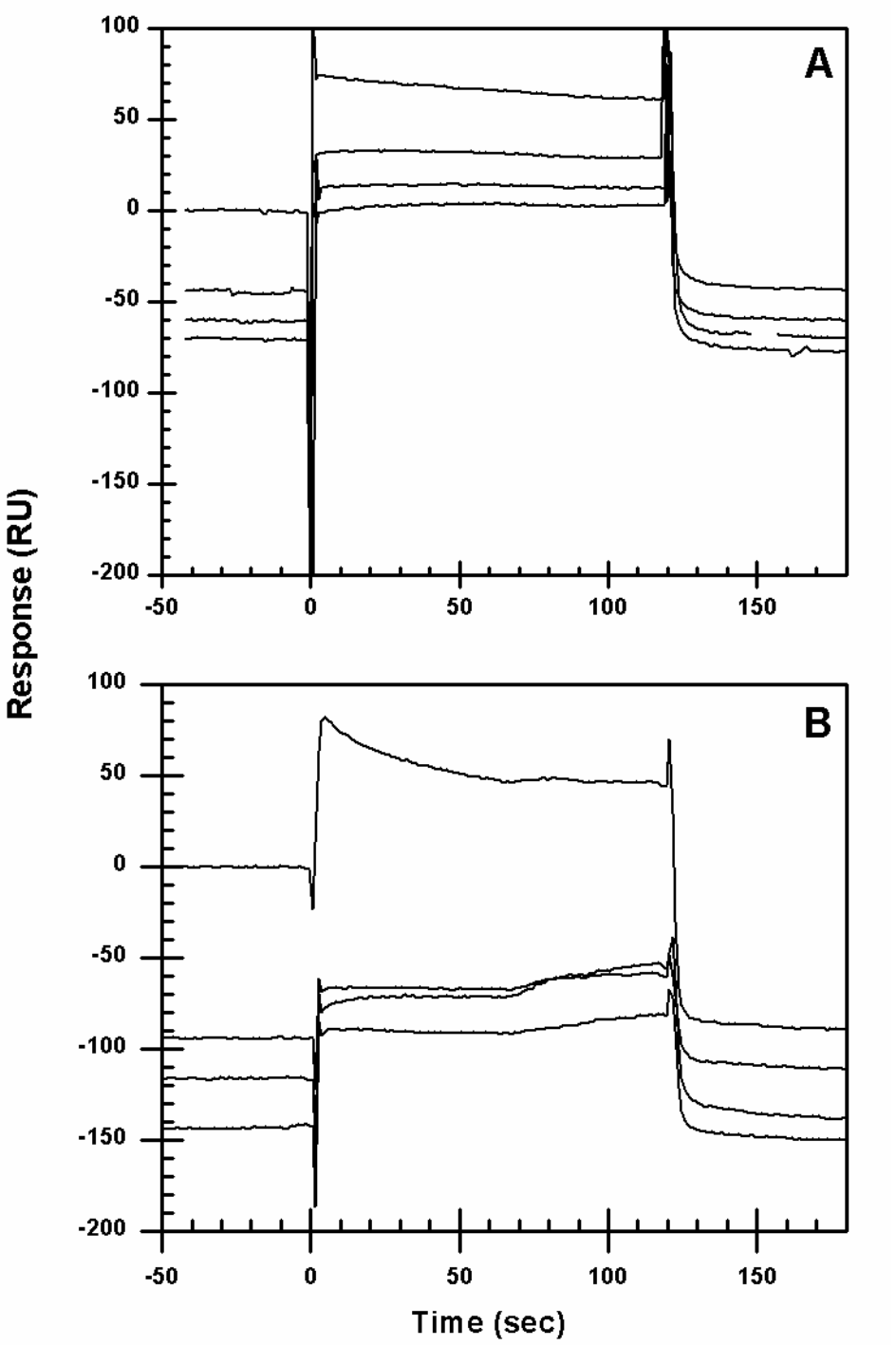

Figure 3.15: Effect of repeated exposure of a fully hybridized dsCTL surface to 0.20 mM Cd^{2+} at pH 7.5 (**A**) and to 20.0 mM Cd^{2+} at pH 8.5 (**B**). A zero value on the response axis corresponds to the starting hybridization level. The baseline becomes lower with each subsequent injection of 0.20 mM Cd^{2+}.

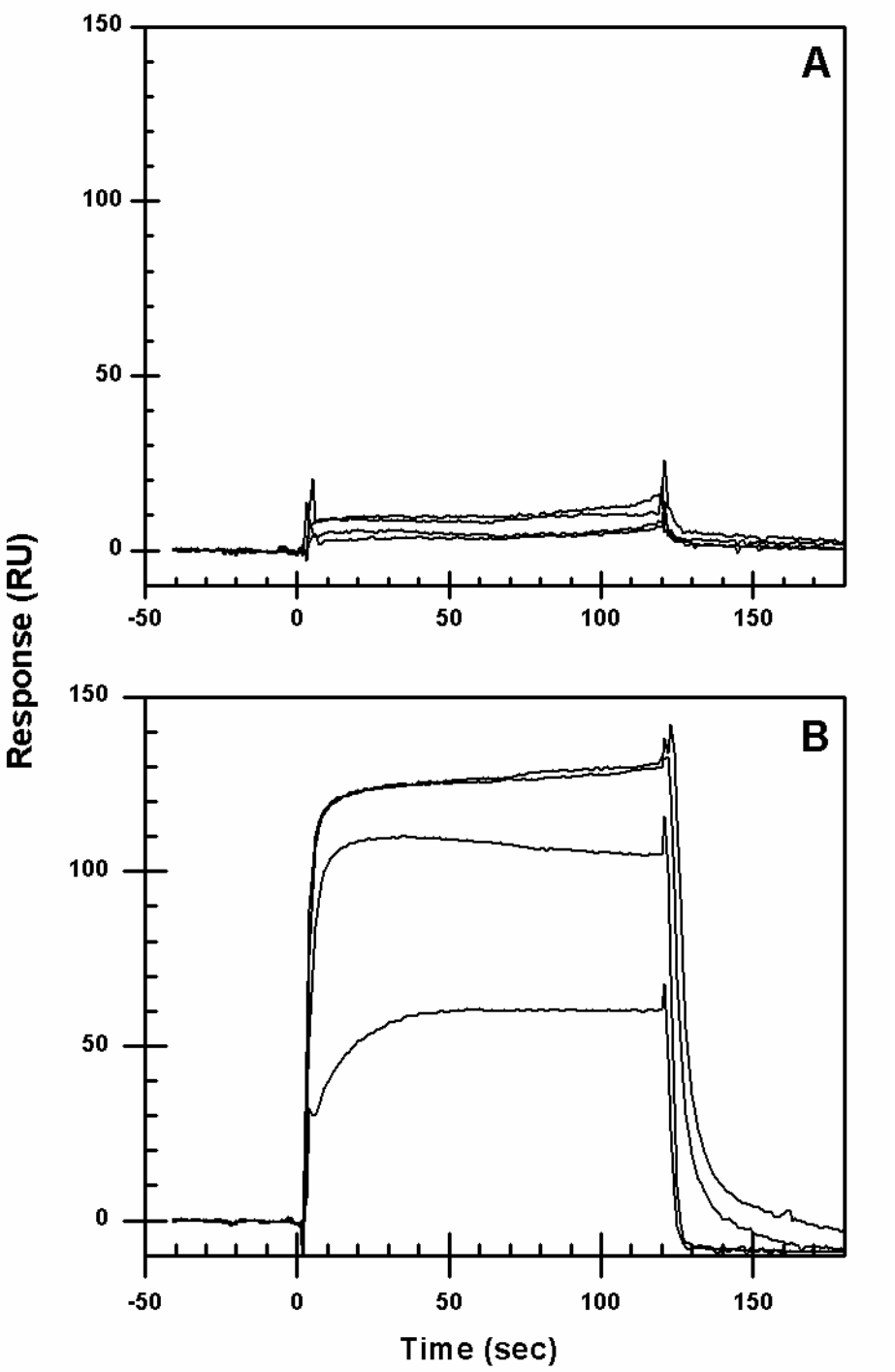

Figure 3.16: Sensorgrams showing the response of dsCTL to various concentrations of Zn^{2+} in pH 7.5 (**A**) and pH 8.5 (**B**) running buffer. The Zn^{2+} concentrations used are 0.05, 0.10, 0.15, and 0.20 mM. The progressively larger responses are due to progressively higher metal ion concentrations. Both of these studies were carried out with the same sensor chip with 370 RU of dsCTL immobilized.

The signals obtained upon exposure of this surface to Ni^{2+} are in many ways similar to those obtained with Zn^{2+}. As with Zn^{2+}, there is little response observed at pH 7.5, whereas signals in excess of $(RU_{pred})_{sat}$ are observed at pH 8.5. These signals are shown over a concentration range of 0.20 - 3.50 mM at pH values 7.5 and 8.5 in figure 3.17. There is no further increase in signal at pH 8.5 upon exposure to 5.00 mM Ni^{2+}. The concentrations at which the maximum signal occurs are an order of magnitude higher than those observed with Zn^{2+}. The amplitude of the peak signal at pH 8.5 is also higher, being ~200 RU compared to ~130 RU. As with Zn^{2+}-induced sensorgrams, the response is very rapid at concentrations that elicit the maximum response. Unlike the responses induced by Zn^{2+}, at concentrations below this threshold, the response continues to rise throughout the injection of Ni^{2+}. The dissociation rate of Ni^{2+} from the DNA is much slower than that of Zn^{2+}. Finally, there is no evidence for denaturation following Ni(II) M-DNA formation. Although the baseline following exposure to TBS is not shown in figure 3.17, following this exposure, the baseline remained at the same value as before the exposure to Ni^{2+}.

When DNA is exposed to metal ions, signals well in excess of $(RU_{pred})_{sat}$ are only obtained in the presence of metal ions known to form M-DNA, Zn^{2+} and Ni^{2+}, and are observed at pH 8.5 but not at pH 7.5. In addition, a higher concentration of Ni^{2+} than Zn^{2+} is required to elicit a maximum response and once this response is obtained, it is more stable than that obtained due to the presence of Zn^{2+}. These results are in agreement with data obtained by the EtBr based assays detailed in section 3.2. A linear relationship is observed between the level of dsCTL immobilized on the surface and the responses obtained from exposure to 0.20 mM Zn^{2+} or 2.00 mM Ni^{2+} at pH 8.5. This is illustrated in

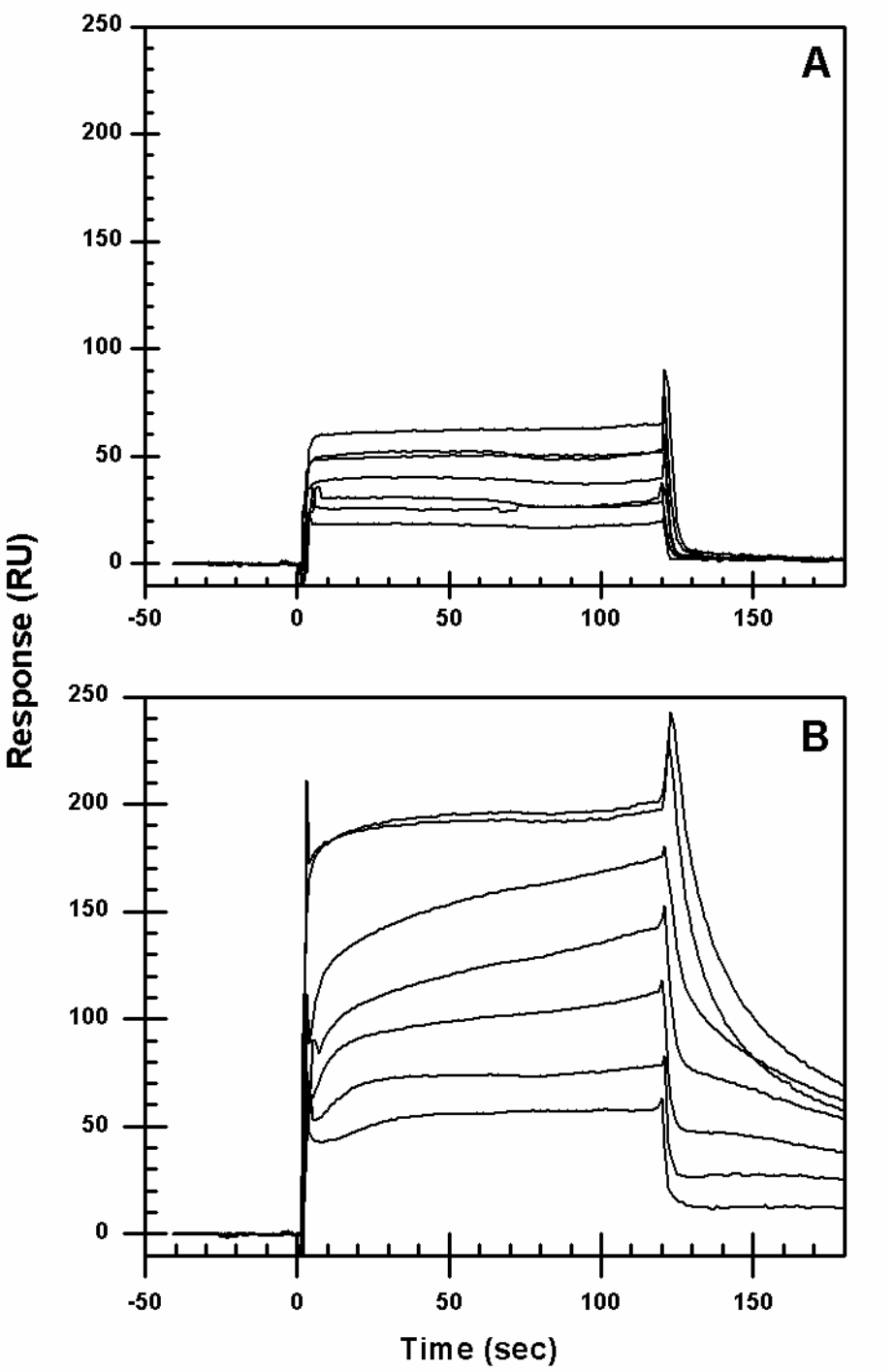

Figure 3.17: Sensorgrams showing the response of dsCTL to various concentrations of Ni^{2+} in pH 7.5 (**A**) and pH 8.5 (**B**) running buffer. The Ni^{2+} concentrations shown are 0.20, 0.40, 0.60, 0.80, 1.00, 2.00, and 3.50 mM. The progressively larger responses are due to progressively higher metal ion concentrations. Both of these studies were carried out with the same sensor chip with 370 RU of dsCTL immobilized.

figure 3.18 and indicates that the signals are due exclusively to changes in the n_d and/or d_d values of the immobilized DNA, suggesting they are due to M-DNA formation.

3.4.2.2 Single-Stranded DNA with 50% GC Content

As with dsCTL, there was a dependence on pH in the response surface to the various metal ions. The responses of btn-CTL-2 to 0.20 mM of Mg^{2+}, Cd^{2+}, Zn^{2+} and Ni^{2+} at each pH are shown in figure 3.19. As with dsCTL, there is little response to Mg^{2+} at either pH while the other metal ions all elicit pH-dependent responses.

The responses of btn-CTL-2 to Zn^{2+} concentrations between 0.05 and 0.20 mM are shown in figure 3.20. The signals obtained at pH 8.5 are roughly twice the amplitude of those obtained at pH 7.5, and at the higher pH are approximately half the amplitude of those obtained with dsCTL. As with dsCTL, the dissociation rates are very rapid. The signals originating from exposure to Ni^{2+} concentrations between 0.20 and 5.00 mM, shown in figure 3.21, are also roughly twice as strong at pH 8.5 relative to pH 7.5. The dissociation rates are very slow. The large positive signals beginning at the end of the injections are due to a rapid reversion to baseline of the background signal but a much slower reversion of the signal on the sample cell, causing a net increase in signal. At pH 7.5, the signals are somewhat higher than those obtained under the same conditions with dsCTL for Zn^{2+} and slightly higher for Ni^{2+}. The signals observed at pH 8.5 upon exposure of btn-CTL-2 to Zn^{2+}, Ni^{2+}, or Cd^{2+} are likely due to formation of a complex similar to M-DNA in which formation of fold-back structures mediate binding of the metal ions and cause the change in signal. The results obtained upon exposure of the

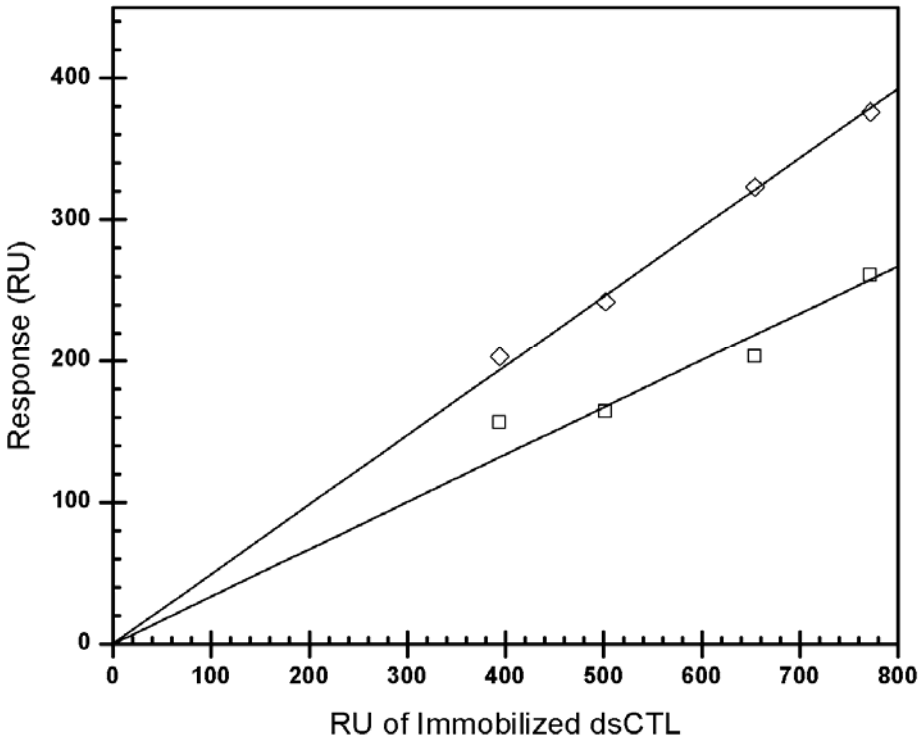

Figure 3.18: Responses of surfaces with increasing levels of immobilized dsCTL to exposure to 0.20 mM Zn^{2+} (diamonds) or 2.00 mM Ni^{2+} (squares) at pH 8.5 as a function of immobilization level of dsCTL. The fits indicated are linear.

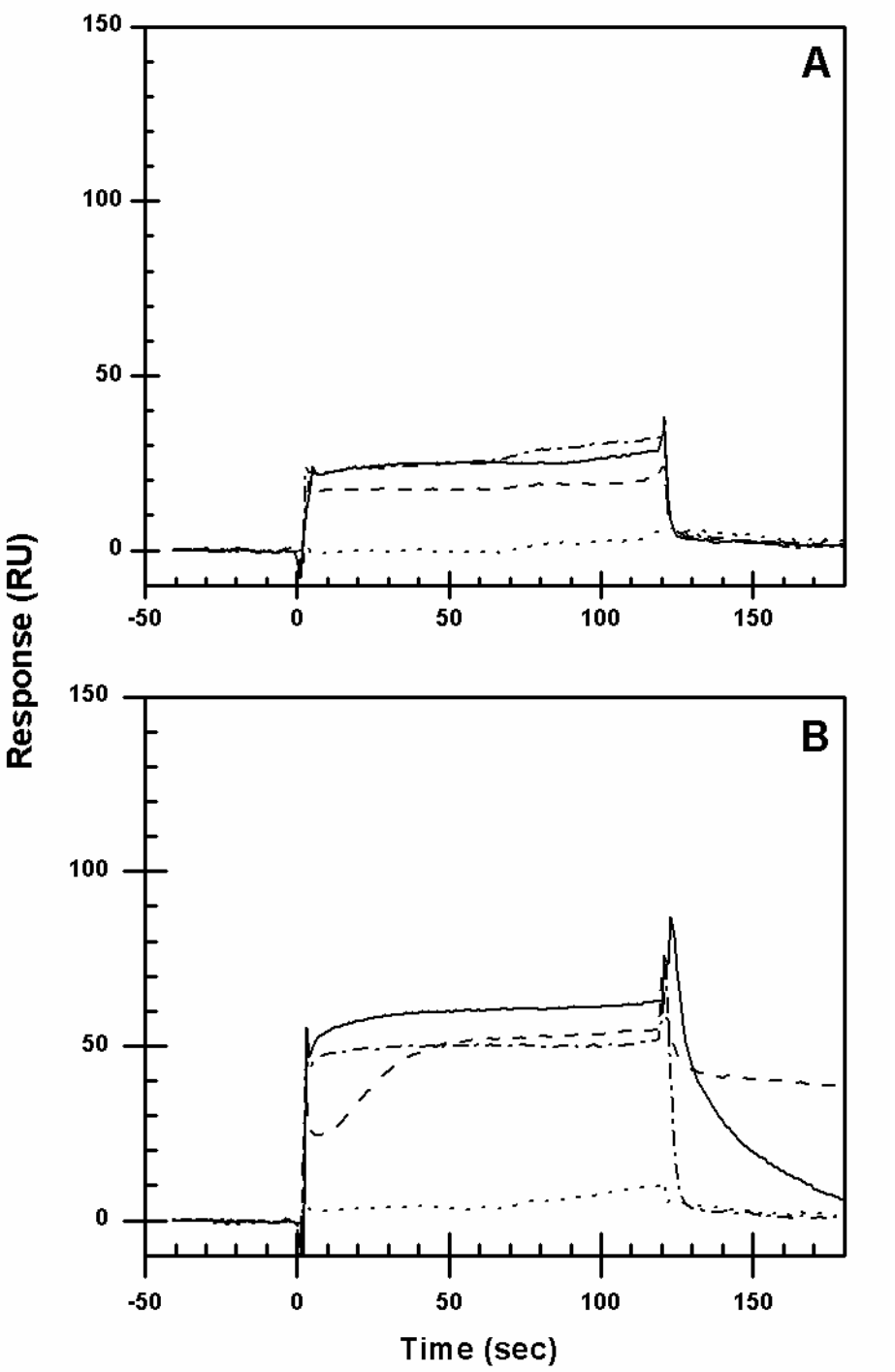

Figure 3.19: Sensorgrams showing the response of 185 RU btn-CTL-2 to 0.20 mM metal ions with a pH 7.5 (**A**) and pH 8.5 (**B**) running buffer. The metal ions used are: solid lines, Zn^{2+} (solid lines), Ni^{2+} (dashed lines), Mg^{2+} (dotted lines), and Cd^{2+} (dot-dashed lines).

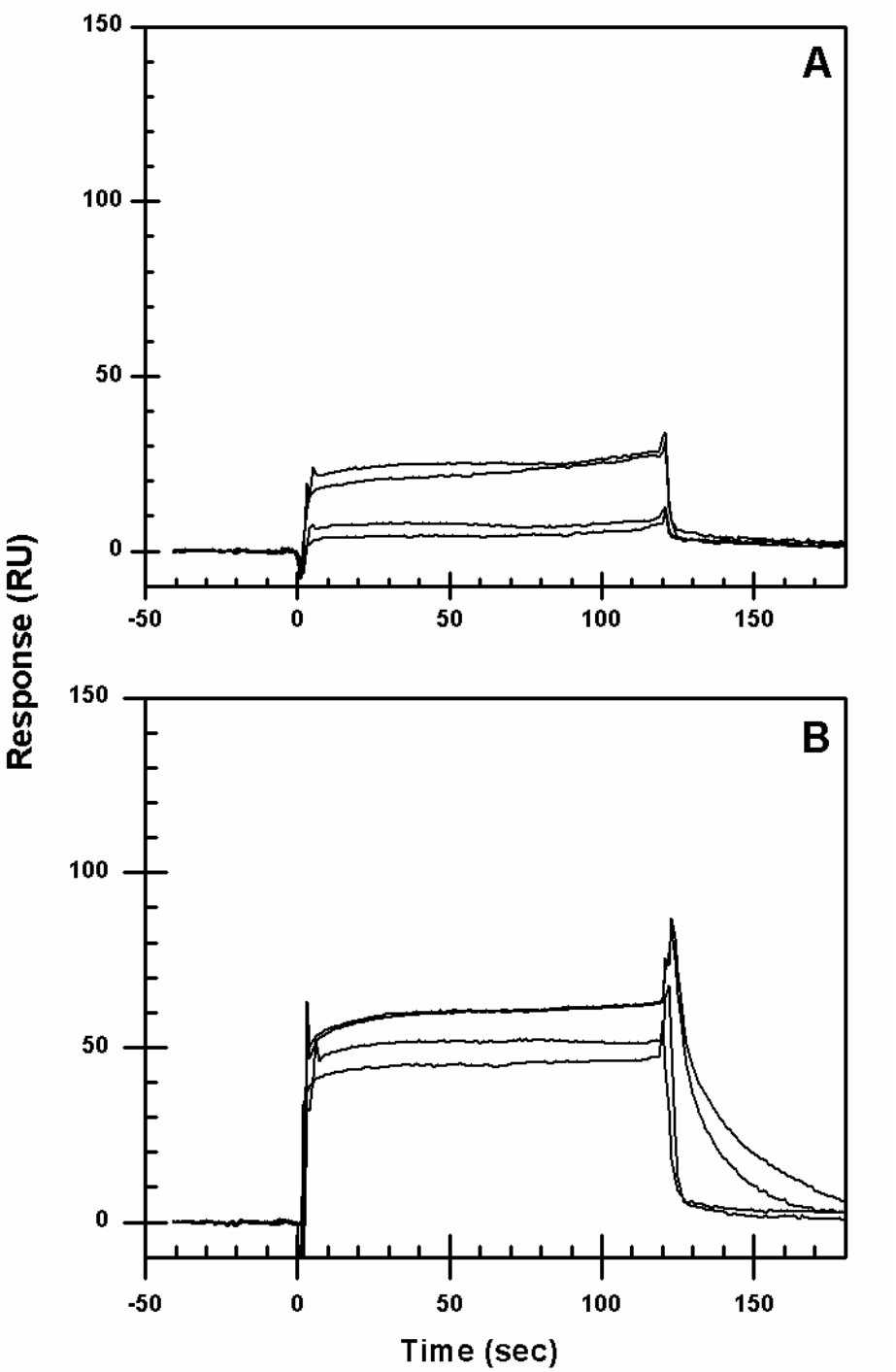

Figure 3.20: Sensorgrams showing the response of btn-CTL-2 to various concentrations of Zn^{2+} in pH 7.5 (**A**) and pH 8.5 (**B**) running buffer. The Zn^{2+} concentrations used are 0.05, 0.10, 0.15, and 0.20 mM. The progressively larger responses are due to progressively higher metal ion concentrations. Both of these studies were carried out with the same sensor chip with 185 RU of btn-CTL-2 immobilized.

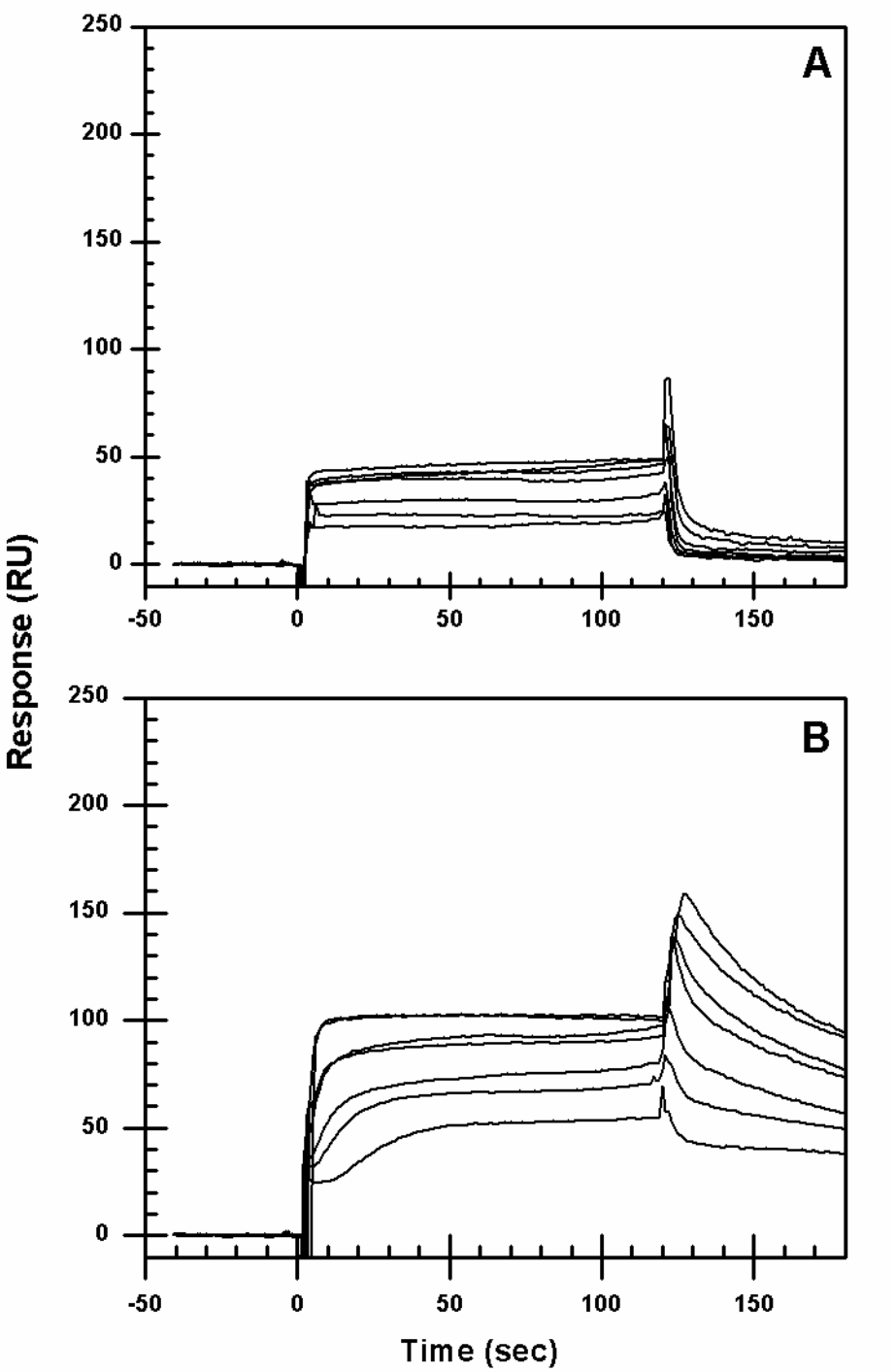

Figure 3.21: Sensorgrams showing the response of btn-CTL-2 to various concentrations of Ni^{2+} in pH 7.5 (**A**) and pH 8.5 (**B**) running buffer. The Ni^{2+} concentrations shown are 0.20, 0.40, 0.60, 0.80, 1.00, 2.00, and 3.50 mM. The progressively larger responses are due to progressively higher metal ion concentrations. Both of these studies were carried out with the same sensor chip with 185 RU of btn-CTL-2 immobilized.

surface to Zn^{2+}, Ni^{2+}, or Cd^{2+} at pH 7.5 are similar to those obtained with dsCTL indicating that these metal ions have little effect on either hybridized or denatured DNA at this pH.

3.4.2.3 Single-Stranded Homopolymers

The homopolymers T30, C30, and A30 were subjected to the same trials as dsCTL and CTL-2; the responses of each of these sequences to 0.20 mM of each metal ion are shown in figures 3.22, 3.25, and 3.28, respectively. As with the 50% GC sequences, Mg^{2+} has little effect at either pH on any of these sequences. T30 displayed a strong pH-dependence in its responses to Zn^{2+}, Ni^{2+}, and Cd^{2+}, while C30 and A30 showed very weak pH-dependences in their responses.

The responses of T30 to Zn^{2+} and Ni^{2+} are shown in figures 3.23 and 3.24, respectively. A dependence on pH is observed in both cases, although it is more pronounced with Zn^{2+} than with Ni^{2+}. C30 has almost no pH-dependence in its responses to increasing Zn^{2+} concentrations, but some degree of pH-dependence in those to increasing Ni^{2+} concentrations, as shown in figures 3.26 and 3.27, respectively. Exposure of A30 to Zn^{2+} at either pH showed signals near the 30-site predictions of $(RU_{pred})_{sat}$; these responses are shown in figure 3.29. On the other hand, signals well in excess of those $(RU_{pred})_{sat}$ were observed at pH values 7.5 and 8.5 when A30 was exposed to Ni^{2+}, as shown in figure 3.30. Thus, a larger difference between the signals obtained at each pH was observed for Zn^{2+} than Ni^{2+} with T30, but with C30 and A30 a stronger pH-dependency was observed with Ni^{2+} than with Zn^{2+}. However, regardless of which metal

ion the surface was exposed, a larger dependence of the signal obtained on pH was observed with T30 than with C30 or A30.

The results obtained by exposure of T30 to Zn^{2+} are, as with btn-CTL-2, likely due to the formation of fold-back structures with metal ions bridging base pairs at pH 8.5 but not at pH 7.5. The lack of large differences between signals obtained with Zn^{2+} at each pH with C30 or A30 are likely due to the absence of binding sites which are likely to undergo proton exchange over this pH range.

T30, C30, btn-CTL-2, and dsCTL all showed similar responses to Ni^{2+} at pH 7.5 while those of A30 were substantially higher. This difference is likely due to conformational changes caused by binding of Ni^{2+} to N7 positions in A30 that could result in formation of a secondary structure. All five sequences showed a larger response to Ni^{2+} at pH 8.5 than at pH 7.5, although the largest pH-difference by far was observed with dsCTL. Of the single-stranded sequences, the responses to 1.00 mM Ni^{2+} at pH 8.5 followed the order T30 ~ A30 > btn-CTL-2 > C30. The responses obtained with T30 and btn-CTL-2 could be due to fold-back M-DNA-like structures as with Zn^{2+} while the weak responses of C30 could be due to a lack of potential secondary structures. The large responses obtained at pH 8.5 with A30 could be due to formation of secondary structures as well as binding at N7 positions. Increased signals at pH 8.5 with C30 or A30 could also be due to changes in the properties of the Ni^{2+} ion and the complexes it forms with solvent molecules. This will be further discussed in section 4.3.

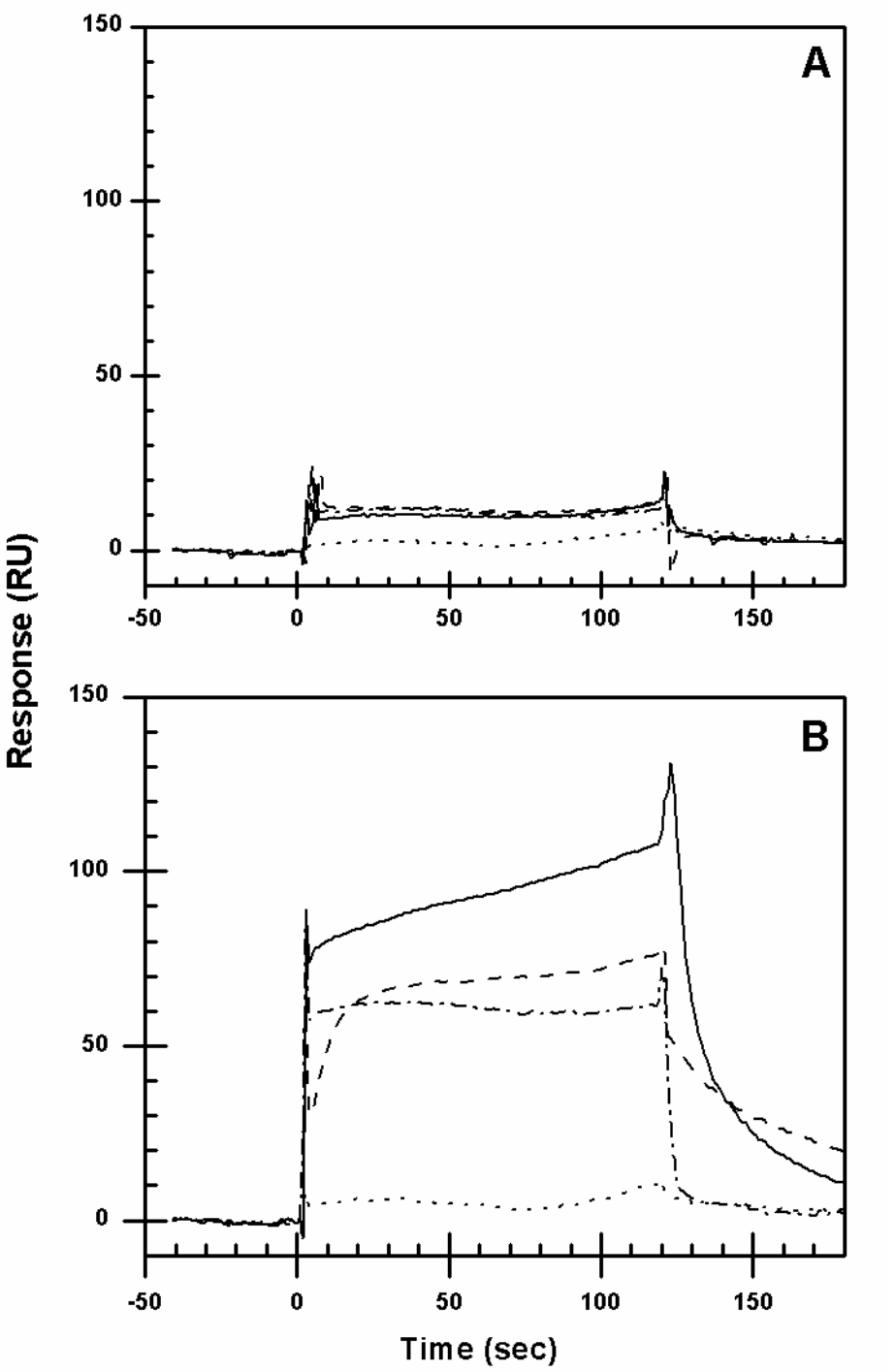

Figure 3.22: Sensorgrams showing the response of 206 RU of T30 to 0.20 mM metal ions with a pH 7.5 (**A**) and pH 8.5 (**B**) running buffer. The metal ions used are: solid lines, Zn^{2+} (solid lines), Ni^{2+} (dashed lines), Mg^{2+} (dotted lines), and Cd^{2+} (dot-dashed lines).

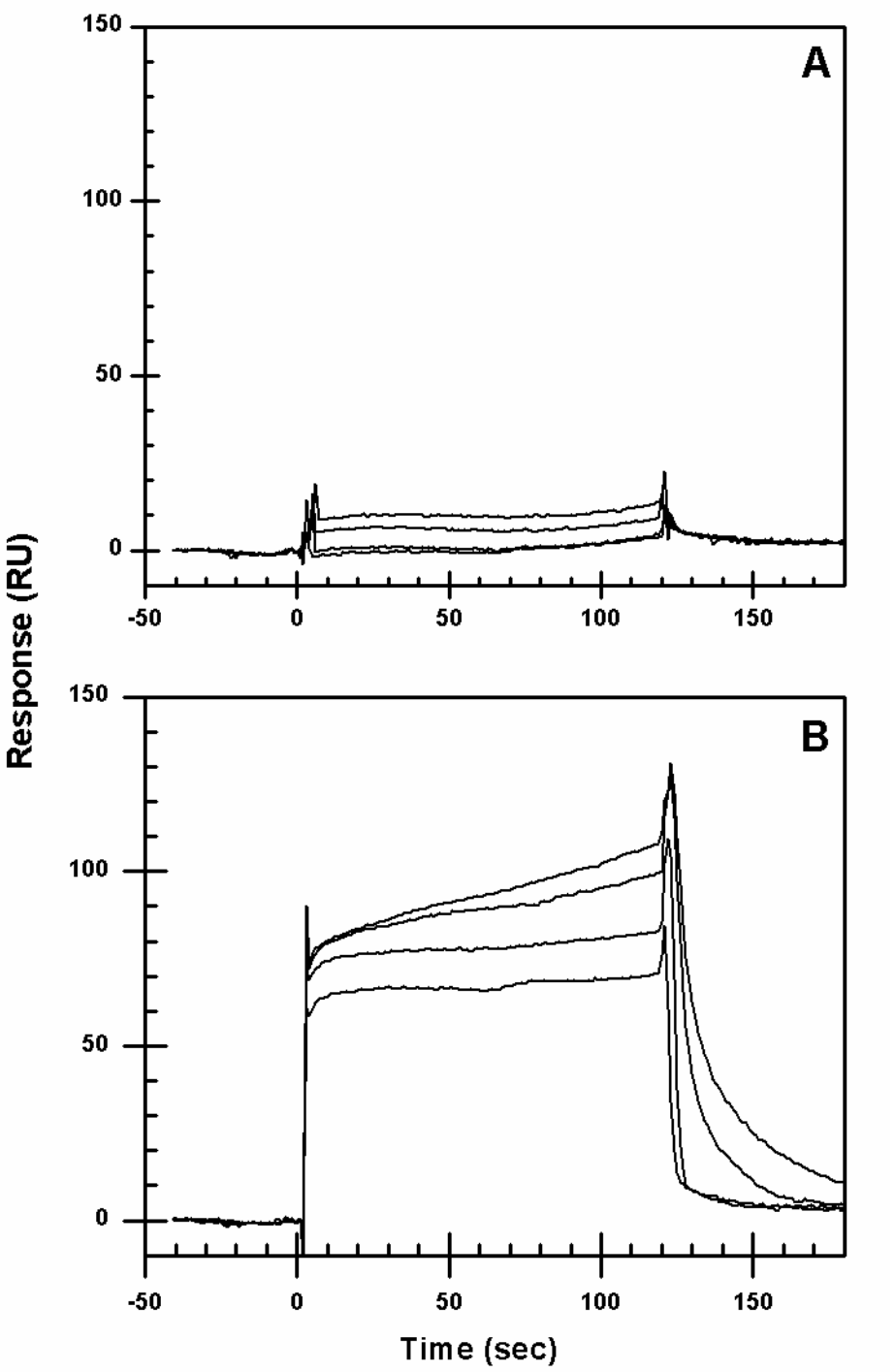

Figure 3.23: Sensorgrams showing the response of T30 to various concentrations of Zn^{2+} in pH 7.5 (**A**) and pH 8.5 (**B**) running buffer. The Zn^{2+} concentrations used are 0.05, 0.10, 0.15, and 0.20 mM. The progressively larger responses are due to progressively higher metal ion concentrations. Both of these studies were carried out with the same sensor chip with 206 RU of T30-immobilized.

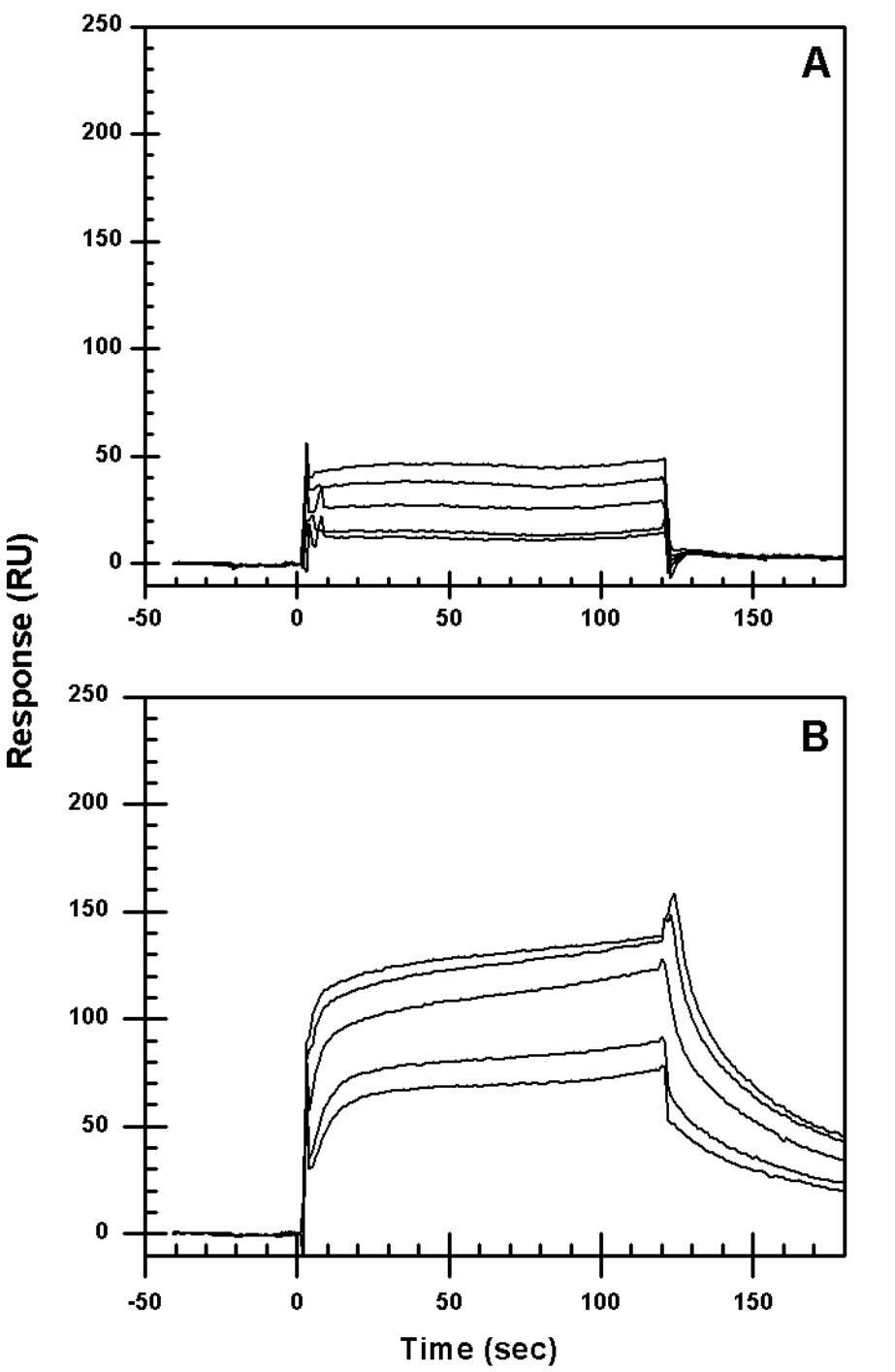

Figure 3.24: Sensorgrams showing the response of T30 to various concentrations of Ni^{2+} in pH 7.5 (**A**) and pH 8.5 (**B**) running buffer. The Ni^{2+} concentrations shown are 0.20, 0.40, 0.60, 0.80, and 1.00 mM. The progressively larger responses are due to progressively higher metal ion concentrations. Both of these studies were carried out with the same sensor chip with 206 RU of T30 immobilized.

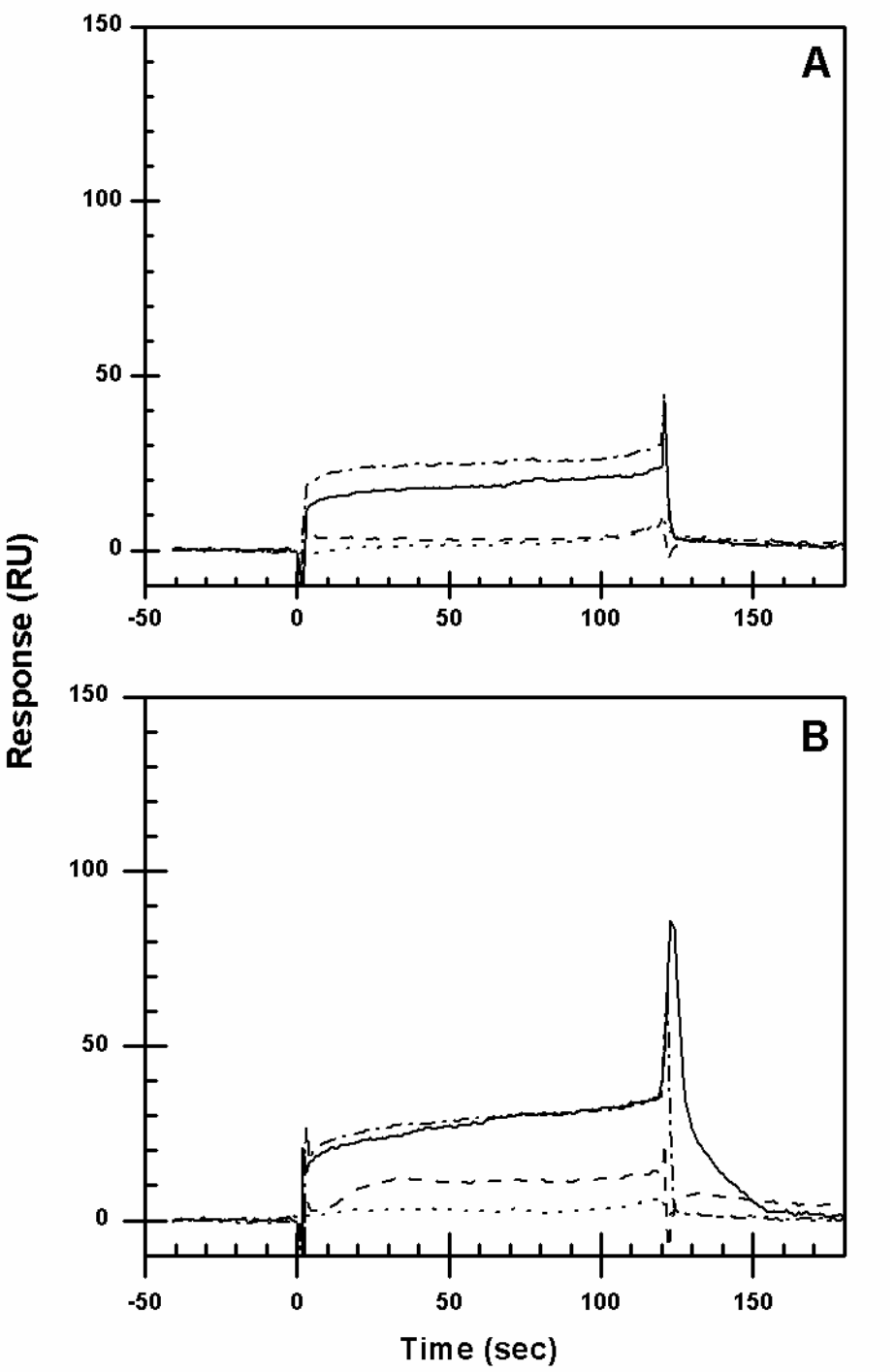

Figure 3.25: Sensorgrams showing the response of 214 RU of C30 to 0.20 mM metal ions with a pH 7.5 (**A**) and pH 8.5 (**B**) running buffer. The metal ions used are: solid lines, Zn^{2+} (solid lines), Ni^{2+} (dashed lines), Mg^{2+} (dotted lines), and Cd^{2+} (dot-dashed lines).

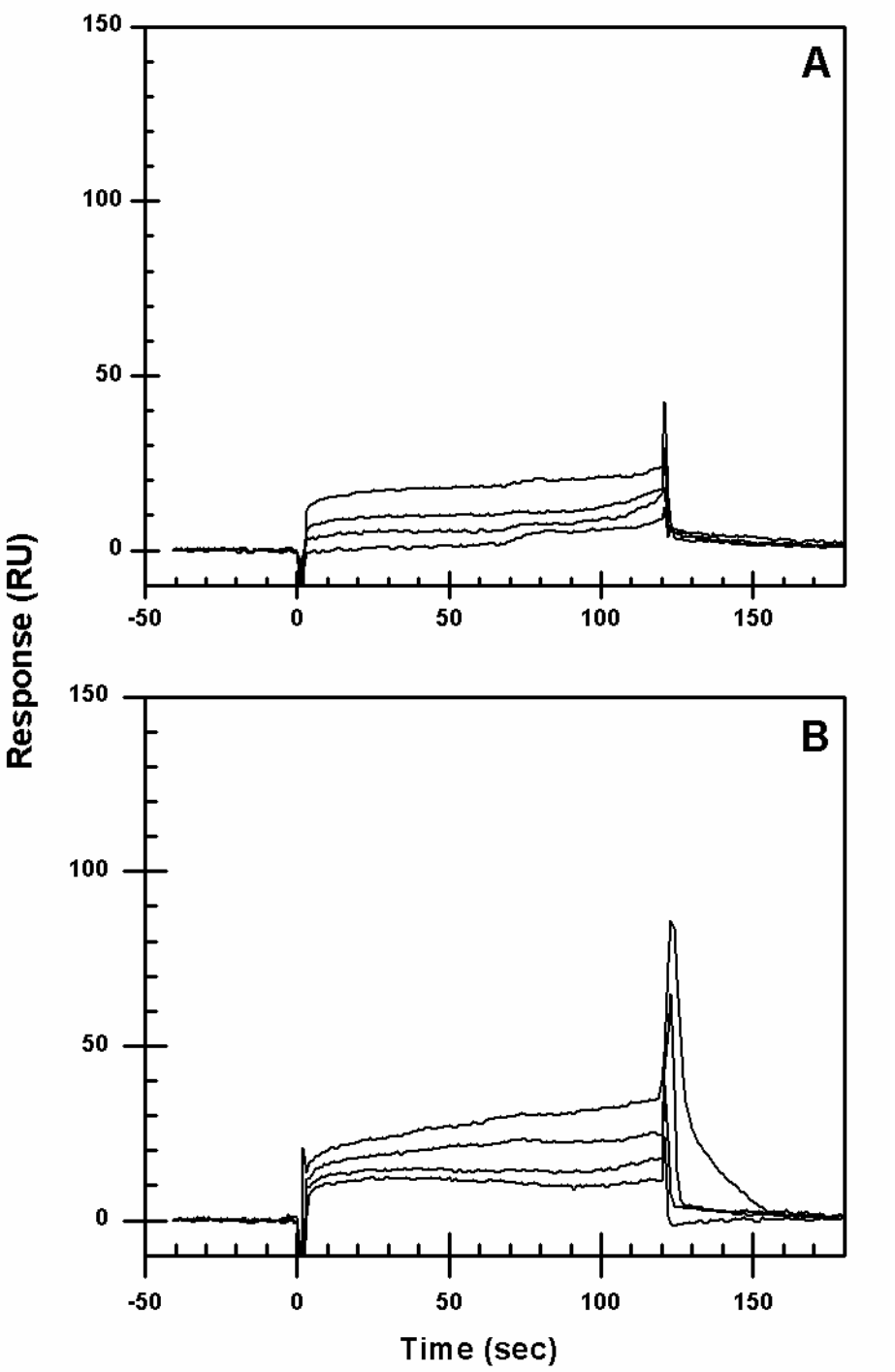

Figure 3.26: Sensorgrams showing the response of C30 to various concentrations of Zn^{2+} in pH 7.5 (**A**) and pH 8.5 (**B**) running buffer. The Zn^{2+} concentrations used are 0.05, 0.10, 0.15, and 0.20 mM. The progressively larger responses are due to progressively higher metal ion concentrations. Both of these studies were carried out with the same sensor chip with 214 RU of C30 immobilized.

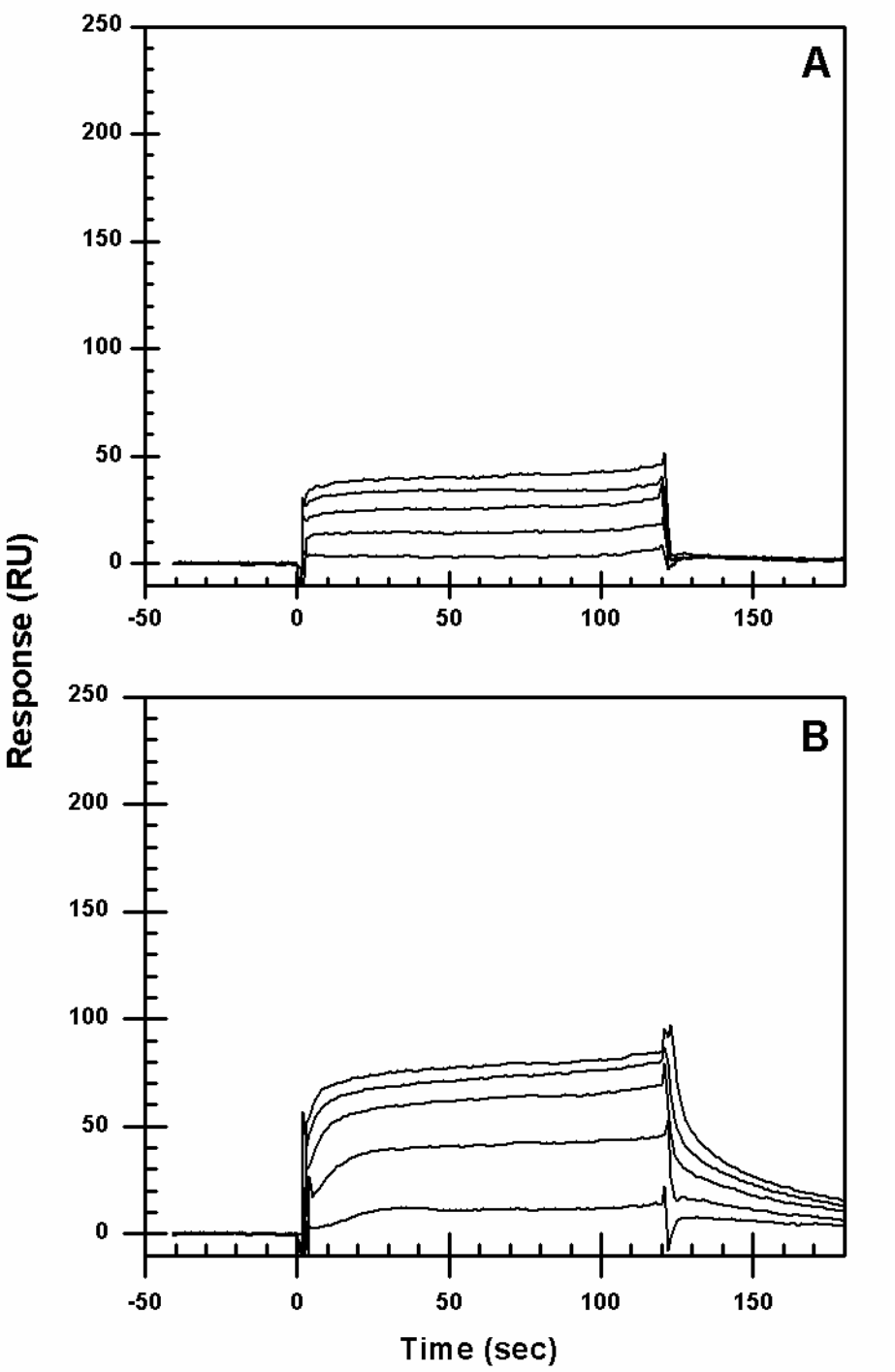

Figure 3.27: Sensorgrams showing the response of C30 to various concentrations of Ni^{2+} in pH 7.5 (**A**) and pH 8.5 (**B**) running buffer. The Ni^{2+} concentrations shown are 0.20, 0.40, 0.60, 0.80, and 1.00 mM. The progressively larger responses are due to progressively higher metal ion concentrations. Both of these studies were carried out with the same sensor chip with 214 RU of C30 immobilized.

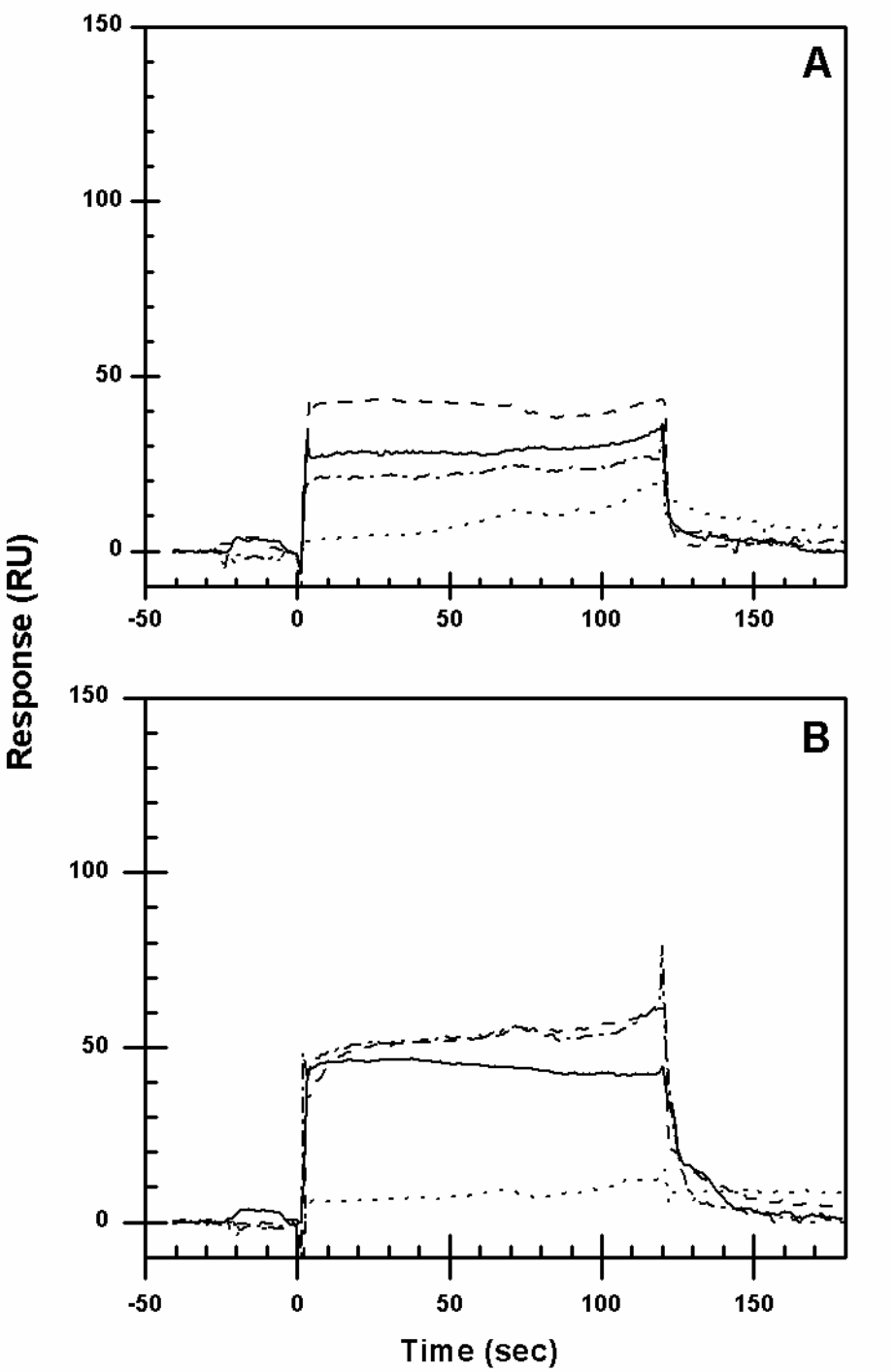

Figure 3.28: Sensorgrams showing the response of 220 RU of A30 to 0.20 mM metal ions with a pH 7.5 (**A**) and pH 8.5 (**B**) running buffer. The metal ions used are: solid lines, Zn^{2+} (solid lines), Ni^{2+} (dashed lines), Mg^{2+} (dotted lines), and Cd^{2+} (dot-dashed lines).

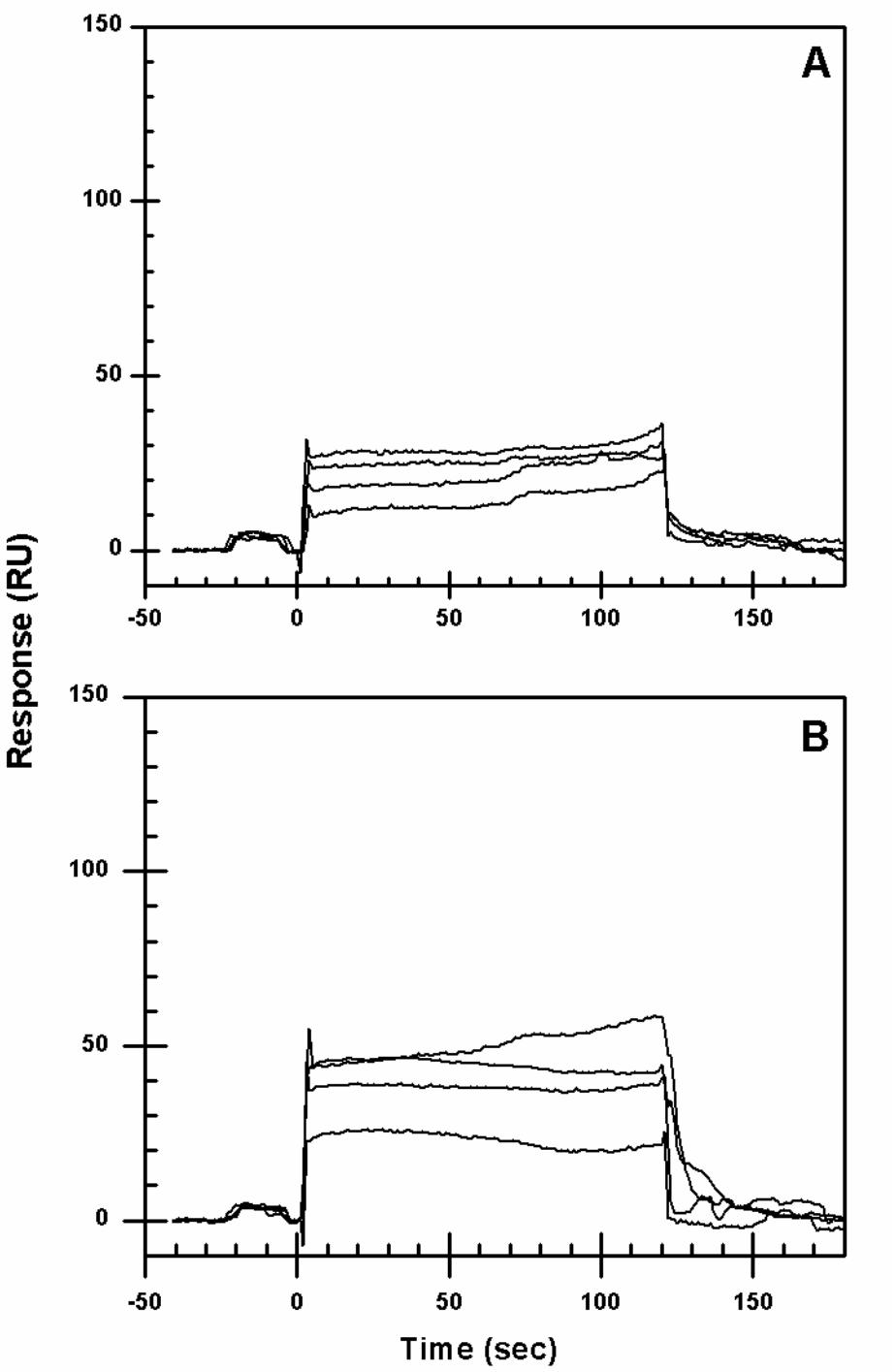

Figure 3.29: Sensorgrams showing the response of A30 to various concentrations of Zn^{2+} in pH 7.5 (**A**) and pH 8.5 (**B**) running buffer. The Zn^{2+} concentrations used are 0.05, 0.10, 0.15, and 0.20 mM. The progressively larger responses are due to progressively higher metal ion concentrations. Both of these studies were carried out with the same sensor chip with 220 RU of A30 immobilized.

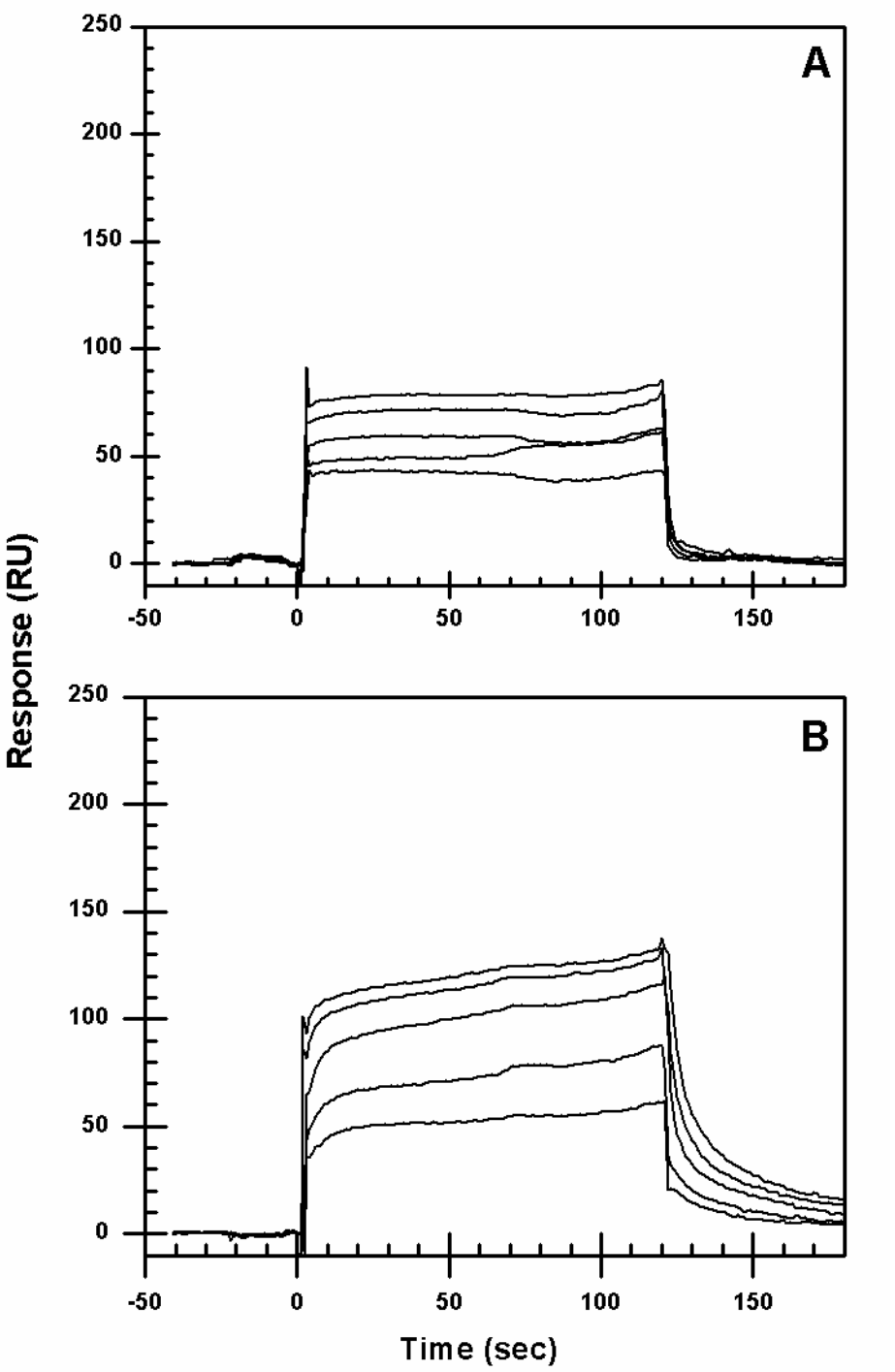

Figure 3.30: Sensorgrams showing the response of A30 to various concentrations of Ni^{2+} in pH 7.5 (**A**) and pH 8.5 (**B**) running buffer. The Ni^{2+} concentrations shown are 0.20, 0.40, 0.60, 0.80, and 1.00 mM. The progressively larger responses are due to progressively higher metal ion concentrations. Both of these studies were carried out with the same sensor chip with 220 RU of A30 immobilized.

3.4.3 Low-pH M-DNA Formation

When dsCTL was exposed to millimolar Zn^{2+} concentrations at pH 7.5, signals indicative of M-DNA formation were observed. At pH 7.5, peak signals were observed at 5 mM Zn^{2+}; they were equal to 95 % of those observed with 0.20 mM Zn^{2+} at pH 8.5. Similar results were not observed upon exposure of dsCTL to millimolar Ni^{2+} at pH 7.5. At pH 7.5, plateau signals were observed upon exposure of dsCTL to 10 mM Ni^{2+}. However, this pleateau was only equal to 39 % of that observed with 2.0 mM Ni^{2+} at pH 8.5.

At pH 6.5, signals of approximately 145 RU were observed upon exposure of dsCTL to 20 mM Zn^{2+}, Ni^{2+}, or Cd^{2+}. Peak responses for all concentrations of Zn^{2+} and Ni^{2+} are shown at all three pH values in figure 3.31A. Although these signals are larger than those observed at pH 7.5 for both metal ions, the signals obtained upon exposure of dsCTL to Mg^{2+} at pH 6.5 are also much higher than those obtained at pH 7.5. Thus, it is difficult to asses M-DNA formation at pH values of 6.5 and 7.5 by SPR. These results are discussed further in section 4.3.

3.4.3.1 5-Fluorouracil Substituted Double-Stranded DNA

Sequences with 6, 9, or 15 T residues replaced with F^5U were assayed in addition to the standard dsCTL sequences detailed in section 3.4.2.1. In no case was there a significantly increased propensity to form M-DNA relative to unsubstituted sequences. The peak values of the responses obtained in these experiments plotted against metal ion

(**A**)

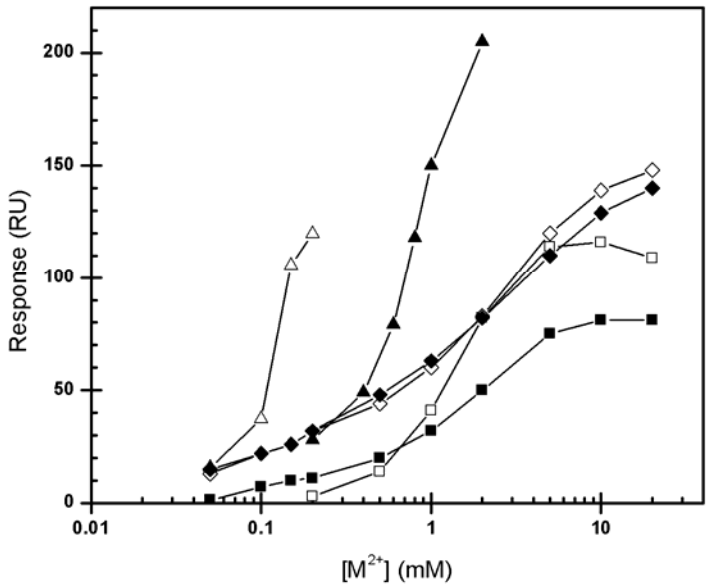

(**B**)

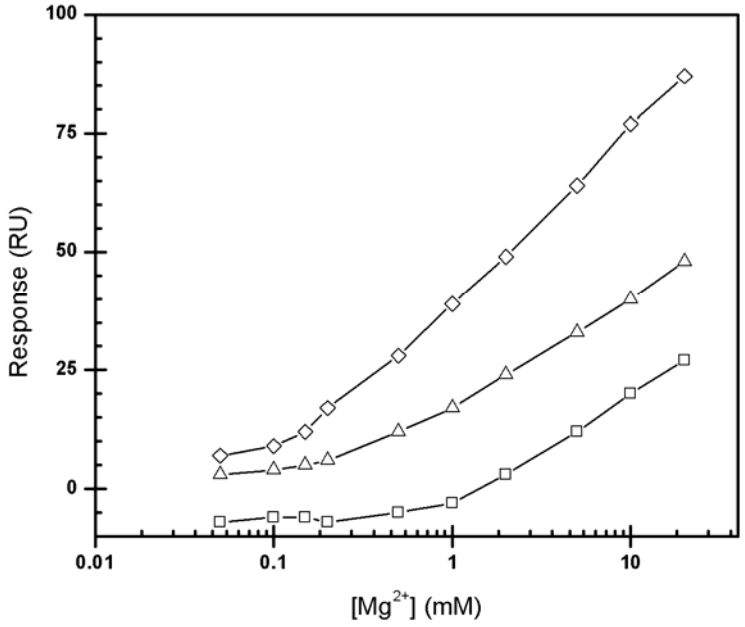

Figure 3.31: Peak values of responses to (**A**) Zn^{2+} (white symbols), Ni^{2+} (black symbols) and (**B**) Mg^{2+} (white symbols). Both sets of data were obtained with the same chip with approximately 370 RU of dsCTL immobilized. The readings were obtained at pH values of 6.5 (diamonds), 7.5 (squares), and 8.5 (triangles).

(**A**)

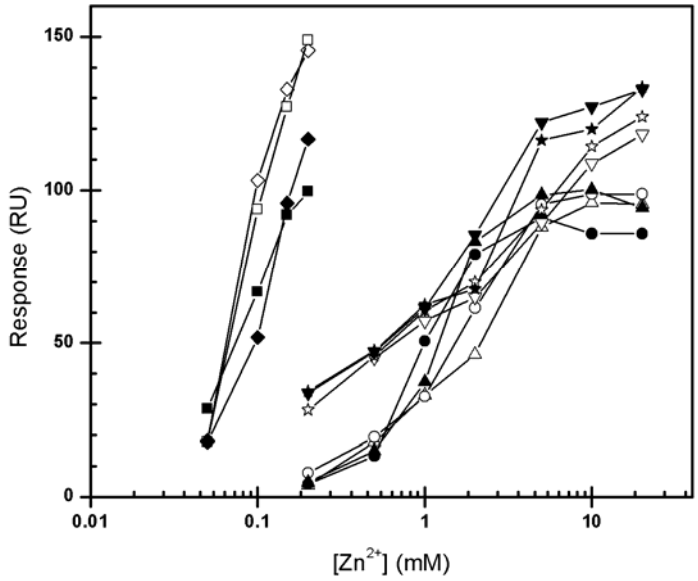

(**B**)

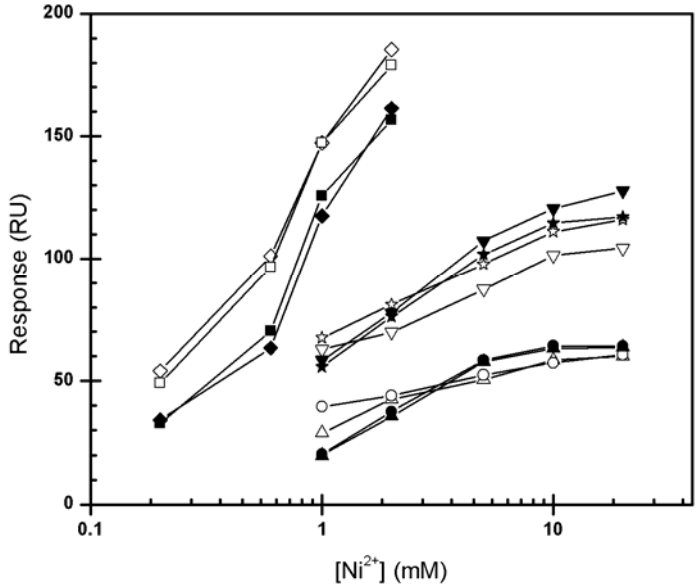

Figure 3.32: The response peaks of dsCTL with varying degrees of F^5U substitution to Zn^{2+} (**A**) and Ni^{2+} (**B**). Four hybridization states are shown: CTL-1 / btn-CTL-2 (pH 8.5, white diamonds; pH 7.5, white triangles; pH 6.5, white inverted triangles), 5FUCTL-1 / btn-CTL-2 (pH 8.5, white squares; pH 7.5, white circles; pH 6.5, white stars), CTL-1 / 5FUCTL-2 (pH 8.5, black diamonds; pH 7.5, black triangles; pH 6.5, black inverted triangles), and 5FUCTL-1 / 5FUCTL-2 (pH 8.5, black squares; pH 7.5, black circles; pH 6.5, black stars).

concentrations at all three pH values with Zn^{2+} and Ni^{2+} are shown in figure 3.32. The only difference between signals obtained with sequences containing F^5U and those that did not was that the substituted sequences were denatured more severely by Zn^{2+} and were denatured by Ni^{2+}. These results are surprising given the increased formation and pH stability of M-DNA observed in F^5U-substituted DNA observed with the EtBr-based assay. Small differences between readings in figures 3.32 and 3.31 are due to deviations encountered when using different sensor chips.

3.5 Quenching of Fluorophore-labeled DNA at Low pH

Fluorescence quenching studies were performed on Fl/QSY7 double-labeled DNA to verify SPR results that suggested low pH M-DNA formation was possible. As the corrected quenching titrations in figure 3.33 show, quenching occurs at all pH values, although the required metal ion concentration raises as the pH drops. The Zn^{2+} concentrations necessary to form M-DNA at pH 7.5 are roughly 100-fold higher than those causing dismutation at pH 8.5. Thus, low-pH quenching was not observed in previous studies since pH 7.5 controls were carried out at the same Zn^{2+} concentrations as the studies at pH 8.5. Further, $MgCl_2$ had no effect on quenching regardless of concentration or pH, while $CdCl_2$ allowed quenching at low pH and denatured the DNA at high pH. The denaturation induced by $CdCl_2$ at pH 8.5 is apparent from the increase to baseline following a small amount of quenching allowed by concentrations of $CdCl_2$ below 0.08 mM. The data from the $MgCl_2$ and $CdCl_2$ trials is presented in figure 3.34.

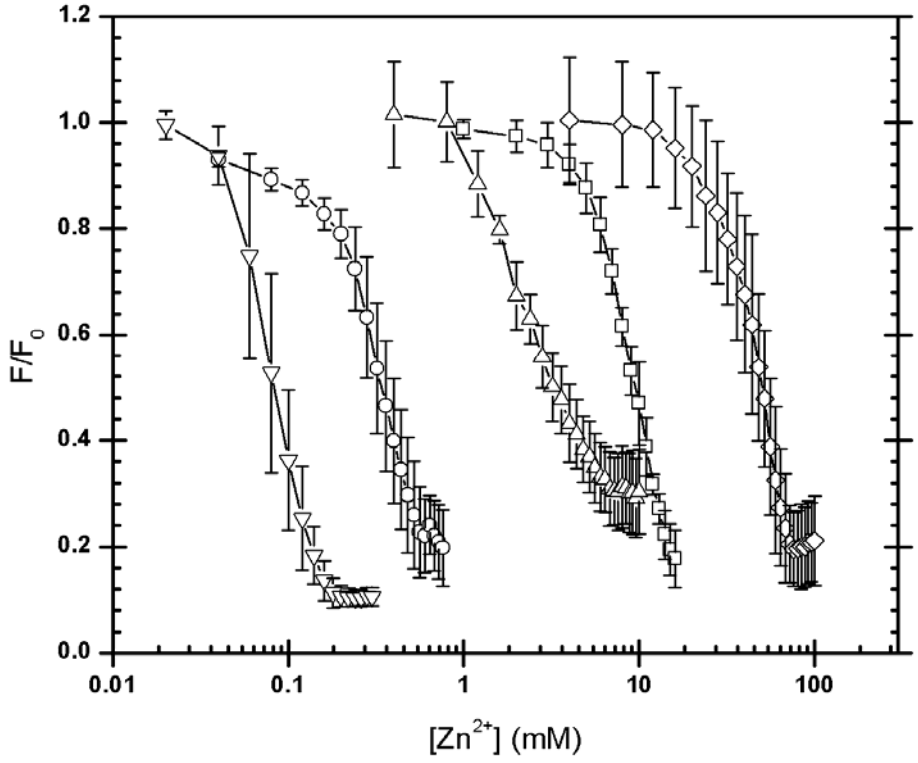

Figure 3.33: Corrected quenching profiles for the Fl-CTL-1 / QSY7-CTL-2 duplex at pH 6.5 (diamonds), pH 7.0 (squares), pH 7.5 (triangles), pH 8.0 (circles), and pH 8.5 (inverted triangles). The remaining fluorescence divided by the initial fluorescence is shown as a function of added Zn^{2+} cocentration.

(**A**)

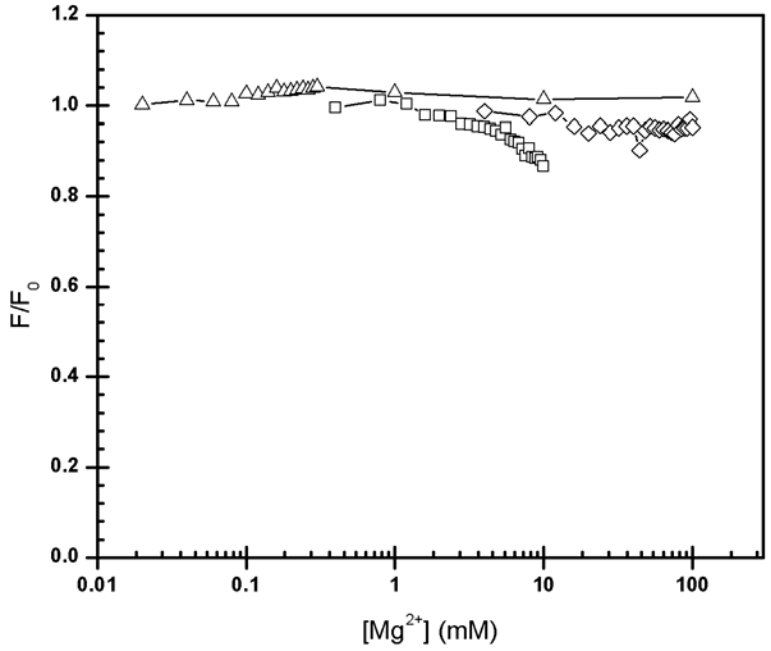

(**B**)

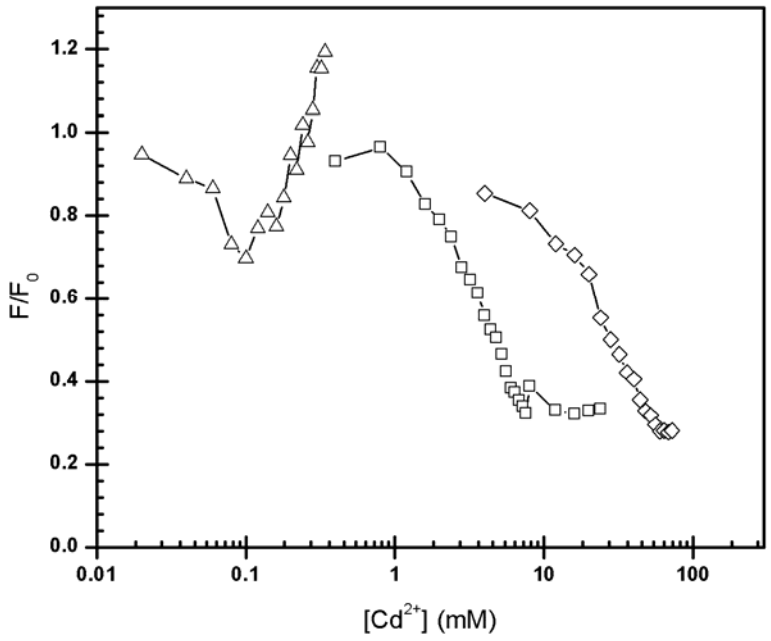

Figure 3.34: Corrected quenching profiles for the Fl-CTL-1 / QSY7-CTL-2 duplex with (**A**) Mg^{2+} at and (**B**) Cd^{2+} at pH 6.5 (diamonds), 7.5 (squares), and pH 8.5 (triangles).

The data shown in figure 3.33 are averages of between 3 and 6 individual experiments, while data shown in figures 3.34 – 3.36 are averages of 2 individual experiments.

Two different $ZnCl_2$ solutions were used for this portion of the study. Both were initially prepared at 2.0 M and diluted to the desired 400X solution for each experiment. The pH of the first was adjusted to 4.0 as described in section 2.1. In the second case, the $ZnCl_2$ was dissolved to 2.0 M without addition of HCl resulting in a solution of pH ~4.40. At all pH values except pH 6.5, no significant difference was observed between the two experiments, and readings with both $ZnCl_2$ stock solutions are averaged together with no effect on the standard deviation. However, as illustrated in figure 3.35, there is a substantial difference between titrations using the two different stock solutions at pH 6.5. When the acidified stock is used, the midpoint of the transition occurs at 50 mM $ZnCl_2$ while with the unacidified $ZnCl_2$, the midpoint of the transition occurs at 9 mM $ZnCl_2$. These figures are the average of several readings and three separately prepared 2.0 M $ZnCl_2$ stocks of each type were used, with all three producing the same results. As illustrated in figure 3.36, the final pH of the solution varies little with addition of either $ZnCl_2$ solution. Finally, there is almost no difference between the changes in pH caused by each stock solution of $ZnCl_2$ over the $ZnCl_2$ concentration range that cause a large change with the unacidified stock but not with the acidified one. As a control, assays were also done using $Zn(ClO_4)_2$ as a titrant, which showed results similar to those obtained with the acidified $ZnCl_2$ solution, as shown in figure 3.35.

Figure 3.37 summarizes the concentrations of $ZnCl_2$ necessary to drop the corrected fluorescence intensities to 50% of their starting values at each pH. For pH 6.5, the values obtained with each stock solution of $ZnCl_2$ as well as $Zn(ClO_4)_2$ are indicated.

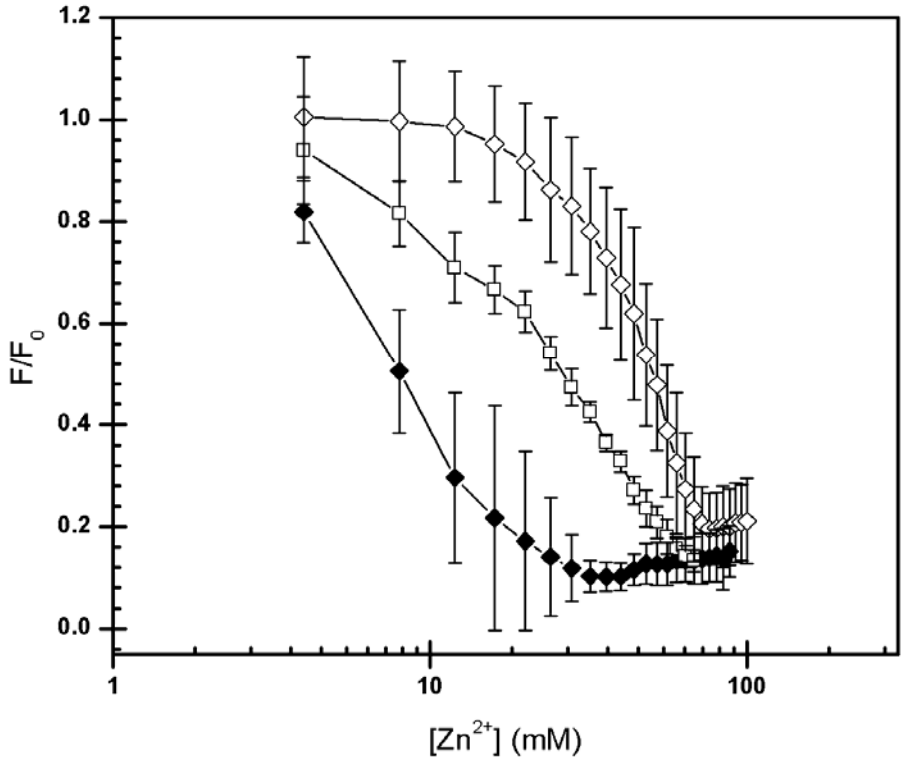

Figure 3.35: Corrected quenching profiles for the Fl-CTL-1 / QSY7-CTL-2 duplex with at pH 6.5 with adjusted pH $ZnCl_2$ stock solution (white diamonds), unadjusted pH $ZnCl_2$ stock solution (black diamonds), and $Zn(ClO_4)_2$ stock solution (white squares).

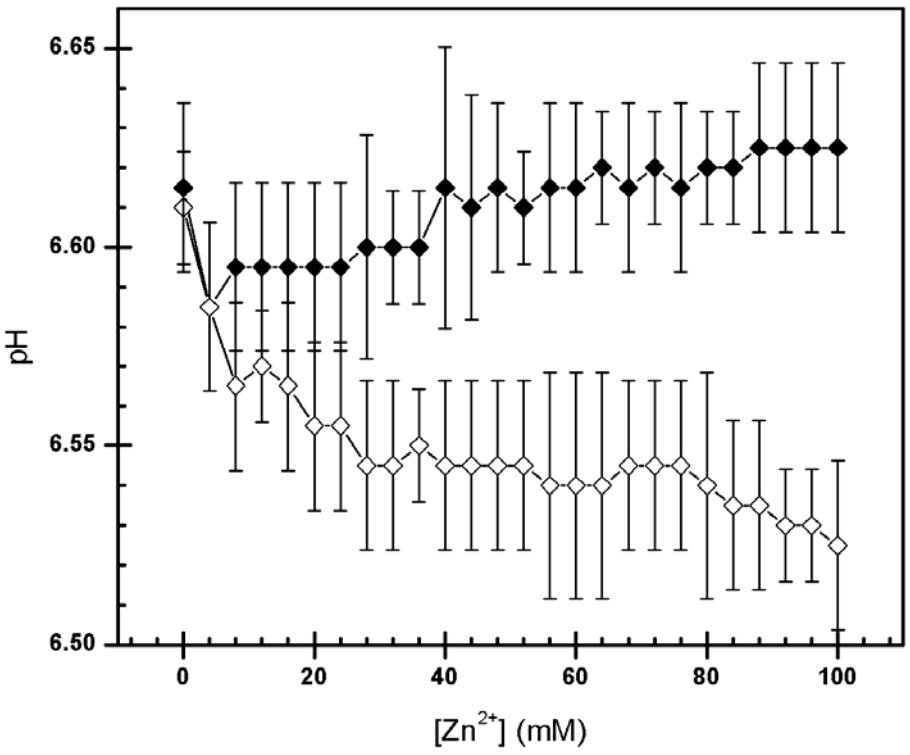

Figure 3.36: The effect of each $ZnCl_2$ stock solution on the pH of a 10 mM MES pH 6.5, 10 mM NaCl as a function of added Zn^{2+} concentration. Values are shown for the adjusted pH $ZnCl_2$ solution (white diamonds) and the unadjusted pH $ZnCl_2$ solution (black diamonds).

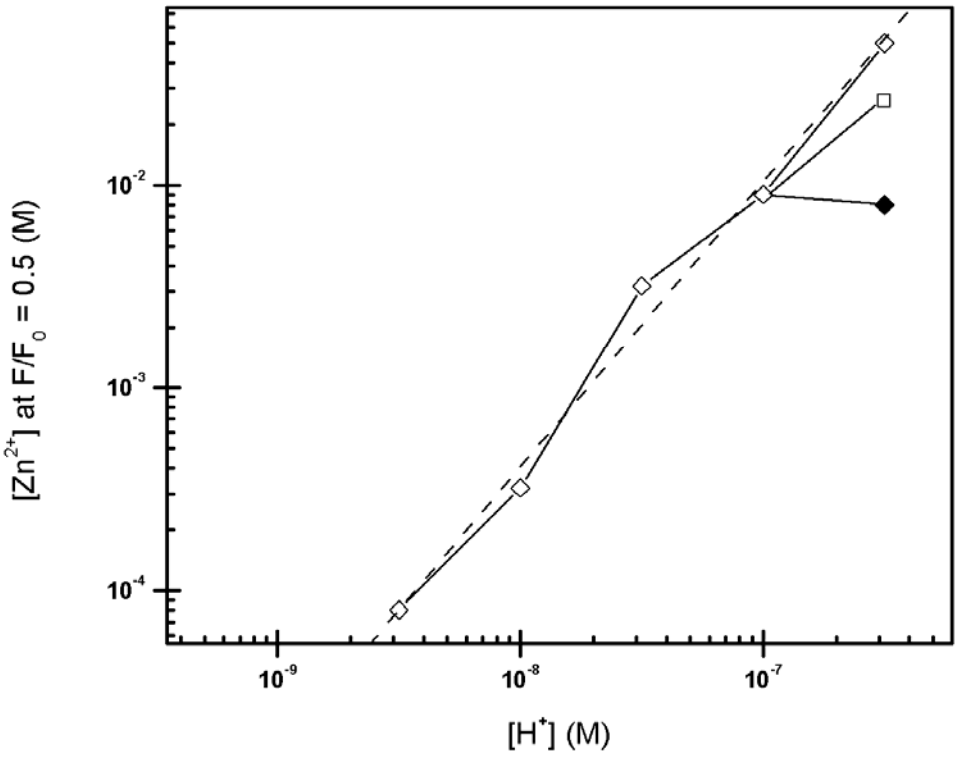

Figure 3.37: The concentration of Zn^{2+} necessary to cause 50% quenching of the Fl-CTL-1 / QSY7-CTL-2 duplex as a function of H^+ concentration. The $[Zn^{2+}]$ values at pH 6.5 are shown for the adjusted pH $ZnCl_2$ stock solution (white diamonds), the unadjusted pH $ZnCl_2$ stock solution (black diamond), and the $Zn(ClO_4)_2$ stock solution (white square). A logarithmic fit is indicated for the acidified $ZnCl_2$ stock solution by the dashed line.

When acidified $ZnCl_2$ or $Zn(ClO_4)_2$ is used at pH 6.5, the relationship between this concentration and the pH is logarithmic. The relationship is similar with unacidified $ZnCl_2$ except that a plateau value is reached at pH 7.0 that does increase with a further decrease in pH.

These results suggest that formation of Zn(II) M-DNA is possible at any pH with sufficient concentrations of Zn^{2+} and reinforce the distinction between M-DNA formation and denaturation. The differences between the readings obtained at pH 6.5 with each stock solution of $ZnCl_2$ are likely due to differences in the ionization states of the Zn^{2+} ions in each solution and this will be further discussed in section 4.4.

4.0 Discussion

4.1 Ethidium Bromide-Based Assay

The lack of EtBr binding to M-DNA was the basis of an early method used to characterize the conformation. This technique was initially used to demonstrate M-DNA formation as a function of time following addition of the metal ion with a variety of variables, including DNA sequence, metal ion, temperature, and pH (Lee *et al.*, 1993). As outlined in section 3.2, two forms of the EtBr-based assay were used in the current study, both of which measured the level of M-DNA formation under equilibrium conditions. The first assay was conducted by exposing DNA to metal ions and adding a final concentration of 0.71 μM to Zn-EFB at pH 8.3. This technique was used to measure M-DNA formation with a variety of metal ions, at different DNA concentrations, and at different temperatures, all as a function of either pH or metal ion concentration. The second assay was performed by adding B- or Zn(II) M-DNA to Zn-EFB at a variety of pH values and allowing an equilibrium to be reached in the presence of 1.3 μM EtBr at a DNA concentration of 0.71 μM in the presence of 0.20 mM Zn^{2+}. The latter technique was used to measure Zn(II) M-DNA formation with a variety of base modifications and different DNA sequences. The second assay allowed measurement of M-DNA formation with sequences or base substitutions that facilitated formation of the conformation at low pH values. Use of the second EtBr assay was necessary since some repetitive sequences or base-substituted DNAs converted immediately and fully to M-DNA upon addition of the DNA to pH 8.3 Zn-EFB.

As shown in figure 3.6, Zn(II) and Co(II) M-DNA have similar degrees of pH stability once formed, but Zn(II) M-DNA forms much more readily than the Co(II) form. Ni(II) M-DNA forms with a propensity intermediate between the other two forms but has the greatest degree of pH-stability once formed. In all cases, however, there is some degree of hysteresis present, indicating that M-DNA formation is likely a cooperative process. As shown in figure 3.7, Ni(II) M-DNA is also far more stable than M-DNA formed by the other metal ions when exposed to EDTA. Further, an excess of EDTA relative to the Ni^{2+} concentration must be added or complete reversion does not occur. This is not due to a lower affinity of EDTA for Ni^{2+} than Zn^{2+}, as the log k values for EDTA-Ni and EDTA-Zn interactions are 18.6 ± 0.1 and 16.4 ± 0.1, respectively (Martell and Smith, 1975).

It was previously known that increasing the metal ion concentration increases the conversion to M-DNA (Lee *et al.*, 1993), but as shown in figure 3.8 the concentration of CT DNA also affects the dismutation. At a DNA concentration of 15 μM and a pH of 8.5, 50 % conversion to M-DNA occurs with 0.25 mM Zn^{2+} but with 150 μM DNA 0.6 mM Zn^{2+} is required and for 1.5 mM DNA 50 % conversion cannot be achieved at a concentration of Zn^{2+} which remains soluble. The Co(II) form of M-DNA is similar to the Zn(II) form but M-DNA conversion induced by Ni^{2+} at pH 8.5 cannot be achieved above a DNA concentration of 10 μM. It is clear that higher DNA concentrations require more metal ion than that which is required to replace the imino protons. A possible explanation is that the negatively charged phosphates on the DNA backbone must be saturated before the metal can occupy sites within the helix. However, at pH 9.0 the Ni(II) form of M-DNA can be prepared readily at much lower concentrations of Ni^{2+}. In addition, the

slopes of the plots for Ni^{2+} are different at pH 8.5 and 9.0 suggesting that the structure of the Ni^{2+} aquo ion may be important for the formation of M-DNA. The differences between Zn(II) and Ni(II) M-DNA observed by this technique as well as by SPR and their implications are further considered in section 4.5.2.

The second form of the EtBr based assay was used to assess the differences in M-DNA formation between repetitive sequences of DNA or those containing various base modifications with the same λ 496 bp fragment used in the assays shown in figure 3.6. This assay was also performed on genomic CT DNA and the CTL-1 / CTL-2 duplex as well as the λ 496mer, which have GC contents of 42, 50, and 54 % respectively. The results were not significantly different with any of these three sequences. Thus it appears that the length of the DNA molecule used to form M-DNA does not have a large impact. The length of the sequence can, however, have an impact on the extent to which M-DNA formation allows communication between 5' end-labeled fluorophores (Aich *et al.*, 2002).

The effect of base substitutions on the λ 496 bp sequence was assayed by the second EtBr method with respect to the formation and stability of Zn(II) M-DNA as a function of pH. The conversion and stability behaviour of representative base substitutions are shown in figures 3.9A and 3.9B, respectively. Complete data for all substitutions are given in table 3.1. In all cases, the pH_m values for the B- to M-DNA transition were higher than those for the M- to B-DNA transition, again indicating hysteresis. Substitution of n^2A or z^7A for A, of m^5C for C, or of U for T all had minor effects on the pH_m values for each transition, being within 0.2 pH units of the control sequence with the exception of the M- to B-DNA transitions for the A substitutions which were 0.3 pH units lower than the control sequence. On the other hand, substitution

of I for G or of Br^5U, F^5U, or s^4T for T had larger effects on the transitions, with changes between 0.3 and 0.6 pH units. In all of these cases, the unusual bases incorporated into the DNA had lower pK_a values than the corresponding standard bases. The pK_a values of Br^5U, F^5U, s^4T, and T are 8.2, 7.8, 8.8 (estimated), and 9.9, respectively. The pK_a value of U, which had little effect on M-DNA formation, is 9.3. Likewise, the pH_m values for the other three T analogues are all close to each other, and the pH_m values for their transitions are also close to each other. Similarly, I has a pK_a of 8.8 while that of G is 9.4, and this substitution also had a large impact on the pH_m values as well. In light of the proposed M-DNA structural model, a lower pK_a on either T or G would favour the conformation since these bases need to be deprotonated in order to form the structure given in figure 1.11. Further structural implications for the effects of some of the base substitutions are considered in detail in section 4.5.1. In addition to the base substitutions inserted into the λ 496 bp fragment with a GC content of 54 %, a 73 % GC 516 bp fragment from the c-*src* oncogene was assayed. The latter sequence was found to have a lower pH_m value for both transitions. This is likely due to the lower pK_a of the titratable imino proton in G•C base pairs relative to the A•T base pairs; G has a pK_a of 9.4, while T has a pK_a of 9.9.

In order to investigate the effects of the sequence in more detail, several synthetic DNAs were evaluated. Representative data for the formation of M-DNA are depicted in figure 3.9C and the complete values obtained are listed in table 3.1. For the conversion of B- to M-DNA $(dG)_n$•$(dC)_n$ has a pH_m value of 7.8 compared with 8.5 for $d(GC)_n$ with $d(GGCC)_n$ having an intermediate value. For AT sequences the homopolymer $(dA)_n$•$(dT)_n$ also has a lower pH_m value than the alternating polymer $d(AT)_n$ (pH_m values

of 8.1 and 8.6, respectively). Therefore, pur•pyr tracts form M-DNA most readily, presumably because the repeating sequence with all purines on one strand allows for better stacking interactions. Alternatively, pur•pyr tracts tend to be overwound compared with B-DNA. M-DNA is also overwound relative to B-DNA so that the increased twist of these sequences might facilitate M-DNA formation (Lee *et al.*, 1993). With respect to base content, the sequences composed exclusively of G•C base pairs consistently formed and stabilized M-DNA at lower pH values than those composed exclusively of A•T base pairs. As with the 73 % GC 516 bp fragment relative to the 54 % GC 496 bp fragment assayed by this method, this difference is likely due to the lower pK_a of G relative to T. Finally, the duplex RNA $r(AU)_n$ showed similar properties to $d(AT)_n$ and $d(AU)_n$ indicating that the M-conformation is also available to RNA sequences.

Substitution of s^4T for T had a predictable effect on the propensity of the λ 496mer to form M-DNA. The lowered pK_a of the base analogue facilitated M-DNA formation similarly to other T analogues as discussed above. The λ 496 bp fragment could not be prepared with s^2T substitutions by PCR as no PCR-compatible DNA polymerase would incorporate it. However, s^2T and s^4T were both incorporated into the sequences d(AT) and $d(TG)_n$•$d(CA)_n$ through use of *E. coli* DNA polymerase. The results of the EtBr assays on these base-substituted repeating sequences are detailed in table 3.1. Incorporation of either analogue into $d(AT)_n$ lowered the pH_m of the B- to M-DNA transition by 0.3 pH units, which was not surprising given that both base analogues have lower pK_a values than T and that transition metals bind well to sulfur-containing functional groups. However, when incorporated into $d(TG)_n$•$d(CA)_n$, the pH_m of M-DNA formation was lowered by 0.4 pH units through substitution with s^4T but raised by 0.2 pH

units by substitution with s^2T. The opposite effects of s^2T substitution on M-DNA formation in $d(AT)_n$ as opposed to $d(TG)_n \bullet d(CA)_n$ could be due to the presence of 2-amino groups on G bases bases which are unfavourable ligands for transition metals. Thus, it appears that the effects of some base substitutions can be sequence-specific.

The EtBr studies done at different temperatures, illustrated in figure 3.10, showed Zn(II) M-DNA formation to be strongly favoured at 37 °C relative to 4 °C. Previous results showed Zn(II) M-DNA formation as a function of time to be much faster at elevated temperatures (Lee *et al.*, 1993). However, increased kinetics at higher temperatures are expected with any process dependent on intermolecular interactions. The current study shows that under equilibrium conditions M-DNA is favoured over B-DNA by elevated temperatures. This shift in equilibrium is manifested as a five-fold decrease in the concentration of Zn^{2+} required to completely form M-DNA at pH 8.5 as the temperature increases from 4 to 37 °C. In light of this, it appears that M-DNA formation is an entropy-driven process, since $\Delta G = \Delta H - T\Delta S$. Direct studies on the ΔH associated with M-DNA were investigated calorimetrically and found to agree with the variable-temperature EtBr assay.

4.2 Isothermal Titration Calorimetry

As outlined in section 3.3, the ITC studies showed M-DNA formation to be an endothermic process. Thus, M-DNA formation is an entropy-driven process in agreement with the EtBr assays carried out at various temperatures under equilibrium conditions (see section 4.1).

Small exothermic changes were observed upon exposure of the DNA to $Mg(ClO_4)_2$ at either pH 7.5 or 8.5 as well as upon exposure of the DNA to $Zn(ClO_4)_2$ at pH 7.5. These changes were likely due to coordination of the metal ions to the phosphate backbone through electrostatic interactions. This type of binding is generally weak and involves hydrated metal ions (Chiu and Dickerson, 2000). Since the hydration sphere of the metal ions remains for the most part intact, large ΔH values are not typically associated with these interactions (Misra and Draper, 1999; Misra and Draper, 2001). Site specific binding, on the other hand, often results in removal of all but the innermost hydration spheres of the metal ion. The disruption of ordered solvent molecules coordinated around the ions provides the source of entropy that is the driving force behind these interactions. Site-specific interactions can also be involved in Z-DNA formation, which is also an entropy-driven process (Klump *et al.*, 1993). When induced by divalent ions, formation of Z-DNA is enhanced when the hydration layers of the metal ions are removed (Taboury *et al.*, 1984).

There was a large degree of error associated with the readings obtained in the ITC experiments. This error was due to a limitation of the system. Since better signals were obtained with higher concentrations of DNA, it was desirable to use as high a DNA concentration as possible. However, as discussed in section 4.1, the higher the concentration of DNA, the more Zn^{2+} is required to convert it to M-DNA. This imposed a limitation on the amount of DNA that could be used in the experiment in order to keep the Zn^{2+} concentration within a range that would remain soluble. Both of these phenomena are apparent in figure 3.11, which shows a larger transition at a higher Zn^{2+} concentration with 0.30 mM DNA compared to 0.15 mM. In addition, the error in the ΔH

values obtained at the higher concentration was three fold lower than at the lower concentration.

In many cases, ITC experiments are undertaken on simple or well-characterized systems and the data can be fit to a model to elucidate ΔG and therefore ΔS values. However, M-DNA formation involves many distinct events. These events include displacement of ions bound to the phosphate backbone of the helix, deprotonation of G and T bases, and binding of metal ions to different sites on the bases. Further, the change in conformation itself is likely to result in a ΔG that would be observed as a ΔH signal. Development of a formula that would account for all of these factors placing the appropriate emphasis on those generating the M-DNA signal would be complex and it would be difficult to test the validity of such a model. There were also difficulties with changing the temperature of the system in order to elucidate the ΔS and ΔG values of the transition. Converting high concentrations of DNA to M-DNA at lower temperatures would have required addition of Zn^{2+} concentrations which would have led to precipitation, while raising the temperature increased the background noise. Thus, detailed thermodynamic information was not obtained, although an estimate of ΔH was obtained. The shape of the ΔH vs Zn^{2+} concentration curve in figure 3.11 is approximately gaussian, indicative of a complex binding process, and the sudden increase in ΔH values around 0.10 mM Zn^{2+} is indicative of a cooperative binding process, in agreement with hysteresis data detailed in section 4.1.

4.3 Surface Plasmon Resonance

In light of the large number of SPR studies in which conformational changes of proteins have been characterized both in the presence and absence of a CMD matrix, it is not unreasonable to attribute the SPR signals observed under some of the conditions employed in this study to M-DNA formation. The results obtained in experiments with dsCTL as the target sequence at pH 8.5 with Zn^{2+} and Ni^{2+} are viewed as being due to M-DNA formation. However, some caution is required when interpreting changes in an SPR signal as being due to a change in conformation of the immobilized species, particularly when dealing with a surface on which the biomolecule is immobilized within a CMD matrix rather than on bare gold. Two studies made this claim when exposing proteins immobilized in a CMD matrix to extreme changes in pH (Mannen *et al.*, 2001; Sota *et al.*, 1998). Subsequent analysis of these studies suggested that the changes observed were due primarily to changing electrostatic interactions between the CMD matrix and the immobilized proteins (Paynter and Russell, 2002).

There are several indications that the changes observed at pH 8.5 upon exposure of dsCTL to Zn^{2+} or Ni^{2+} are due to M-DNA formation. First, the signals are much larger than $(RU_{pred})_{sat}$, indicating that factors other than an increase in mass due to condensation of divalent metal ions on the DNA are causing the signal. Second, it is unlikely that this data is an artifact as was the case in the studies described in the previous paragraph since large pH changes that would change the ionization state of the CMD matrix are not employed. Third, if the signal were primarily due to enhanced electrostatic interactions between the DNA and the CMD matrix, then it is likely that Mg^{2+} or Ca^{2+} ions would

elicit signals comparable to those induced by Zn^{2+} or Ni^{2+} ions, and that a change in pH over the range of 7.5-8.5 would have little effect on the signal. In summary, the signal which results from M-DNA formation is likely due to a combination of an increase in mass on the surface due to replacement of imino protons by Zn^{2+} or Ni^{2+} and a change in shape of the DNA upon converting to M-DNA. This shape change is likely to be to a more compact state, as this would increase the mass closer to the surface of the chip and therefore result in a positive signal.

Formation of M-DNA by Zn^{2+} or Ni^{2+} shows distinct conversion and reversion kinetics, depending on which metal ion is present. Unfortunately, quantitative evaluation of these kinetics is complicated by the contributions from mass and conformational change together in a system which has at least 30 potential binding sites outside the helix and another 30 inside the helix per molecule, all of which are likely involved in a cooperative reaction to form M-DNA. Thus, the high stoichiometry of the interaction contributes in part to the presence of the signal but also makes detailed evaluation of it difficult. However, a qualitative assessment was possible and yielded some interesting observations.

The Zn^{2+} induced M-DNA profiles show rapid equilibrium values regardless of concentration, while the Ni^{2+} profiles reach equilibrium at concentrations below 0.60 mM or above 2.00 mM. Between these low and high points, the Ni^{2+} induced signals rise continuously throughout the exposure, suggesting that little Ni(II) M-DNA formation occurs below 0.60 mM and that it plateaus at 2.00 mM. Also, Ni(II) M-DNA reverts more slowly than Zn(II) M-DNA, as is apparent from figure 3.17. Further, the concentration that gives 50% of the maximum response for dsCTL at pH 8.5 is 0.50 mM

for Ni^{2+}, while that of Zn^{2+} is 0.06 mM, an order of magnitude difference. These results are supported by those obtained with the EtBr assay (discussed in section 4.1), which demonstrated that to convert equivalent concentrations of DNA at pH 8.5, substantially more Ni^{2+} is required than Zn^{2+}. The maximum responses which each metal ion elicits in dsCTL are different as well; +130 RU for Zn^{2+} compared to +185 RU for Ni^{2+} on the same sensor surface. The higher maximum response with Ni^{2+} relative to Zn^{2+} could be due to stronger interactions between the DNA and the Ni^{2+}, meaning that in a dynamic process, the ions spend more of their time bound to the DNA, resulting in a larger signal. The larger signal could be due in part to stronger interactions between Ni^{2+} and the phosphate backbone relative to those of Zn^{2+}. This interpretation is supported by the slower dissociation rate of Ni^{2+}. None of these changes are observed at pH 7.5. At pH 7.5, weak signals arise from interactions between the metal ions and dsCTL. Further, weak signals are detected in the presence of Mg^{2+} and Ca^{2+}. These findings are consistent with M-DNA formation being dependent on a high pH.

In figure 3.15, 0.20 mM Cd^{2+} at pH 8.5 is shown to cause an initial increase in signal which then drops off sharply as the Cd^{2+} denatures the DNA. Part of this large increase in signal could be due to the higher mass of Cd^{2+} relative to the other metal ions, but it is likely that it is forming a complex with the DNA similar to M-DNA. It is apparent from the change in baseline following a 0.20 mM Cd^{2+} injection at pH 8.5 that the Cd^{2+} denatures roughly 40 % of the dsDNA. A stoichiometric excess of Cd^{2+} is known to destabilize dsDNA at acidic pH (Duguid *et al.*, 1995; Eichhorn and Shin, 1968). However, figure 3.15 shows the first observation of denaturation of DNA at room temperature by Cd^{2+}, which is dependent on an alkaline pH. Subsequent injections of

$CdCl_2$ further dropped the baseline. At pH 7.5, an initial exposure of 5.00 mM Cd^{2+} was required to cause denaturation of roughly 20 % of the dsCTL, while subsequent exposures had little effect as illustrated in figure 3.15. Similar results were obtained upon exposure of the surface to Cd^{2+} concentrations of up to 20 mM. At pH 6.5, Cd^{2+} did not denature dsCTL regardless of the concentration of Cd^{2+} used. It is not surprising that Cd^{2+} can complex with DNA in a similar manner to Zn^{2+} or Ni^{2+} as it has similar coordination properties to Zn^{2+} (Cotton and Wilkinson, 1966), and both metal ions are known to interact with base nitrogens of dsDNA (Eichhorn and Shin, 1968). It is possible that the larger atomic radius of Cd^{2+} compared with Zn^{2+} or Ni^{2+} (1.13 Å compared with ~0.70 Å) disrupts the helix due to coordination with the imino nitrogen atoms at position 1 in purines and 3 in pyrimidines. In addition to the interactions of Zn^{2+}, Ni^{2+}, and Cd^{2+} with dsCTL, there were significant interactions between these metals and the four single-stranded sequences studied.

For comparison, the responses of each sequence to 0.20 mM of every metal ion at pH values 7.5 and 8.5 are presented in figure 4.1. The data in figure 4.1 were normalized by dividing the background subtracted RU observed at 95% of the injection volume by the value RU_M/MW_{ratio}. Following this, the highest response was set at a value of 1.00, and all other responses are shown relative to that. RU_M is the amount of immobilized DNA in RU, and MW_{ratio} is the molecular weight of the polymer in question divided by the molecular weight of dsCTL. This normalization accounts for differences in the amount of DNA the metal ions are interacting with as well as the varying molecular weights of the different polymers. The only uniform results across all sequences was that Mg^{2+} did not cause a large signal regardless of pH.

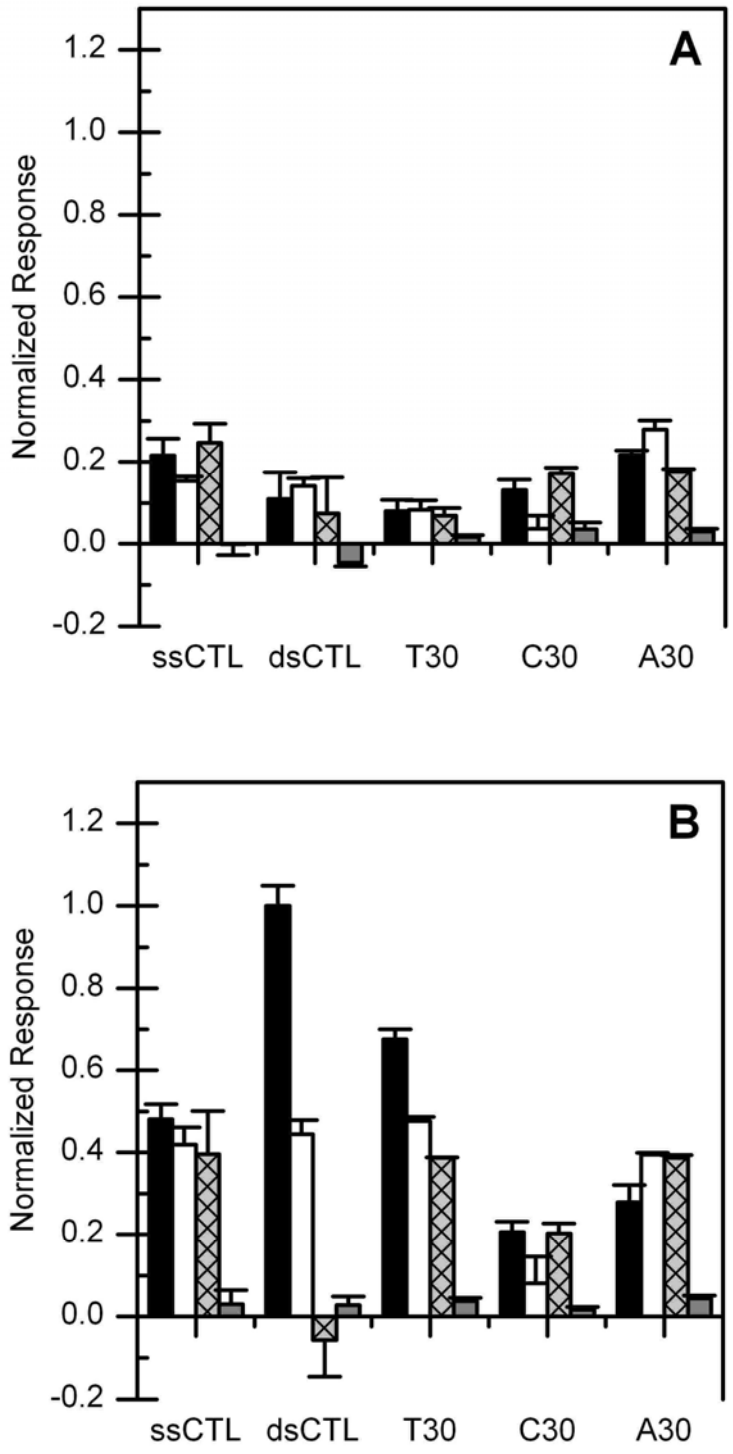

Figure 4.1: Bar graphs showing responses of all DNA sequences to all metal ions at 0.20 mM concentration at pH values 7.5 (**A**) and 8.5 (**B**). In each case the legend is as follows: black bar, $ZnCl_2$; white bar, $NiCl_2$; patterned grey bar, $CdCl_2$; dark grey bar, $MgCl_2$.

As is apparent from figure 4.1, there were substantial pH-dependent signals observed with btn-CTL-2 and T30 in the presence of Zn^{2+}, Ni^{2+}, and Cd^{2+} as was the case when dsCTL was exposed to Zn^{2+} and Ni^{2+}. The response of these sequences could be due to metal ions coordinating to the deprotonated bases as well as to the phosphate backbone of the DNA, folding the DNA back upon itself with subsequent alteration of the refractive index of the polymer. It is possible that the btn-CTL-2 and T30 sequences are folding back upon themselves to allow Zn^{2+}, Ni^{2+}, or Cd^{2+} to bridge base pairs in the resulting hairpin or between T bases as has been observed previously with Hg^{2+} and 1-methylthymine monomers (Kosturko *et al.*, 1974). The slower dissociation of Ni^{2+} at pH 8.5 observed with CTL-2 and T30 relative to A30 or C30 is likely due to tighter binding of the metal ion to deprotonated imino positions on G and T bases. The pH-dependence of the signals induced by Zn^{2+} with btn-CTL-2 and T30 but not A30 or C30 is likely also due to interactions with deprotonated imino positions on the former sequences. A $d(G)_{30}$ sequence was not assayed as it would likely form parallel tetrameric structures which would interefere with the analysis, and also due to the low solubility of guanine rich DNA. The signals obtained with the btn-CTL-2 surface due to Zn^{2+} exposure at pH 7.5 were slightly higher than those obtained with dsCTL which could be due to the higher accessibility of N1 and N3 binding sites on A and C residues, respectively, which do not require deprotonation for binding, and would allow them to participate in formation of hairpin loops.

Unlike single-stranded sequences with titratable protons, C30 did not display a large signal upon exposure to any of the metal ions at either pH, likely due to the lack of potential secondary structures or protons titratable over the pH range studied. C30 did,

however, display a small difference in its responses to Ni^{2+} at concentrations above 0.40 mM, as illustrated in figure 3.27. The behavior of A30 was less straightforward; this sequence did not show any pH-dependence in its responses to Zn^{2+} and displayed very weak responses at either pH, close to those of $(RU_{pred})_{sat}$ as shown in figure 3.29. However, in the presence of Ni^{2+} or Cd^{2+}, A30 showed much larger responses at pH 8.5 than at 7.5 and in the case of Ni^{2+} concentrations above 0.60 mM, the responses at pH 8.5 were more than double $(RU_{pred})_{sat}$. It is possible that Ni^{2+} is inducing a helical structure in A30 that is facilitated by a high pH. It has been observed in DNA melting studies that $d(A)_n$ sequences can form a helical structure. As with the observations shown in figure 3.8, facilitation of this structure by Ni^{2+} at high pH could be due to changes in the coordination properties of the Ni^{2+} ion. In contrast to the data obtained by the EtBr assay, SPR studies did not detect differences in M-DNA formation when F^5U was substituted for T in the sequences, as illustrated in figure 3.32. A possible explanation is that this system was already allowing complete M-DNA formation at pH 8.5, while pH 7.5 was too low to allow enhanced formation of M-DNA even with the base substitution. Further, the data being assessed in the EtBr assay was shown as a function of pH, while SPR data was evaluated as a function of metal ion concentration. Another difference between the results obtained by SPR and those of the EtBr assay was that SPR showed maximum responses at the same Zn^{2+} concentration regardless of the level of immobilized DNA on the surface. However, the amount of immobilized dsCTL on the surface was increased only two fold at most in the SPR experiments. As illustrated in figure 3.8, the increase in Zn^{2+} concentration required for dismutation to M-DNA increased linearly as the DNA concentration increased logarithmically. Further, at low DNA concentrations, there is

little difference in the amount of Zn^{2+} required to convert the DNA to M-DNA at pH 8.5. Thus lack of dependence of the Zn^{2+} concentration required for a maximal response in SPR could be due in part to the large excess of metal ions in the system and the rapid establishment of an equilibrium as well as to the small DNA concentration range studied.

When Zn^{2+} concentrations in excess of 2.0 mM were added to the system with dsCTL at pH 7.5, significant signals that appeared to be indicative of M-DNA formation were observed. These signals reached a plateau of ~115 RU for exposure to 5 mM Zn^{2+}. The signals resulting from exposure to similarly high concentrations of Ni^{2+} reached a lower plateau of ~80 RU at 5 mM Ni^{2+}. Due to the very large concentrations of divalent metal ions employed in these experiments, the interactions between Mg^{2+} and the DNA also gave substantial signals, reaching a plateau of ~25 RU at 20 mM. The peak values of these experiments are listed as a function of metal ion concentration in figure 4.2. When the signals due to Mg^{2+} were subtracted from those occurring during exposure to the other metal ions, only Zn^{2+} still displayed signals which were over double the $(RU_{pred})_{sat}$ values, as illustrated in figure 4.3. Thus, it appears that Zn(II) M-DNA formation is detectable at pH 7.5 by SPR but that Ni(II) M-DNA formation is not.

Exposure of dsCTL to Zn^{2+}, Ni^{2+}, and Cd^{2+} at pH 6.5 all gave similar results well in excess of $(RU_{pred})_{sat}$ at concentrations over 2.0 mM. However, as shown in figure 4.2, exposure to Mg^{2+} had a similar effect albeit with lower plateau values. All of these signals were larger than those observed with the same metal ions at pH 7.5. When the signals due to Mg^{2+} exposure were subtracted from those of the other metal ions, as shown in figure 4.3, the low values observed were not believed to be indicative of M-DNA formation. It is unclear why the signals are all so much larger at pH 6.5 than at 7.5,

(**A**)

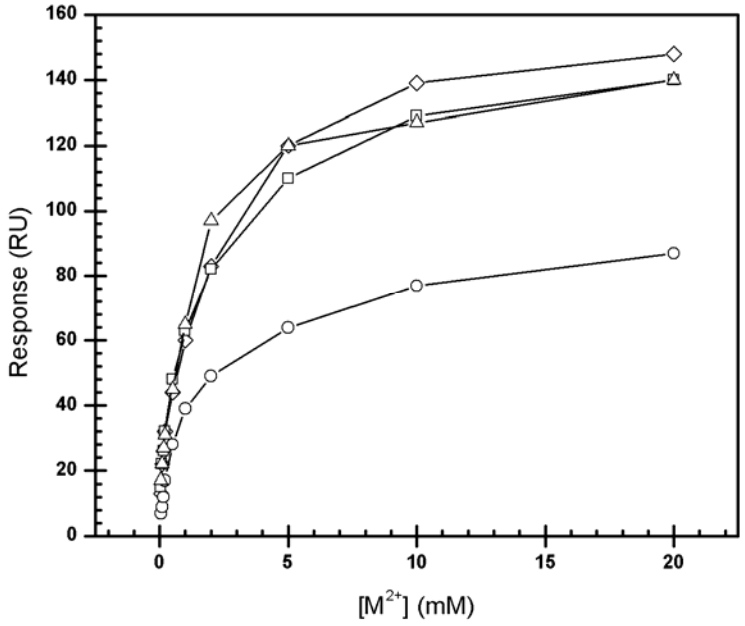

(**B**)

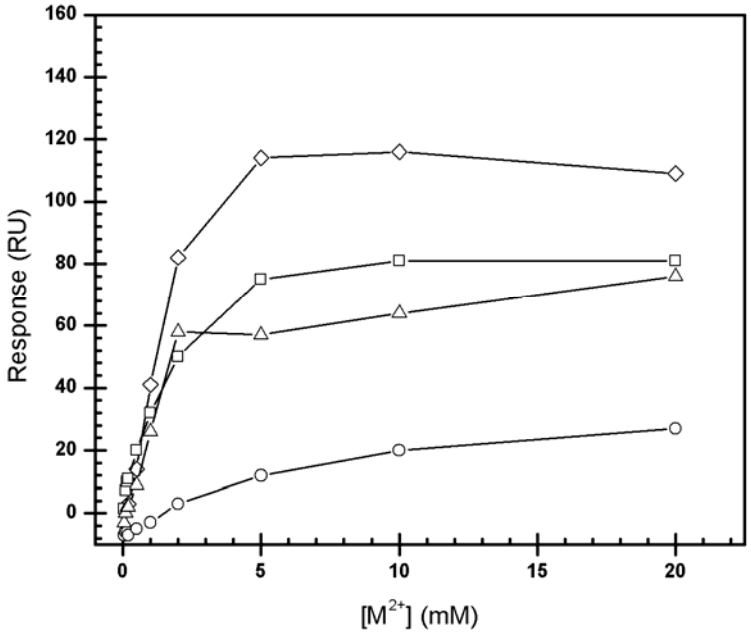

Figure 4.2: The responses of dsCTL to high concentrations of Zn^{2+} (diamonds), Ni^{2+} (squares), Cd^{2+} (triangles), and Mg^{2+} (circles) at pH 6.5 (**A**) and pH 7.5 (**B**). The data are averages of 2 individual experiments with a standard deviation of less than 2 %.

(**A**)

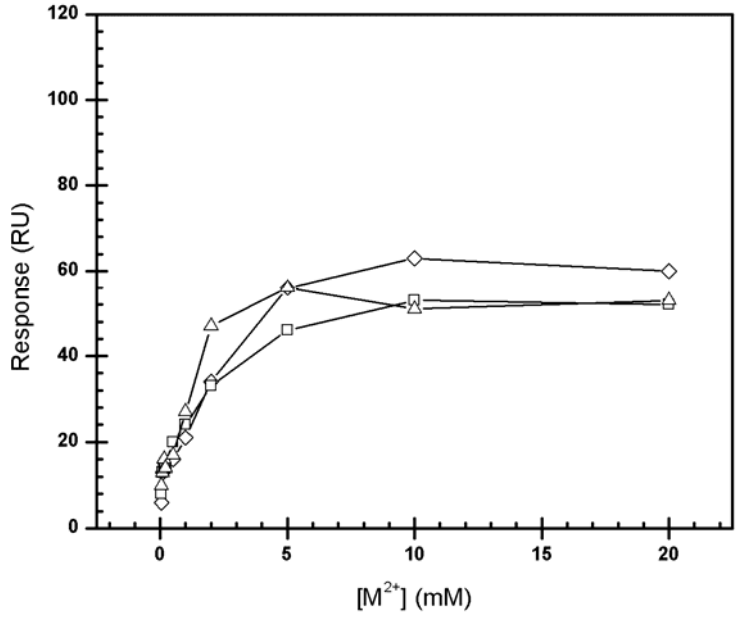

(**B**)

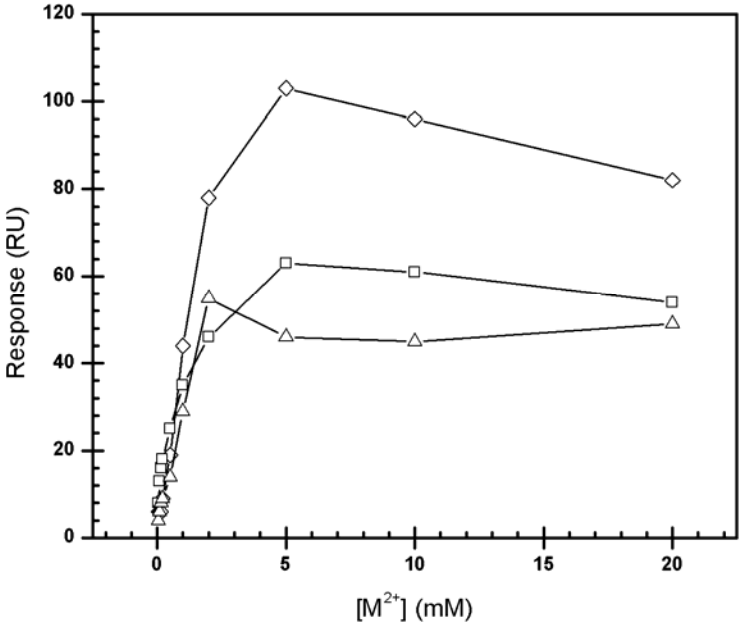

Figure 4.3: The responses of dsCTL to high concentrations of Zn^{2+} (diamonds), Ni^{2+} (squares), Cd^{2+} (triangles) after subtraction of the responses due to the same concentrations of Mg^{2+} at pH 6.5 (**A**) and pH 7.5 (**B**).

but it appears that they are largely due to an interaction independent of M-DNA formation. The results obtained by SPR at low-pH prompted parallel quenching studies with Fl/QSY7-double labeled DNA in the presence of Zn^{2+} as a control, which yielded very compelling findings.

4.4 Quenching of Fluorophore-labeled DNA

In order to verify whether the results observed by SPR at pH 7.5 were indicative of Zn(II) M-DNA formation, quenching experiments were undertaken. These were performed with the same sequence used in the SPR experiments with Fl labels attached to the 5' end of CTL-1 and QSY7 attached to the 5' end of CTL-2. All quenching data was corrected by taking into account the background quenching of Fl on a duplex with the Fl attached to the 5' end of CTL-1 hybridized to unlabeled CTL-2.

As shown in figure 3.34A, Mg^{2+} did not induce quenching at any pH or concentration. This acted as a control against the possibility that aggregation would allow quenching of the QSY7 at very high Zn^{2+} concentrations. In the case of aggregation, a quenching mechanism mediated by FRET would be likely. However, at the DNA concentrations employed, this did not occur even at very high concentrations of Mg^{2+}. In addition, Cd^{2+} caused denaturation of the DNA at pH 8.5 but allowed some degree of quenching at pH 6.5 and pH 7.5. As explained in section 4.3, the SPR data was inconclusive as to whether a complex similar to M-DNA is formed by Cd^{2+} at either pH 6.5 or 7.5. However, this study indicates that some degree of M-DNA formation is occurring in the presence of elevated Cd^{2+} concentrations at pH 6.5 and 7.5. Although it

is possible that the Cd^{2+} denatures small amounts of the DNA at pH 7.5, it appears that sufficient amounts of dsDNA remain to allow quenching of most of the Fl fluorescence.

When $ZnCl_2$ stock solutions are prepared, a small amount of HCl is typically added to the solution to prevent formation of insoluble $Zn(OH)_2$. Addition of HCl results in a drop in pH from 4.4 ± 0.1 to 4.0 ± 0.1 for a 2.0 M stock solution. Whether or not HCl is added typically has no effect on the results obtained by experiments in which the solutions are used, and as indicated in section 3.5, results from both stock solutions were collated to generate the averaged quenching profiles at all pH values except pH 6.5 in figure 3.33. However, at pH 6.5, there is a large difference between the quenching profiles obtained with the two stock solutions, as illustrated in figure 3.35. Thus, when an acidified $ZnCl_2$ stock solution is used, a logarithmic relationship between the concentration of Zn^{2+} required to convert 50 % of the DNA to M-DNA and the proton concentration is observed over all pH values. However, as illustrated in figure 3.37, this relationship does not hold up at pH 6.5 when the unacidified stock solution is employed. The possibility of high Zn^{2+} concentrations lowering the pH of the solution is ruled out by the data in figure 3.36, which shows no significant difference in the final pH of the buffered 6.5 mM solution between titrations of each $ZnCl_2$ solution.

When a stock solution of $Zn(ClO_4)_2$ is used rather than $ZnCl_2$, 50 % M-DNA formation occurs around 26 mM Zn^{2+}. Thus, the data obtained with $Zn(ClO_4)_2$ is more similar to that of the acidified $ZnCl_2$, suggesting that the acidification of the stock solution causes Zn^{2+} to show weaker interactions with Cl^-. This inference follows from studies on $CdCl_2$ and $Cd(ClO_4)_2$ which show that in the former ion pair, there is a much tighter association between the two ions than in the latter. Similar behaviour by

compounds formed between the respective anions and Zn^{2+} is likely since Zn^{2+} has similar coordination properties to Cd^{2+}. There are many distinct equilibria in which the Zn^{2+} ion could be participating in order to bind to the DNA, some of which are shown below, where "B" represents a T or G base:

$$Zn^{2+}\text{-}H_2O + BH \leftrightarrow Zn^{+}\text{-}B + H_3O^{+}$$

$$ZnCl_2 + BH \leftrightarrow Zn^{+}\text{-}B + HCl + H^{+}$$

$$Zn^{+}OH + BH \leftrightarrow Zn^{+}\text{-}B + H_2O$$

In view of the possibility that the above examples and other equilibria play a role in determining the exact state of the Zn^{2+} ion interacting with the DNA, it is difficult to determine the exact cause of the differences between the acidified $ZnCl_2$, unacidified $ZnCl_2$, and $Zn(ClO_4)_2$ stock solutions on the Zn^{2+} concentration at which M-DNA occurs at pH 6.5. This already complicated analysis would be exacerbated by the fact that Zn^{2+} is usually coordinated to six different inner-sphere ligands, meaning that different combinations of the above indicated equilibria could play a role in M-DNA formation. These differences do, however, show that the interaction between Zn^{2+} and its counterion have an effect on the interaction between Zn^{2+} and DNA that only manifests itself at very high Zn^{2+} concentrations. Since the data obtained with $Zn(ClO_4)_2$, which likely represents a nearly completely dissociated form of Zn^{2+}, agree more with the data obtained with the acidified $ZnCl_2$ stock, data from that stock solution will be considered in the following discussion.

The results obtained upon exposure of Zn^{2+} to the double-labeled DNA at each pH were indicative of M-DNA formation regardless of pH. As the pH was lowered, the concentration of Zn^{2+} required changes on a similar scale, with roughly a 10-fold increase

in required Zn^{2+} concentration per 10-fold increase in H^+ concentration as depicted in figure 3.33. The midpoints of the transition are 3.2 and 50 mM Zn^{2+} at pH values 7.5 and 6.5, respectively, in keeping with the observation of M-DNA formation at pH 7.5 but not at pH 6.5 by SPR. The logarithmic relationship between the concentration of Zn^{2+} required to induce quenching and the pH at which the experiment is conducted is summarized in figure 3.37. The trend in figure 3.37 was then fit to the following model for M-DNA formation, where "B" represents a T or G base:

$$BH + Zn^{2+} \leftrightarrow Zn^{+}\text{-}B + n\ H^{+}$$

This model can be expressed as an equation, with an an equilibrium constant K_{eq} as follows:

(2) $$K_{eq} = \frac{[\text{Zn-DNA}]\ [H^+]^n}{[\text{DNA}]\ [Zn^{2+}]}$$

Thus, at 50% M-DNA formation, equation 2 becomes:

$$K_{eq} = \frac{[H^+]^n}{[Zn^{2+}]}$$

In this form, equation 2 can be expressed as a plot of log $[Zn^{2+}]$ vs log $[H^+]$ with a slope of n and a y-intercept of $-(\log K_{eq})$ as such:

$$\log [Zn^{2+}] = n \log [H^+] - \log K_{eq}$$

This yielded a line with the following equation fit with an R^2 value of 0.995:

$$y = 1.4\ x + 7.9$$

Thus, n = 1.4 and $K_{eq} = 1.3 \times 10^{-8}$. This suggests that roughly 1.4 protons are released per base pair upon M-DNA formation, in agreement with previous observations (Aich *et al.*, 1999). It also indicates that the K_{eq} for Zn(II) M-DNA formation is on the order of 10^{-8}

indicating a fairly strong interaction. However, this interaction is still dependent on the presence of Zn^{2+} ions to maintain the M-DNA conformation as illustrated by the effect of EDTA in EtBr experiments or in SPR experiments upon termination of the exposure to metal ions. Thus, the interaction between DNA and Zn^{2+} to form M-DNA necessitates a roughly 10^5-fold excess of Zn^{2+} compared to H^+ in order to maintain a K_{eq} of 1.3×10^{-8}. The difference between this ratio and the K_{eq} value is due to the non-unity value of n.

4.5 Implications for Data on M-DNA Model

Data gathered from the different assays support the M-DNA structural model in many ways. They also outline some of the differences between the Zn(II) and Ni(II) forms of M-DNA. Finally, data obtained in this study have shown directly and conclusively that M-DNA is distinct from denaturation of the DNA.

4.5.1 Support for the Structural Model

There are several lines of evidence produced by this study that support the structural model for M-DNA depicted in figure 1.11. Foremost is the fact that of the base modifications studied in section 3.2.4, those that had the largest impact on M-DNA formation were also those that replaced T or G with bases having much lower pK_a values for their imino protons than T or G. This relationship is illustrated in figure 4.4, which shows a linear relationship between the pK_a of the base pairing with A and the pH at which 50 % M-DNA formation occurs in the presence of EtBr. It is also interesting that

n^2A had little effect since ring amine groups are not good ligands for transition metal ions. Likewise, the loss of a ring amino group from G did not negatively impact M-DNA formation; rather, the lowered pK_a of this analogue facilitated the conversion to M-DNA. It is worth noting that in the X-ray crystallography study carried out by Thiyagarajan *et al*. in 2004, Co(III) hexamine bound the 4-amino group of C through a hydrogen bond mediated by one of the amines coordinated to the Co(III) ion. The model is also supported by the fact that purine N7 positions are not important for M-DNA formation since z^7A substituted DNA also formed the conformation. A sequence containing z^7G could not be assayed by EtBr since it does not fluoresce. Further, the fact that "M-RNA" formation was similar to M-DNA formation with $r(AU)_n$ as compared to $d(AT)_n$ suggests that the interaction is primarily with the bases of the DNA.

A more subtle effect observed in the EtBr study was that n^2A and m^5C substitutions, both of which increases the T_m of DNA, shift the B- to M-DNA pH_m to higher values but conversely lower the M- to B-DNA pH_m value. These effects support the notion that the metal ion is bound in the middle of the DNA, as a helix which denatures less easily would breath less thereby making exchange between the inside of the helix and the solvent more difficult. This is analogous to raising the activation energy of conversion in either direction. It is worth noting that a higher GC content raises the T_m as well lowering the pH_m values of transitions in both directions. This is not in contradiction to the reasoning presented above, since the pK_a of the available imino protons are lower in G•C base pairs than in A•T base pairs.

The SPR studies also supported the structural model since M-DNA formation was only observed when deprotonation of imino protons was possible. In addition, the

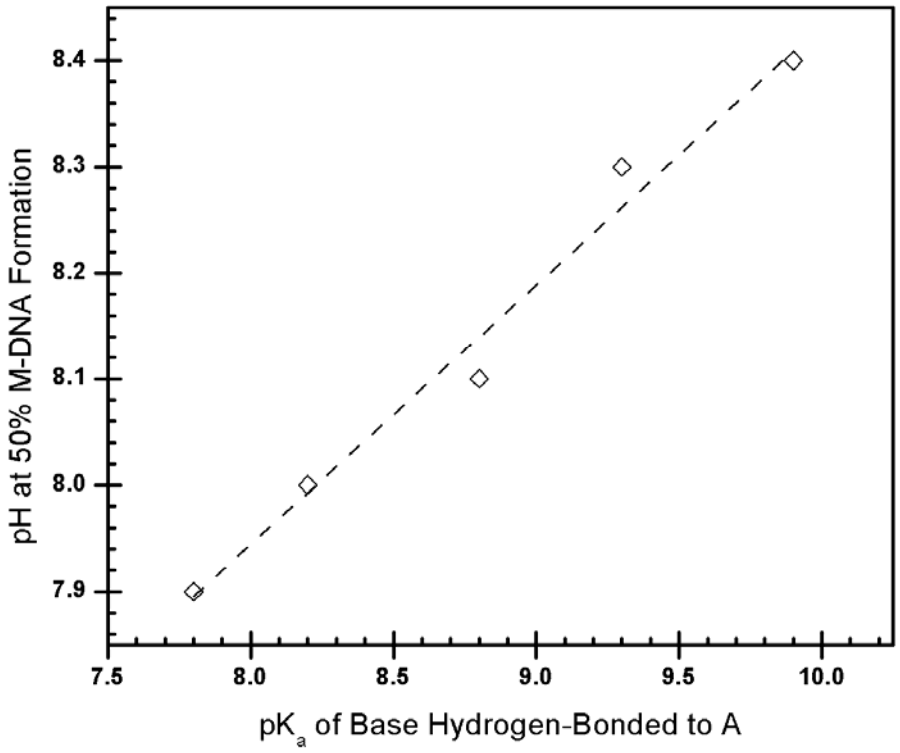

Figure 4.4: The relationship between the pK_a of the base pairing with A and the pH at which 50% M-DNA formation occurs as determined by the EtBr assay detailed in section 2.3.5. The pK_a values displayed are, from lowest to highest, those of F^5U, Br^5U, s^4T, U, and T. A linear fit is indicated by the dashed line.

foldback structures that were believed to have formed with btn-CTL-2 or T30 sequences were not present with C30 or A30. In addition, the Cd^{2+} induced denaturation of DNA at pH 8.5 suggests that Cd^{2+} is forming a complex with the bases in the middle of the helix. Since the coordination properties of Cd^{2+} and Zn^{2+} are similar, it is likely that this type of binding is also occurring between Zn^{2+} and DNA at elevated pH, although it obviously does not result in denaturation of the dsDNA to the same extent as with complexes between DNA and Cd^{2+}. A similar phenomenon is likely occurring between Ni^{2+} and DNA, although many differences between Ni(II) M-DNA and Zn(II) M-DNA were apparent from this study.

4.5.2 Differences Between Zn(II) and Ni(II) M-DNA

When the data obtained by SPR and through the EtBr assay are considered together, several differences between these two forms of M-DNA are apparent. In the EtBr assay, Ni(II) M-DNA was shown to be more stable than Zn(II) M-DNA as a function of pH as well as in the presence of EDTA. Similarly, the SPR work showed Ni(II) M-DNA to be more stable in the absence of Ni^{2+} compared to Zn(II) M-DNA in the absence of Zn^{2+}. In both the EtBr and SPR assays, a higher concentration of Ni^{2+} than Zn^{2+} is required to elicit a plateau response at pH 8.5. The greater propensity for Zn^{2+} to induce M-DNA formation could be due to the higher affinity of Zn^{2+} than Ni^{2+} for positions on the bases as well as to differences in the coordination preferences between the two ions. The small amount of denaturation observed by SPR following formation of Zn(II) M-DNA but not Ni(II) M-DNA is also likely due to this difference in affinity.

Thus, although Ni(II) M-DNA is more stable, it is also more difficult to form than Zn(II) M-DNA. It is possible that these differences arise from the coordination chemistries of Zn^{2+} and Ni^{2+}. Since it has a completed 3d shell, there are no ligand field stabilization effects in Zn^{2+} and consequently it is among the most conformationally labile transition metals, with the most common coordination environments being tetrahedral or octahedral. The coordination environment of Ni^{2+} is octahedral for the aquo ion, and tetrahedral and square planar structures are preferred with some ligands. Further, the coordination environment adopted by this ion is often affected by temperature or concentration (Cotton and Wilkinson, 1966). Characterization of the coordination environment of Ni^{2+} in M-DNA has not been possible owing to weak extinction coefficients (Aich *et al.*, 1999). It is also possible that the coordination environment of Ni^{2+} changes upon an increase in pH from 8.5 to 9.0, as there is a sudden increase in Ni(II) M-DNA formation observed at that pH as opposed to the gradual increase in Zn(II) M-DNA formation observed as the pH is increased. This is also supported by the differing slopes of the Ni(II) M-DNA data at each pH shown in figure 3.8.

4.5.3 Evidence Against Denaturation

Since early data on M-DNA formation relied heavily on EtBr-based assays that showed a lack of binding to the conformation, it was suspected that what was actually being measured was denaturation of DNA. The basis for this suspicion was that since elevated pH and the presence of transition metals capable of binding the bases could drastically lower the T_m of a duplex (Eichhorn and Shin, 1968), the two together could be

inducing denaturation. However, the fact that the T_m of a given sequence could be raised substantially in the presence of certain transition metals only at high pH was compelling evidence that denaturation was not taking place. This study has provided two further strong pieces of evidence that only a small amount of denaturation occurs concomitantly with Zn(II) M-DNA formation and that this cannot account for the observations made. Further, it has shown that the most stable form of M-DNA, Ni(II) M-DNA, does not incur any denaturation of a normal duplex.

Since the SPR experiments take place in a system with a mobile phase, any denaturation would be obvious. This is because there is no possibility that the strands can rehybridize since upon denaturation, the strand that is not anchored to the surface would be carried away by the flowing buffer resulting in a lowered baseline. As the data in figure 3.16 shows, there is only a small amount of denaturation (about 3%) occurring upon Zn(II) M-DNA formation in a normal DNA duplex. Further, no denaturation occurs at all upon formation of Ni(II) M-DNA. On the other hand, exposure of dsDNA to Cd^{2+} seems to transiently form a complex similar to M-DNA, but which results in denaturation of over 40% of the duplex on the first exposure and further loss of dsDNA upon further exposure, as illustrated in figure 3.15. Therefore the SPR assay conclusively demonstrated that Cd^{2+} denatures DNA at room temperature under alkaline conditions and also shows that Zn(II) M-DNA formation results in only a small amount of denaturation whereas Ni(II) M-DNA formation does not denature the duplex at all. These results are strongly supported by parallel quenching studies.

While exposure to Zn(II) causes quenching of fluorophore-labelled DNA at different concentrations depending on the pH, exposure to Mg^{2+} and Cd^{2+} have markedly

different effects on the emission spectra of labeled molecules. In agreement with SPR studies, exposure to Mg^{2+} has little effect regardless of pH or concentration. Further, exposure to Cd^{2+} at pH 6.5 or 7.5 causes some degree of quenching suggestive of formation of an M-DNA-like complex as depicted in figure 3.34B. However, at pH 8.5, as shown in figure 3.34B, there is a drop in fluorescence initially up to a concentration of about 0.10 mM after which the signal climbs back to baseline. Further addition of Cd^{2+} has little effect on this signal, presumably since the DNA is now denatured. Since the DNA is denatured, it is not possible for the QSY7 to communicate electronically with the excited Fl, and the fluorescence cannot be quenched. The differing effects of Cd^{2+} and Zn^{2+} at pH 8.5 not only strongly support the notion that M-DNA formation is distinct from denaturation but also verifies the validity of the quenching approach to measurement of M-DNA formation.

4.6 Summary

The EtBr and SPR studies demonstrated many qualitative differences between Zn(II) and Ni(II) M-DNA, likely due to the differing ligand affinities and coordination properties of the respective transition metal ions involved in their formation. The EtBr experiments also provided support for the proposed structural model of M-DNA based on the effect of base substitutions on the B- to M-DNA equilibrium. The ITC experiments unambiguously showed that M-DNA formation is an entropy-driven process, while the SPR work indicated that a process similar to M-DNA formation is also possible with single-stranded DNA provided that titratable protons are present in the sequence. The

SPR work also unambiguously demonstrated that M-DNA formation is distinct from denaturation. These two techniques are typically used to obtain quantitative thermodynamic and kinetic data, respectively. Unfortunately, in both cases, detailed quantitative data about the M-DNA formation process were unobtainable due to the complexity of the process being studied. These results would include ΔG and ΔS values, and rates of association and dissociation as well as interaction constants from ITC and SPR experiments, respectively. Quenching experiments did yield some quantitative data, showing that Zn(II) M-DNA formation is possible regardless of pH, provided that Zn^{2+} concentration is in roughly 10^{11}-fold excess over the H^{+} concentration, although at pH 6.5 and presumably lower, the activity of the metal ion is extremely sensitive to its ionization state. This mass-action view of M-DNA formation is also supported by the fact that higher concentrations of metal ion are necessary to form M-DNA at higher DNA concentrations.

The data obtained by the EtBr assay indicates that M-DNA formation is possible with any sequence of DNA, as both CT and a 496 bp random sequence DNA form the conformation. In addition, the propensities of different repeating sequences of DNA to form M-DNA are different, indicating that there is some degree of sequence specificity in the conformation. In particular, the data shown by EtBr indicating that d(G)•d(C) tracts can form M-DNA at particularly near-physiological pH values in the presence of 0.20 mM Zn^{2+} suggest that there is a possibility for M-DNA to play a role *in vivo*, whether in the normal functioning of the cell or in the pathogenesis of a disease. This is further reinforced by the observation that M-DNA formation is entropy driven and therefore facilitated by higher temperatures.

4.7 Future Directions

This study has shown that M-DNA formation is facilitated by some base substitutions and in certain sequences. It has also shown that Zn(II) M-DNA formation is possible regardless of the pH as long as the correct ratio of metal ions to protons is maintained. These findings suggest two logical extensions of the current work. The first would be to localize M-DNA to different parts of a DNA molecule. Localization could be achieved by creating a sequence in which one portion has a high propensity for M-DNA formation perhaps also containing base substitutions that facilitate the conformation with the remainder of the molecule being comprised of a sequence that does not favour M-DNA formation. These findings should also facilitate crystallization of M-DNA since it has been demonstrated that certain base substitutions and sequences favour M-DNA formation. Further, M-DNA formation at low pH values could be exploited to solve the problem of base-induced precipitation of divalent metal ions, particularly Zn^{2+} by attempting to crystallize the conformation at a lower pH.

More detailed SPR studies could also be undertaken, perhaps with an in-house built system that does not immobilize the DNA to a CMD matrix but rather measures the properties of DNA monolayers immobilized on a gold surface. Such a system would allow measurements of the thickness of the DNA in addition to measurements on the bulk refractive index, yielding more information about the structural changes occurring upon formation of M-DNA. In short, application of the findings of this study towards a specific goal or product involving M-DNA would be a logical future direction, as would refinement of a potentially powerful technique developed during this study.

5.0 Bibliography

Agazie, Y. M., Lee, J. S. and Burkholder, G. D. (1994) Characterization of a New Monoclonal Antibody to Triplex DNA and Immunofluorescent Staining of Mammalian Chromosomes. *J Biol Chem*. 269: 7019-7023.

Agazie, Y. M., Burkholder, G. D. and Lee, J. S. (1996) Triplex DNA in the Nucleus: Direct Binding of Triplex-specific Antibodies and their Effect on Transcription, Replication and Cell Growth. *Biochem J*. 316: 461-466.

Aich, P., Labiuk, S. L., Tari, L. W., Delbaere, L. J., Roesler, W. J., Falk, K. J., Steer, R. P. and Lee, J. S. (1999) M-DNA: A Complex Between Divalent Metal Ions and DNA Which Behaves as a Molecular Wire. *J Mol Biol*. 294(2): 477-485.

Aich, P., Kraatz, H. B. and Lee, J. S. (2000) M-DNA: pH Stability, Nuclease Resistance and Signal Transmission. *J Biomol Struct Dyn*. 11: 297-301.

Aich, P., Skinner, R. J. S., Wettig, S. D., Steer, R. P. and Lee, J. S. (2002) Long Range Molecular Wire Behavior in a Metal Complex of DNA. *J Biomol Struct Dyn*. 20: 1-6.

Akimoto, T., Sasaki, S., Ikebukuro, K. and Karube, I. (2000) Effect of Incident Angle of Light on Sensitivity and Detection Limit for Layers of Antibody with Surface Plasmon Resonance Spectroscopy. *Biosens Bioelectron*. 15: 355-362.

Allauzen, S., Mani, J. C., Granier, C., Pau, B. and Bouanani, M. (1995) Epitope Mapping and Binding Analysis of Insulin-Specific Monoclonal Antibodies Using a Biosensor Approach. *J Immunol Methods*. 183: 27-32.

Anderson, J. A., Kuntz, G. P. P., Evans, H. H. and Swift, T. J. (1971) Preferential Interaction of Manganous Ions with Guanine Moiety in Nucleosides, Dinucleoside Monophosphates, and Deoxyribonucleic Acid. *Biochemistry*. 4368-4374.

Angerer, L. M. and Moudrianakis, E. N. (1972) Interaction of Ethidium Bromide with Whole and Selectively Deproteinized Deoxynucleoproteins from Calf Thymus. *J Mol Biol*. 63: 505-521.

Angerer, L. M., Georghio, S. and Moudrianakis, E. N. (1974) Structure of Deoxyribonucleoproteins. III. Spectroscopic Characterization of the Ethidium Bromide Binding Sites. *Biochemistry*. 13: 1075-1082.

Arkin, M. R., Stemp, E. D. A., Holmlin, R. E., Barton, J. K., Hormann, A., Olson, E. J. C. and Barbara, P. F. (1996) Rates of DNA-Mediated Electron Transfer Between Metallointercalators. *Science*. 273: 475-480.

Asensio, J. L., Dosanjh, H. S., Jenkins, T. C. and Lane, A. N. (1998) Thermodynamic, Kinetic, and Conformational Properties of a Parallel Intermolecular DNA Triplex Containing 5 ' and 3' Junctions. *Biochemistry*. 37: 15188-15198.

Bates, P. J., Dosanjh, H. S., Kumar, S., Jenkins, T. C., Laughton, C. A. and Neidle, S. (1995) Detection and Kinetic-Studies of Triplex Formation by Oligodeoxynucleotides Using Real-Time Biomolecular Interaction Analysis (BIA). *Nucleic Acids Res*. 23: 3627-3632.

Bauer, C. and Wang, A. H. J. (1997) Bridged Cobalt Amine Complexes Induce DNA Conformational Changes Effectively. *J Inorg Biochem*. 68: 129-135.

Behe, M. and Felsenfeld, G. (1981) Effects of Methylation on a Synthetic Polynucleotide - The B-Z Transition in polyd(G-m^{5}C).polyd(G-m^{5}C). *Proc Natl Acad Sci USA*. 78: 1619-1623.

Bischoff, G., Bischoff, R., Birch-Hirschfeld, E., Gromann, U., Lindau, S., Meister, W. V., Bambirra, S. D. A., Bohley, C. and Hoffmann, S. (1998) DNA-drug Interaction Measurements Using Surface Plasmon Resonance. *J Biomol Struct Dyn*. 16(2): 187-203.

Bittman, R. (1969) Studies of Binding of Ethidium Bromide to Transfer Ribonucleic Acid - Absorption, Fluorescence, Ultracentriguation and Kinetic Investigations. *J Mol Biol*. 46: 251-268.

Blaszak, R. T., Potaman, V., Sinden, R. R. and Bissler, J. J. (1999) DNA Structural Transitions Within the PKD1 Gene. *Nucleic Acids Res*. 27: 2610-2617.

Blume, S. W., Lebowitz, J., Zacharias, G., Guarcello, V., Mayfield, C. A., Ebbinghaus, S. W., Bates, P., Jones, D. E., Trent, J., Vigneswaran, N. and Miller, D. M. (1999) The Integral Divalent Cation Within the Intermolecular Purine*Purine Pyrimidine Structure: A Variable Determinant of the Potential for and Characteristics of the Triple Helical Association. *Nucleic Acids Res*. 27: 695-702.

Boussaad, S., Pean, J. and Tao, N. J. (2000) High-Resolution Multiwavelength Surface Plasmon Resonance Spectroscopy for Probing Conformational and Electronic Changes in Redox Proteins. *Anal Chem*. 72: 222-226.

Braun, R. P. and Lee, J. S. (1986) Variations in Duplex DNA Conformation Detected by the Binding of Monoclonal Autoimmune Antibodies. *Nucleic Acids Res*. 14: 5049-5065.

Bresloff, J. L. and Crothers, D. M. (1981) Equilibrium Studies of Ethidium-Polynucleotide Interactions. *Biochemistry*. 20: 3547-3553.

Cain, K. D., Jones, D. R. and Raison, R. L. (2000) Characterisation of Mucosal and Systemic Immune Responses in Rainbow Trout (*Oncorhynchus mykiss*) Using Surface Plasmon Resonance. *Fish Shellfish Immun*. 651-666.

Champ, P. C., Maurice, S., Vargason, J. M., Camp, T. and Ho, P. S. (2004) Distributions of Z-DNA and Nuclear Factor I in Human Chromosome 22: A Model for Coupled Transcriptional Regulation. *Nucleic Acids Res*. 32: 6501-6510.

Chargaff, E., Lipschitz, R., Green, C. and Hodes, M. E. (1951) The Composition of the Desoxyribonucleic Acid of Salmon Sperm. *J Biol Chem*. 192: 223-230.

Chiu, T. K. and Dickerson, R. E. (2000) 1 Angstrom Crystal Structures of B-DNA Reveal Sequence-specific Binding and Groove-specific Bending of DNA by Magnesium and Calcium. *J Mol Biol*. 301: 915-945.

Ciolkowski, M. L., Fang, M. M. and Lund, M. E. (2000) A Surface Plasmon Resonance Method for Detecting Multiple Modes of DNA-ligand Interactions. *J Pharmaceut Biomed*. 22: 1037-1045.

Clegg, R. M. (1992) Fluorescence Resonance Energy Transfer and Nucleic Acids. In *Method Enzymol* 211 (Edited by D. M. J. Lilley and J. E. Dahlberg), Academic Press, Inc., San Diego, pp. 335-353

Cotton, F. A. and Wilkinson, G. (1966) Advanced Inorganic Chemistry. Interscience Publishers, New York

Cowan, J. (1997) Inorganic Biochemistry. Wiley-VCH, New York

Crothers, D. M. (1968) Calculation of Binding Isotherms for Heterogeneous Polymers. *Biopolymers.* 575-584.

Dandiker, P. J., Holmlin, R. E. and Barton, J. K. (1997) Oxidative Thymine Dimer Repair in the DNA Helix. *Science*. 275: 1465-1468.

Davis, T. M. and Wilson, W. D. (2000) Determination of the Refractive Index Increments of Small Molecules for Correction of Surface Plasmon Resonance Data. *Anal Biochem*. 284: 348-353.

Ditusa, C. A., Christensen, T., Mccall, K. A., Fierke, C. A. and Toone, E. J. (2001) Thermodynamics of Metal Ion Binding. 1. Metal Ion Binding by Wild-type Carbonic Anhydrase. *Biochemistry*. 40: 5338-5344.

Duguid, J., Bloomfield, V. A., Benevides, J. and Thomas, G. J. (1993) Raman Spectral Studies of Nucleic Acids 4. Raman-Spectroscopy of DNA-Metal Complexes 1. Interactions and Conformational Effects of the Divalent Cations - Mg, Ca, Sr, Ba, Mn, Co, Ni, Cu, Pd, and Cd. *Biophys J*. 65: 1916-1928.

Duguid, J. G., Bloomfield, V. A., Benevides, J. M. and Thomas, G. J. (1995) Raman Spectroscopy of DNA-Metal Complexes 2. The Thermal Denaturation of DNA in the

Presence of Sr^{2+}, Ba^{2+}, Mg^{2+}, Ca^{2+}, Mn^{2+}, Co^{2+}, Ni^{2+}, and Cd^{2+}. *Biophys J*. 69: 2623-2641.

Eichhorn, G. L. and Shin, Y. A. (1968) Interaction of Metal Ions with Polynucleotides and Related Compounds. XII. The Relative Effect of Various Metal Ions on DNA Helicity. *J Am Chem Soc*. 90: 7232-7238.

Felsenfeld, G., Davies, D. and Rich, A. (1957) Formation of a 3-stranded Polynucleotide Molecule. *J Am Chem Soc*. 79: 2023-2024.

Felsenfeld, G. and Rich, A. (1957) Studies on the Formation of 2-Stranded and 3-Stranded Polyribonucleotides. *Biochim Biophy Acta*. 26: 457-468.

Flatmark, T., Stokka, A. J. and Berge, S. V. (2001) Use of Surface Plasmon Resonance for Real-time Measurements of the Global Conformational Transition in Human Phenylalanine Hydroxylase in Response to Substrate Binding and Catalytic Activation. *Anal Biochem*. 294: 95-101.

Frank-Kamenetskii, M. and Mirkin, S. (1995) Triplex DNA Structures. *Annu Rev Biochem*. 64: 65-95.

Franklin, R. E. and Gosling, R. G. (1953) Molecular Configuration in Sodium Thymonucleate. *Nature*. 171: 740-741.

Gambari, R., Feriotto, G., Rutigliano, C., Bianchi, N. and Mischiati, C. (2000) Biospecific Interaction analysis (BIA) of Low-molecular Weight DNA-Binding Drugs. *J Pharmacol Exp Ther*. 294(1): 370-377.

Gaus, K. and Hall, E. A. H. (1998) Surface Plasmon Resonance Sensor for Heparin Measurements in Blood Plasma. *Biosens Bioelectron*. 13: 1307-1315.

Georgiadis, R., Peterlinz, K. P. and Peterson, A. W. (2000) Quantitative Measurements and Modeling of Kinetics in Nucleic Acid Monolayer Films Using SPR Spectroscopy. *J Am Chem Soc*. 122: 3166-3173.

Gestwicki, J. E., Hsieh, H. V. and Pitner, J. B. (2001) Using Receptor Conformational Change to Detect Low Molecular Weight Analytes by Surface Plasmon Resonance. *Anal Chem*. 221: 5732-5737.

Giese, B., Amaudrut, J., Kohler, A. K., Spormann, M. and Wessely, S. (2001) Direct Observation of Hole Transfer through DNA by Hopping Between Adenine Bases and by Tunnelling. *Nature*. 412: 318-320.

Gilbert, D. E. and Feigon, J. (1999) Multistranded DNA Structures. *Curr Opin Struc Biol*. 305-314.

Gonzales, N. R., Schuck, P., Schlom, J. and Kashmiri, S. V. S. (2002) Surface Plasmon Resonance-based Competition Assay to Assess the Sera Reactivity of Variants of Humanized Antibodies. *J Immunol Methods*. 268: 197-210.

Goobes, R. and Minsky, A. (2001) Thermodynamic Aspects of Triplex DNA Formation in Crowded Environments. *J Am Chem Soc*. 123: 12692-12693.

Gotfresden, C. H., Schultze, P. and Feigon, J. (1998) Solution Structure of an Intramolecular Pyrimidine-Purine-Pyrimidine Triplex Containing an RNA Third Strand. *J Am Chem Soc*. 120: 4281-4289.

Hahn, B. H. (1998) Systemic Lupus Erythematosus. In *Harrison's Principles of Internal Medicine* (Edited by A. S. Fauci, E. Brauwald, K. J. Isselbacher, J. D. Wilson, J. B. Martin, D. L. Kasper, S. L. Hauser and D. L. Longo), McGraw-Hill, New York, pp. 1874-1880

Haimovich, J., Czerwinski, D., Wong, C. P. and Levy, R. (1998) Determination of Anti-idiotype Antibodies by Surface Plasmon Resonance. *J Immunol Methods*. 214: 113-119.

Hall, B. D., Holmlin, R. E. and Barton, J. K. (1996) Oxidative DNA Damage Through Long-Range Electron Transfer. *Nature*. 382: 731-735.

Hampel, K. J., Crosson, P. and Lee, J. S. (1991) Polyamines Favor DNA Triplex Formation at Neutral pH. *Biochemistry*. 30: 4455-4459.

Hardin, C. C., Henderson, E., Watson, T. and Prosser, J. K. (1991) Monovalent Cation Induced Structural Transitions in Telomeric DNAs - G-DNA Folding Intermediates. *Biochemistry*. 30: 4460-4472.

Homola, J. (1997) On the Sensitivity of Surface Plasmon Resonance Sensors with Spectral Interrogation. *Sensor Actuat B*. 41: 207-211.

Hoogsteen, K. (1963) The Crystal and Molecular Structure of a Hydrogen-Bonded Complex of 1-Methylthymine and 9-Methyladenine. *Acta Crystallogr.* 16: 907-916.

Hudson, B. and Jacobs, R. (1975) Ultraviolet Transitions of the Ethidium Cation. *Biopolymers.* 14: 1309-1312.

Ivanov, V. I., Minchenk, L. E., Minyat, E. E., Frankkam, M. D. and Schyolki, A. K. (1974) The B To A Transition of DNA in Solution. *J Mol Biol*. 87: 817-833.

Jain, S. C., Tsai, C. and Sobell, H. M. (1977) Visualization of Drug-Nucleic Acid Interactions at Atomic Resolution 2. Structure of an Ethidium-Dinucleoside Monophosphate Crystalline Complex, Ethidium-5-Iodocytidylyl (3'-5') Guanosine. *J Mol Biol*. 114: 317-331.

Jain, S. C. and Sobell, H. M. (1984) Visualization of Drug-Nucleic Acid Interactions at Atomic Resolution. VIII. Structures of Two Ethidiumdinucleoside Monophosphate Crystalline Complexes Containing Ethidium: Cytidylyl(3'-5')Guanosine. *J Biomol Struct Dyn*. 1: 1179-1194.

Jensen, K. K., Orum, H., Nielsen, P. E. and Norden, B. (1997) Kinetics for Hybridization of Peptide Nucleic Acids (PNA) with DNA and RNA Studied with the BIAcore Technique. *Biochemistry*. 36: 5072-5077.

Johnsson, B., Lofas, S. and Lindquist, G. (1991) Immobilization of Proteins to a Carboxymethyldextran-Modified Gold Surface Biospecific Interaction Analysis in Surface Plasmon Resonance Sensors. *Anal Biochem*. 198: 268-277.

Jonsson, U., Fagerstam, L., Ivarsson, B., Johnsson, B., Karlsson, R., Lundh, K., Lofas, S., Persson, B., Roos, H., Ronnberg, I., Sjolander, S., Stenberg, E., Stahlberg, R., Urbaniczky, C., Ostlin, H. and Malmqvist, M. (1991) Real-Time Biospecific Interaction Analysis Using Surface-Plasmon Resonance and a Sensor Chip Technology. *Biotechniques*. 11: 620-627.

Jonsson, U. and Malmqvist, M. (1992) Real Time Biospecific Interaction Analysis. In *Advances in Biosensors* (Edited by A. P. F. Turner), JAI Press, London, pp. 291-336

Jost, J. P., Munch, O. and Andersson, T. (1991) Study of Protein-DNA Interactions by Surface-Plasmon Resonance (Real-Time Kinetics). *Nucleic Acids Res*. 19: 2788-2788.

Kang, C., Zhang, X. H., Ratliff, R., Moyzis, R. and Rich, A. (1992) Crystal Structure of 4-Stranded *Oxytrichia* Telomeric DNA. *Nature*. 356: 126-131.

Kang, S. and Wells, R. D. (1992) Central Non-Pur.Pyr Sequences in Oligo(dG.dC) Tracts and Metal Ions Influence the Formation of Intramolecular DNA Triplex Isomers. *J Biol Chem*. 267: 20887-20891.

Kang, S., Wohlrab, F. and Wells, R. D. (1992) Metal Ions Cause the Isomerization of Certain Intramolecular Triplexes. *J Biol Chem*. 267: 1259-1264.

Karlsson, R., Fagerstam, L., Nilshans, H. and Persson, B. (1993) Analysis of Active Antibody Concentration - Separation of Affinity and Concentration Parameters. *J Immunol Methods*. 166: 75-84.

Karlsson, R. and Stahlberg, R. (1995) Surface-Plasmon Resonance Detection and Multispot Sensing for Direct Monitoring of Interactions Involving Low-Molecular-Weight Analytes and for Determination of Low Affinities. *Anal Biochem*. 228: 274-280.

Keller, M., Tagawa, T., Preuss, M. and Miller, A. D. (2002) Biophysical Characterization of the DNA Binding and Condensing Properties of Adenoviral Core Peptide mu. *Biochemistry*. 41: 652-659.

Klump, H. H., Schmid, E. and Wosgien, M. (1993) Energetics of Z-DNA Formation in Poly-d(AT), Poly-d(GC), and Poly-d(AC).poly-d(GT). *Nucleic Acids Res*. 21: 2343-2348.

Kohwi, Y. and Kohwi-Shigematsu, T. (1988) Magnesium Ion-Dependent Triple-Helix Structure Formed by Homopurine-Homopyrimidine Sequences in Supercoiled Plasmid DNA. *Proc Natl Acad Sci USA*. 85: 3781-3785.

Kosturko, L. D., Folzer, C. and Stewart, R. F. (1974) Crystal and Molecular Structure of a 2-1 Complex of 1-Methylthymine-Mercury(II). *Biochemistry*. 3949-3952.

Labiuk, S. L., Delbaere, L. T. J. and Lee, J. S. (2001) Gamma and Ultraviolet Radiation Cause DNA Crosslinking in the Presence of Metal Ions at High pH. *Photochem Photobiol*. 73: 579-584.

Labiuk, S. L., Delbaere, L. T. J. and Lee, J. S. (2003) Cobalt(II), Nickel(II) and Zinc(II) do not Bind to Intra-helical N(7) Guanine Positions in the B-form Crystal Structure of d(GGCGCC). *J Biol Inorg Chem*. 715-720.

Lafer, E. M., Moller, A., Nordheim, A., Stollar, B. D. and Rich, A. (1981) Antibodies Specific for Left-Handed Z-DNA. *Proc Natl Acad Sci USA*. 78: 3546-3550.

Lafer, E. M., Sousa, R. and Rich, A. (1985) Anti-Z-DNA Antibody Binding can Stabilize Z-DNA in Relaxed and Linear Plasmids Under Physiological Conditions. *EMBO J*. 3655-3660.

Laricchia-Robbio, L., Silvana, B., Ghione, S., Montali, U. and Revoltella, R. P. (1998) Detection of Digitalis Compounds Using a Surface Plasmon Resonance-based Biosensor. *Biosens Bioelectron*. 13: 1055-1060.

Latimer, L. J. P., Hampel, K. J. and Lee, J. S. (1989) Synthetic Repeating Sequence DNAs Containing Phosphorothioates - Nuclease Sensitivity and Triplex Formation. *Nucleic Acids Res*. 17: 1549-1561.

Latimer, L. J. P. and Lee, J. S. (1991) Ethidium Bromide Does Not Fluoresce When Intercalated Adjacent to 7-Deazaguanine in Duplex DNA. *J Biol Chem*. 266: 13849-13851.

Latimer, L. J. P., Agazie, Y. M., Braun, R. P., Hampel, K. J. and Lee, J. S. (1995) Specificity of Monoclonal Antibodies Produced against Phosphorothioate and Ribo Modified DNAs. *Mol Immunol*. 32: 1057-1064.

Lee, J. S., Johnson, D. A. and Morgan, A. R. (1979) Complexes Formed by $(Pyrimidine)_n.(Purine)_n$ DNAs on Lowering the pH are 3-Stranded. *Nucleic Acids Res*. 6: 3073-3091.

Lee, J. S., Evans, D. H. and Morgan, A. R. (1980) Polypurine DNAs and RNAs form Secondary Structures which May Be Tetra-Stranded. *Nucleic Acids Res*. 8: 4305-4320.

Lee, J. S., Dombroski, D. F. and Mosmann, T. R. (1982) Specificity of Autoimmune Monoclonal FAB Fragmenst Binding to Single-Stranded Deoxyribonucleic Acid. *Biochemistry*. 21: 4940-4945.

Lee, J. S., Woodsworth, M. L., Latimer, L. J. P. and Morgan, A. R. (1984) Poly(pyrimidine).poly(purine) Synthetic DNAs Containing 5-Methylcytosine form Stable Triplexes at Neutral pH. *Nucleic Acids Res*. 12: 6603-6614.

Lee, J. S., Latimer, L. J. P. and Woodsworth, M. L. (1985) A Monoclonal Antibody Specific for the Duplex DNA poly [d(TC)].poly[d(GA)]. *Febs Lett*. 190: 120-124.

Lee, J. S., Burkholder, G. D., Latimer, L. J. P., Haug, B. L. and Braun, R. P. (1987) A Monoclonal Antibody to Triplex DNA Binds Eukaryotic Chromosomes. *Nucleic Acids Res*. 15: 1047-1061.

Lee, J. S., Latimer, L. J. P., Haug, B. L., Pulleyblank, D. E., Skinner, D. M. and Burkholder, G. D. (1989) Triplex DNA in Plasmids and Chromosomes. *Gene*. 82: 191-199.

Lee, J. S. (1990) The Stability of Polypurine Tetraplexes in the Presence of Monovalent and Divalent Cations. *Nucleic Acids Res*. 18: 6057-6060.

Lee, J. S., Latimer, L. J. and Reid, R. S. (1993) A Cooperative Conformational Change in Duplex DNA Induced by Zn^{2+} and Other Divalent Metal Ions. *Biochem Cell Biol*. 71(3-4): 162-168.

Lepecq, J. B. and Paoletti, C. (1967) A Fluorescent Complex Between Ethidium Bromide and Nucleic Acids - Physical-Chemical Characterization. *J Mol Biol*. 27: 87-106.

Lewis, F. D., Wu, T., Zhang, Y., Letsinger, R. L., Greenfield, S. R. and Wasielewski, M. R. (1997) Distance-Dependent Electron Transfer in DNA. *Science*. 277: 675-676.

Li, C. Z., Long, Y. T., Kraatz, H. B. and Lee, J. S. (2003) Electrochemical investigations of M-DNA self-assembled monolayers on gold electrodes. *J Phys Chem B*. 107: 2291-2296.

Liedberg, B., Lundstrom, I. and Stenberg, E. (1993) Principles of Biosensing with an Extended Coupling Matrix and Surface Plasmon Resonance. *Sensor Actuat B*. 11: 63-72.

Lofas, S. and Johnsson, B. (1990) A Novel Hydrogel Matrix on Gold Surfaces in Surface Plasmon Resonance Sensors for Fast and Efficient Covalent Immobilization of Ligands. *J Chem Soc Chem Comm*. 1526-1528.

Lofas, S., Malmqvist, M., Ronnberg, I., Stenberg, E., Liedberg, B. and Lundstrom, I. (1991) Bioanalysis with Surface Plasmon Resonance. *Sensor Actuat B*. 5: 79-84.

Long, Y. T., Li, C. Z., Kraatz, H. B. and Lee, J. S. (2003) AC impedance spectroscopy of native DNA and M-DNA. *Biophys J*. 84: 3218-3225.

Malkov, V. A., Voloshin, O. N., Soyfer, V. N. and Frank-Kamenetskii, M. D. (1993) Cation and Sequence Effects on Stability of Intermolecular Pyrimidine-Purine-Purine Triplex. *Nucleic Acids Res*. 21: 585-591.

Mannen, T., Yamaguchi, S., Honda, J., Sugimoto, S., Kitayama, A. and Nagamune, T. (2001) Observation of Charge State and Conformational Change in Immobilized Protein Using a Surface Plasmon Resonance Sensor. *Anal Biochem*. 293: 185-193.

Marmur, J. and Doty, P. (1962) Determination of Base Composition of Deoxyribonucleic Acids From its Thermal Denaturation Temperature. *J Mol Biol*. 5: 109-118.

Martell, A. E. and Smith, R. M. (1975) Critical Stability Constants. Plenum Press, London

Martin, R. B. and Yitbarek, H. M. (1979) Interactions Between Metal Ions and Nucleic Bases, Nucleosides, and Nucleotides in Solution. In *Metal Ions in Biological Systems* 8 (Edited by H. Sigel), Marcel Dekker, Inc., New York, pp. 57-114

Martin, R. B. (1996) Dichotomy of Metal Ion Binding to N1 and N7 of Purines. In *Metal Ions in Biological Systems* 32 (Edited by A. Sigel and H. Sigel), Marcel Dekker, Inc., New York, pp. 61-87

Matulis, D., Rouzina, I. and Bloomfield, V. A. (2000) Thermodynamics of DNA Binding and Condensation: Isothermal Titration Calorimetry and Electrostatic Mechanism. *J Mol Biol*. 296: 1053-1063.

May, L. M. and Russell, D. A. (2002) The Characterization of Biomolecular Secondary Structures by Surface Plasmon Resonance. *Analyst.* 127: 1589-1595.

May, L. M. and Russell, D. A. (2003) Novel Determination of Cadmium Ions Using an Enzyme Self-assembled Monolayer with Surface Plasmon Resonance. *Anal Chim Acta*. 500: 119-125.

Meggers, E., Michel-Beyerle, M. E. and Giese, B. (1998) Sequence Dependent Long Range Hole Transport in DNA. *J Am Chem Soc*. 120: 12950-12955.

Mirkin, S. M., Lyamichev, V. I., Drushlyak, K. N., Dobrynin, V. N., Filippov, S. A. and Frank-Kamenetskii, M. D. (1987) DNA H-form requires a Homopurin Homopyrimidine Mirror Repeat. *Nature*. 330: 495-497.

Misra, V. K. and Draper, D. E. (1999) The Interpretation of Mg^{2+} Binding Isotherms for Nucleic Acids using Poisson-Boltzmann Theory. *J Mol Biol*. 294: 1135-1147.

Misra, V. K. and Draper, D. E. (2001) A Thermodynamic Framework for Mg^{2+} Binding to RNA. *P Natl Acad Sci USA*. 98: 12456-12461.

Moghaddam, A., Lobersli, I., Gebhardt, K., Braunagel, M. and Marvik, O. J. (2001) Selection and Characterisation of Recombinant Single-chain Antibodies to the Hapten Aflatoxin-B1 from Naive Recombinant Antibody Libraries. *J Immunol Methods*. 254: 169-181.

Mohr, S. C., Sokolov, N. V. H. A., He, C. M. and Setlow, P. (1991) Binding of Small Acid-Soluble Spore Proteins from *Bacillus subtilis* Changes the Conformation of DNA from B to A. *Proc Natl Acad Sci USA*. 88: 77-81.

Moller, A., Gabriels, J. E., Lafer, E. M., Nordheim, A., Rich, A. and Stollar, B. D. (1982) Monoclonal Antibodies Recognize Different Parts of Z-DNA. *J Biol Chem*. 257: 2081-2085.

Moller, A., Nordheim, A., Kozlowski, S. A., Patel, D. J. and Rich, A. (1984) Bromination Stabilizes polyd(G)-d(C) in the Z-DNA Form Under Low Salt Conditions. *Biochemistry*. 23: 54-62.

Morgan, A. R. and Wells, R. D. (1968) Specificity of 3-Stranded Complex Formation Between Double-Stranded DNA and Single-Stranded RNA Containing Repeating Nucleotide Sequences. *J Mol Biol*. 37: 63-80.

Morgan, A. R., Evans, D. H., Lee, J. S. and Pulleyblank, D. E. (1979) Ethidium Fluorescence Assay 2. Enzymatic Studies and DNA-Protein Interactions. *Nucleic Acids Res*. 7: 571-594.

Morgan, A. R., Lee, J. S., Pulleyblank, D. E., Murray, N. L. and Evans, D. H. (1979) Ethidium Fluorescence Assays 1. Physiochemical Studies. *Nucleic Acids Res*. 7: 547-569.

Nagata, K. and Handa, H. (2000) Real-Time Analysis of Biomolecular Interactions: Applications of BIAcore. Springer Verlag, Kyoto

Nilsson, P., Persson, B., Uhlen, M. and Nygren, P. A. (1995) Real-Time Monitoring of DNA Manipulations Using Biosensor Technology. *Anal Biochem*. 224: 400-408.

Olmsted, J. and Kearns, D. R. (1977) Mechanism of Ethidium-Bromide Fluorescence Enhancement on Binding to Nucleic Acids. *Biochemistry*. 16: 3647-3654.

Oshannessy, D. J., Brighamburke, M. and Peck, K. (1992) Immobilization Chemistries Suitable for Use in the Biacore Surface Plasmon Resonance Detector. *Anal Biochem*. 205: 132-136.

Ozawa, T., Sasaki, K. and Umezawa, Y. (1999) Metal Ion Selectivity for Formation of the Calmodulin-metal-target Peptide Ternary Complex Studied by Surface Plasmon Resonance Spectroscopy. *Biochim Biophys Acta*. 1434: 211-220.

Patel, H. P., Lu, L., Blaszak, R. T. and Bissler, J. J. (2004) PKD1 Intron 21: Triplex DNA Formation and Effect on Replication. *Nucleic Acids Res*. 32: 1460-1468.

Paynter, S. and Russell, D. A. (2002) Surface Plasmon Resonance Measurement of pH-induced Responses of Immobilized Biomolecules: Conformational Change or Electrostatic Interaction Effects? *Anal Biochem*. 309: 85-95.

Peck, L. J., Nordheim, A., Rich, A. and Wang, J. C. (1982) Flipping of Cloned d(pCpG)n.d(pCpG)n DNA Sequences from Right-handed to Left-handed Helical Structure by Salt, Co(III), or Negative Supercoiling. *Proc Natl Acad Sci USA*. 79: 4560-4564.

Perlmann, G. E. and Longsworth, L. G. (1948) The Specific Refractive Index Increment of Some Purified Proteins. *J Am Chem Soc*. 70: 2719-2724.

Peterlinz, K. A. and Georgiadis, R. (1996) Two-color Approach for Determination of Thickness and Dielectric Constant of Thin Films Using Surface Plasmon Resonance Spectroscopy. *Opt Commun*. 130: 260-266.

Peterlinz, K. A. and Georgiadis, R. (1996) In Situ Kinetics of Self-assembly by Surface Plasmon Resonance Spectroscopy. *Langmuir.* 12: 4731-4740.

Peterlinz, K. A., Georgiadis, R. M., Herne, T. M. and Tarlov, M. J. (1997) Observation of Hybridization and Dehybridization of Thiol-tethered DNA Using Two-color Surface Plasmon Resonance Spectroscopy. *J Am Chem Soc*. 119: 3401-3402.

Peterson, A. W., Heaton, R. J. and Georgiadis, R. (2000) Kinetic Control of Hybridization in Surface Immobilized DNA Monolayer Films. *J Am Chem Soc*. 122: 7837-7838.

Peterson, A. W., Heaton, R. J. and Georgiadis, R. M. (2001) The Effect of Surface Probe Density on DNA Hybridization. *Nucleic Acids Res*. 29: 5163-5168.

Peterson, A. W., Wolf, L. K. and Georgiadis, R. M. (2002) Hybridization of Mismatched or Partially Matched DNA at Surfaces. *J Am Chem Soc*. 124: 14601-14607.

Phipps, A. K., Tarkoy, M., Schultze, P. and Feigon, J. (1998) Solution Structure of an Intramolecular DNA Triplex Containing 5-(1-Propynyl)-2'-deoxyuridine Residues in the Third Strand. *Biochemistry*. 37: 5820-5830.

Pohl, F. M. and Jovin, T. M. (1972) Salt-Induced Cooperative Conformational Change of a Synthetic DNA - Equilibrium and Kinetic Studies with Poly (dG-dC). *J Mol Biol*. 67: 375-396.

Polymenis, M. and Stollar, B. D. (1995) Domain Interactions and Antigen-Binding of Recombinant Anti-Z-DNA Antibody Variable Domains - the Role of Heavy and Light-Chains Measured by Surface-Plasmon Resonance. *J Immunol*. 154: 2198-2208.

Portmann, R., Magnani, D., Stoyanov, J. V., Schmechel, A., Multhaup, G. and Solioz, M. (2004) Interaction Kinetics of the Copper-responsive CopY Repressor With the Cop Promoter of *Enterococcus hirae*. *J Biol Inorg Chem*. 396-402.

Qu, Y., Harris, A., Hegmans, A., Petz, A., Kabolizadeh, P., Penazova, H. and Farrell, N. (2004) Synthesis and DNA Conformational Changes of Non-covalent Polynuclear Platinum Complexes. *J Inorg Biochem*. 98: 1591-1598.

Rakitin, A., Aich, P., Papadopoulos, C., Kobzar, Y., Vedeneev, A. S., Lee, J. S. and Xu, J. M. (2001) Metallic Conduction Through Engineered DNA: DNA Nanoelectronic Building Blocks. *Phys Rev Lett*. 86(16): 3670-3673.

Ren, J. S., Jenkins, T. C. and Chaires, J. B. (2000) Energetics of DNA Intercalation Reactions. *Biochemistry*. 39: 8439-8447.

Rich, A., Nordheim, A. and Wang, A. H. J. (1984) The Chemistry and Biology of Left-Handed Z-DNA. *Annu Rev Biochem*. 53: 791-846.

Rich, A. and Zhang, S. G. (2003) Z-DNA: the long road to biological function. *Nat Rev Genet*. 4: 566-572.

Rich, R. L. and Myszka, D. G. (2002) Survey of the Year 2001 Commercial Optical Biosensor Literature. *J Mol Recognit*. 15: 352-376.

Saenger, W. (1984) Principles of Nucleic Acid Structure. Springer Verlag, New York

Salamon, Z., Wang, Y., Brown, M. F., Macleod, H. A. and Tollin, G. (1994) Conformational-Changes in Rhodopsin Probed by Surface-Plasmon Resonance Spectroscopy. *Biochemistry*. 33: 13706-13711.

Salamon, Z., Wang, Y., Tollin, G. and Macleod, H. A. (1994) Assembly and Molecular Organization of Self-Assembled Lipid Bilayers on Solid Substrates Monitored by Surface Plasmon Resonance Spectroscopy. *Biochim Biophys Acta*. 1195: 267-275.

Salamon, Z., Macleod, H. A. and Tollin, G. (1997) Surface Plasmon Resonance Spectroscopy as a tool For Investigating the Biochemical and Biophysical Properties of Membrane Protein Systems 2. Applications to Biological Systems. *Biochim Biophys Acta*. 1331: 131-152.

Salamon, Z., Macleod, H. A. and Tollin, G. (1997) Surface Plasmon Resonance Spectroscopy as a Tool for Investigating the Biochemical and Biophysical Properties of Membrane Protein Systems 1. Theoretical Principles. *Biochim Biophys Acta*. 1331: 117-129.

Salamon, Z., Cowell, S., Varga, E., Yamamura, H. I., Hruby, V. J. and Tollin, G. (2000) Plasmon Resonance Studies of Agonist/antagonist Binding to the Human Delta-opioid Receptor: New Structural Insights into Receptor-ligand Interactions. *Biophys J*. 79: 2463-2474.

Sarkar, D. and Somasundaran, P. (2004) Conformational Dynamics of poly(acrylic acid). A Study Using Surface Plasmon Resonance Spectroscopy. *Langmuir.* 20: 4657-4664.

Schade, M., Behlke, J., Lowenhaupt, K., Herbert, A., Rich, A. and Oschkinat, H. (1999) A 6 bp Z-DNA Hairpin Binds two Z alpha Domains from the Human RNA Editing Enzyme ADAR1. *Febs Lett*. 458: 27-31.

Schaffitzel, C., Berger, I., Postberg, J., Hanes, J., Lipps, H. J. and Pluckthun, A. (2001) In Vitro Generated Antibodies Specific for Telomeric Guanine-Quadruplex DNA React With *Stylonychia lemnae* Macronuclei. *Proc Natl Acad Sci USA*. 98: 8572-8577.

Schwartz, T., Rould, M. A., Lowenhaupt, K., Herbert, A. and Rich, A. (1999) Crystal Structure of the Z Alpha Domain of the Human Editing Enzyme ADAR1 Bound to left-handed Z-DNA. *Science*. 284: 1841-1845.

Sen, D. and Gilbert, W. (1988) Formtaion of Parallel 4-Stranded Complexes by Guanine-Rich Motifs in DNA and its Implications for Meiosis. *Nature*. 334: 364-366.

Sen, D. and Gilbert, W. (1990) A Sodium-Potassium, Switch in the Formation of 4-Stranded G4-DNA. *Nature*. 344: 410-414.

Sen, D. and Gilbert, W. (1992) Novel DNA Superstructures Formed by Telomere-Like Oligomers. *Biochemistry*. 31: 65-70.

Sharp, P. A., Sugden, B. and Sambrook, J. (1973) Detection of 2 Restriction Endonuclease Activities in *Haemophilus parainfluenzae* Using Analytical Agarose-Ehtidium Bromide Electrophoresis. *Biochemistry*. 12: 3055-3063.

Sibille, P., Ternynck, T., Nato, F., Buttin, G., Strosberg, D. and Avrameas, A. (1997) Mimotopes of Polyreactive anti-DNA Antibodies Identified Using Phage-display Peptide Libraries. *Eur J Immunol*. 27: 1221-1228.

Sinden, R. R. (1994) DNA Structure and Function. Academic Press, San Diego

Sklenar, V. and Feigon, J. (1990) Formation of a Stable Triplex from a Single DNA Strand. *Nature*. 345: 836-838.

Smith, F. W. and Feigon, J. (1992) Quadruplex Structure of *Oxytricha* Telomeric DNA Oligonucleotides. *Nature*. 356: 164-168.

Sobell, H. M., Tsai, C., Jain, S. C. and Gilbert, S. G. (1977) Visualization of Drug-nucleic Acid Interactions at Atomic Resolution: III. Unifying Structural Concepts in Understanding Drug-DNA Interactions and their Broader Implications in Understanding Protein-DNA Interactions. *J Mol Biol*. 114: 333-365.

Sota, H., Hasegawa, Y. and Iwakura, M. (1998) Detection of Conformational Changes in an Immobilized Protein using Surface Plasmon Resonance. *Anal Chem*. 70: 2019-2024.

Stenberg, E., Persson, B., Roos, H. and Urbaniczky, C. (1991) Quantitative Determination of Surface Concentration of Protein with Surface Plasmon Resonance Using Radiolabeled Proteins. *J Colloid Interf Sci*. 143: 513-526.

Stirdivant, S. M., Klysik, J. and Wells, R. D. (1982) Energetic and Structural Interrelationship Between DNA Supercoiling and the Right-Handed to Left-Handed Z-Helix Transitions in Recombinant Plasmids. *J Biol Chem*. 257: 159-165.

Stollar, B. D., Zon, G. and Pastor, R. W. (1986) A Recognition Site on Synthetic Helical Oligonucleotides for Monoclonal Anti-Native DNA Autoantibody. *Proc Natl Acad Sci USA*. 83: 4469-4473.

Sugimoto, N. and Wakizaka, N. (1998) Effect of Cu^{2+} on Complex Formation Between a Deoxyribozyme and its Substrates. *Nuclos Nucleot*. 17: 565-574.

Sugimoto, N., Wu, P., Hara, H. and Kawamoto, Y. (2001) pH and Cation Effects on the Properties of Parallel Pyrimidine Motif DNA Triplexes. *Biochemistry*. 40: 9396-9405.

Swanson, P. C., Ackroyd, C. and Glick, G. D. (1996) Ligand Recognition by Anti-DNA Autoantibodies. Affinity, Specificity, and Mode of Binding. *Biochemistry*. 35: 1624-1633.

Taboury, J. A., Bourtayre, P., Liquier, J. and Taillandier, E. (1984) Interaction of Z-Form Poly(dGdC).poly(dGdC) with Divalent Metal Ions - Localization of the Binding Sites by IR Spectroscopy. *Nucleic Acids Res*. 12: 4247-4258.

Takacs, M. A., Jacobs, S. J., Bordens, R. M. and Swanson, S. J. (1999) Detection and Characterization of Antibodies to PEG-IFN-alpha 2b Using Surface Plasmon Resonance. *J Interf Cytok Res*. 19: 781-789.

Tanha, J., Forsyth, G., Schorr, P., Crosby, W. and Lee, J. S. (1997) Sequence and Structure Specific Antibodies from Phage Display Libraries. *MOL IMMUNOL*. 34: 109-113.

Tanha, J. and Lee, J. (1997) Thermodynamic analysis of monoclonal antibody binding to duplex DNA. *Nucleic Acids Res*. 25: 1442-1449.

Tanner, J. A., Abowath, A. and Miller, A. D. (2002) Isothermal Titration Calorimetry Reveals a Zinc Ion as an Atomic Switch in the Diadenosine Polyphosphates. *J Biol Chem*. 277: 3073-3078.

Tao, T., Nelson, J. H. and Cantor, C. R. (1970) Conformational Studies on Transfer Ribonucleic Acid. Fluroescence Lifetime and Nanosecond Depolarization Measurements on Bound Ethidium Bromide. *Biochemistry*. 9: 3514-3524.

Taubes, G. (1997) Double Helix Does Chemistry at a Distance-- But How? *Science*. 275: 1420-1421.

Testa, S. M., Disney, M. D., Turner, D. H. and Kierzek, R. (1999) Thermodynamics of RNA-RNA Duplexes with 2- or 4-thiouridines: Implications for Antisense Design and Targeting a Group I Intron. *Biochemistry*. 38: 16655-16662.

Thiyagarajan, S., Rajan, S. S. and Gautham, N. (2004) Cobalt Hexammine Induced Tautomeric Shift in Z-DNA: The Structure of d(CGCGCA).d(TGCGCG) in Two Crystal Forms. *Nucleic Acids Res*. 32: 5945-5953.

Tsoi, P. Y. and Yang, M. S. (2004) Surface Plasmon Resonance Study of the Molecular Recognition Between Polymerase and DNA Containing Various Mismatches and Conformational Changes of DNA-protein Complexes. *Biosens Bioelectron*. 19: 1209-1218.

Tufvesson, E. and Westergren-Thorsson, G. (2002) Tumour Necrosis Factor-alpha Interacts with Biglycan and Decorin. *Febs Lett*. 530: 124-128.

Vales-Gomez, M., Erskine, R. A., Deacon, M. P., Strominger, J. L. and Reyburn, H. T. (2001) The role of Zinc in the Binding of Killer Cell Ig-like Receptors to Class I MHC Proteins. *Proc Natl Acad Sci USA*. 98: 1734-1739.

Van De Sande, J. H., Mcintosh, L. P. and Jovin, T. M. (1982) Mn^{2+} and other Transition Metals at Low Concentration Induce the Right-to-Left Helical Transformation of poly[d(GC)]. *EMBO J*. 1: 777-782.

Van De Sande, J. H., Ramsing, N. B., Germann, M. W., Elhorst, W., Kalisch, B. W., Vonkitzing, E., Pon, R. T., Clegg, R. C. and Jovin, T. M. (1988) Parallel Stranded DNA. *Science*. 241: 551-557.

Vikinge, T. P., Askendal, A., Liedberg, B., Lindahl, T. and Tengvall, P. (1998) Immobilized chicken antibodies improve the detection of serum antigens with surface plasmon resonance (SPR). *Biosens Bioelectron*. 13: 1257-1262.

Wang, A. H. J., Quigley, G. J., Kolpak, F. J., Crawford, J. L., Vanboom, J. H., Vandermarel, G. and Rich, A. (1979) Molecular Structure of a Left-Handed Doble Helical DNA Fragment at Atomic Resolution. *Nature*. 282: 680-686.

Waring, M. J. (1965) Complex Formation Between Ethidium Bromide and Nucleic Acids. *J Mol Biol*. 13: 269-282.

Watson, J. D. and Crick, F. H. C. (1953) Genetic Implications of the Structure of Deoxyribonucleic Acid. *Nature*. 171: 964-967.

Wettig, S. D., Bare, G. A., Skinner, R. J. S. and Lee, J. S. (2003) Signal transduction through dye-labeled M-DNA Y-branched junctions: Switching modulated by chemical reduction of anthraquinone. *Nano Lett*. 3: 617-622.

Winzor, D. J. (2003) Surface Plasmon Resonance as a Probe of Protein Isomerization. *Anal Biochem*. 318: 1-12.

Wood, S. J. (1993) DNA DNA Hybridization in Real-Time Using Biacore. *Microchem J*. 47: 330-337.

Xu, Y., Ikeda, R. and Sugiyama, H. (2003) 8-methylguanosine: A Powerful Z-DNA Stabilizer. *J Am Chem Soc*. 125: 13519-13524.

Yamaguchi, O., Odani, A., Masuda, H. and Sigel, H. (1996) Stacking Interactions Involving Nucleotides and Metal Ions. In *Metal Ions in Biological Systems* 32 (Edited by A. Sigel and H. Sigel), Marcel Dekker, Inc., New York, pp. 207-262

Yi, J. Z., Asante-Appiah, E. and Skalka, A. M. (1999) Divalent Cations Stimulate Preferential Recognition of a Viral DNA End by HIV-1 Integrase. *Biochemistry*. 38: 8458-8468.

Zahler, A. M., Williamson, J. R., Cech, T. R. and Prescott, D. M. (1991) Inhibition of Telomerase by G-quartet Structures. *Nature*. 350: 718-720.

Zhang, Y., Akilesh, S. and Wilcox, D. E. (2000) Isothermal Titration Calorimetry Measurements of Ni(II) and Cu(II) Binding to His, GlyGlyHis, HisGlyHis, and Bovine Serum Albumin: A Critical Evaluation. *Inorg Chem*. 39: 3057-3064.

Zhao, Y., Kan, Z., Zeng, Z., Hao, Y., Chen, H. and Tan, Z. (2004) Determining the Folding and Unfolding Rate Constants of Nucleic Acids by Biosensor. Application to Telomere G-Quadruplex. *J Am Chem Soc*. 126: 13255-13264.

Zimmerman, S. B., Cohen, G. H. and Davies, D. R. (1975) X-ray Fiber Diffraction and Model-building Study of Polyguanylic Acid and Polyinosinic Acid. *J Mol Biol*. 92: 181-184.

Zouali, M., Stollar, B. D. and Schwartz, R. S. (1988) Origin and Diversitfication of Anti-DNA Antibodies. *Immunol Rev*. 105: 137-159.